

# **Growth of Carbon Nanotubes on Model and Supported Catalysts**

by

Vinay S. Medhekar

## **A Dissertation**

Submitted to the Faculty of

**WORCESTER POLYTECHNIC INSTITUTE**

in partial fulfillment of the requirement for the

Degree of Doctor of Philosophy

in

Chemical Engineering

---

August 2004

Approved by:

---

Prof. Fabio H. Ribeiro, Advisor, Purdue University

---

Prof. Robert W. Thompson, WPI

---

Prof. Venkat R. Thalladi, WPI

# Outline of Ph.D. Dissertation

Outline of Ph.D. Dissertation.....	i
Abstract.....	v
1. Introduction to Study of Growth of Carbon Nanotubes on Model and Supported Catalyst.....	1
1) <i>Introduction</i> .....	5
2) <i>Nanotube Growth Method</i> .....	12
3) <i>Research Proposal</i> .....	19
4) <i>References</i> .....	25
2. Spin coating of catalyst clusters on model support.....	29
1) <i>Introduction</i> .....	37
2) <i>Background</i> .....	39
3) <i>Experimental Section</i> .....	41
4) <i>Spin Coating Experiments</i> .....	45
5) <i>Temperature effects on Catalyst clusters on Si(100) support</i> .....	55
6) <i>Iron Nitrate</i> .....	66
7) <i>Discussion and Conclusion</i> .....	87
8) <i>References</i> .....	89

3. Growth of Carbon Nanotubes on Iron clusters on model support.....	91
1) <i>Aim of Experiments</i> .....	97
2) <i>Deposition of catalyst of various sizes</i> .....	97
3) <i>Effect of temperature on the catalyst particle size</i> .....	99
4) <i>Reaction with FeCl<sub>2</sub> on SiO<sub>2</sub>/Si with benzene as carbon source</i> .....	102
5) <i>Reaction with FeCl<sub>2</sub> on SiO<sub>2</sub>/Si with propylene as carbon source</i> .....	112
6) <i>Discussion and Conclusion</i> .....	120
7) <i>References</i> .....	121
4. Growth of Carbon Nanotubes on Nickel clusters on model support.....	122
1) <i>Experimental procedure to produce carbon nanotubes</i> .....	126
2) <i>Spin coating of NiCl<sub>2</sub> on SiO<sub>2</sub>/Si support and blank reaction</i> .....	128
3) <i>Production of carbon nanotubes on NiCl<sub>2</sub></i> .....	133
4) <i>Conclusion</i> .....	144
5. Growth and Study of MWNT from Ferrocene.....	145
1) <i>Background</i> .....	150
2) <i>Experimental</i> .....	153
3) <i>Results and Discussion</i> .....	155
4) <i>TEM Analysis</i> .....	161

5) Oxidation of sample covered with carbon nanotubes grown from ferrocene.....	163
6) Discussion and Conclusion.....	166
7) References.....	168
6. Growth and Study of SWNT on Supported Catalyst.....	169
1) Introduction.....	175
2) Experimental.....	176
3) Results and Discussion.....	178
4) Discussion.....	191
5) Conclusion.....	193
6) Reference.....	194
7. Atomic Layer Deposition of Alumina on Silica/Si (100) substrate and their Thermal Properties.....	197
1) Introduction.....	205
2) Background of Atomic Layer Deposition.....	206
3) Characterization of thin films using Ellipsometry.....	208
4) Effect of support on production and growth of carbon nanotubes.....	210
5) Atomic layer deposition equipment design.....	212
6) Atomic layer deposition of Alumina on SiO <sub>2</sub> /Si model support.....	215
7) Thermal stability of thin film.....	230
8) Deposition of catalyst clusters on Alumina coated SiO <sub>2</sub> /Si wafer.....	239

9) <i>Reaction on iron salt deposited on Alumina coated SiO<sub>2</sub>/Si wafer</i> .....	248
10) <i>Discussion</i> .....	252
11) <i>Conclusion</i> .....	255
12) <i>References</i> .....	256
8. Discussion and Conclusions.....	259
9. Future Work.....	266
Acknowledgements.....	vii

# Abstract

Catalytic growth of Carbon Nanotubes (CNT) provides important advantages of controlling their diameters and possibly chirality. Our work involved growing CNT on model and supported catalyst by catalytic decomposition of carbon source such as benzene, methane and propylene. On supported catalyst, iron nitrate was deposited on alumina and reduced to form metallic iron clusters. These were reacted at 700 – 950 °C under varying benzene concentrations. Multi Walled CNT (MWNT) grew below 800 °C and Single Wall CNT (SWNT) are observed at 850 °C and above as confirmed by TEM and Raman. Model catalysts were studied by producing CNT from ferrocene which acted as the carbon and catalyst source on Silica/Si (100). Large yield of MWNT was observed at 900 °C. MWNT grew perpendicular to the model support as seen by SEM. In another model catalyst study, iron salt clusters were deposited on silica/Si (100) by spin coating, controlling their diameters by solution concentration and speed of spinning. Agglomeration of clusters at high temperatures produces only MWNT on silica/Si (100). Cluster agglomeration can be reduced with strong support metal interaction such as with alumina. We deposited alumina on silica/Si (100) by atomic layer deposition, with conformal coatings on surface and low relative roughness. Alumina film was stable under reaction temperatures of 900 °C. Cluster deposition on alumina by spin coating was difficult because of different surface acidity compared to silica. Clusters on alumina did not agglomerate at high reaction temperatures. We report effect of parameters such as the temperature of reaction, conditions of pretreatment such as reduction and oxidation of catalyst precursor, type of precursor, type of carbon source, and type of support material on growth of CNT. The role of spin coating in controlling the diameter of salt clusters

deposited is discussed. We also report deposition of alumina on top of silica/Si (100) by atomic layer deposition and the effect of deposition and calcination temperatures on the alumina film integrity.

# **Chapter 1**

**Introduction to Study of Growth of Carbon  
Nanotubes on Model and Supported Catalyst**

# Table of Contents

<b>CHAPTER 1.....</b>	<b>1</b>
<b>INTRODUCTION TO STUDY OF GROWTH OF CARBON NANOTUBES ON MODEL AND SUPPORTED CATALYST.....</b>	<b>1</b>
<b>TABLE OF CONTENTS .....</b>	<b>2</b>
<b>LIST OF FIGURES .....</b>	<b>3</b>
<b>1 INTRODUCTION.....</b>	<b>5</b>
<b>2 NANOTUBE GROWTH METHODS.....</b>	<b>12</b>
2.1 ARC-DISCHARGE TECHNIQUE .....	12
2.2 LASER ABLATION METHOD .....	14
2.3 CHEMICAL VAPOR DEPOSITION (CVD) .....	15
<b>3 RESEARCH PROPOSAL .....</b>	<b>19</b>
3.1 BACKGROUND.....	19
3.2 SPIN COATING .....	20
3.3 AIM OF RESEARCH.....	23
<b>4 REFERENCE.....</b>	<b>25</b>

## List of Figures

Figure 1 Structure of single and multi-walled carbon nanotubes. ....	6
Figure 2 Typical TEM images of MWNT show a central hollow core surrounded by graphite layers (Iijima et al. 1993).....	7
Figure 3 Chirality of carbon nanotubes determines the properties of the CNT that depend on the direction in which the graphite sheet is cut and joined together. ....	7
Figure 4 A model design of carbon nanotube based transistor (IBM Corp.). The source and drain are metallic conductors. ....	11
Figure 5 Arc-discharge technique for production of MWNT and SWNT. The arcing current is passed between carbon anode and cathode in an inert atmosphere. <i><a href="http://www.iljinnanotech.co.kr/en/material/r-4-1.htm">http://www.iljinnanotech.co.kr/en/material/r-4-1.htm</a></i> .....	13
Figure 6 Laser ablation of carbon target to produce SWNT. The laser is incident on the target, which is kept in the furnace at a temperature around 1200 °C. Inert gas flowing removes the nanotubes formed in the furnace and carries it to the cold zone to be collected separately. ....	14
Figure 7 CVD method of producing carbon nanotube from a hydrocarbon source. The catalyst is placed inside a tube furnace maintained at reaction temperature of 500 – 900 °C. Hydrocarbon is flowed through the reactor over the catalyst. The carbon nanotubes are collected at the end of the reaction. ....	17
Figure 8 Carbon nanotubes growth takes by two mechanisms; base mode where the catalyst stay attached to the base to the support and other tip mode where the catalyst is lifted from the surface of support.....	18

Figure 9 Aligned carbon nanotube growth from in-situ deposition of iron from ferrocene.

Each pillar consists of several tens of nanotubes grown in vertical alignment and in a normal direction to SiO<sub>2</sub> patterns on the Si/SiO<sub>2</sub> template. Vertical and horizontal growth of aligned nanotubes, viewed in a cross-section of a patterned Si/SiO<sub>2</sub> wafer is observed. Scale bars, 100 μm [31]. ..... 18

Figure 10 Stages of spin coating process are shown in temporal order. After initial

deposition, the excess of liquid is thrown away by centrifugal force. At some point, centrifugal force is balanced by viscous force and only a very small net flow of liquid occurs. The inert gas flowing over the top leads to evaporation of the liquid film, resulting in super saturation and ultimately in crystallization of catalyst particles..... 22

# 1 Introduction

Carbon nanotubes are essentially long graphite sheets rolled in to a tube with their edges joined to form a seamless cylinder and a cap placed on the open ends of the tube (Figure 1a). The tube made out of a single layer of carbon atoms is called single-walled carbon nanotube (SWNT). If there occur layers of carbon sheets all wrapped one over other (Figure 1b), they are termed as Multi-walled carbon nanotubes (MWNT). MWNT were first observed by Dr. Iijima of the NEC laboratory in Japan in 1991 [1]. About two years later, he made the observation of SWNT [2]. The TEM images of MWNT are given in Figure 2. The diameter of a SWNT is typically about 1 – 3 nm and that of MWNT varies from 5 to 100 nm depending on the number of layers growing co-axially.

Carbon nanotubes are unique nanostructures with remarkable electronic and mechanical properties. The initial interest in the molecule was because of its one – dimensional quantum effects that lead to its remarkable electronic properties. The subsequent interest was the promise that the remarkable structure and properties of carbon nanotubes might give rise to some unique applications. The most important development was the prediction that carbon nanotubes could be either semi-conducting or metallic depending on their geometrical characteristics, namely their diameter and the chirality [3,4,5]. The chirality of the carbon nanotube molecule depends on the direction in which the sheet is cut and joined at the edges to make the carbon nanotube. Two examples of the chirality of the carbon nanotubes are zigzag ( $\theta = 0^\circ$ ) and armchair ( $\theta = 30^\circ$ ) as shown in Figure 3. Zigzag chirality leads to semi-conductor or quasi-metallic properties of carbon nanotube whereas armchair behaves as metallic. The property of

carbon nanotube that depends only on the chirality of the structure but essentially form the same molecules has great implication in electronics. Armchair carbon nanotube is single tube with pure metallic properties, which makes it truly a one-dimensional quantum wire. Most of the theoretical predictions of the electrical properties were done in 1992, a year after their discovery but it was not until 1998 that these remarkable properties were corroborated experimentally [6,7].

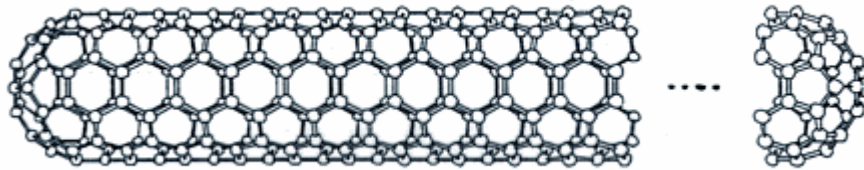


**Figure 1a** Single walled carbon nanotube.

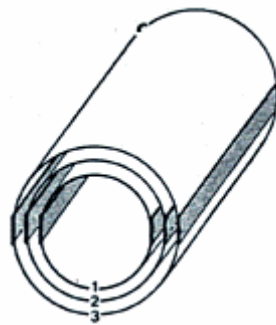


**Figure 1b** Multi-walled carbon nanotube showing layers of single graphitic layers wrapped around a common axis.

**Figure 1** Structure of single and multi-walled carbon nanotubes.

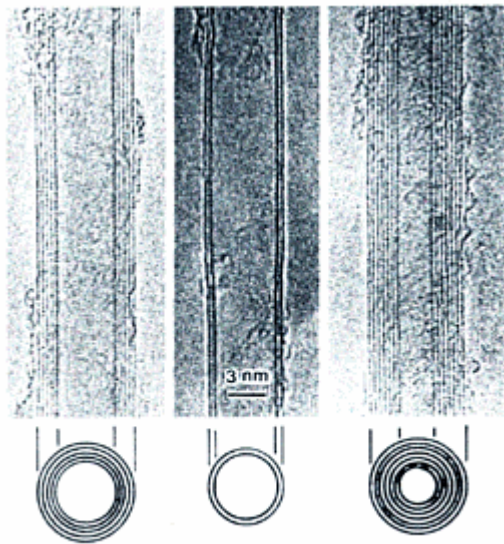


**Figure 2** Typical TEM images of MWNT show a central hollow core surrounded by graphite layers (Iijima et al. 1993).

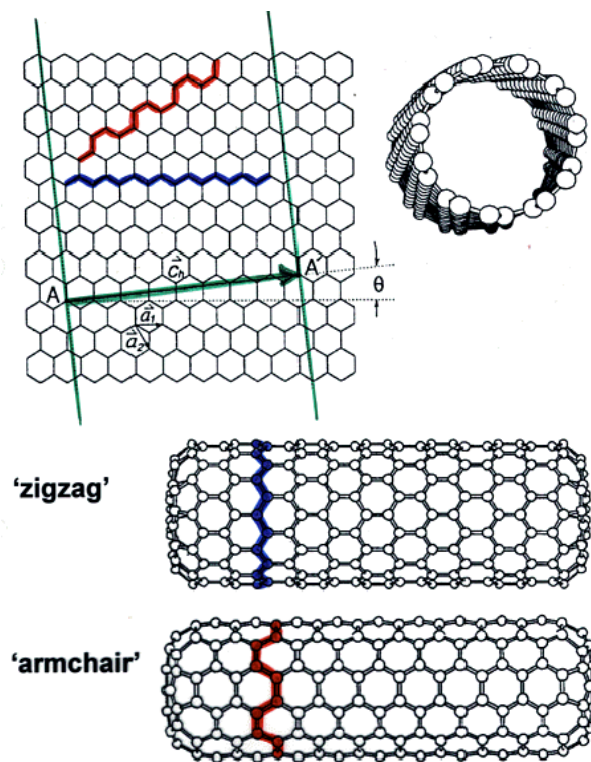


**Figure 3** Chirality of carbon nanotubes determines the properties of the CNT that depend on the direction in which the graphite sheet is cut and joined together.

Carbon nanotube is the strongest material to find utility in nano-scale devices and composite materials and remains a powerful motivation for the research in this area. Carbon nanotube has combination of high strength and high stiffness, a combination desired in airplanes and space shuttles. Early theoretical work and experiments on individual nanotubes (mostly MWNT) had confirmed that nanotubes are one of the stiffest structures ever made [8, 9, 10]. Yu et al [11] showed by direct measurement that the tensile strength of individual SWNT is about 50 GPa, comparing with that of carbon fibers used in space shuttles, which has tensile strength of 5 GPa while steel breaks at 3 GPa. Such high tensile strength makes them a promising candidate in reinforcement applications. Most importantly, nanotubes, for the first time represent the ideal, most perfect and ordered, carbon fiber, the structure of which is entirely known at the atomic level.

The small size of the carbon nanotubes is currently employed in preparing Scanning Force Microscope probes [12]. Since the MWNT are conducting, they can be easily used in the Scanning tunneling microscopy. MWNT and SWNT tip were used in a tapping mode to image biological molecules such as amyloid-b-protofibrils (related to Alzheimer's disease), with resolution never achieved before [13]. In addition, due to the high elasticity of the nanotubes, the tips do not suffer from crashes on contact with the substrates. Any impact will cause buckling of the nanotube, which generally is reversible on retraction of the tip from the substrate.

Carbon nanotubes are cylindrical hollow tubes with nanometer-scale diameters, which provide storage of atoms, molecules and metallic wires, thereby forming nanocomposites with new electronic and magnetic properties. Approaches of filling of carbon nanotube essentially employ the nanotube capillarity [14]. The current application of the filling properties of nanotubes is employed for storage of hydrogen. Extraordinarily high and reversible hydrogen adsorption in SWNT containing materials [15, 16, 17, 18] has been reported and has attracted considerable interest in both academia and industry. It has been predicted that the carbon nanotubes can store liquid and gases in the inner cores through a capillary effect [19]. Measurements performed on relatively large amount of materials (~50% purity, 500 mg) showed a hydrogen capacity of 4.2% when samples were exposed to 10 MPa hydrogen pressure at room temperature. About 80% of the adsorbed H<sub>2</sub> could be released at room temperature, providing an application for storage of H<sub>2</sub> for fuel cell. The benchmark is 6.5% set by DOE and the target is easily exceeded under special conditions of high pressure and low temperatures and greater purity of carbon nanotubes.

Among few other application, energy storage is promising. Graphite, carbonaceous materials, and carbon fiber electrodes have been used for decades in fuel cells, battery and several other electrochemical applications [20]. Nanotubes have small dimensions, smooth surface topology and perfect surface specificity that provide the fastest electron transfer kinetics following ideal Nernstian behavior [21]. SWNT are currently being employed as field emitters with application in cathode ray lighting elements. Ise Electronic Co. in Japan produced the first cathode ray tube from SWNT [22]. Prototype

matrix-addressable diode flat panel displays have been fabricated using carbon nanotubes as the electron emission source [23]. Samsung has already developed the world's first flat display panel [24]. A flat panel diode consists of SWNT stripes on the cathode and phosphor-coated Indium-Tin-Oxide stripes on the anode running orthogonal to the cathode stripes.

IBM has recently announced the production of first transistor chip to be successfully used in electronic devices [25]. The size of a carbon nanotube based transistor is about 500 times smaller than silicon-based transistor (Figure 4) and is thought to beat the Moore's law of hitting the size limit for transistors in near future. More transistors per unit area of support imply greater applicability, speed and information processing capability.

The greatness of SWNT lies in the fact that it is a macromolecule as well as a crystal at the same time. A carbon nanotube is extremely versatile material; it is one of the strongest materials, yet highly elastic, highly conducting, small in size, but stable, and quite robust in most chemically harsh environments. It is hard to think of any another material that can compete carbon nanotube in versatility.

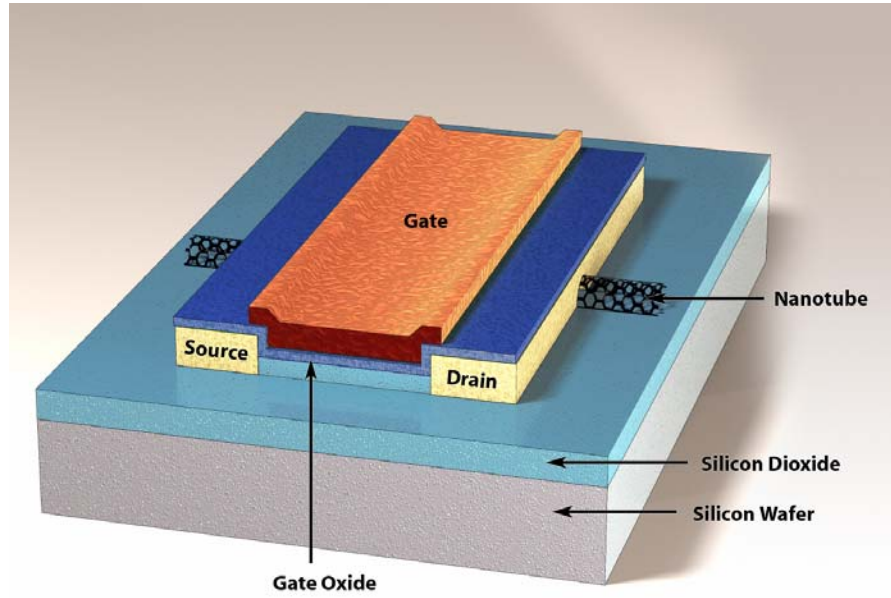


**Figure 4** A model design of carbon nanotube based transistor (IBM Corp.). The source and drain are metallic conductors.

## 2 Nanotube Growth Methods

### 2.1 Arc-discharge technique

The method employed by Iijima for growth of carbon nanotube was Arc-discharge between two graphitic sources placed in an inert chamber. A representative experimental setup for arc-discharge technique is shown in Figure 5. A high current discharge is passed through two opposing carbon anode and cathode, evaporating carbon atoms by plasma of helium gas. Arc-discharge method has developed into an excellent method of producing high quality multi-walled carbon nanotube and single wall carbon nanotube. MWNT can be obtained by controlling the growth conditions such as the pressure of inert gas in the discharge chamber and the arcing current. Ebbesen and Ajayan made a breakthrough in arc-discharge method by producing and purifying MWNT at gram level [26]. The length of the multi-walled carbon nanotubes is about few tens of microns and the diameter varies from 5 to 30 nm. The MWNT are usually kept together by van der Waal's forces and are usually found in bundles. They grow straight in arc-discharge method, which is indicative of the high crystallinity of the material. The number of defects in the carbon nanotube is less in form of pentagons and heptagons instead of regular hexagons. For the growth of single walled carbon nanotubes, metal catalyst particles are needed in the graphitic electrodes. Bethune and coworkers [27] first produced substantial amount of SWNT by arc-discharge method using cobalt as the catalyst.

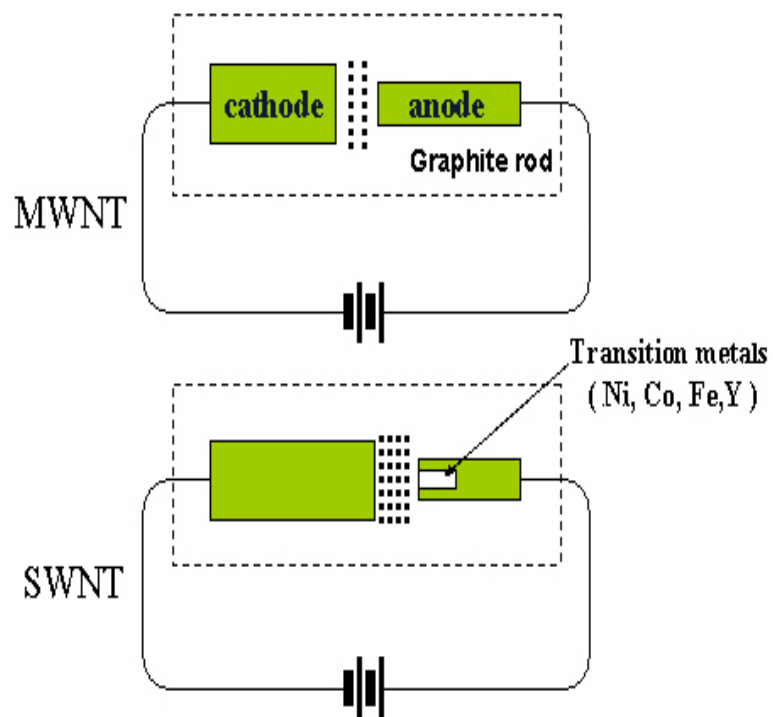


**Figure 5** Arc-discharge technique for production of MWNT and SWNT. The arcing current is passed between carbon anode and cathode in an inert atmosphere. <http://www.iljinnanotech.co.kr/en/material/r-4-1.htm>

## 2.2 Laser Ablation method

Smalley and coworkers first grew high quality SWNT at 1 – 10 gm scale using the technique of laser ablation of carbon target [28]. The method involves intense laser pulses to ablate carbon target containing 0.5 atomic percent of nickel and cobalt. The target was placed in a tube furnace heated to 1200 °C. During the ablation, inert gas was passed through the reaction chamber to carry the grown nanotubes to be collected in a cold region (Figure 6). The SWNT produced are essentially in the form of ropes that are in bundles of tens of individual carbon nanotubes that are close-packed in crystals via van der Waal's forces.

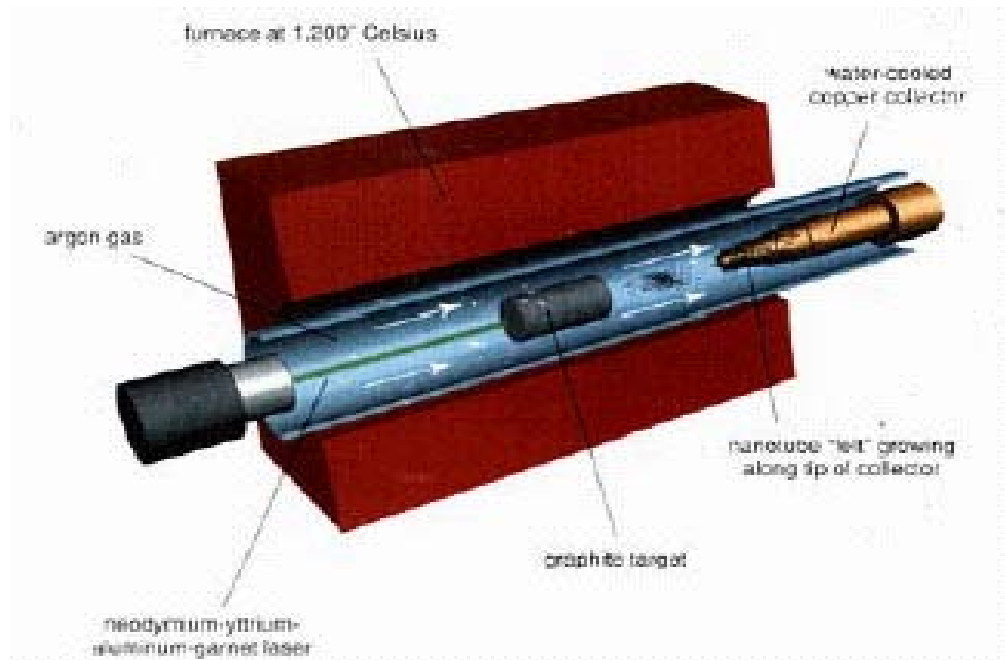


**Figure 6** Laser ablation of carbon target to produce SWNT. The laser is incident on the target, which is kept in the furnace at a temperature around 1200 °C. Inert gas flowing removes the nanotubes formed in the furnace and carries it to the cold zone to be collected separately.

### 2.3 Chemical Vapor Deposition (CVD)

Chemical vapor deposition involves placing suitable catalyst in a tube furnace and flowing hydrocarbon gas through the tube for a period of time. The catalyst decomposes the hydrocarbon releasing hydrogen and carbon is free to form nanotubes. At the right conditions of temperature, hydrocarbon flow rate and temperature, carbon nanotubes are formed (Figure 7). The catalyst, the temperature of reaction, the type of hydrocarbon and the time of reaction control the growth of carbon nanotube. Catalysts employed for CVD are essentially transition metals dispersed on a support such as silica. A carbon nanotube formation is preferred at high temperature over the formation of graphitic carbon because of the absence of dangling bonds on graphite. For MWNT, the temperature of operation is in the range of 550 to 900 °C. Transition metals viz. iron, nickel and cobalt are used as catalyst. The reason for using these metals as catalysts is the finite solubility of carbon in the metals that lead to the formation of metal-carbon solution and ultimately the formation of carbon nanotubes. The mechanism of growth of nanotubes is not clearly understood but what is essentially observed is that carbon can dissolve at the base of the catalyst and the catalyst particles remain attached to the surface of the support and carbon nanotubes grow out. This is called the base mode growth. In other case, the catalyst is picked from the support surface and nanotube keeps forming below the catalyst. This is called tip growth mode (Figure 8).

The major disadvantage of the CVD technique is the large number of defects observed in the structure. This can be related to the low temperature of growth of carbon

nanotubes that does not provide enough energy to iron out the defects. The challenge currently faced is the ability to grow perfect crystals of MWNT.

The advantages of the arc-discharge and the laser ablation techniques lie in the fact that very uniform and almost defect free nanotubes can be formed. The major drawback of these techniques is the large temperature needed for growth of carbon nanotubes. The temperature at the reaction phase exceeds 3000 °C and limits the scale of the process for industrial manufacture of nanotubes. The second disadvantage lies in the usability of these nanotubes. The nanotubes required for all the applications listed above needs a linear orientation while those formed in arc-discharge and laser ablation are essentially in tangled form. This reduces the applicability of the material to be manipulated or purified. CVD has shown growth of very structured MWNT, growing out of the support surface in a linear direction [29, 30, 31, 32, 33, 34]. The catalyst precursors used were of transition metals and variety of hydrocarbon such as methane, benzene, ethylene, acetylene and host of their derivatives were used. The temperature of preparation varied from 500 to 1000 °C.

Aligned carbon nanotubes that grow straight out from the surface of support has several applications in flat panel display, field emission transistors and also help characterize effect of catalyst size on the growth parameters of the carbon nanotubes. Such a study is possible only on a flat catalyst support. Studies have employed several techniques in making supported catalysts such as evaporating metals directly on to a flat support, producing catalyst in-situ or depositing catalyst by crystallization or

precipitation on the surface. Wei et al. [31] exposed silica/silicon surface to a mixture of ferrocene in xylene. Ferrocene decomposes to nascent iron, which is deposited on the silica surface (does not adhere to the silicon surface) producing catalyst in-situ. The carbon atoms are available in the form of its own 5 carbon ring and from xylene. The carbon nanotubes form at 800 °C and grow straight, aligned and away from the surface. Their results are reproduced in Figure 9. Zhang et al. employed evaporating iron on a flat silica support up to a thickness of 5 to 50 nm and passing ethylene diamine (8% in N<sub>2</sub>) for 5 to 45 minutes at 800 – 900 °C. They observed straight aligned multi-walled carbon nanotubes. They also observed that the flat surface of metal layer agglomerates to form clusters on which the carbon nanotubes are formed. The cluster diameter is however dependent on the metal thickness deposited and is not controlled. The above research studies have made giant leaps in the production of carbon nanotubes and are currently pursued to meet the application end.

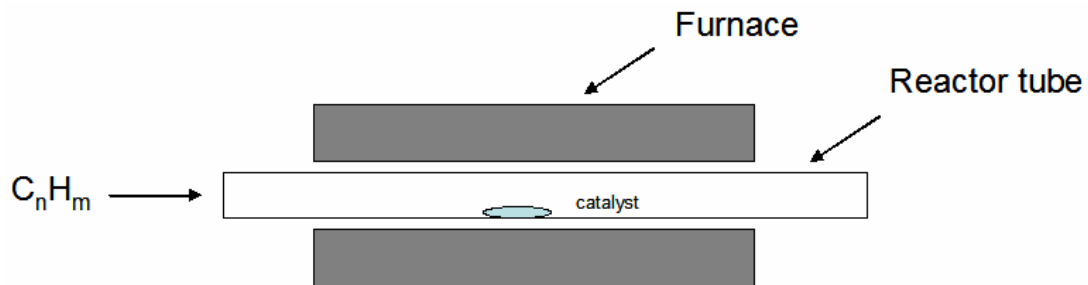


**Figure 7** CVD method of producing carbon nanotube from a hydrocarbon source. The catalyst is placed inside a tube furnace maintained at reaction temperature of 500 – 900 °C. Hydrocarbon is flowed through the reactor over the catalyst. The carbon nanotubes are collected at the end of the reaction.

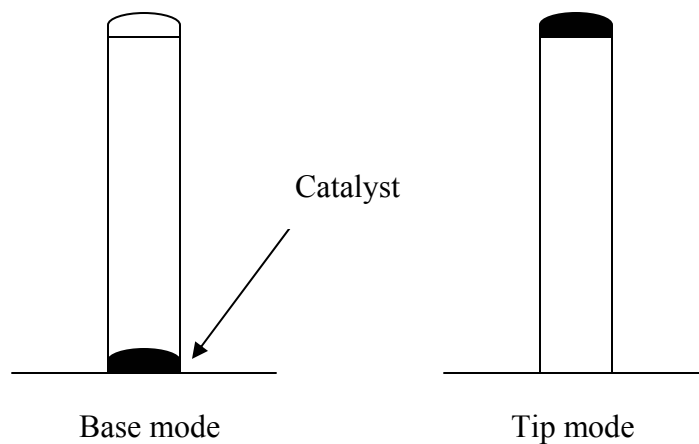


**Figure 8** Carbon nanotubes growth takes by two mechanisms; base mode where the catalyst stay attached to the base to the support and other tip mode where the catalyst is lifted from the surface of support.

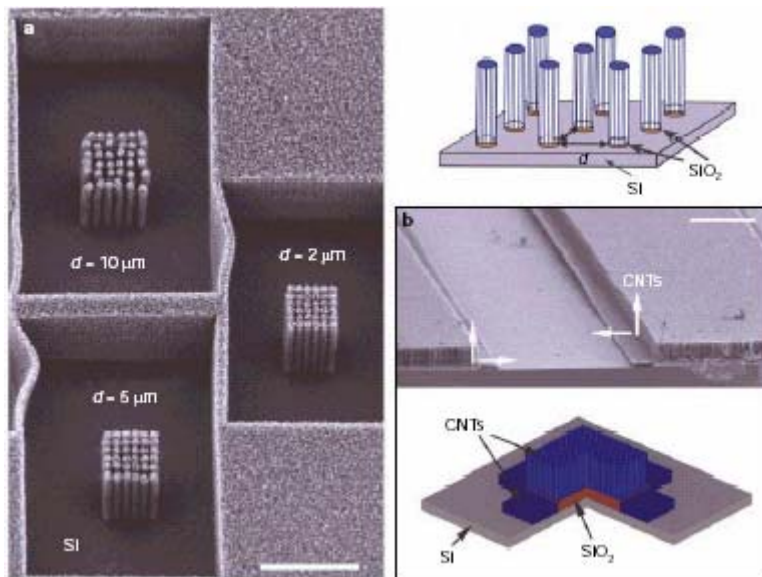


**Figure 9** Aligned carbon nanotube growth from in-situ deposition of iron from ferrocene. Each pillar consists of several tens of nanotubes grown in vertical alignment and in a normal direction to SiO<sub>2</sub> patterns on the Si/SiO<sub>2</sub> template. Vertical and horizontal growth of aligned nanotubes, viewed in a cross-section of a patterned Si/SiO<sub>2</sub> wafer is observed. Scale bars, 100 μm [31].

## **3 Research Proposal**

### **3.1 Background**

The techniques mentioned in previous section definitely are a great leap in the process of manufacture of carbon nanotubes but the formation of catalyst cluster on flat surface is not completely controlled or understood. This provides a serious limitation to the study of the growth of carbon nanotube in correlation to the effect of catalyst clusters deposited. Further the nanotubes grown by CVD techniques are essentially multi-walled carbon nanotubes. Effectively manipulating the catalyst clusters for growing SWNT is still not achieved. The chirality of SWNT controlling properties such as semiconductor or metallic in nature cannot be controlled by above mentioned techniques. The limitation has provided us with the need to employ a technique, which can control the size of the catalyst deposited on a flat support to a higher degree of accuracy. In this regards, we propose to use Si (100) single crystal surface as support as it has implications in semiconductor industry and silica formed by calcining the Si (100) surface is commonly studied catalyst support. The catalyst particles are then deposited from its solution by a technique called spin coating. We propose to employ chemical vapor deposition to grow single wall carbon nanotubes.

## 3.2 Spin coating

Spin coating is a very simple process of depositing catalysts on a flat support such as single crystal alumina ( $\text{Al}_2\text{O}_3$ ) or silica ( $\text{SiO}_2$ ). The use of flat support consisting of  $\text{Al}_2\text{O}_3$  or  $\text{SiO}_2$  layer on a conducting layer of Al or Si respectively instead of commercial catalysts has a number of benefits with respect to surface sensitive spectroscopic techniques [35, 36, 37]. One is that the catalyst is directly available for analysis. Flat support also facilitates the use of techniques such as atomic force microscopy (AFM) and scanning tunneling microscopy (STM). The transport limitations such as mass and heat transfer to the catalyst surface from reaction mixture are usually absent and make interpretation of the results fairly easy. Spin coating has been employed for the deposition of thin layers of inorganic salts on flat supports, in order to prepare model catalysts [38].

The silicon (100) single crystal flat wafer was oxidized in air at 750 °C for 24 hours. This forms a small layer of  $\text{SiO}_2$  (about 80 nm), which has oxygen atoms on the surface in the bound state. The  $\text{SiO}_2/\text{Si}$  wafer is then cleaned using standard cleaning procedure 1 developed by Kern and Poutinen [39] for semi conductor industry. The technique is also called RCA-1 which will be used in this dissertation. The advantage of this technique is the minimal loss of oxide surface while preserving excellent particle removal. The process involves first heating at 70 °C, the  $\text{SiO}_2/\text{Si}$  wafer with 70:30 v/v solutions of ammonium hydroxide (30%) and hydrogen peroxide (35%) for 10 minutes and then cleaned with boiling DI water [40].

The schematic representation of the stages involved in the process is shown in Figure 10. They are explained as given below:

- Stage one:** The first stage is the deposition of the coating fluid onto the flat substrate.
- Stage Two:** The second stage is when the substrate is accelerated up to its final, desired, rotation speed.
- Stage three:** The substrate reaches a constant speed and fluid's viscous forces dominate fluid thinning behavior. The extra fluid is thrown out with the centrifugal force. Now thin layer of liquid remain as a result of balance between viscous force and the centrifugal force.
- Stage four:** A flow of inert gas over the surface causes the liquid to evaporate leading to the process of super saturation. The salt crystals crystallize out uniformly. Since the time of evaporation is very short (about the order of few seconds), the crystals are formed in the nanometer size range.

Variation of the spin coating parameters namely the spin coating speed and the concentration of the solution helps control two important characteristic of the model catalyst viz. catalyst loading and the morphology of the catalyst particles [35, 38, 41].

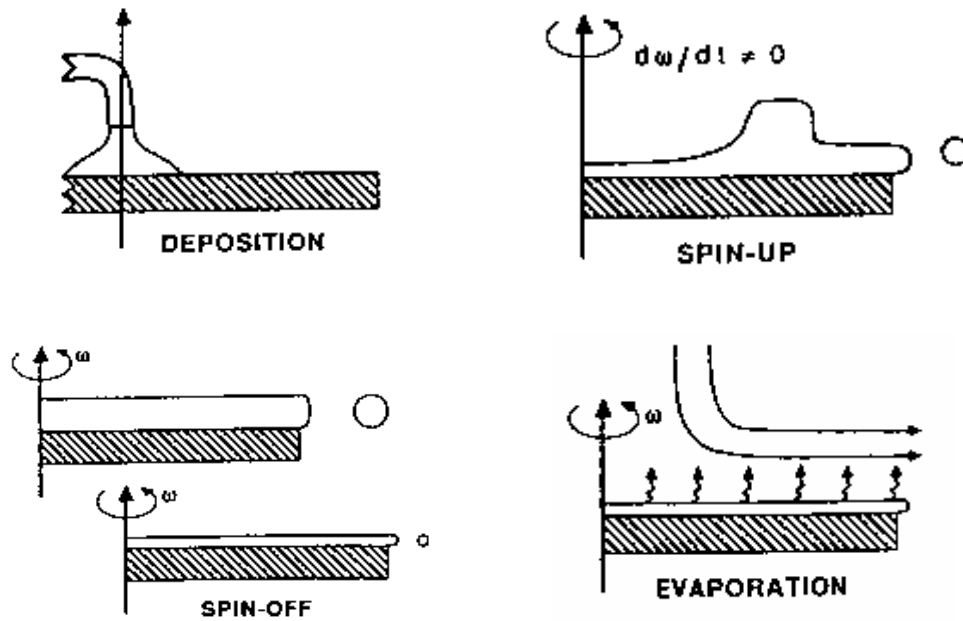


**Figure 10** Stages of spin coating process are shown in temporal order. After initial deposition, the excess of liquid is thrown away by centrifugal force. At some point, centrifugal force is balanced by viscous force and only a very small net flow of liquid occurs. The inert gas flowing over the top leads to evaporation of the liquid film, resulting in super saturation and ultimately in crystallization of catalyst particles.

### **3.3 Aim of Research**

Most of the techniques employed including CVD do not exercise much control over the growth and the properties of the carbon nanotubes. Growing carbon nanotubes of the right orientation and properties in bulk quantities is the goal of all the research groups who are occupied with the growth of carbon nanotubes. From previous research, we have been able to glimpse that the diameter of the catalyst deposited would control the diameter of the nanotubes [42, 43]. The nature of catalyst effect on the growth of the nanotubes is dependent on the support-surface and catalyst interaction. All these parameters are within the scope of investigation of the model catalyst study. The size of the clusters deposited can be well controlled within a narrow window by spin coating process. The surface-catalyst interaction can be manipulated using different catalyst and/or a suitable surface.

Our first aim is to stabilize the catalyst clusters on the silica surface and keep it under the narrow size bracket of 1 to 10 nm under all conditions of reduction and reaction since this size range is known to produce SWNT. The second aim is to grow SWNT in a controlled manner over the catalyst and predict the properties of SWNT grown based on the properties of the clusters deposited. This is to be achieved using various surface science techniques such as AFM, Raman, XPS and bulk techniques such as SEM and TEM.

The third aim is to perform reactions on well known systems of supported catalyst and organic metallocene for growth of both multi-walled and single walled carbon nanotubes. This system will help decide some of the suitable conditions for reduction/reaction besides those determined for model system. These systems are by far the most successful in growing single and multi walled carbon nanotubes. It will enable to draw parallel between the two systems and improve up on the model catalyst systems. A better insight is also obtained in to the working of the model system.

Fourth aim is to try to grow multi and single walled carbon nanotubes on different model catalyst using different carbon source, and with different reduction/oxidation and reaction conditions. The interaction between metal solid and its support plays an important role in the growth of carbon nanotubes. The final aim is to modify the support on model catalyst and observe its effect on growth of carbon nanotubes. We hope to gain understanding on the mechanism behind the growth of carbon nanotubes based on evidence provided by both supported and model catalyst and solve some of the questions facing us in growth of carbon nanotubes.

## 4 Reference

1. Iijima, S., *Nature (London, United Kingdom)*, 354, (1991), p. 56.
2. Iijima, S. and Ichihashi, T., *Nature (London, United Kingdom)*, 363, (1993), p. 603.
3. Dresselhaus, M. S., Dresselhaus, G. and Saito, R., *Physical Review B*, 45, (1992), p. 6234.
4. Mintmire, J. W., Dunlap, B. I. and White, C. T., *Physical Review Letters*, 68, (1992), p. 631.
5. Hamada, N., Sawada, S. and Oshiyama, A., *Physical Review Letters*, 68, (1992), p. 1579.
6. Wildoer, J. W. G., Venema, L. C., Rinzler, A. G., Smalley, R. E. and Dekker, C., *Nature (London)*, 391, (1998), p. 59.
7. Odom, T. W., Huang, J.-L., Kim, P. and Lieber, C. M., *Nature (London)*, 391, (1998), p. 62.
8. Yakobson, B. I., Brabec, C. J. and Bernholc, J., *Physical Review Letters*, 76, (1996), p. 2511.
9. Treacy, M. M. J., Ebbesen, T. W. and Gibson, J. M., *Nature (London)*, 381, (1996), p. 678.
10. Wong, E. W., Sheehan, P. E. and Lieber, C. M., *Science (Washington, D. C.)*, 277, (1997), p. 1971.
11. Yu, M.-F., Files, B. S., Arepalli, S. and Ruoff, R. S., *Physical Review Letters*, 84, (2000), p. 5552.
12. Dai, H., Hafner, J. H., Rinzler, A. G., Colbert, D. T. and Smalley, R. E., *Nature (London)*, 384, (1996), p. 147.

13. Wong, S. S., Harper, J. D., Lansbury, P. T., Jr. and Lieber, C. M., *Journal of the American Chemical Society*, 120, (1998), p. 603.
14. Ajayan, P. M., Ebbesen, T. W., Ichihashi, T., Iijima, S., Tanigaki, K. and Hiura, H., *Nature (London, United Kingdom)*, 362, (1993), p. 522.
15. Dillon, A. C., Jones, K. M., Bekkedahl, T. A., Kiang, C. H., Bethune, D. S. and Heben, M. J., *Nature (London)*, 386, (1997), p. 377.
16. Chen, P., Wu, X., Lin, J. and Tan, K. L., *Science (Washington, D. C.)*, 285, (1999), p. 91.
17. Liu, C., Fan, Y. Y., Liu, M., Cong, H. T., Cheng, H. M. and Dresselhaus, M. S., *Science (Washington, D. C.)*, 286, (1999), p. 1127.
18. Nutzenadel, C., Zuttel, A., Chartouni, D. and Schlapbach, L., *Electrochemical and Solid-State Letters*, 2, (1999), p. 30.
19. Pederson, M. R. and Broughton, J. Q., *Physical Review Letters*, 69, (1992), p. 2689.
20. Chu, X. and Kinoshita, K., *Materials Science & Engineering, B: Solid-State Materials for Advanced Technology*, B49, (1997), p. 53.
21. Nugent, J. M., Santhanam, K. S. V., Rubio, A. and Ajayan, P. M., *Nano Letters*, 1, (2001), p. 87.
22. Saito, Y., Hamaguchi, K., Uemura, S., Uchida, K., Tasaka, Y., Ikazaki, F., Yumura, M., Kasuya, A. and Nishina, Y., *Applied Physics A: Materials Science & Processing*, A67, (1998), p. 95.
23. Wang, Q. H., Setlur, A. A., Lauerhaas, J. M., Dai, J. Y., Seelig, E. W. and Chang, R. P. H., *Applied Physics Letters*, 72, (1998), p. 2912.

24. Choi, W. B., Chung, D. S., Kang, J. H., Kim, H. Y., Jin, Y. W., Han, I. T., Lee, Y. H., Jung, J. E., Lee, N. S., Park, G. S. and Kim, J. M., *Applied Physics Letters*, 75, (1999), p. 3129.
25. Martel, R., Schmidt, T., Shea, H. R., Hertel, T. and Avouris, P., *Applied Physics Letters*, 73, (1998), p. 2447.
26. Ebbesen, T. W. and Ajayan, P. M., *Nature (London, United Kingdom)*, 358, (1992), p. 220.
27. Bethune, D. S., Kiang, C. H., de Vries, M. S., Gorman, G., Savoy, R., Vazquez, J. and Beyers, R., *Nature (London)*, 363, (1993), p. 605.
28. Thess, A., Lee, R., Nikolaev, P., Dai, H., Petit, P., Robert, J., Xu, C., Lee, Y. H., Kim, S. G., Rinzler, A. G., Colbert, D. T., Scuseria, G. E., Tománek, D., Fischer, J. E. and Smalley, R. E., *Science (Washington, D. C.)*, 273, (1996), p. 483.
29. Mauron, P., Emmenegger, C., Zuttel, A., Nutzenadel, C., Sudan, P. and Schlapbach, L., *Carbon*, 40, (2002), p. 1339.
30. Zhang, W. D., Wen, Y., Liu, S. M., Tjiu, W. C., Xu, G. Q. and Gan, L. M., *Carbon*, 40, (2002), p. 1981.
31. Wei, B. Q., Vajtai, R., Jung, Y., Ward, J., Zhang, R., Ramanath, G. and Ajayan, P. M., *Nature (London, United Kingdom)*, 416, (2002), p. 495.
32. Ren, Z. F., Huang, Z. P., Xu, J. W., Wang, J. H., Bush, P., Siegel, M. P. and Provencio, P. N., *Science (Washington, D. C.)*, 282, (1998), p. 1105.
33. Cui, S., Lu, C. Z., Qiao, Y. L. and Cui, L., *Carbon*, 37, (1999), p. 2070.
34. Andrews, R., Jacques, D., Rao, A. M., Derbyshire, F., Qian, D., Fan, X., Dickey, E. C. and Chen, J., *Chemical Physics Letters*, 303, (1999), p. 467.

35. van Hardeveld, R. M., Gunter, P. L. J., van Ijzendoorn, L. J., Wieldraaijer, W., Kuipers, E. W. and Niemantsverdriet, J. W., *Appl. Surf. Sci.*, 84, (1995), p. 339.
36. Niemantsverdriet, J. W., Engelen, A. F. P., De Jong, A. M., Wieldraaijer, W. and Kramer, G. J., *Appl. Surf. Sci.*, 144-145, (1999), p. 366.
37. Borg, H. J., Van den Oetelaar, L. C. A., Van Ijzendoorn, L. J. and Niemantsverdriet, J. W., *Journal of Vacuum Science & Technology, A: Vacuum, Surfaces, and Films*, 10, (1992), p. 2737.
38. Kuipers, E. W., Laszlo, C. and Wieldraaijer, W., *Catal. Lett.*, 17, (1993), p. 71.
39. Kern, W. and Puotinen, D. A., *RCA Rev.*, 31, (1970), p. 187.
40. Eom, D.-H., Lim, G.-B., Park, J.-G. and Busnaina, A. A., *Japanese Journal of Applied Physics, Part 1: Regular Papers, Short Notes & Review Papers*, 43, (2004), p. 3335.
41. Kuipers, E. W., Doornkamp, C., Wieldraaijer, W. and van den Berg, R. E., *Chemistry of Materials*, 5, (1993), p. 1367.
42. Dai, H., Li, Y., Kim, W., Zhang, Y., Rolandi, M. and Wang, D., *Journal of Physical Chemistry B*, 105, (2001), p. 11424.
43. Cheung, C. L., Kurtz, A., Park, H. and Lieber, C. M., *Journal of Physical Chemistry B*, 106, (2002), p. 2429.

# **Chapter 2**

## **Spin coating of catalyst clusters on model support**

## Table of contents

<b>CHAPTER 2.....</b>	<b>29</b>
<b>SPIN COATING OF CATALYST CLUSTERS ON MODEL SUPPORT .....</b>	<b>29</b>
<b>LIST OF FIGURES .....</b>	<b>32</b>
<b>LIST OF TABLES .....</b>	<b>35</b>
<b>1 INTRODUCTION.....</b>	<b>37</b>
<b>2 BACKGROUND .....</b>	<b>39</b>
<b>3 EXPERIMENTAL SECTION.....</b>	<b>41</b>
<b>4 SPIN COATING EXPERIMENTS.....</b>	<b>45</b>
4.1 AIM OF STUDY.....	45
4.2 STUDIES ON SPIN COATING OF SALT CLUSTERS ON Si (100) MODEL SUPPORT .....	46
4.2.1 Concentration of solution .....	46
4.2.2 Speed of spin coating.....	47
4.2.3 Position of clusters from the center to the edge of the wafer.....	48
4.2.4 Type of salt deposited .....	50
4.2.5 Distribution of clusters: Effect of solvent .....	51
<b>5 TEMPERATURE EFFECTS ON CATALYST CLUSTERS ON SI (100)</b>	
<b>SUPPORT .....</b>	<b>55</b>
5.1 REDUCTION AND REACTION TREATMENT OF VARIOUS CATALYST SALTS .....	55
5.2 OXIDATION AND REACTION OF CATALYST CLUSTERS .....	58
5.2.1 Iron Citrate.....	58
5.2.2 Iron Acetate .....	61
5.2.3 Iron Chloride .....	63

<b>6</b>	<b>IRON NITRATE.....</b>	<b>66</b>
6.1	CALCINATION OF MODEL Si (100) SUPPORT AT 750 °C.....	67
6.1.1	<i>Reduction of iron nitrate.....</i>	67
6.1.2	<i>Oxidation of iron nitrate at 150 °C and 250 °C .....</i>	69
6.1.3	<i>Oxidation of iron nitrate at 300 °C.....</i>	72
6.1.4	<i>Oxidation of iron nitrate at 450 and 800 °C.....</i>	73
6.2	CALCINATION OF MODEL Si (100) SUPPORT AT 350 °C.....	76
6.2.1	<i>Oxidation with air to form oxide and reaction with benzene in absence of hydrogen.....</i>	77
6.2.2	<i>Oxidation followed by reduction and reaction with benzene in absence and presence of hydrogen .....</i>	79
6.2.3	<i>Oxidation with air to form oxide and reaction with benzene in presence of hydrogen.....</i>	81
6.2.4	<i>Effect of reduction of iron nitrate followed by reaction.....</i>	84
<b>7</b>	<b>DISCUSSION AND CONCLUSION .....</b>	<b>87</b>
<b>8</b>	<b>REFERENCE:.....</b>	<b>89</b>

## List of Figures

- Figure 1 An illustration of  $\text{FeCl}_2$  clusters are shown in Figure 1a obtained by AFM in tapping mode. For determining the diameter of the clusters, a calibration grating is used (Figure 1b) to first determine the diameter of the tip used to scan the surface and then determine the diameter of the clusters deposited on the surface. .... 42
- Figure 2 The average size of the calibration grating is assumed to be 10 nm at the tip for our calculation of size of the AFM tip (left). The size of the AFM tip is about 24 nm (right) ..... 43
- Figure 3 The distribution of clusters deposited on the surface shows a large percentage of clusters within the size range of 5 – 15 nm and tails on towards larger diameter size clusters. .... 44
- Figure 4 Cluster density and size of clusters increase with increasing concentration of catalyst salt. .... 46
- Figure 5 Cluster size and density decrease with increasing speed of spin coating for a given concentration of salt. .... 47
- Figure 6 Cluster density, the size of clusters and the size range decrease from the center to the edge of the wafer because of the effect of centrifugal force variation from the center to the edge. .... 49
- Figure 7 Different salts show different affinity for the deposition. This in turn governs the size and density of clusters formed. .... 50
- Figure 8 The size distribution of catalyst clusters for different solvents and salt concentrations ..... 54

Figure 9	Reduction of catalyst salts under hydrogen atmosphere shows clusters that have reduced size in general.....	57
Figure 10	Iron citrate gives a very fine cluster deposition on silica surface with small diameter. They are stable at oxidation temperature of up to 250 °C. They did not show any carbon nanotubes formation with dicyclopentadiene as carbon source.....	60
Figure 11	Oxidation study on Iron acetate spin coated from 1 mmol/L solution at 10000 rpm.....	62
Figure 12	Reaction was carried at 700 °C in absence of dicyclopentadiene and H <sub>2</sub> . The reaction time was 40 minutes. The scale of Figure 12 c is 2 μm as compared to previous pictures of spin coating and oxidation, which is 5 μm. ....	65
Figure 13	The deposition of clusters on the calcined model silicon wafer shows good density of iron nitrate clusters. After reaction conditions, almost all of the clusters are lost with very few remaining on the surface.....	68
Figure 14	Oxidation of iron nitrate at 250 °C and reaction at 950 °C in presence of benzene does not produce any carbon nanotubes (right). The clusters are absent after the blank reaction condition (left). ....	71
Figure 15	The iron oxide clusters after oxidation at 300 °C appear stable on silica surface as observed with AFM. Reaction at 950 °C with benzene shows diffuse clusters. No carbon nanotubes were observed.....	73
Figure 16	Oxidation of iron nitrate on model silica support remains stable up to calcination temperature of 800 °C in flowing air. ....	75

Figure 17 The oxidation of iron nitrate at 400 °C on silicon wafer calcined at 350 °C and reacted with benzene at 900 °C in absence of hydrogen shows a large deposition of carbonaceous material..... 78

Figure 18 The blank reaction at 900 °C of clusters produced by oxidation of iron nitrate at 400 °C in presence of only inert helium atmosphere shows large clusters on the surface. .... 79

Figure 19 Iron oxide clusters obtained after calcination were reduced at 300 – 400 °C to form metallic iron particles. Results for reaction of these metallic clusters in absence (left) and presence of hydrogen (right) are shown. The cluster sizes vary when hydrogen was used in the reaction. .... 81

Figure 20 The reaction of iron oxide in presence of hydrogen shows presence of large clusters. The cluster density does not vary based on the calcination temperatures of iron nitrate..... 82

Figure 21 Reaction of iron nitrate with hydrogen as the carrier gas for benzene. The agglomeration of clusters is observed in this case too. The agglomeration is large in case of slow heating ramp..... 84

Figure 22 Clusters agglomeration increases with the concentration of hydrogen. .... 86

## List of Tables

Table 1 Table shows variation of FeCl <sub>2</sub> cluster average size with spin coating speed and the solvent of dissolution. Size range indicates the range of diameters observed for the clusters.....	52
Table 2 Oxidation and reaction of catalyst clusters derived from iron citrate with dicyclopentadiene at various conditions of oxidation temperature and flow rate of dicyclopentadiene. The reaction did not yield any carbon nanotubes.....	59
Table 3 Catalyst clusters from iron acetate were obtained by calcining at different oxidation temperature and varying the flow rate of dicyclopentadiene. No carbon nanotubes were observed by SEM.....	61
Table 4 Catalyst clusters from iron chloride were produced by reduction and reaction at temperatures of 650 °C – 700 °C and optimum conditions of growth of MWNT were determined.....	63
Table 5 Catalyst clusters were produced from iron chloride by oxidation in air and reaction with dicyclopentadiene at temperatures of 650 °C – 700 °C was carried out. The optimum temperature was determined to be 675 °C.....	64
Table 6 Conditions of reaction for clusters obtained by reducing iron nitrate at 300 °C.	68
Table 7 Reaction of clusters derived from iron nitrate after oxidation at 250 °C in presence and absence of benzene.....	70
Table 8 The oxidation of iron nitrate clusters produces iron oxide clusters at 300 °C.....	72
Table 9 The table shows the oxidation and reaction temperature and the benzene concentration for growth of carbon nanotubes.....	77

Table 10 Oxidation of iron nitrate produces iron oxide which is reduced in hydrogen to form metallic iron clusters. The clusters were then reacted with benzene in presence and absence of hydrogen.....	80
Table 11 Oxidation of iron nitrate and reaction with benzene leads to formation of carbon nanotubes. Helium is used as the carrier gas. ....	82
Table 12 Reaction of iron nitrate at 900 – 950 °C with benzene carried by hydrogen instead of helium.....	83
Table 13 The conditions for reduction of iron nitrate and reaction with benzene at varying concentrations of hydrogen.....	85

# 1 Introduction

An important part of catalytic study is the ability to characterize the catalyst well for its reactivity. The catalyst prepared in bulk on supported catalyst has inherent limitations of mass and heat transfer. The number of techniques available for characterization of catalyst is also limited. Model catalyst which is the active catalyst deposited on flat surface provides several advantages over bulk catalyst. One is the absence of bulk mass and heat transfer limitation. The other is the accessibility of various surface sensitive techniques including the bulk techniques that help characterize the catalyst that can provide information on the structure, composition, size and dispersion [1]. The challenge in the surface science study is the preparation of catalyst of defined size and morphology. Spin coating is a novel technique for the deposition of clusters of nanometer size on a flat surface, first developed by Kuipers et al. [2] and explained with theory by Hardeveld et al. [3]. The technique involves deposition of thin film of salt containing solution on a flat support. The surface is rotated at  $10^3 - 10^4$  rpm. The excess liquid is thrown off the surface. A very thin layer exist which is kept in place by the centrifugal force and the surface interaction force between the liquid and the support surface. The excess liquid is evaporated resulting in nucleation and growth of clusters. The parameters that affect the size and distribution of clusters chiefly depend on the type of salt, the spin coating speed, temperature of evaporation and the concentration of salt. Cluster size increases with the concentration of salt [4,5] and with increase in speed [6]. Different salts have different interaction with the surface resulting in different nucleation and growth rate. Higher temperatures would lead to faster evaporation and thereby

smaller clusters. This process can also be achieved with changing the solvent of evaporation such as ethanol which is more volatile compared to water. So in order to keep the system simple, the spin coating was performed at room temperature.

One of the major useful techniques for determination of size of clusters is the atomic force microscopy (AFM). AFM has been extensively used for the determination of size and distribution of clusters. AFM has the ability to scan clusters in the nanometer size range (as low as 1 nm) in ambient conditions.

## 2 Background

Studies have suggested that the size and nature of catalyst particles determine the type of carbon nanotubes formed. The size of carbon nanotubes formed is usually commensurate with the size of catalyst clusters. A single wall carbon nanotube has a diameter of about 0.5 – 3 nm. The catalysts used for the growth of carbon nanotubes have essentially been supported on porous catalyst support such as alumina and silica. In such systems, the distribution of catalyst clusters and their characteristics is made difficult by the inability to determine the exact nature of clusters that lead to the formation of the carbon nanotubes. Further the control of the catalyst size is very difficult. To overcome these limitations, we proposed to employ model catalysts, which are essentially catalyst clusters deposited on a flat support. The advantage of such system is easy accessibility of the catalyst to the reactants and ease of studying the growth of carbon nanotubes using surface science technique such as AFM, STM, and bulk techniques such as SEM, TEM and Raman spectroscopy.

Spin coating is a novel technique of preparing model catalysts in a simple manner. The physical process involves removal of excess of liquid from a flat support surface such as alumina or silica resulting in a thin film, which is then evaporated by inert gas flowing over it. The process of evaporation results in crystallization of catalyst clusters. The current study details the distribution of catalyst clusters using spin coating technique and the measurement of the clusters using atomic force microscopy. The distribution of

clusters is strongly dependent on the type of salt, support and the distance from the center of the support to the edge.

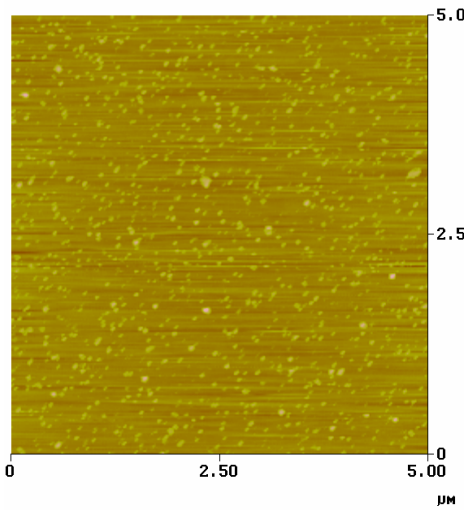
### 3 Experimental Section

The support used for the current study was silica thermally grown on silicon [100] surface. Silicon [100] was heated to 750 °C for 24 hours in air. It was cleaned using RCA-1. The process involves first heating the SiO<sub>2</sub>/Si wafer at 70 °C, with 70:30 v/v solutions of ammonium hydroxide (30%) and hydrogen peroxide (35%) for 10 minutes. This wafer is immediately transferred to the boiling water and kept immersed for 10 minutes. This leads to the formation of –OH groups on the wafer that help anchor the cluster particles during nucleation. The wafer is then immediately transferred to the spin coating assembly and salt solution is placed at the center. The spin coating is done at the desired rpm and stopped after the visible Newton's rings formed by the evaporating thin film of solvent disappear. Variation of the spin coating parameters namely the spin coating speed and the concentration of the solution helps control two important characteristics of the model catalyst viz. catalyst loading and the morphology of the catalyst particles.

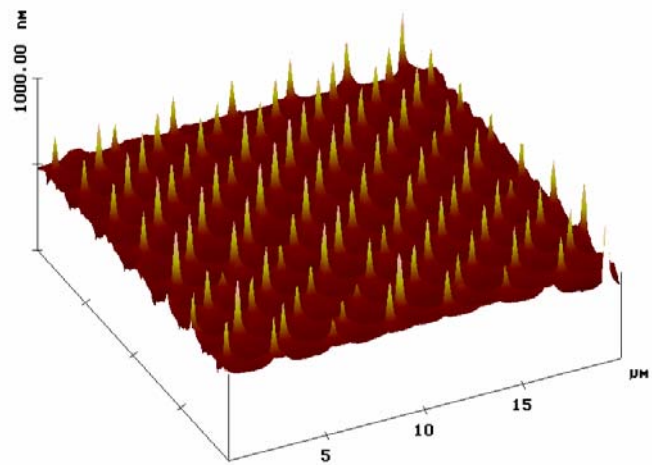
The catalyst loaded on the surface is characterized employing atomic force microscopy (AFM). For our experiments, the size of the clusters needs to be determined as accurately as possible. Whenever the cluster size is determined by AFM, there is an addition of size of the tip to the size of the clusters known as tip effect. The size of tip is difficult to determine and in most spin coating techniques employed for catalyst cluster deposition, the height of the clusters is thought to give the best estimate of the size of clusters. In our studies, we used very fine tips (of the order of 10 nm at the tip). To

ascertain the effect of tip size, the tip was calibrated using a delta calibration grating (which has a thickness less than 10 nm). This helps to estimate the diameter of the tip at a particular height, which is then subtracted from the measured value of the diameter of the clusters to obtain almost true diameter of clusters.

To take a case, we spin coated  $\text{FeCl}_2$  from a 2 mmol/L solution in water at 4000 rpm. The AFM shows dense cluster distribution on the surface (Figure 1a). The tip was calibrated using the delta calibration grating, AFM image of which is shown in Figure 1b.



1a) AFM image of the  $\text{FeCl}_2$  particles deposited with spin coating



1b) AFM image of the calibration grating

**Figure 1** An illustration of  $\text{FeCl}_2$  clusters are shown in Figure 1a obtained by AFM in tapping mode. For determining the diameter of the clusters, a calibration grating is used (Figure 1b) to first determine the diameter of the tip used to scan the surface and then determine the diameter of the clusters deposited on the surface.

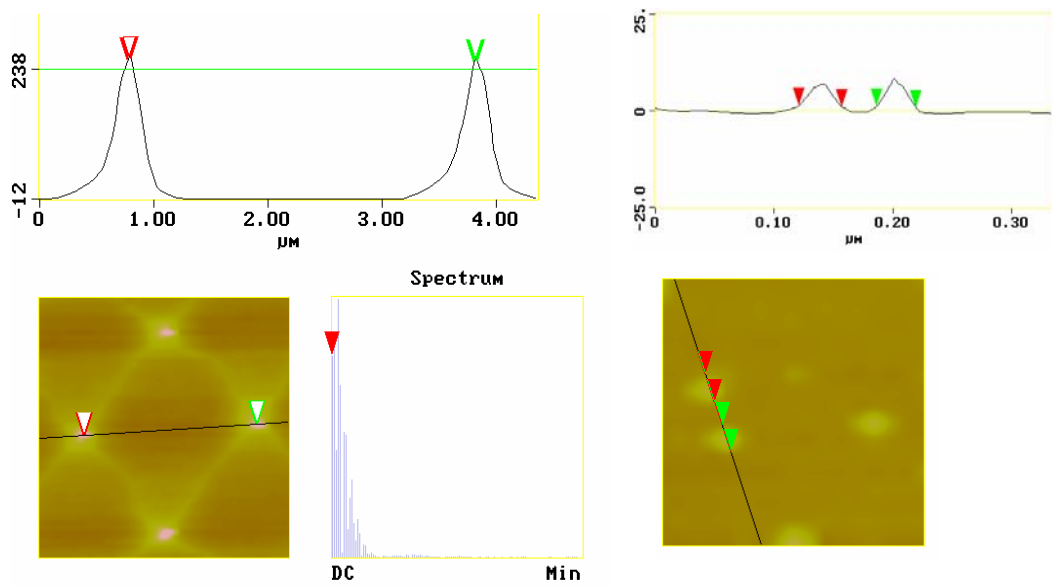


**Figure 2a** The average size of calibration grating was assumed to be 10 nm

**Figure 2b** The average diameter of the particle is about 12 nm.

**Figure 2** The average size of the calibration grating is assumed to be 10 nm at the tip for our calculation of size of the AFM tip (left). The size of the AFM tip is about 24 nm (right)

The grating image diameter is then measured at a particular height say 10 nm from its tip. Figure 2a shows the measured diameter of the AFM tip at this height to be 34 nm. Since we know that to this diameter of the tip, the known size of the calibration grating will add its own diameter (10 nm from manufacturer's manual); we then subtract this value to obtain the approximate size of tip to be about 24 nm. Cluster sizes were measured (Figure 2b) from the AFM image using Sigma ScanPro® software and the tip diameter is subtracted from it to give average cluster size of 12 nm. Particle size distribution follows a bell shaped distribution after spin coating (Figure 3) at any given radial direction.

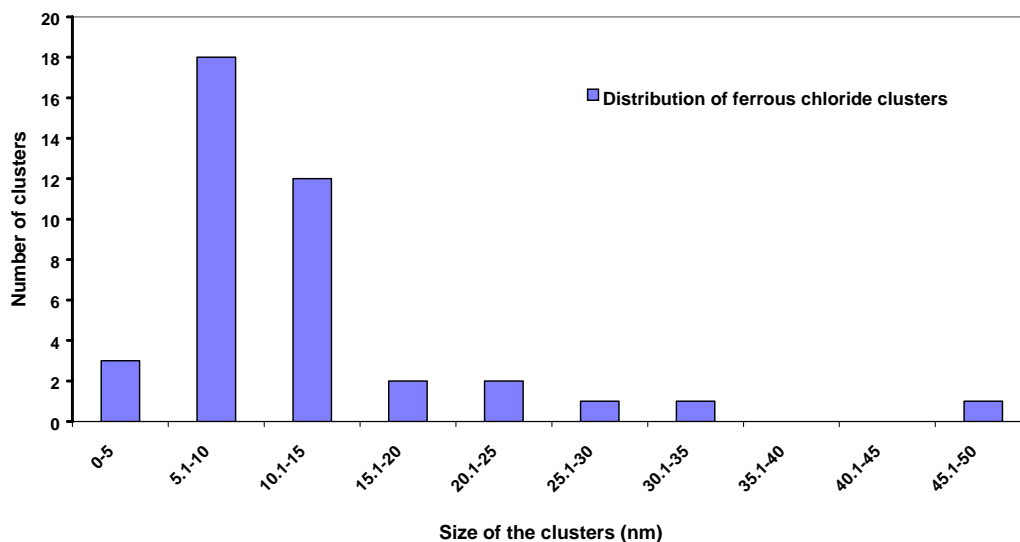


**Figure 3** The distribution of clusters deposited on the surface shows a large percentage of clusters within the size range of 5 – 15 nm and tails on towards larger diameter size clusters.

Varying the concentration of salt deposited, type of salt, spin coating speed, position of the salt clusters on the surface of wafer (support) and solvent of salt dissolution controlled cluster deposition. The size of clusters being in the nanometer size range, they will essentially be in crystalline form. The effects of the aforementioned parameters and many other effects such as calcination of clusters and their reaction in carbon (reducing) environment are described in following sections.

## 4 Spin coating Experiments

### 4.1 Aim of study

In order to control the size and distribution of catalyst clusters on the surface, it is necessary to have the good picture of the deposition of clusters and the factors that affect its distribution. To study the deposition of clusters, we make a systematic study of the deposition of clusters using spin coating by varying the parameters such as spin coating speed, concentration of salt solution one at a time. The following are the aims:

- 1) To prepare catalyst clusters on the flat support (model catalyst) employing spin coating.
- 2) To control the diameter of clusters deposited using the concentration of salt and speed of spin coating within a range of 1 to 5 nm.
- 3) To study the size distribution of clusters deposited.
- 4) To study the density of clusters deposited (numbers per unit area) as a function of salt concentration and speed of spin coating.
- 5) To study the behavior of clusters and their stability at various reduction/oxidation and reaction conditions.
- 6) To grow carbon nanotubes on deposited clusters at various reaction temperatures, flow rates of gases, various carbon source etc. and to optimize for more carbon nanotubes to carbon ratio.
- 7) To correlate the diameter of the carbon nanotubes to the size of clusters deposited.

## 4.2 Studies on spin coating of salt clusters on Si (100) model support

Spin coating studies were done with transition metal salt concentration. The salts employed were both inorganic such as chlorides, nitrates and organic such as acetate, citrates for iron and nickel chloride.

### 4.2.1 Concentration of solution

Higher the concentration of salt, greater is the solid amount present in the solution to crystallize out. It also provides enough material for formation of more number of clusters. For a given speed of spin coating, the number of clusters deposited and their size increases with concentration of solution. Figure 4 shows results for spin coating speed  $\text{NiCl}_2$  salt at 4000 rpm with increasing concentration.

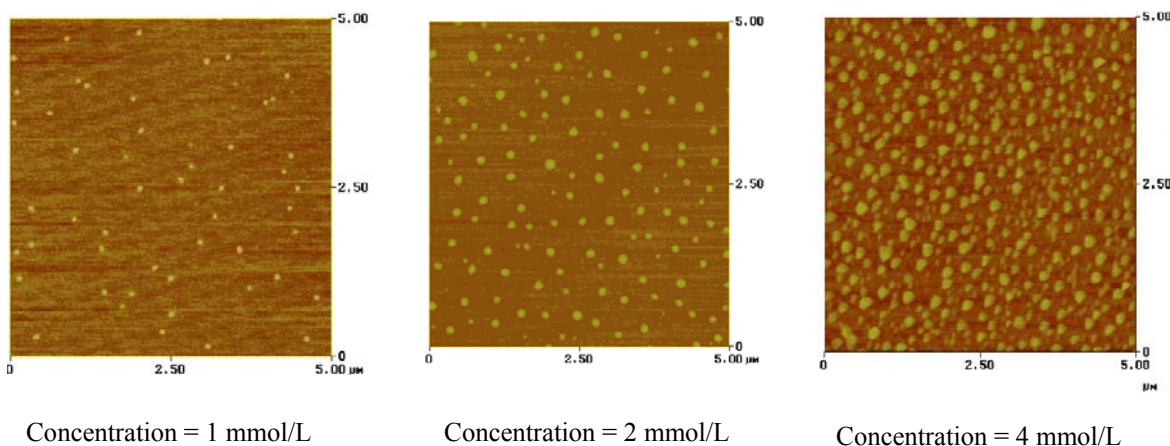


**Figure 4** Cluster density and size of clusters increase with increasing concentration of catalyst salt.

### 4.2.2 Speed of spin coating.

With increase in the speed of the spin coating, the centrifugal force acting on the catalyst salt solution lying on the substrate surface increases. The thickness of the film that remains on the surface under the influence of capillary force reduces thereby reducing the amount of salt containing solution. The amount of solid deposited on the surface after the evaporation of the liquid is less and is manifested in the form of smaller size of clusters on the surface. This parameter can be effectively used for controlling and getting the desired size of clusters. A 2 mmol/L of  $\text{FeCl}_2$  was spin coated at 4000, 7000, and 9000 rpm. The average size of clusters was respectively 15 nm, 13.6 nm, and 13 nm (Figure 5). Distribution of cluster size is given in Figure 8, sample no. 1, 2 and 3 respectively.

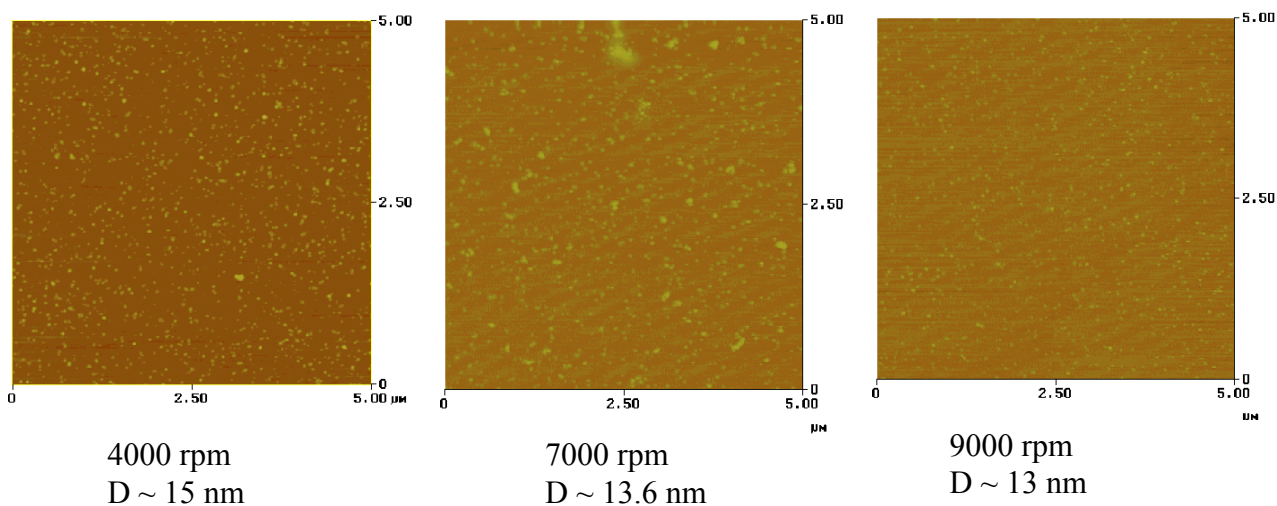


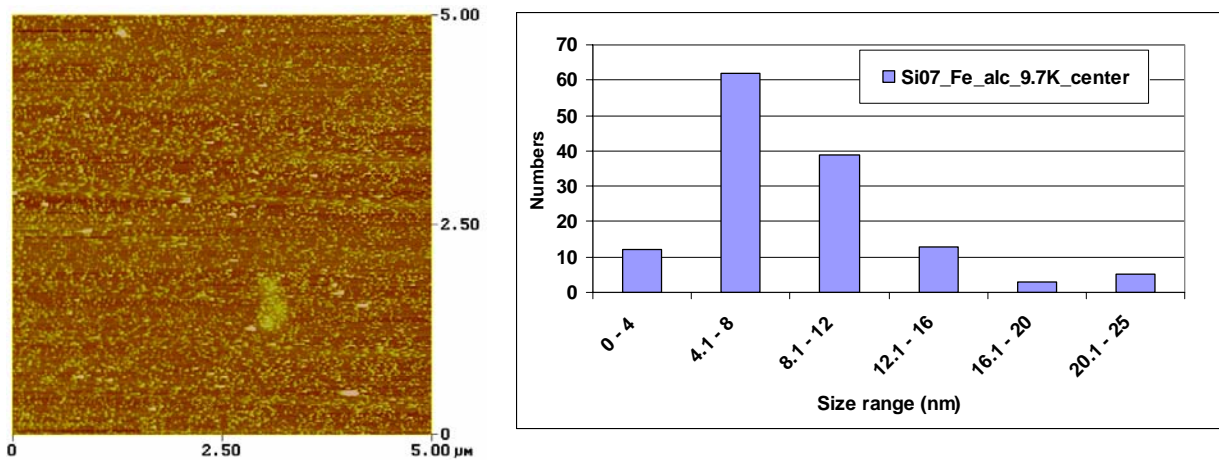
**Figure 5** Cluster size and density decrease with increasing speed of spin coating for a given concentration of salt.

### 4.2.3 Position of clusters from the center to the edge of the wafer

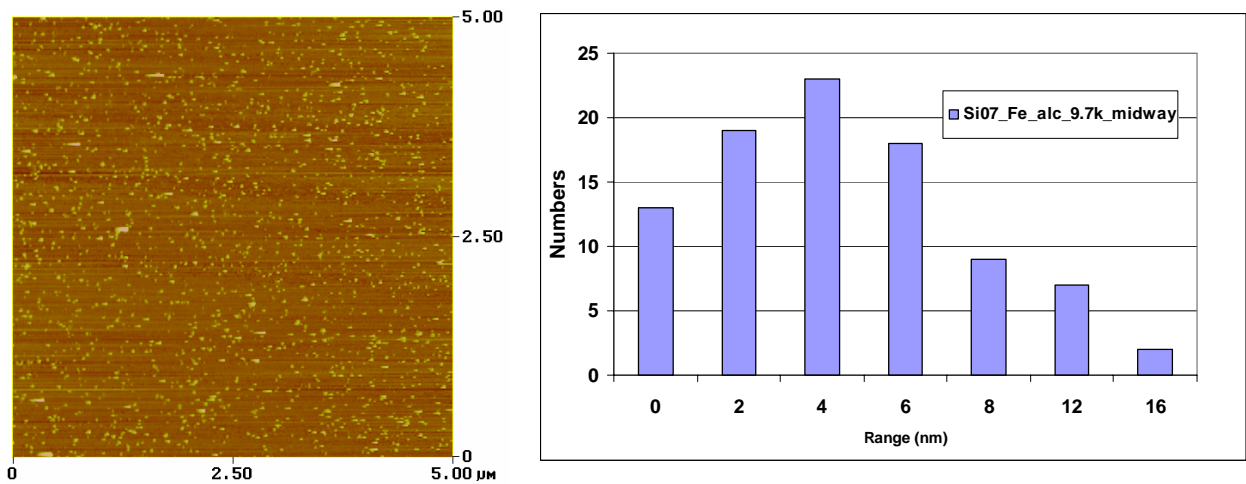
The centrifugal force varies from the center to the edge of the wafer thereby varying liquid film thickness with more liquid at the center than at the edge. The large liquid film thickness at the center has more inorganic salt content than at the edge. This leads to larger number density and size of clusters at the center compared to that at edge. AFM images of 2 mmol/L FeCl<sub>2</sub> spin coated at 9700 rpm from ethanol solution is shown in Figure 6. The results indicate two things:

- a. The density of particles decreased away from the center to the edge of the wafer.
- b. The average size of clusters decreased from 8.5 nm at the center to 5.9 nm at the midway region. The distribution of particles also becomes narrower as observed from the decrease in the size range of clusters.

In case of using the model catalyst in reaction system, the position from which the clusters are picked up needs to be carefully chosen. It will bear an effect on the characterization of the products formed.



AFM image obtained at the center of the wafer shows presence of dense clusters of catalyst. The distribution is much wider with average particle size at 8.5 nm.



AFM image obtained at the region between the center and edge of wafer. The density is less compared to that at center with average cluster size to be 5.9 nm.

**Figure 6** Cluster density, the size of clusters and the size range decrease from the center to the edge of the wafer because of the effect of centrifugal force variation from the center to the edge.

#### 4.2.4 Type of salt deposited

Different salts have different rate of crystallization from the solution, and would result in different agglomeration of clusters. The size of clusters will essentially depend on the choice of salt. As an example, 4 mmol/L of  $\text{NiCl}_2$ ,  $\text{FeCl}_2$ , Fe acetate and Fe citrate were all spin coated at 6000 rpm. The results are shown in Figure 7. The Fe citrate has shown to form the smallest clusters while Fe acetate forms the largest. The second largest are  $\text{NiCl}_2$  followed by  $\text{FeCl}_2$ . Depending on the choice of salt, the cluster size could be manipulated.

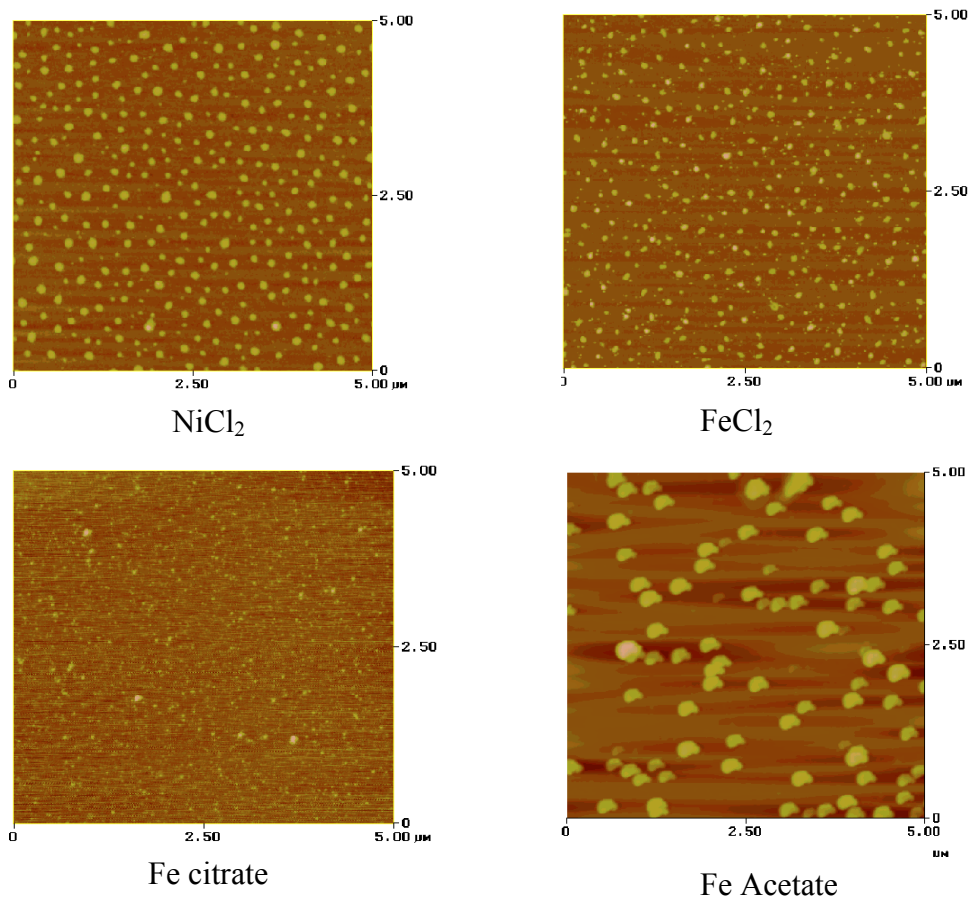


**Figure 7** Different salts show different affinity for the deposition. This in turn governs the size and density of clusters formed.

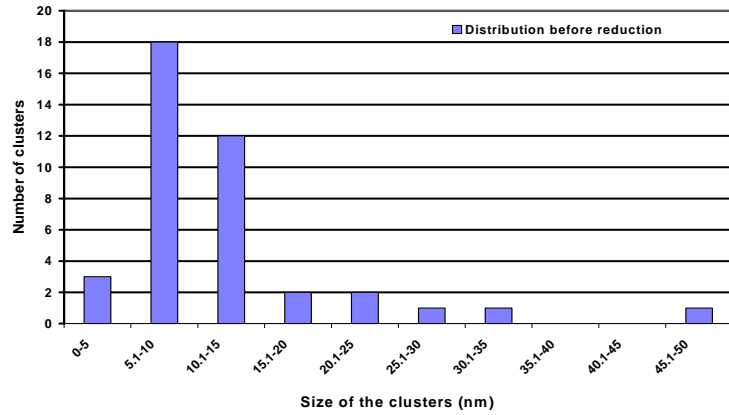
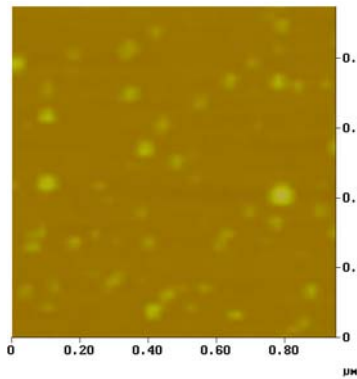
This essentially means that reaction conditions will vary for the final products (carbon nanotubes) desired as each salt will have appreciable rate at different reaction conditions.

#### **4.2.5 Distribution of clusters: Effect of solvent**

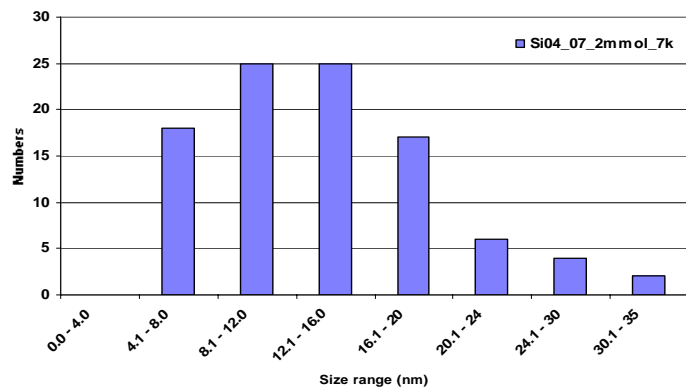
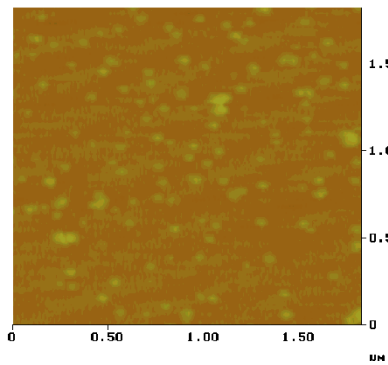
Size distribution of catalyst clusters invariably depends on the availability of nucleation site and the interaction between the support and catalyst. On surface we would have a range of diameters of particles deposited. Our aim is to restrict diameter of clusters deposited in the range of 1 to 10 nm with *distribution* of particles to the range of 1 – 2 nm about the mean. FeCl<sub>2</sub> was employed as the catalyst salt for our study. The effect of spin coating speed, the concentration of salt along with the effect of solvent was studied. Water and ethanol were chosen as solvents. Force of adhesion of ethanol and water are different based on the hydrogen bonding between the solvent and the substrate, with water having higher adhesion compared to ethanol. Correspondingly the liquid film formed at a given speed of rotation is smaller in thickness for alcohol compared to water leading to formation of smaller clusters. It was observed that deposition from alcohol produced smaller size clusters with narrower distribution. Results are summarized in Table 1. The figures corresponding to sample numbers are given in Figure 8. We observe that it is possible to achieve the size range of 1 – 10 nm though for water the distribution is large. The advantage for alcohol as solvent is the small size of clusters with narrow distribution around the average.

**Table 1** Table shows variation of FeCl<sub>2</sub> cluster average size with spin coating speed and the solvent of dissolution. Size range indicates the range of diameters observed for the clusters.

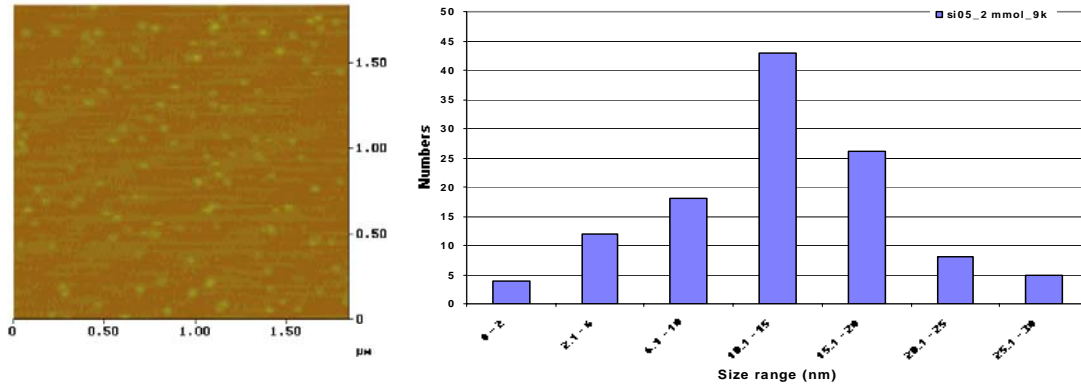
Sample No.	Solvent	Concentration	RPM	Size range	Average size
1	Water	2 mmol/L	4000	5 – 50 nm	15 nm
2	Water	2 mmol/L	7000	4 – 35 nm	13.6 nm
3	Water	2 mmol/L	9000	2 – 30 nm	13 nm
4	Water	2 mmol/L	9700	1 – 27 nm	9.7 nm
5	Ethanol	2 mmol/L	7000	1 – 18 nm	6.9 nm
6	Ethanol	2 mmol/L	9700	1 – 12 nm	7.3 nm
7	Ethanol	1 mmol/L	9000	1 – 10 nm	6.18 nm
8	Ethanol	0.4 mmol/L	10000	1 – 10 nm	3.85 nm



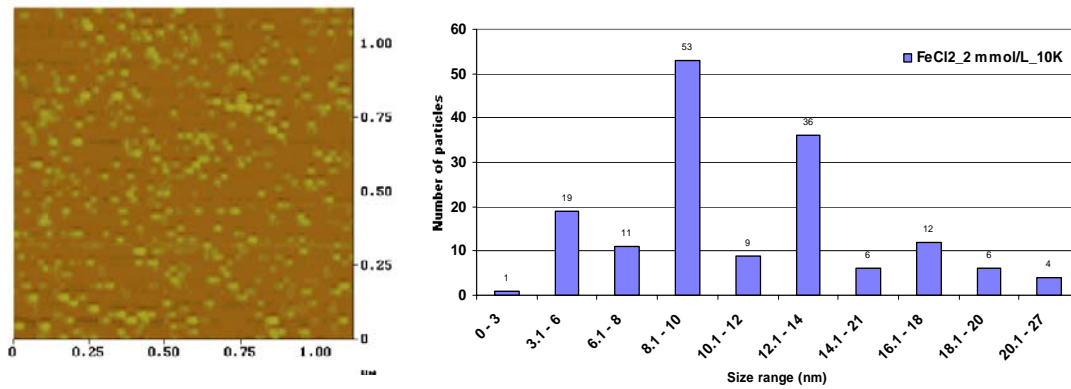
Sample 1 spin coated at 4000 rpm. Average size is 15 nm.



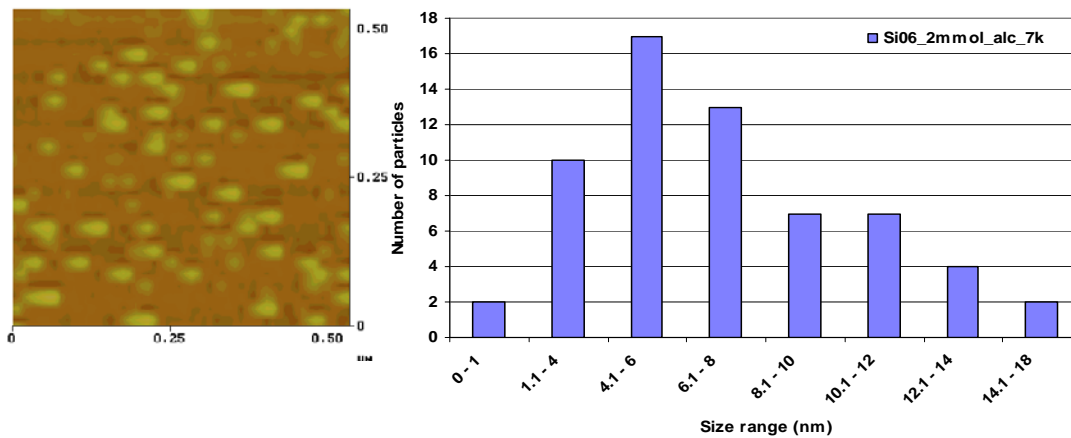
Sample 2 shows size distribution of particles after spin coating at 7000 rpm. The average size of particles is 13.64 nm



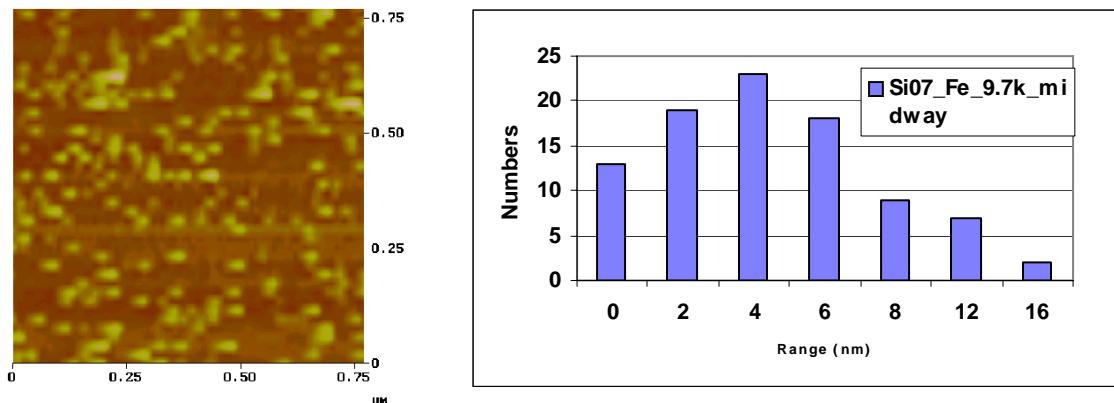
Sample 3 shows size distribution of particles after spin coating at 9000 rpm. Average size of clusters is 13 nm.



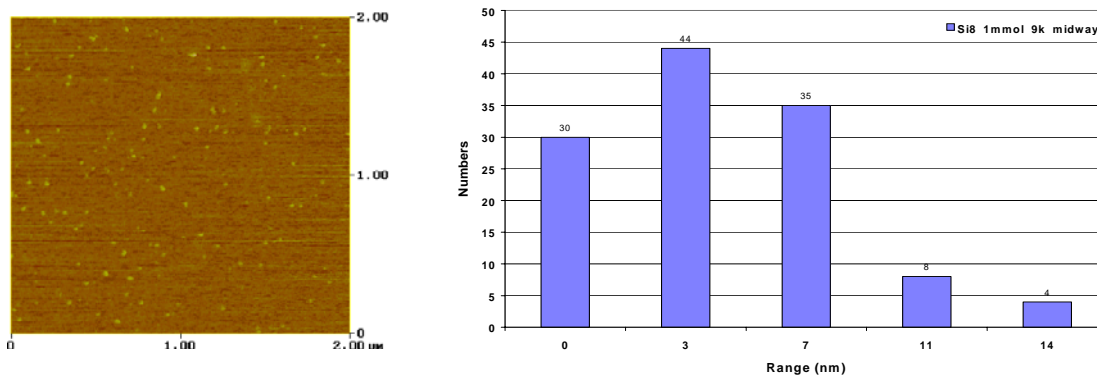
Sample 4 shows size distribution of particles after spin coating at 9700 rpm. The average size is 9.66 nm.



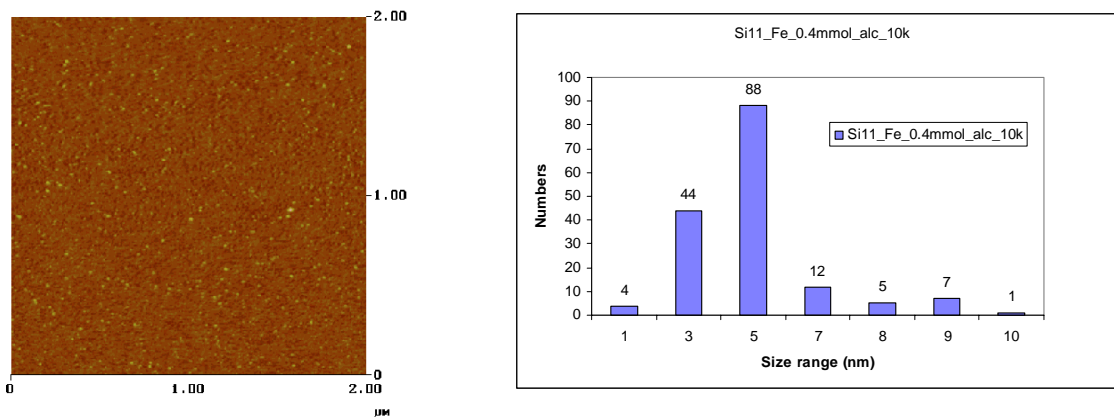
Sample 5 shows size distribution of particles after spin coating at 7000 rpm from ethanol solution. The average size of clusters is 6.9 nm.



Sample 6 shows size distribution of particles after spin coating at 9700 rpm from 2 mmol/L ethanol solution. The average size of particles is 7.3 nm



Sample 7 shows size distribution of particles after spin coating at 9000 rpm from 1 mmol/L ethanol solution. The average size of clusters is 6.18 nm.



Sample 8 shows distribution of particles deposited from a 0.4 mmol/L at 10000 rpm. Average size is about 3.84 nm.

**Figure 8** The size distribution of catalyst clusters for different solvents and salt concentrations

## **5 Temperature effects on catalyst clusters on Si (100) support**

Stability of clusters plays an important part in their reactivity towards formation of carbon nanotubes and their properties. Clusters agglomerate at higher temperatures of reduction/oxidation and reaction when salt precursors are treated to obtain the metal catalyst. There is practically no way to maintain the size or other properties of clusters under the reduction/reaction conditions as system is highly energetic. Under the scope of our experiments, we can only try to determine how the clusters would behave under high temperatures and help correlate these behaviors to the properties of carbon nanotubes formed. Reactions were carried with dicyclopentadiene and benzene as carbon source. Reactions were very successful with ferrocene in growing multi-walled carbon nanotubes (discussed in later chapter). Ferrocene is derived from dicyclopentadiene; hence attempt was made to grow carbon nanotubes using it as the carbon source. The other advantage is the reduced temperature of growth since multi-walled carbon nanotubes are formed at temperatures of 500 – 700 °C with ferrocene. Some of the further reactions were again continued with benzene because of results based on supported catalyst.

### **5.1 Reduction and Reaction treatment of various catalyst salts**

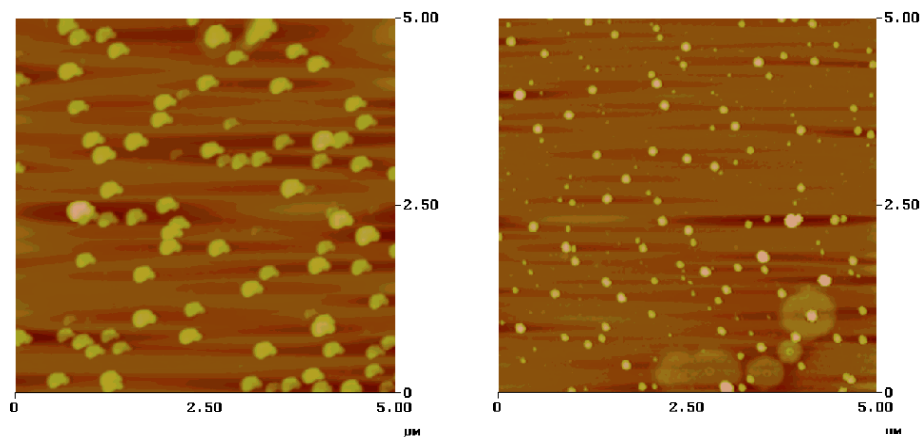
To prevent large agglomeration of iron salt, it would be possible to employ metal salts that have large ligand molecule that will prevent clusters from coming close to each other during reduction and reaction process. The other effective technique is to calcine

the salt to form their respective oxide, which are fairly stable under reaction conditions because oxides are usually more stable compared to their metallic counterpart.

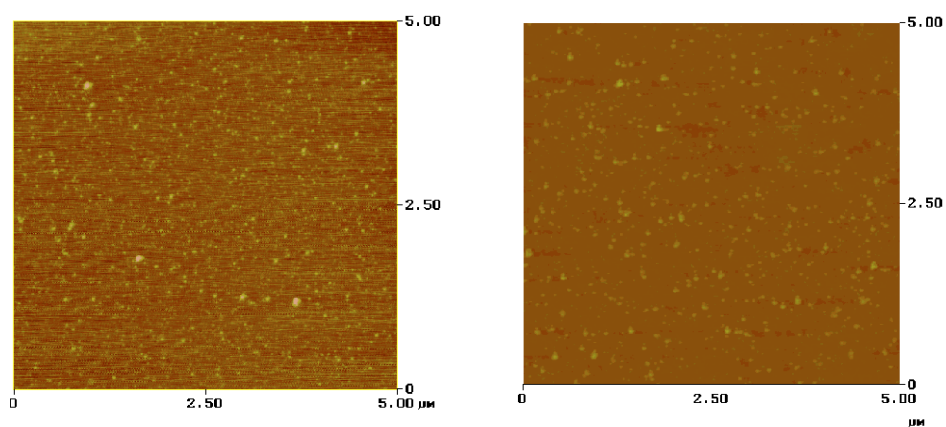
To study the effect of reduction temperature on the size of clusters, following salts were reduced in hydrogen atmosphere:

- 1) Iron acetate at 120 °C.
- 2) Iron citrate at 120 °C.
- 3) Nickel chloride at 300 °C.
- 4) Iron chloride at 400 °C and 500 °C.

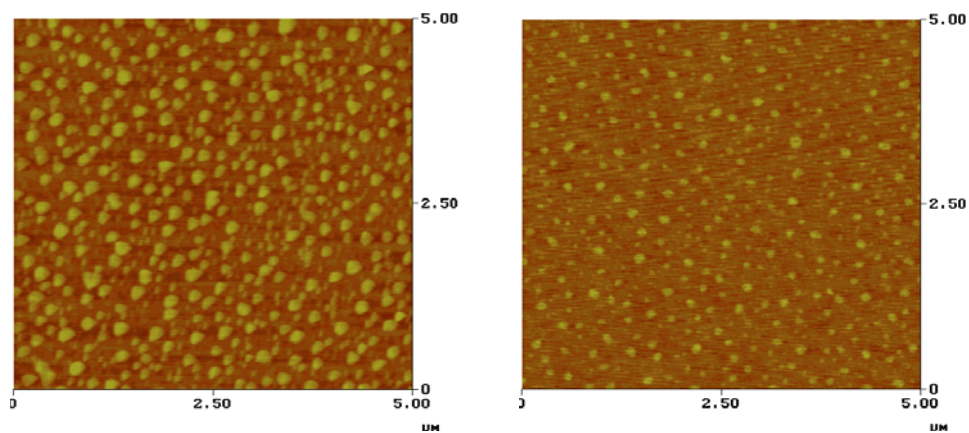
All salts showed decrease in the cluster size after reduction. The results for iron acetate, iron citrate and nickel chloride are shown in Figure 9. The distribution of clusters appears to remain same. The scan is taken on the same piece broken from the wafer so AFM analysis is almost at the same position.



Fe acetate before and after reduction, reduced at 120 °C.



Fe citrate before and after reduction, reduced at 120 °C



NiCl<sub>2</sub> before and after reduction, reduced at 300 °C.

**Figure 9** Reduction of catalyst salts under hydrogen atmosphere shows clusters that have reduced size in general.

## 5.2 Oxidation and reaction of catalyst clusters

To keep the cluster size stable under reaction conditions, oxidation of iron salts to iron oxide is an effective technique. Iron oxide adheres strongly to the support material and has a very high melting point, which can prevent their agglomeration to a large extent. Iron oxide also provides a route for decomposition of carbon source by reduction of iron oxide to iron in situ and production of carbon nanotubes. Oxidation studies were carried on salts of iron viz. chlorides, acetates and citrates.

### 5.2.1 Iron Citrate

Iron citrate was spin coated from 1 mmol/L solution in water and at 10000 rpm (Figure 10). A sample from the wafer was oxidized at 170 °C for 60 minutes (Figure 10b). AFM studies showed almost no trace of clusters as most likely the salt melts at 170 °C. Hence, oxidation was carried out at 150 °C for 30 minutes followed by increment in temperature at 5 °C/min up to 250 °C and maintaining it at 250 °C for 30 minutes (Figure 10c). Clusters are observed. All attempts at production of carbon nanotubes at 675 °C from dicyclopentadiene with catalyst clusters derived from iron citrate failed and hence further studies were discontinued. Growth of carbon nanotubes was analyzed with SEM. Conditions for growth of carbon nanotubes are given in Table 2.

**Table 2** Oxidation and reaction of catalyst clusters derived from iron citrate with dicyclopentadiene at various conditions of oxidation temperature and flow rate of dicyclopentadiene. The reaction did not yield any carbon nanotubes.

Oxidation Temp.	Reaction Temp.	Time	Dicyclopentadiene Flow rate	Results
170 °C	675 °C	40 min	1.824 ml/hr	Only Carbon. No CNT
170 °C	675 °C	20 min	1.2 ml/hr	Only Carbon. No CNT
150 °C, 250 °C	675 °C	40 min	1.2 ml/hr	Only Carbon. No CNT

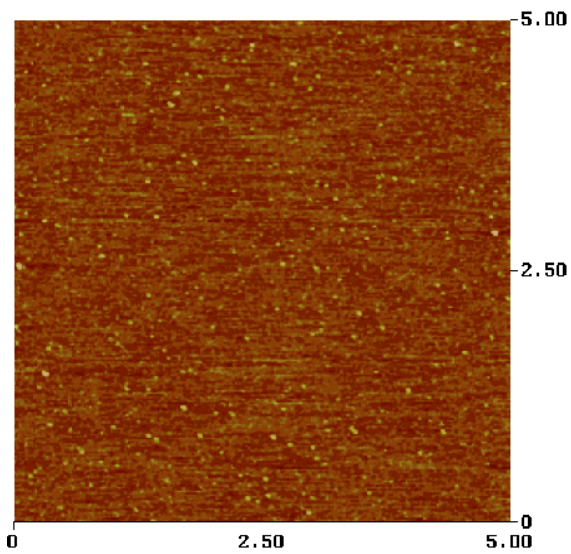


**Figure 10a** 1 mmol/L iron citrate deposited at 10000 rpm.

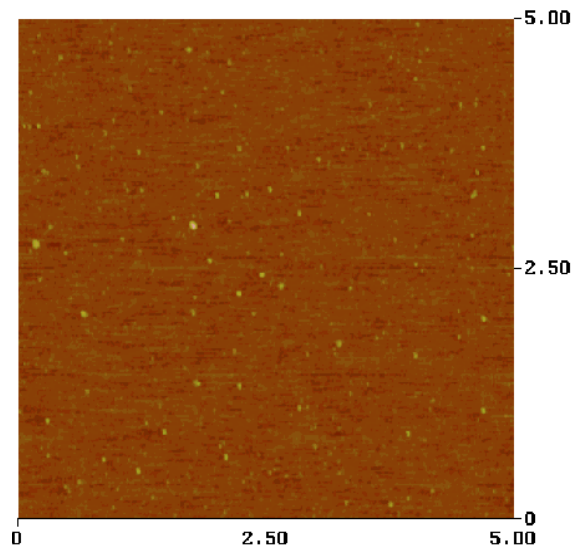


**Figure 10b** Surface after oxidation at 170 °C in air.

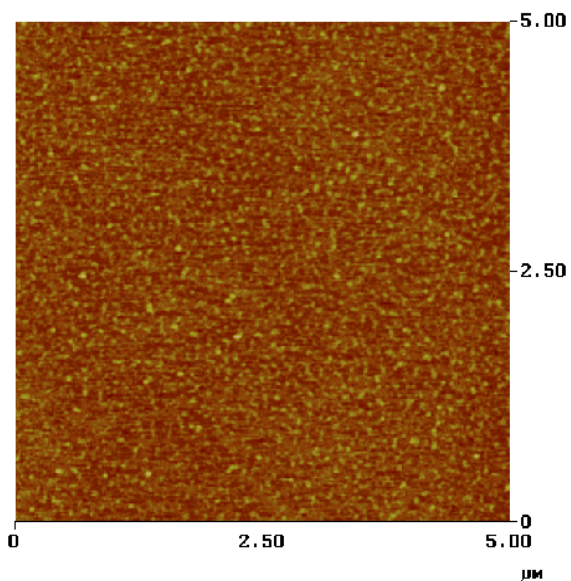


**Figure 10c** Oxidation at 150 °C for 30 minutes followed by oxidation at 250 °C for 30 minutes.

**Figure 10** Iron citrate gives a very fine cluster deposition on silica surface with small diameter. They are stable at oxidation temperature of up to 250 °C. They did not show any carbon nanotubes formation with dicyclopentadiene as carbon source.

## 5.2.2 Iron Acetate

Iron acetate was spin coated from 1 mmol/L solution in alcohol at 10000 rpm (Figure 11a). Sample was oxidized at 170 °C for one hour, which showed presence of no clusters (Figure 11b). Experiment was repeated at 150 °C (Figure 11c), which showed presence of clusters. Attempts to grow carbon nanotubes under reaction conditions did not yield any results. Oxidation was then carried at 150 °C for 30 minutes followed by oxidation at 250 °C for 30 minutes (Figure 11d). No growth of CNT occurred after oxidation at any of these temperatures as observed with SEM. The oxidation and reaction conditions are shown in Table 3.

**Table 3** Catalyst clusters from iron acetate were obtained by calcining at different oxidation temperature and varying the flow rate of dicyclopentadiene. No carbon nanotubes were observed by SEM.

Oxidation Temp.	Reaction Temp.	Time	Dicyclopentadiene Flow rate	Results
170 °C	675 °C	40 min	1.824 ml/hr	Only Carbon. No CNT
150 °C	675 °C	30 min	1.824 ml/hr	Only Carbon. No CNT
150 °C, 250 °C	675 °C	40 min	1.2 ml/hr	Only Carbon. No CNT

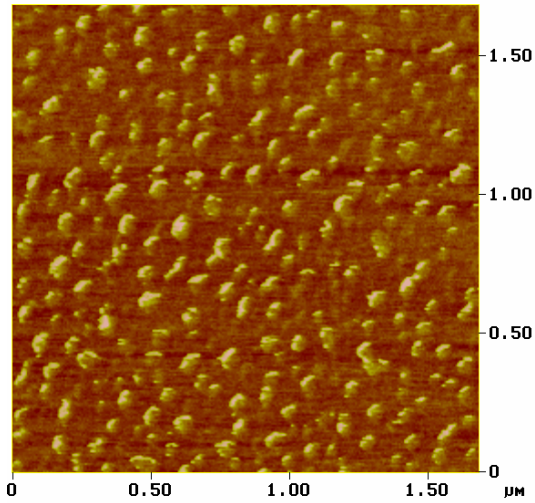


**Figure 11a** AFM image of Fe acetate spin coated at 10,000 rpm from 1mmol/L solution.

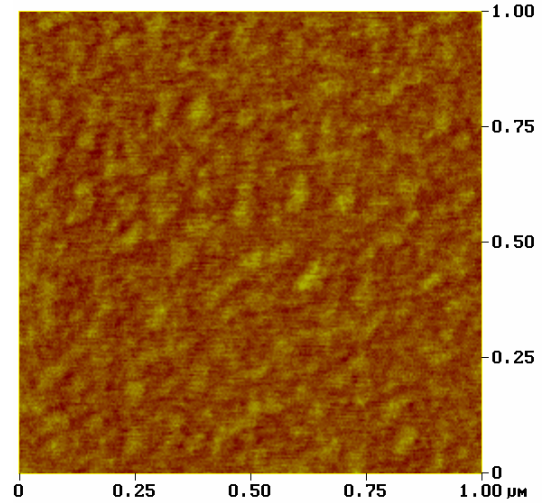


**Figure 11b** AFM image of Fe acetate after oxidation at 170 °C.

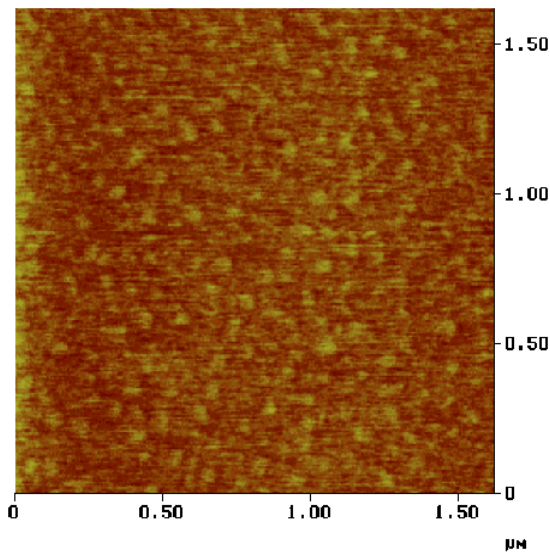


**Figure 11c** Oxidation of Fe acetate at 150 °C in air.

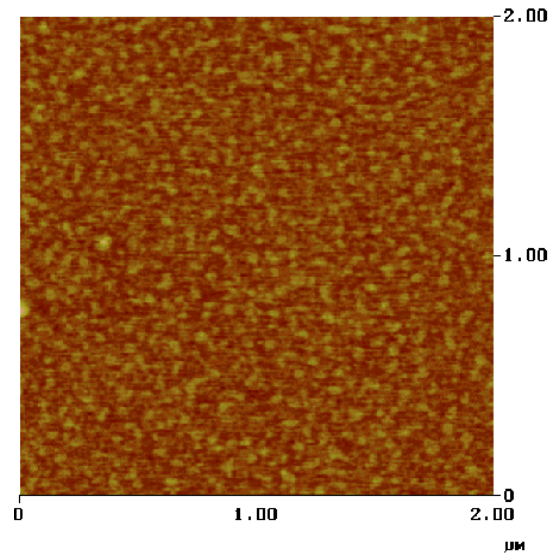


**Figure 11d** Oxidation at 150 °C for 30 minutes followed by oxidation at 250 °C for 30 minutes.

**Figure 11** Oxidation study on Iron acetate spin coated from 1 mmol/L solution at 10000 rpm.

### 5.2.3 Iron Chloride

Iron chloride oxidizes to iron oxide at 400 - 600 °C [7, 8, 9, 10, 11]. Iron chloride was spin coated at 9000 rpm from 1 mmol/L solution of ethanol. The average size of clusters was about 8.6 nm (Figure 12a). A sample was oxidized at 500 °C for one hour. Clusters were stable after oxidation treatment and the size was about the same ~9 nm (Figure 12b). It was then treated to high temperature of 700 °C in inert atmosphere to observe the effect of reaction conditions. Cluster size reduced dramatically to average 3.5 nm (Figure 12c). The clusters seemed to be stable under reaction conditions. Reaction of oxidized iron at 675 °C with dicyclopentadiene was successful in growing single MWNT. The various conditions of reduction and oxidation along with reaction at 675 °C are given in Table 4 and 5 respectively. The reduction of catalyst followed by reaction with dicyclopentadiene from the SEM results showed few multi-walled carbon nanotubes as compared to the clusters that were oxidized.

**Table 4** Catalyst clusters from iron chloride were produced by reduction and reaction at temperatures of 650 °C – 700 °C and optimum conditions of growth of MWNT were determined.

Reduction Temp.	Reaction Temp.	Time (minutes)	Results
500 °C	650 °C	5	No CNT
500 °C	700 °C	5	CNT & C deposit
500 °C	700 °C	5	CNT & large C
500 °C	675 °C	5	Low CNT and large C. Reduction may not be suitable for production of CNT.

**Table 5** Catalyst clusters were produced from iron chloride by oxidation in air and reaction with dicyclopentadiene at temperatures of 650 °C – 700 °C was carried out. The optimum temperature was determined to be 675 °C.

Oxidation Temp.	Reaction Temp.	Time (minutes)	Results
500 °C	650 °C	5	No CNT
500 °C	650 °C	40	Large C and pockets of CNT
500 °C	700 °C	40	C deposit
500 °C	700 °C	40 (higher flow rate of helium)	Low no. of CNT.
500 °C (benzene)	700 °C	40	C deposit with very few CNT
200 °C oxidation 250 °C reduction	650 °C	40	C deposit with small CNT pockets
500 °C	675 °C	40	Single MWNT and C deposit
500 °C	675 °C	40	Single MWNT (large and entangled) and C deposit

The reaction produced multi-walled carbon nanotubes and the diameter of the nanotubes was in the range of 100 – 250 nm. The agglomeration of clusters derived from iron chloride did not agglomerate to such a large extent under reaction conditions starting with the precursor size of 5 – 10 nm. The large diameter is probably because of large molecules of dicyclopentadiene that provides more than enough carbon molecules to form large diameter multi-walled carbon nanotubes. The other reason may be that the amorphous carbon deposits on the walls of the multi-walled carbon nanotubes. In any case, dicyclopentadiene is not a suitable carbon source for formation of small diameter multi-walled carbon nanotubes and especially single walled carbon nanotubes. This carbon source was thereby abandoned in favor of benzene which though decomposes at higher temperature, does not provide amorphous carbon deposition at lower temperature and is known to produce single walled carbon nanotubes.

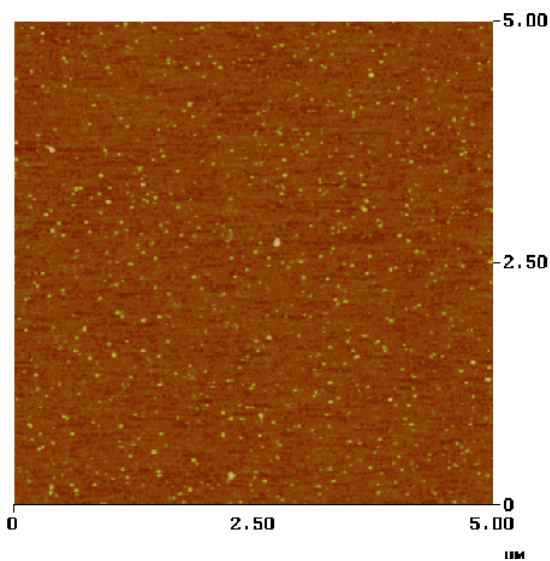


Figure 12a AFM image of  $\text{FeCl}_2$  spin coated at 9000 rpm from 1 mmol/L alcohol solution.

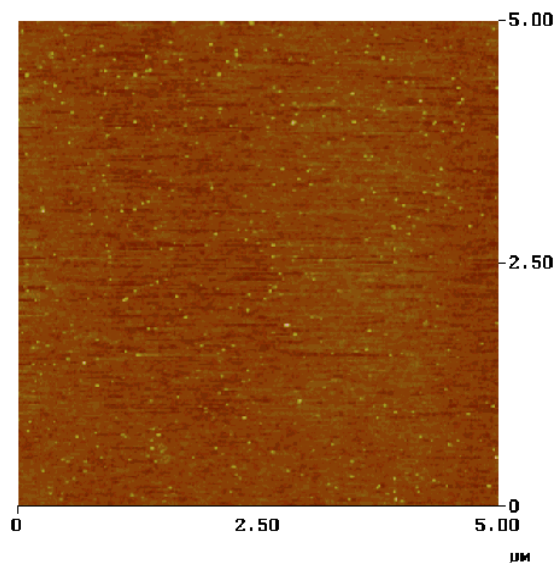


Figure 12b AFM image of  $\text{FeCl}_2$  clusters after oxidation at 500 °C for one hour.

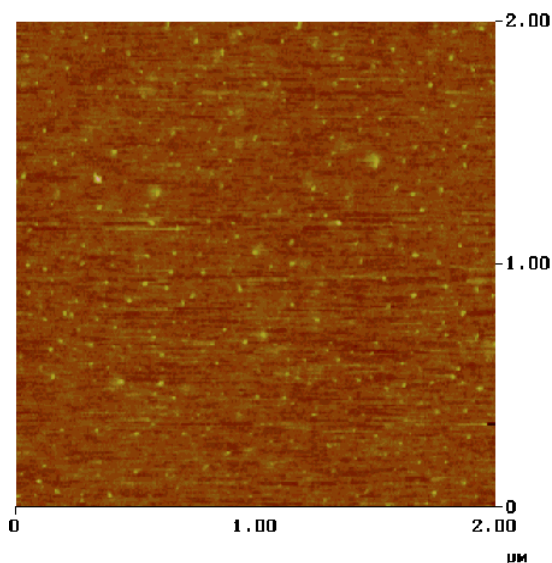


Figure 12c Treatment of  $\text{Fe}_2\text{O}_3$  clusters produced after oxidation with inert atmosphere at reaction temperature of 700 °C reduced the size of clusters dramatically.

**Figure 12** Reaction was carried at 700 °C in absence of dicyclopentadiene and  $\text{H}_2$ . The reaction time was 40 minutes. The scale of Figure 12 c is 2  $\mu\text{m}$  as compared to previous pictures of spin coating and oxidation, which is 5  $\mu\text{m}$ .

## 6 Iron Nitrate

Nitrates of iron are easily decomposed to their respective oxides at low temperatures compared to iron citrates or iron acetates which are not stable at temperatures of their oxidation. Other inorganic counter ions of iron salts take high temperatures for their oxidation or reduction. An oxide can be reduced quite easily at reduced temperatures. The results on supported catalyst with iron nitrate as the precursor provided some very good results with respect to growth of single walled carbon nanotubes (to be discussed in later chapters). There were some very interesting results with respect to the behavior of catalyst clusters deposited on silica wafer calcined at low and high temperature with respect to their stability under reaction conditions. With these points of view, we performed detailed study on the behavior of iron nitrate deposited on model catalyst support by spin coating under reduction/oxidation and reaction conditions. Benzene was employed as the carbon source for reasons mentioned in the previous section.

As mentioned before, the calcination temperature of silicon wafer prior to the spin coating of the salt clusters on the surface seems to make a big difference to the presence of clusters during the reaction conditions. Calcination of silicon wafer was carried at two temperatures: 750 °C for 24 hours and 350 °C for 24 hours. The difference between the two supports was the thickness of the silica over the model silicon wafer. We take the case in following two sections.

## 6.1 Calcination of model Si (100) support at 750 °C

The silicon wafer was calcined at 750 °C in open air furnace for 24 hours. The surface was then cleaned with RCA-1 solution at 70 °C for 10 minutes and then boiled in DI water for 10 minutes. The surface was then immediately transferred to the spin coating machine and spin coated with 1 mmol/L of iron nitrate at 8500 rpm.

### 6.1.1 Reduction of iron nitrate

Iron nitrate clusters were reduced in pure hydrogen for a period of 30 minutes, the total flow rate being maintained at 20 ml/min. The temperature of reduction was 300 °C. At the same temperature, after 30 minutes, helium flow was started to accommodate the reaction conditions to follow. The reaction was carried at 950 °C. The conditions of reduction are as follows and the conditions of reaction are given in Table 6:

Temperature  $T = 300\text{ °C}$     Time  $t = 30\text{ min.}$     Ramp  $R = 2\text{ °C/min}$

H<sub>2</sub> flow rate = 20 ml/min

Temperature  $T = 300\text{ °C}$     Time  $t = 30\text{ min.}$     Ramp  $R = 2\text{ °C/min}$

H<sub>2</sub> flow rate = 20 ml/min

He flow rate = 200 ml/min

**Table 6** Conditions of reaction for clusters obtained by reducing iron nitrate at 300 °C.

Reaction no.	Temp.	Time (min)	Total flow rate (ml/min)	He flow through saturator	Conc. of benzene	H <sub>2</sub> flow rate (ml/min)	AFM Results
1	950 °C	10	264.39	40	0.91 %	20	Clusters absent
2	950 °C	10	236.64	15	0.69 %	20	Clusters absent

No clusters were observed after reaction conditions as compared to large deposition of clusters after spin coating. The surface appeared completely blank after the reaction conditions. There were very few clusters of very large diameter (70 – 100 nm) spaced at a large distance. Either the clusters agglomerated to a great extent or they were lost in to the surface. The reason for such a behavior is not very clear at present. Results are shown in Figure 13.

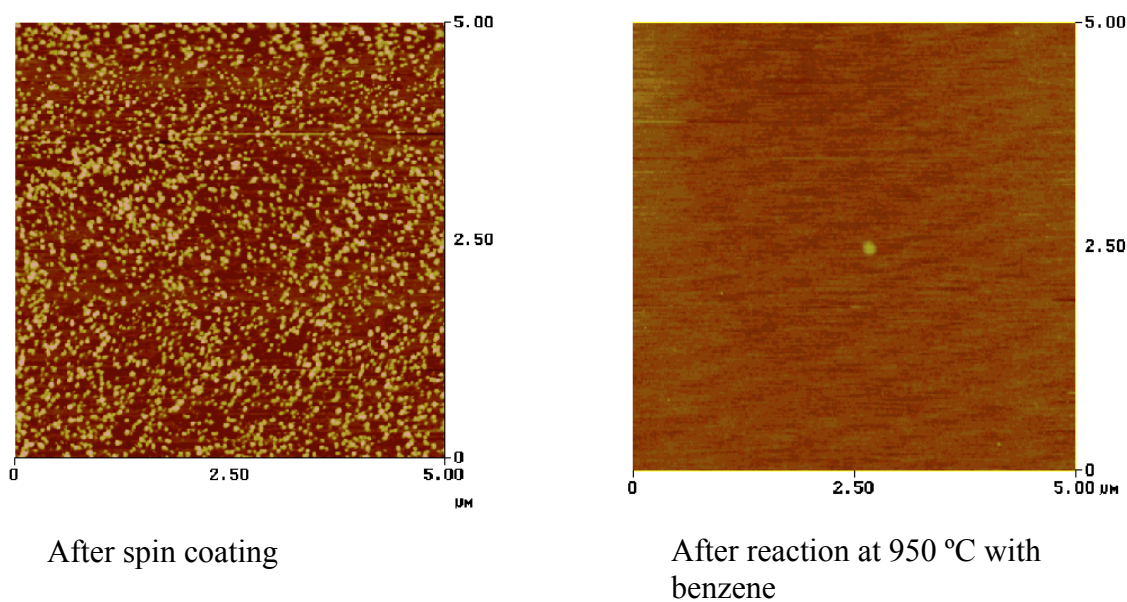


**Figure 13** The deposition of clusters on the calcined model silicon wafer shows good density of iron nitrate clusters. After reaction conditions, almost all of the clusters are lost with very few remaining on the surface.

### 6.1.2 Oxidation of iron nitrate at 150 °C and 250 °C

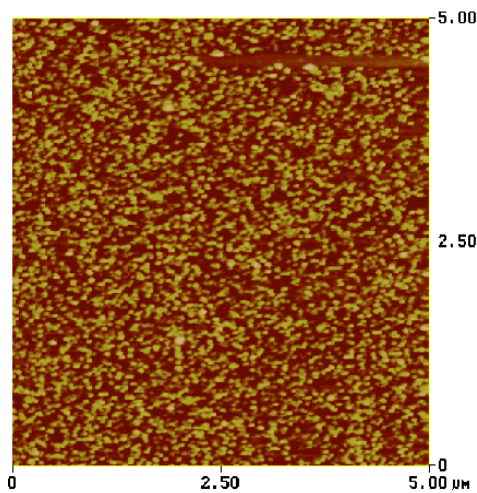
Iron nitrate decomposes completely at 110 °C and forms the corresponding iron oxide which is amorphous in nature. Oxidation of iron oxide at about 250 °C starts crystallization of clusters [12]. The transition of phase crystallinity begins with formation of incomplete oxide of iron magnetite  $\text{Fe}_3\text{O}_4$  and then proceeds to form hematite  $\text{Fe}_2\text{O}_3$ , the transition being complete at about 500 °C [13]. In current study we employ the oxidation of clusters to only iron oxide to form their amorphous state and observe the effect on their stability. Oxidation was carried in stagnant air followed by reaction at 950 °C in absence and presence of benzene. The AFM images of the surface after spin coating, oxidation at 250 °C and reaction in presence and absence of carbon source are given in Figure 14. The reaction conditions are summarized in Table 7. The blank reaction was performed in presence of hydrogen and helium only but no benzene was flowed. The surface shows almost no clusters, the case is similar to the ones where reduction and reaction of clusters were carried out as discussed in section 6.1.1. The reaction carried out with benzene shows carbon deposition in the form of large hillock type structures. No carbon nanotube growth was observed. The reduction conditions are given below:

Temperature  $T_1 = 150$  °C      Time  $t_1 = 5$  min      Ramp  $R = 1$  °C/min

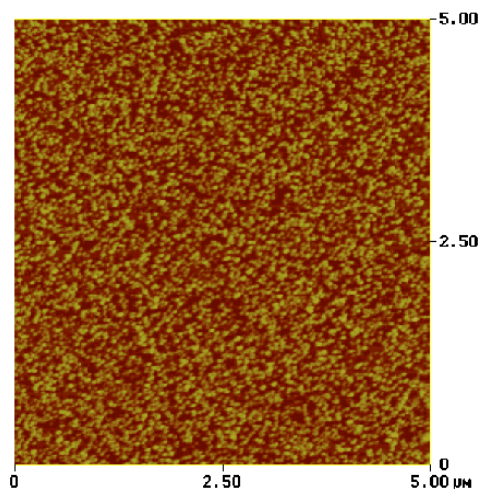
Temperature  $T_2 = 250$  °C      Time  $t_2 = 5$  min      Ramp  $R = 1$  °C/min

**Table 7** Reaction of clusters derived from iron nitrate after oxidation at 250 °C in presence and absence of benzene.

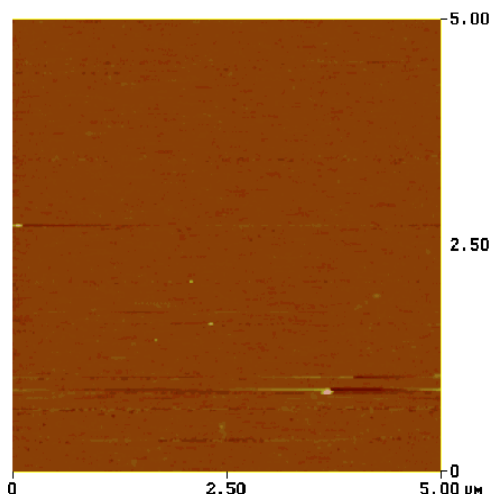
Reaction no.	Temp.	Time (min)	Total flow rate (ml/min)	He flow through saturator	Conc. of benzene	H <sub>2</sub> flow rate (ml/min)	AFM Results
1	950 °C	10	236.64	15	0.69 %	20	No clusters
2	950 °C	10	220	0	0	20	No clusters



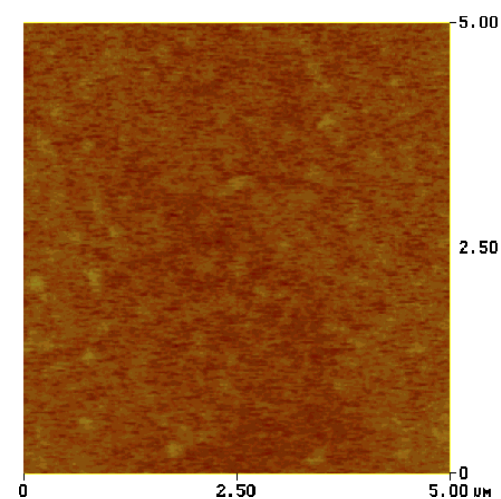
After spin coating



After calcinations at 250 °C  
in stagnant air



Blank reaction at 950 °C in  
flow of Helium and H<sub>2</sub>



Reaction at 950 °C with 0.69%  
benzene concentration

**Figure 14** Oxidation of iron nitrate at 250 °C and reaction at 950 °C in presence of benzene does not produce any carbon nanotubes (right). The clusters are absent after the blank reaction condition (left).

### 6.1.3 Oxidation of iron nitrate at 300 °C

Oxidation carried out at 250 °C did not make the clusters stable enough for reaction conditions so the temperature was increased to 300 °C. Air was also flowed through the reactor so as not to allow stagnant environment over the catalyst. Following conditions for oxidation were employed:

T = 300 °C    t = 30 min    R = 1 °C/min

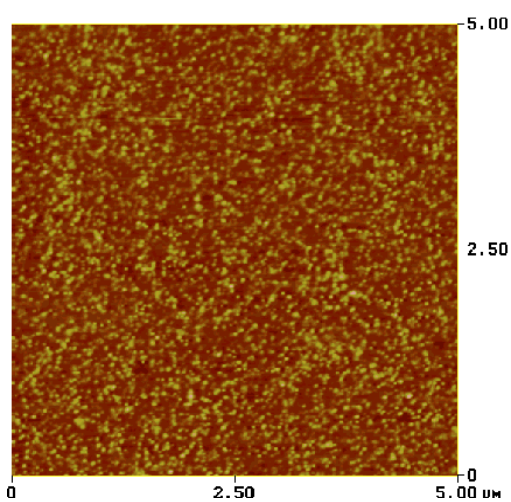
Air flow rate = 189 ml/min

The reaction conditions are given in Table 8 and the AFM results are shown in Figure 15. After reaction, clusters were observed but no formation of carbon nanotubes occurred. These results were confirmed both with Raman as well as AFM.

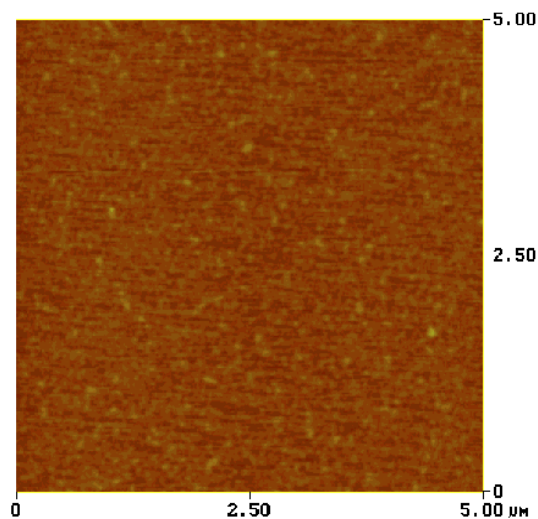
**Table 8** The oxidation of iron nitrate clusters produces iron oxide clusters at 300 °C.

Reaction no.	Temp.	Time (min)	Total flow rate (ml/min)	He flow through saturator	Conc. Of benzene	H <sub>2</sub> flow rate (ml/min)	AFM Results
1	950 °C	10	236.64	15	0.69 %	20	Clusters with reduced height
2	950 °C	10	236.64	15	0.69 %	20	Large clusters. No CNT

\* The tube was placed inside the furnace between the transition period of oxidation and reaction.



After calcination at 300 °C in flowing air for 30 minutes



Reaction with benzene (0.69%) for 10 minutes

**Figure 15** The iron oxide clusters after oxidation at 300 °C appear stable on silica surface as observed with AFM. Reaction at 950 °C with benzene shows diffuse clusters. No carbon nanotubes were observed.

#### 6.1.4 Oxidation of iron nitrate at 450 and 800 °C

Based on the work done on oxidation of iron crystallites [14], oxidation was further carried out at 450 °C and 800 °C. The initial oxidation was carried out at 300 °C for 30 minutes to form amorphous iron oxide. The clusters turn crystalline above this temperature. There are two phases initially, magnetite ( $\text{Fe}_3\text{O}_4$ , FCC packed) and hematite ( $\text{Fe}_2\text{O}_3$ , HCP packed). As the annealing temperature increases, magnetite is gradually converted to hematite. At ~500 °C, the conversion is almost complete. Above 600 °C, growth of misaligned hematite begins and continues as temperature goes up. We studied

the clusters with AFM at oxidation temperatures up to 800 °C. The details of oxidation are as follows:

**Oxidation at 450 °C**

$T_1 = 300\text{ °C}$              $t_1 = 30\text{ min}$      $R_1 = 1\text{ °C/min}$

$T_2 = 450\text{ °C}$              $t_2 = 30\text{ min}$      $R_2 = 5\text{ °C/min}$

Air flow rate = 189 ml/min

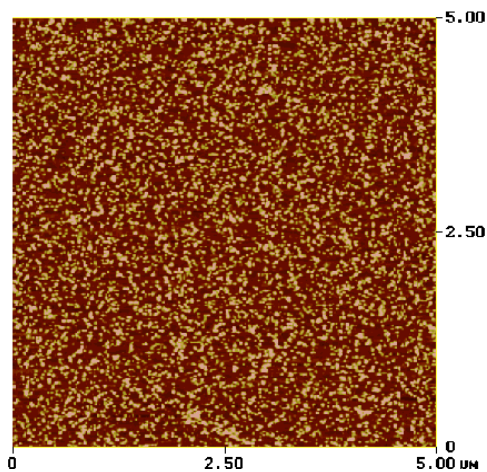
**Oxidation at 800 °C**

$T_1 = 300\text{ °C}$              $t_1 = 30\text{ min}$      $R_1 = 1\text{ °C/min}$

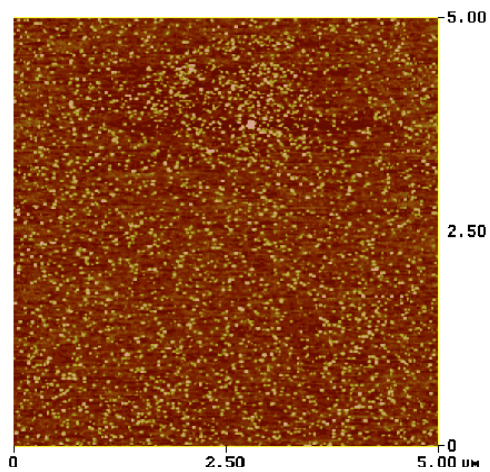
$T_2 = 800\text{ °C}$              $t_2 = 5\text{ min}$        $R_2 = 5\text{ °C/min}$

Air flow rate = 189 ml/min

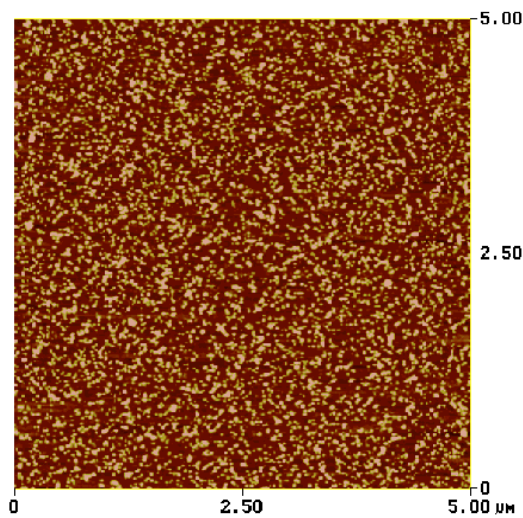
AFM indicates diffused clusters about 2 – 4 nm in size (Figure 16). Clusters of oxide are present up to 800 °C of oxidation temperature. They “disappear” under the reaction conditions especially under the presence of hydrogen. The exposure of surface at a very high temperature makes the silica surface rough and porous (thickness of about 80 nm) compared to the native silicon oxide (2 nm). Reaction in presence of benzene leads to formation of structures that seem to trace the presence of clusters. In any case if the clusters are present in the reaction system, they are not discernible by AFM. No carbon nanotubes were observed by AFM and Raman spectroscopy.



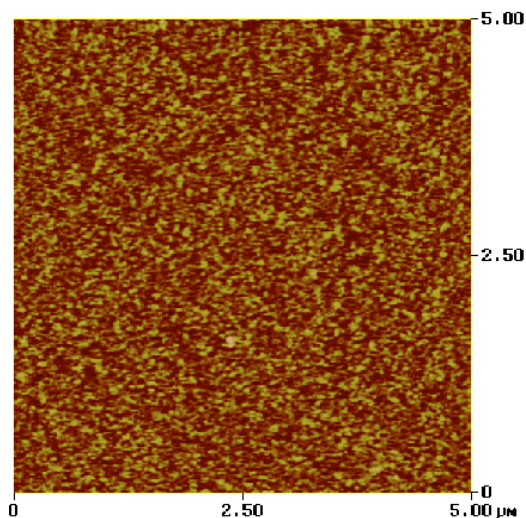
After spin coating



After oxidation at 450 °C for 30 minutes in flowing air



After spin coating



After oxidation at 800 °C for 5 minutes in flowing air

**Figure 16** Oxidation of iron nitrate on model silica support remains stable up to calcination temperature of 800 °C in flowing air.

## 6.2 Calcination of model Si (100) support at 350 °C

Silicon (100) wafer was calcined at 350 °C for 24 hours in an open air furnace. The furnace did provide provision for preventing any contamination to be deposited on the surface as the sample was enclosed and only air was allowed to flow in to the furnace. We did not find any contamination on the surface from air after calcination as observed by AFM. The surface was treated with RCA-1 solution for 10 minutes at 70 °C and then boiled in DI water for 10 minutes. It was rinsed with DI water and then spin coated with iron nitrate. The specifications of spin coating are as follows:

Concentration of iron nitrate: 1 mmol/L

Speed of spin coating: 9000 rpm

Following types of reactions were performed to study the behavior of clusters:

1. Oxidation with air to form oxide and reaction with benzene in *absence* of hydrogen (with tube inside and outside during ramp).
2. Oxidation followed by reduction and reaction with benzene in *absence* and *presence* of hydrogen.
3. Oxidation with air to form oxide and reaction with benzene and *presence* of hydrogen.
4. Reduction of iron nitrate to form metallic iron and reaction with benzene.

### 6.2.1 Oxidation with air to form oxide and reaction with benzene in *absence* of hydrogen

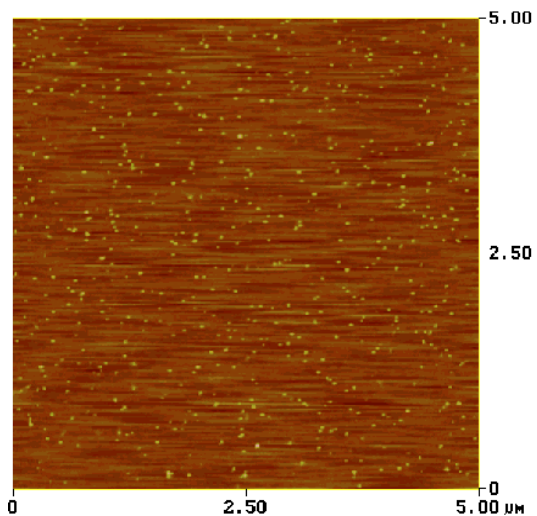
Oxidation of clusters was performed at two temperatures: 300 °C and 400 °C. The former temperature was reached at a very slow ramp of 1 °C/min while from 300 °C to 400 °C was reached at the rate of 5 °C/min. Clusters were present after the calcination process. The sample was then taken to the reaction temperature of 900 °C in inert atmosphere of helium. The temperature was raised at different ramps and the sample was maintained inside the furnace or outside with the help of a sliding mechanism without exposing the sample to the atmosphere. The conditions of reactions are given in Table 9. The surface shows large cluster formation (Figure 17) on the surface at the position of iron catalyst. The iron catalyst could lead to larger deposition of carbon on itself because of absence of hydrogen in the reaction system. No carbon nanotubes were observed by AFM or SEM.

**Table 9** The table shows the oxidation and reaction temperature and the benzene concentration for growth of carbon nanotubes.

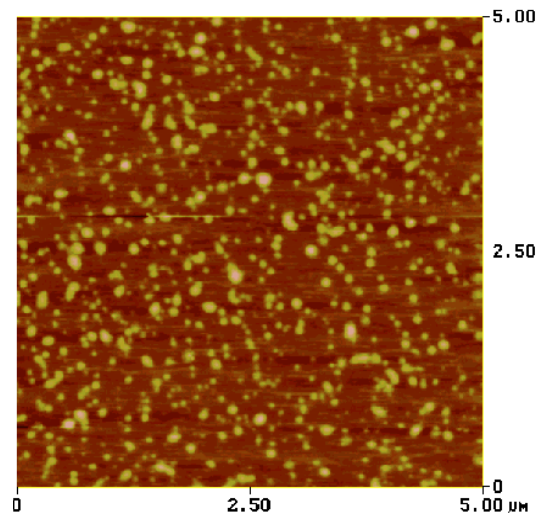
Rxn no.	Oxid <sup>n</sup> Temp.	Time (min)	Rxn temp.	Total flow rate	He flow through saturator (ml/min)	Conc. of benzene	H <sub>2</sub> flow rate (ml/min)	Result
1	300 °C 400 °C	30 30	900 °C	216.64	15	0.76 %	0	Large clusters
2*	300 °C 400 °C	30 30	900 °C <sup>†</sup>	216.64	15	0.76 %	0	Large clusters
3*	300 °C 400 °C	30 30	900 °C	216.54	15	0.76 %	0	Large clusters

\* Tube was kept inside the furnace during temperature ramp.

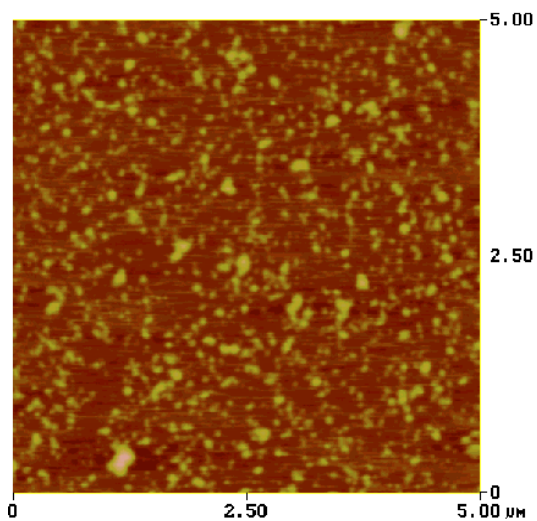
† Reaction temperature was reached at 5 °C/min.



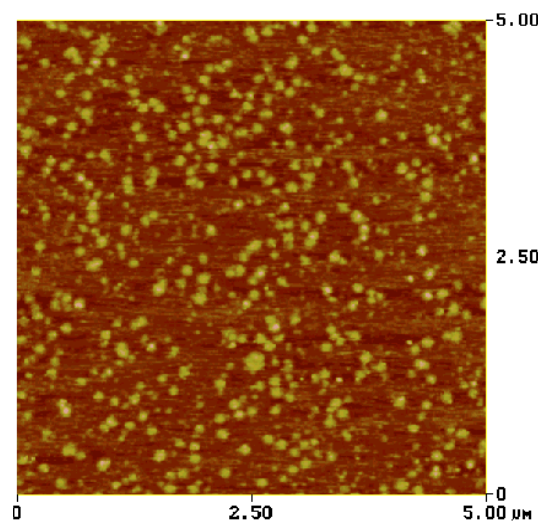
After spin coating, the clusters are well dispersed.



Tube inside furnace during temperature ramp of 5 °C/min



Tube outside the furnace during temperature ramp of 70 °C/min



Tube inside the furnace during temperature ramp of 70 °C/min

**Figure 17** The oxidation of iron nitrate at 400 °C on silicon wafer calcined at 350 °C and reacted with benzene at 900 °C in absence of hydrogen shows a large deposition of carbonaceous material.

## 6.2.2 Oxidation followed by reduction and reaction with benzene in *absence* and *presence* of hydrogen

A blank reaction was first performed in the absence of both hydrogen and benzene at 900 °C after oxidizing iron nitrate at 400 °C. This was to ascertain whether the cluster distribution on the surface changed just by the effect of temperature alone. Catalyst was oxidized at 300 °C (ramp = 1 °C/min) and 400 °C (ramp = 5 °C/min) for 30 minutes each. The clusters were then removed from the furnace and the temperature of the furnace was raised to 900 °C. A blank reaction involving *absence* of benzene and hydrogen but presence of only inert helium atmosphere was carried out. The AFM results after the blank reaction conditions are given in Figure 18. No benzene or hydrogen was present in the system during the reaction conditions, so the large clusters could only be because of agglomeration of clusters or covering of the iron clusters with silicon from underneath the silica surface. At present the case is not resolved.

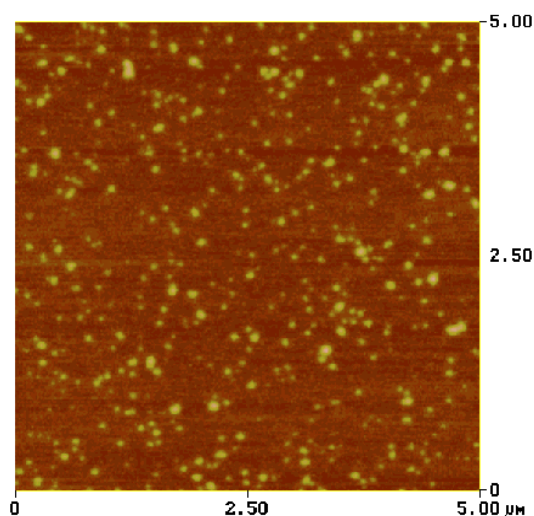


**Figure 18** The blank reaction at 900 °C of clusters produced by oxidation of iron nitrate at 400 °C in presence of only inert helium atmosphere shows large clusters on the surface.

To observe the effect of benzene and hydrogen, the clusters after being oxidized were then reduced in 1% hydrogen at 300 °C – 400 °C and employed for growth of carbon nanotubes at 900 °C both in presence and absence of hydrogen. The results are given in Figure 19. The clusters obtained are still large as compared to the ones deposited or obtained after calcination when hydrogen is absent during reaction. The sizes of clusters vary a lot in the presence of hydrogen. The reaction conditions are given in Table 10. Presence of reducing atmosphere under reaction conditions may not be the reason for large agglomeration of cluster as observed from the blank reaction. The presence of large clusters can be attributed to the high temperature and thin film of silica maybe unable to prevent effective migration of silicon from underneath the surface and covering the iron clusters. Presence of hydrogen during reaction prevents excess of carbon from being deposited and provides a large variation in the size of the clusters. Further the chemistry of metallic iron clusters as compared to iron oxide may be the reason for different results.

**Table 10** Oxidation of iron nitrate produces iron oxide which is reduced in hydrogen to form metallic iron clusters. The clusters were then reacted with benzene in presence and absence of hydrogen.

Rxn no.	Oxid <sup>n</sup> Temp.	Time	Red <sup>n</sup> temp.	Time
1	300 °C	30 min	300 °C	10 min
2	300 °C	30 min	300 °C	10 min
3	300 °C 400 °C	30 min 30 min	400 °C	10 min

Rxn no.	Total flow rate	He flow through saturator (ml/min)	Conc. of benzene	H <sub>2</sub> flow rate (ml/min)	Result
1	216.64	15	0.76 %	0	Large clusters
2	218.64	15	0.75 %	2	Large clusters
3	216.64	15	0.76 %	0	Large clusters

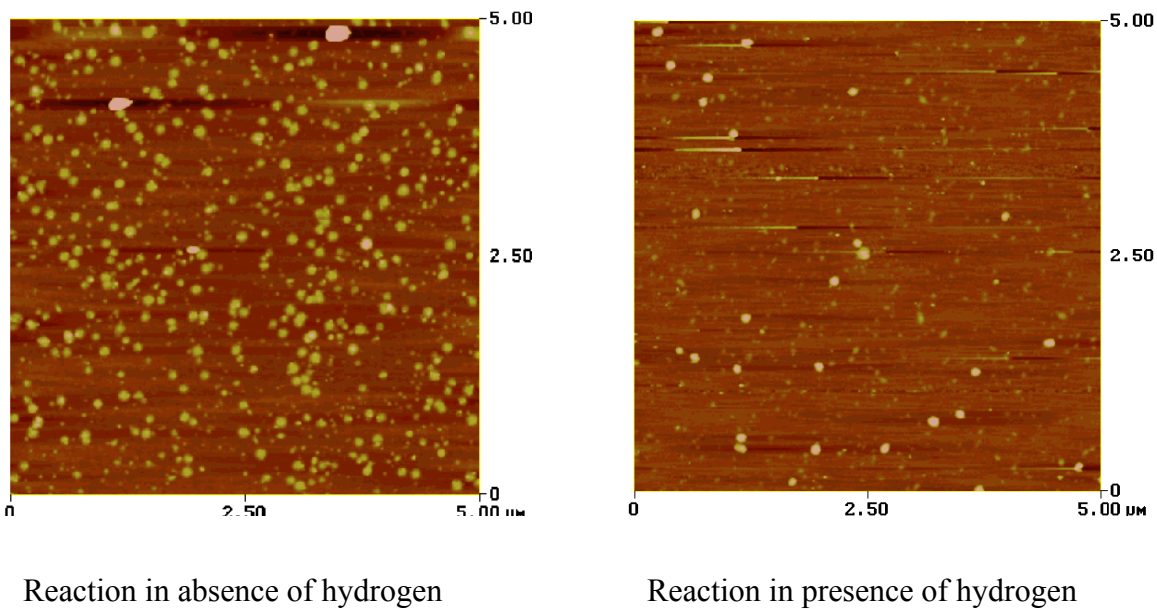


**Figure 19** Iron oxide clusters obtained after calcination were reduced at 300 – 400 °C to form metallic iron particles. Results for reaction of these metallic clusters in absence (left) and presence of hydrogen (right) are shown. The cluster sizes vary when hydrogen was used in the reaction.

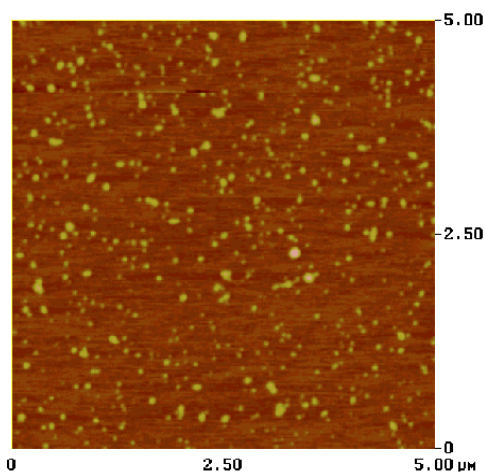
### 6.2.3 Oxidation with air to form oxide and reaction with benzene in presence of hydrogen

Oxidation was performed at 120 °C to 800 °C in flowing air. The iron oxide clusters were then reacted with benzene at 900 °C in presence of hydrogen. The concentration of hydrogen was varied to prevent the deposition of carbon from benzene to as much extent as possible. This helps in ascertaining whether the large clusters were because of large decomposition of carbon or from the interaction of iron clusters with the support surface. In second case hydrogen was used as the carrier gas for benzene to ensure intimate mixing of hydrogen and benzene. The reaction conditions are given in Table 11 for helium as the carrier gas for benzene. The reaction condition for hydrogen as carrier gas is given in Table 12. With helium as the carrier gas for benzene and 8.45% hydrogen

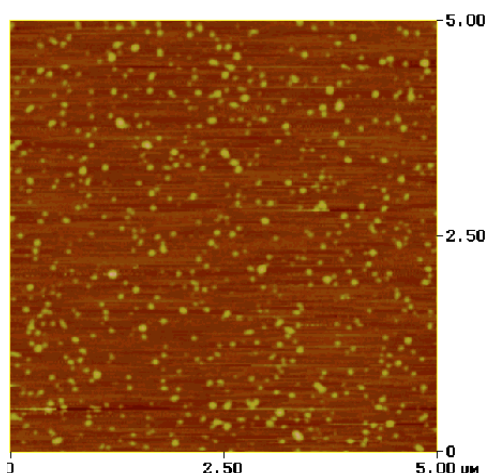
concentration, the surface showed large clusters in the size range of 50 – 90 nm (Figure 20). Under similar conditions on silicon surface calcined at 750 °C, the clusters were absent. The difference in the behavior of clusters under different calcining conditions of support at different temperatures is evident from this reaction.

**Table 11** Oxidation of iron nitrate and reaction with benzene leads to formation of carbon nanotubes. Helium is used as the carrier gas.

Rxn no.	Oxid <sup>n</sup> Temp.	Time (min)	Rxn temp.	Total flow rate	He flow through saturator (ml/min)	Conc. Of benzene	H <sub>2</sub> flow rate (ml/min)	Result
1	300 °C 400 °C	30 30	900 °C	236.64	15	0.69 %	20 (8.45%)	Large clusters
2	120 °C 800 °C	5 (1 °C/min) 5 (70 °C/min)	900 °C	236.64	15	0.69 %	20 (8.45%)	Clusters



Oxidation performed at 300 °C followed by at 400 °C for 30 minutes each



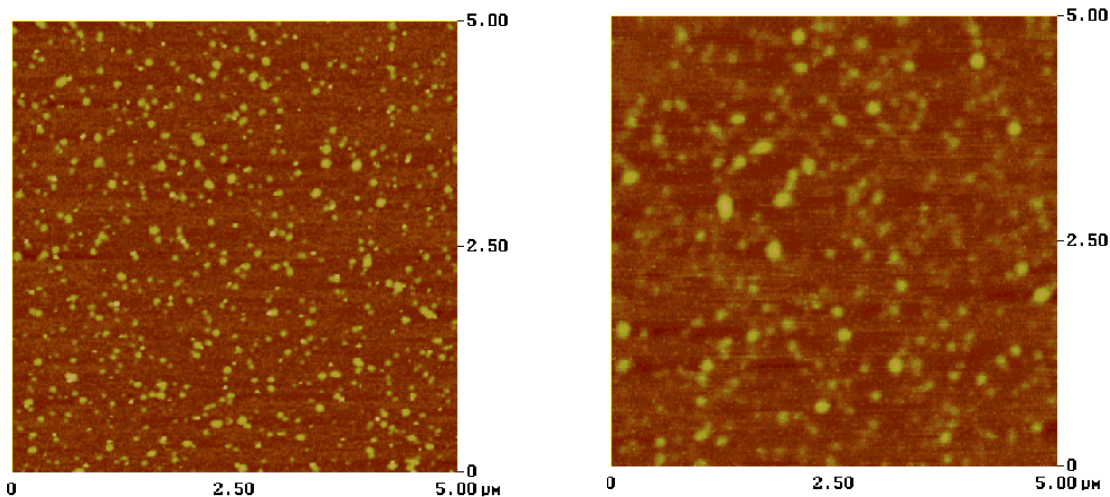
Oxidation performed at 120 °C followed by at 800 °C for 5 minutes each

**Figure 20** The reaction of iron oxide in presence of hydrogen shows presence of large clusters. The cluster density does not vary based on the calcination temperatures of iron nitrate.

The large clusters formed on the surface, if produced by deposition of large amount of carbon, could only be because of the slow diffusion of hydrogen to the surface of silicon. To remove this possibility, hydrogen was employed as the carrier gas so that benzene and hydrogen are intimately mixed. The results are given in Figure 21. The clusters are still comparable to the ones in Figure 20 except for slow oxidation of iron nitrate clusters (Table 12, reaction 2) where we see the size increased (150 – 250 nm). The large cluster diameter under these conditions is because of very slow heating ramp of the surface providing enough time for agglomeration. This further confirms the fact that the large clusters formation is a result of agglomeration and not carbon deposition since slow heating ramp will result in higher agglomeration.

**Table 12** Reaction of iron nitrate at 900 – 950 °C with benzene carried by hydrogen instead of helium.

Rxn no.	Oxid <sup>n</sup> Temp.	Time (min)	Rxn temp.	Total flow rate	He flow through saturator (ml/min)	Conc. of benzene	H <sub>2</sub> flow rate (ml/min)	Result
1	120 °C 800 °C	5 (1 °C/min) 5 (70 °C/min)	900 °C	221.64	0	0.99 %	20	Clusters
2	250 °C 800 °C	5 (1 °C/min) 1 (1 °C/min)	950 °C	221.64	0	0.99 %	20	Large clusters with C



Oxidation at 120 °C followed by at 800 °C for 5 minutes each.

Slow oxidation temperature ramp to 800 °C causes huge agglomeration of particles.

**Figure 21** Reaction of iron nitrate with hydrogen as the carrier gas for benzene. The agglomeration of clusters is observed in this case too. The agglomeration is large in case of slow heating ramp.

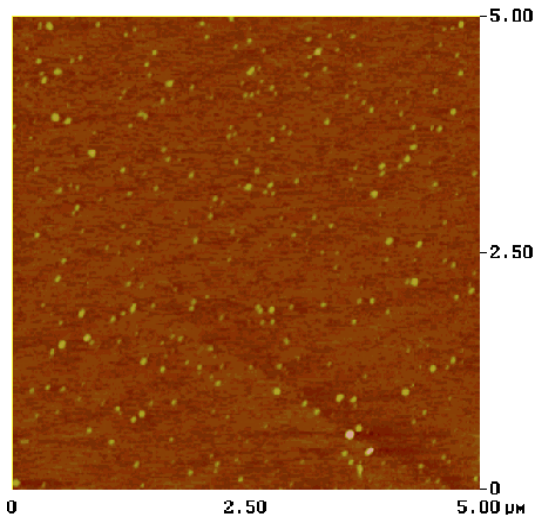
#### 6.2.4 Effect of reduction of iron nitrate followed by reaction

Effect of reduction of iron nitrate was interesting in observing the effect of hydrogen on the agglomeration of clusters during reaction conditions. Reduction of iron nitrates was performed under pure hydrogen with very slow heating rate (1 °C/min). The temperature of reduction was 250 °C and 500 °C, maintained at these temperatures for 5 minutes. Concentration of hydrogen was varied to observe its effect on the cluster size. The cluster size increases with the concentration of hydrogen indicating that the presence of hydrogen plays an important role in the stability of clusters at elevated temperatures. The reaction conditions are given in Table 13. The results are shown in Figure 22.

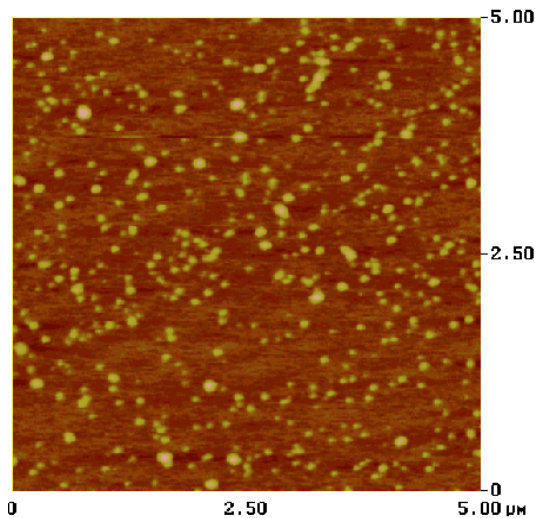
**Table 13** The conditions for reduction of iron nitrate and reaction with benzene at varying concentrations of hydrogen.

Rxn no.	Red <sup>n</sup> Temp.	Time (min)	Rxn temp.	Total flow rate (ml/min)	He flow through saturator (ml/min)	Conc. of benzene	H <sub>2</sub> flow rate (ml/min)	Result
1	250 °C 500 °C	5 (1 °C/min) 5 (5 °C/min)	900 °C	242.19	20	0.90 %	20	Small clusters
2	250 °C 500 °C	5 (1 °C/min) 5 (1 °C/min)	800 °C	239.34	15	0.69 %	22.7	Large clusters
3	250 °C 500 °C	5 (1 °C/min) 5 (1 °C/min)	800 °C	316.64	15	0.52 %	100	Clusters

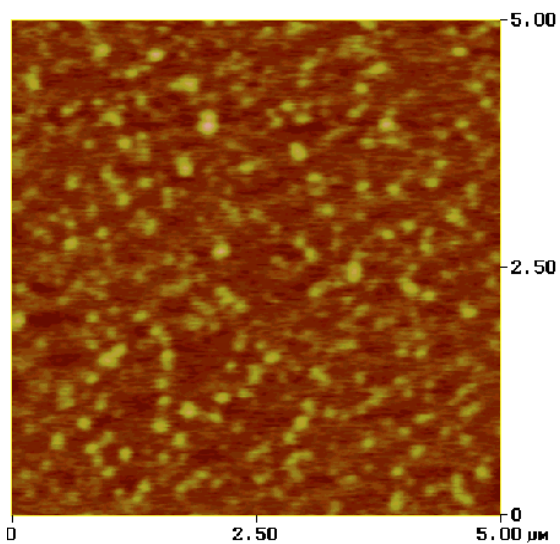
The growth of carbon nanotubes on iron nitrate was minimal with very few tubes growing on the surface. The best catalyst is iron chloride on model silicon wafer as deduced from reproducible growth of carbon nanotubes from them. They had a good yield over a given surface and also resulted in the formation of nanotubes of size comparable to the clusters deposited.



Reaction performed at 900 °C at H<sub>2</sub> flow rate of 20 ml/min



Reaction performed at 800 °C at H<sub>2</sub> flow rate of 22.7 ml/min



Reaction performed at 800 °C at H<sub>2</sub> flow rate of 100 ml/min

**Figure 22** Clusters agglomeration increases with the concentration of hydrogen.

## 7 Discussion and Conclusion

Catalyst cluster formation with spin coating is very effective technique to form clusters in the nanometer range. The various factors that affect the size of clusters are the concentration of salt, speed of spin coating, type of solvent, and type of salt used. The type of salt is important since producing metallic clusters from different salts entails different chemistry, and different reaction conditions for reduction/oxidation. The size distribution of clusters is difficult to control. Depending on the type of site for nucleation, the distribution exists at a given area. The limitation of spin coating process leads to variation in size and density of clusters from the center of the wafer to the edge. The cluster size distribution varies from the center to the edge of the support wafer. Alcohol evaporates easily leaving lesser time for growth of nucleated crystals that helps produce smaller crystals compared to the same concentration of salt in water.

Reduction of salt to produce metallic clusters, which catalyze the reaction, needs to be done carefully. Iron acetate and iron citrate carry larger groups attached to their end and have low melting and boiling point. They are easy to reduce and hence lower temperatures for large time are usually capable for complete reduction. The disadvantage is that they have low melting and boiling point and can be lost from the surface before complete oxidation or reduction takes place. A slow heating rate makes it necessary for maintaining the stability of clusters. Nickel chloride reduces at 300 – 400 °C and iron chloride has been shown to reduce at 500 °C. Agglomeration of clusters at higher temperature of reaction (> 400 °C) is difficult to prevent. Agglomeration of clusters is a

function of temperature and time of reaction. Agglomeration can be prevented to some extent by keeping the temperature of reaction low and by choosing appropriate carbon source.

Oxidation of salt to its oxide produces stable clusters. Iron oxide has a very high melting point, which prevents its agglomeration at higher temperatures. Iron chloride was shown to oxidize at 500 °C and remained stable with reduction in size of clusters at 700 °C under inert gas treatment. A direct reaction with iron oxide at 675 °C with dicyclopentadiene was able to produce single MWNT. Iron acetate and iron citrate did not seem to be stable during oxidation process. They did not produce any CNT under reaction conditions.

Iron nitrate showed a peculiar behavior with respect to the calcination of support. The silicon (100) wafer was calcined at two temperatures: 350 °C and 750 °C. Clusters deposited on silicon wafer calcined at 750 °C remained stable after calcination conditions while they were absent during the reaction conditions. In case of silicon wafer calcined at 350 °C, the clusters agglomerated to a large extent after reaction conditions. The agglomeration was about 5 – 10 times larger than the original deposited clusters. The wafer calcined at 350 °C had a small thickness of silica compared to that at 750 °C. The relative roughness and porosity of silica surface was also small at 350 °C as compared to 750 °C. The reason for this is not very clear as of now. The growth of carbon nanotubes is also limited on these clusters. Among the catalyst that we tried, iron chloride provides the best precursor for the growth of carbon nanotubes.

## 8 Reference:

1. Niemantsverdriet, J. W. and Editor, Spectroscopy in Catalysis: An Introduction, p. 289 pp. (1995).
2. Kuipers, E. W., Laszlo, C. and Wieldraaijer, W., *Catal. Lett.*, 17, (1993), p. 71.
3. van Hardeveld, R. M., Gunter, P. L. J., van Ijzendoorn, L. J., Wieldraaijer, W., Kuipers, E. W. and Niemantsverdriet, J. W., *Appl. Surf. Sci.*, 84, (1995), p. 339.
4. Partridge, A., Toussaint, S. L. G. and Flipse, C. F. J., *Appl. Surf. Sci.*, 103, (1996), p. 127.
5. Brookshier, M. A., Chusuei, C. C. and Goodman, D. W., *Langmuir*, 15, (1999), p. 2043.
6. Niemantsverdriet, J. W., Engelen, A. F. P., De Jong, A. M., Wieldraaijer, W. and Kramer, G. J., *Appl. Surf. Sci.*, 144-145, (1999), p. 366.
7. Kang, Y. S., Risbud, S., Rabolt, J. F. and Stroeve, P., *Chemistry of Materials*, 8, (1996), p. 2209.
8. Gurov, A. N. and Orlov, A. K., *Novye Issledovaniya v Khimii, Metallurgii i Obogashchenii*, No. 3, (1971), p. 48.
9. Krashennnikova, A. A., Syrkina, I. G. and Ul'yankina, G. S., *Zhurnal Fizicheskoi Khimii*, 52, (1978), p. 2255.
10. Suganuma, K. and Yagi, T., *Nippon Kagaku Kaishi*, (1978), p. 319.
11. Basu, A. and Roy, N. C., *Indian Journal of Technology*, 10, (1972), p. 119.
12. Gadalla, A. M. and Yu, H. F., *Thermochimica Acta*, 164, (1990), p. 21.
13. Gota, S., Guiot, E., Henriot, M. and Gautier-Soyer, M., *Surface Science*, 454-456, (2000), p. 796.

14. Doh, S. J., Je, J. H. and Cho, T. S., *Journal of Crystal Growth*, 240, (2002), p. 355.

# **Chapter 3**

**Growth of Carbon Nanotubes on Fe catalysts on  
Silica/Si model support**



5.1	REACTION WITH 1.5% PROPYLENE CONCENTRATION AT 900 °C.....	113
5.2	REACTION WITH 3% PROPYLENE CONCENTRATION AT 900 °C.....	115
5.3	REACTION WITH 3% PROPYLENE CONCENTRATION AT 850 °C.....	116
5.4	REACTION WITH 3% PROPYLENE CONCENTRATION AT 800 °C.....	117
5.5	TEM ANALYSIS OF REACTION PERFORMED AT 900 °C WITH 3% PROPYLENE CONCENTRATION.....	118
<b>6</b>	<b>DISCUSSION AND CONCLUSION .....</b>	<b>120</b>
<b>7</b>	<b>REFERENCE.....</b>	<b>121</b>

## List of Figures

Figure 1 AFM scan and size distribution of particles deposited from 2 mmol/L solution at 4000 rpm. The average size is about 12 nm.....	98
Figure 2 AFM scan and size distribution of particles deposited from 2 mmol/L solution at 7000 rpm. The average size is about 8 – 9 nm.....	98
Figure 3 AFM scan and size distribution of particles after reduction at 400 °C. The average size of clusters is about 16 nm.....	101
Figure 4 AFM scan and size distribution of particles after sample was treated at reaction conditions. The average size of the particles is about 37 nm with increase in the range of the distribution.....	101
Figure 5 MWNT grown in flat silica surface at 800 °C employing benzene as the carbon source. The MWNT are seen growing in single strand and are about 70 – 100 nm in diameter .....	104
Figure 6 Growth of carbon nanotubes at 900 °C and 180 ml/min flow rate of helium that leads to higher benzene to hydrogen flow rate .....	106
Figure 7 SEM scan of sample reacted at 900 °C at reduced benzene to hydrogen ratio shows ample amount of carbon nanotubes formed. Helium flow rate through saturator was 87.3 ml/min.....	108
Figure 8 Growth of carbon nanotubes occurs both at 800 and 900 °C from iron catalyst deposited from 40 mmol/L salt solutions. A dense growth of carbon nanotubes is observed throughout especially so for reaction at 900 °C.....	111

Figure 9 The reaction of iron clusters at 900 °C after being reduced at 400 °C from iron chloride shows a large agglomeration of clusters. The average diameter is about 30 - 70 nm. .... 114

Figure 10 High concentration of propylene leads to its homogenous pyrolysis resulting in deposition of high amount of carbon as observed by AFM. The Raman indicates the presence of carbon deposition..... 115

Figure 11 Drop in reaction temperature does reduce the size of carbon deposited but also indicates that the pyrolysis of propylene does take place. The analysis does not conclusively prove about the nature of clusters after reaction conditions. .... 116

Figure 12 The reaction at reduced temperature of 800 °C at 3% propylene concentration does not lead to formation of carbon nanotubes as observed by AFM. Very few clusters are seen in this case with heights considerably reduced (1 – 3 nm) compared to the ones spin coated with (4 – 7 nm). .... 117

Figure 13 TEM images of multi-walled carbon nanotubes grown on iron deposited on silica/Si wafer using spin coating. The diameter varied between 30 – 60 nm. Walls of the nanotubes do not show uniformity of structure showing many defects. .... 119

## List of Tables

Table 1 Results for reaction at 900 °C and no removal of sample between the reduction and reaction conditions. ....	105
Table 2 Experimental conditions and results for samples kept out of the furnace between the reduction and reaction period.....	110

## 1 Aim of Experiments

The following are the research aim to produce carbon nanotubes (CNT) and study their growth on iron catalyst on model silica/Si (100) support.

- 1) To deposit catalyst (Fe) clusters in the size range of 1 to 10 nm. Study the catalyst behavior under reduction and reaction conditions.
- 2) To pursue growth of carbon nanotubes on the deposited catalyst under variety of conditions such as loading of catalysts, size of clusters, effect of temperatures, flow rates of reactants etc.
- 3) Vary the reactant for the growth of CNT to find a good carbon source.

## 2 Deposition of catalyst of various sizes

Catalyst salt employed is  $\text{FeCl}_2$  that is deposited using spin coating technique on flat silica wafer. The concentration is varied to control the amount of catalyst deposited. The speed of spinning allows us to control the size of the particles deposited. Both the concentration and the speed of coating can very effectively help control the size of the clusters deposited. The wafers for our experiments were coated with 2 mmol/L solution of  $\text{FeCl}_2$  at 4000 rpm. The size of the particles has a distribution with mean size at 12 nm. The AFM image of the particles deposited on the surface with the size distribution is given in Figure 1. As noted in previous chapters, the size of the particles deposited goes on decreasing with increasing revolution speed. At 7000 rpm and 2 mmol/L  $\text{FeCl}_2$  concentration, we observe a reduction in the size of the particles that meet our expectation of producing clusters in the size range of 1 to 10 nm. The average sizes of the

particles deposited are 8 – 9 nm. The AFM scan of the surface and the particle distribution is given in Figure 2.

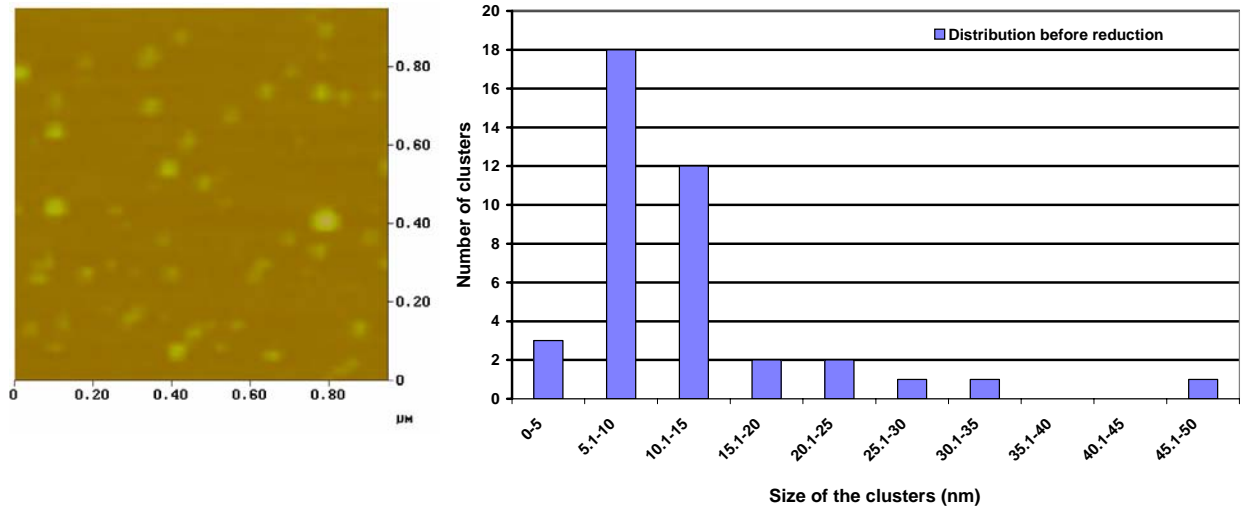


**Figure 1** AFM scan and size distribution of particles deposited from 2 mmol/L solution at 4000 rpm. The average size is about 12 nm

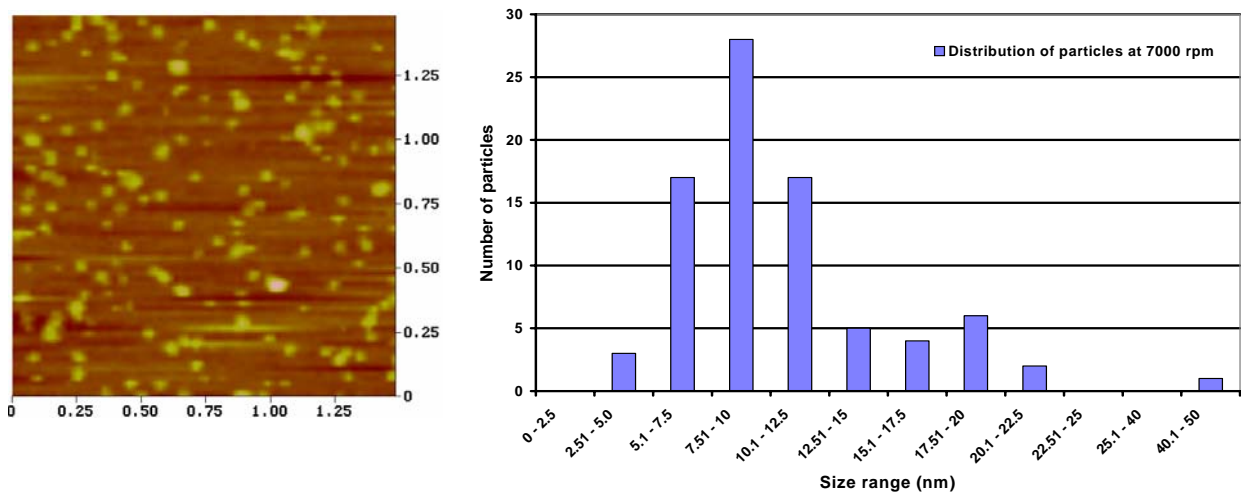


**Figure 2** AFM scan and size distribution of particles deposited from 2 mmol/L solution at 7000 rpm. The average size is about 8 – 9 nm

### **3 Effect of temperature on the catalyst particle size**

The catalyst plays its role in the production of carbon nanotubes at very high temperatures. At such temperatures, the catalyst particles have a tendency to agglomerate and form large clusters than what is intended in our 2 mmol/L solution at 4000 rpm aim. It is necessary to have a good idea about the extent to which this agglomeration occurs so as to correlate the size of the carbon nanotubes formed to the agglomerated catalyst cluster size. The typical conditions, which the catalyst particles face is the reduction and the reaction conditions. The typical reduction is done at 400 to 500 °C and reaction temperature goes as high as 900 °C. The effect of temperature was studied using sample coated with 2 mmol/L FeCl<sub>2</sub> solution at 4000 rpm. The reduction temperature was reached with a ramp of 10 °C under pure hydrogen flow. The temperature was raised at 70 °C to reach reaction temperature. The conditions and flow rates of various reactants are given as follows:

#### **Reduction:**

Temperature: 500 °C

Time: 60 minutes

H<sub>2</sub> flow rate: 20 ml/min

#### **Reaction conditions:**

Temperature: 900 °C

Time: 5 min.

H<sub>2</sub> flow rate: 20 ml/min

He flow rate: 200 ml/min

No benzene was flown during reaction conditions as we are only measuring the effect of temperature. The size distribution after spin coating is as given in Figure 1. After reduction, the AFM scan and the corresponding size distribution is given in Figure 3. We calculate 16 nm to be the average size of the particles. Other perceptible change is the slight increase in the range of size distribution around the mean. After reaction conditions, we observe about 3 - 7 times increase in the average size of the clusters. The average size of the clusters is about 37 nm and the maximum can go to about 80 nm. Results are given in Figure 4. We observe clearly that spin coated particles with an average size of about 12 nm easily goes up to average size of about 37 nm under reaction conditions. The agglomeration is also accompanied with increase in the range of the size distribution. The ideal case will be to produce 1 - 10 nm size clusters and also to retain this size under reaction conditions so as to produce carbon nanotubes of these dimensions. Under the conditions that we employ, we were not able to achieve it as was perceptible by techniques (AFM) available to us. In all the figures from 1 to 4, we only show a very small scan size of AFM so as to make the clusters more visible for calculating its size.

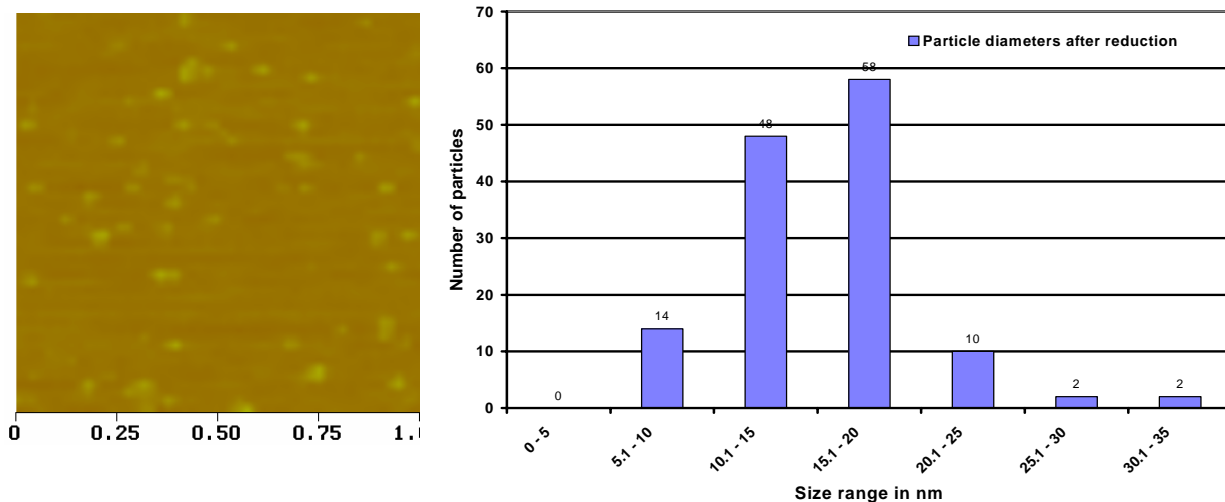


**Figure 3** AFM scan and size distribution of particles after reduction at 400 °C. The average size of clusters is about 16 nm

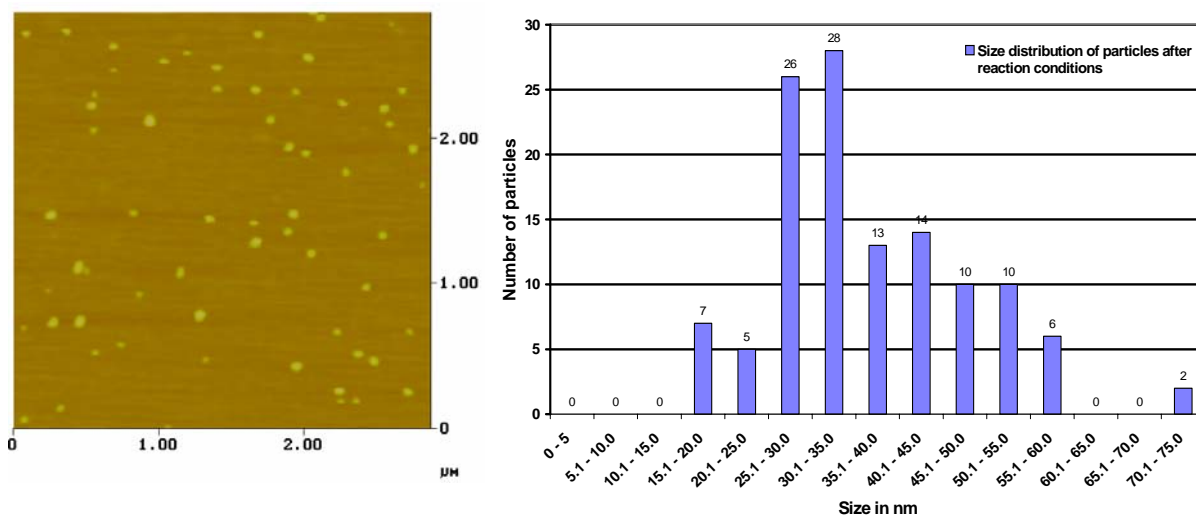


**Figure 4** AFM scan and size distribution of particles after sample was treated at reaction conditions. The average size of the particles is about 37 nm with increase in the range of the distribution

## 4 Reaction of FeCl<sub>2</sub> on SiO<sub>2</sub>/Si with Benzene as carbon source

All samples were reduced under hydrogen at around 400 °C to 500 °C with slowly reaching these temperatures at 10 °C/min. The reduction time was 60 minutes for all cases. *The hydrogen flow rate under reduction and reaction conditions was 20 ml/min.* The temperature was then ramped at 70 °C/min till it reached the reaction temperature of 700 to 900 °C. The reaction time was varied from 5 to 15 minutes. The samples were then cooled under inert atmosphere to room temperature and then collected for Raman, AFM, and SEM analysis.

### 4.1 Reduction at 400 °C and reaction at 800 °C

The wafer was spin coated with FeCl<sub>2</sub> solution (2 mmol/L) at 4000 rpm. The sample containing the FeCl<sub>2</sub> sample was reduced in pure hydrogen at 400 °C for one hour. The temperature was raised to 800 °C with the sample placed in the furnace in inert gas and then benzene and hydrogen was started immediately at the reaction temperature. The reaction was carried for 5 minutes. Benzene flow was stopped followed by terminating hydrogen flow. The sample was analyzed using SEM, AFM and RAMAN. Following are the details of the experiment:

#### **Reduction:**

Temperature: 400 °C.

Time: 60 minutes

H<sub>2</sub> flow rate: 20 ml/min

**Reaction conditions:**

Temperature: 800 °C.                      Time: 5 min.

H<sub>2</sub> flow rate: 20 ml/min

He flow rate (through saturator): 180 ml/min

Corresponding Benzene flow rate: 19.71 ml/min (8.97 %)

**4.1.1 Results**

The SEM results are given in Figure 5. We clearly observe the growth of *single* tubes of MWNT. The tubes are well separated. They have an average diameter of 70 - 100 nm. Since the particle size agglomerate to around 4 to 7 times the size of the clusters deposited, the size of the carbon nanotubes is within the range of cluster sizes. The SEM scan shows that CNT grow everywhere on the surface. It was difficult to catch this image because of the limitation of the resolution of the machine. The growth of CNT is uniform over the entire surface. SEM scans from various sections of the wafer is shown in Figure 5. Such results were not observed with Ni previously implying that iron forms an important catalyst for the growth of CNT.

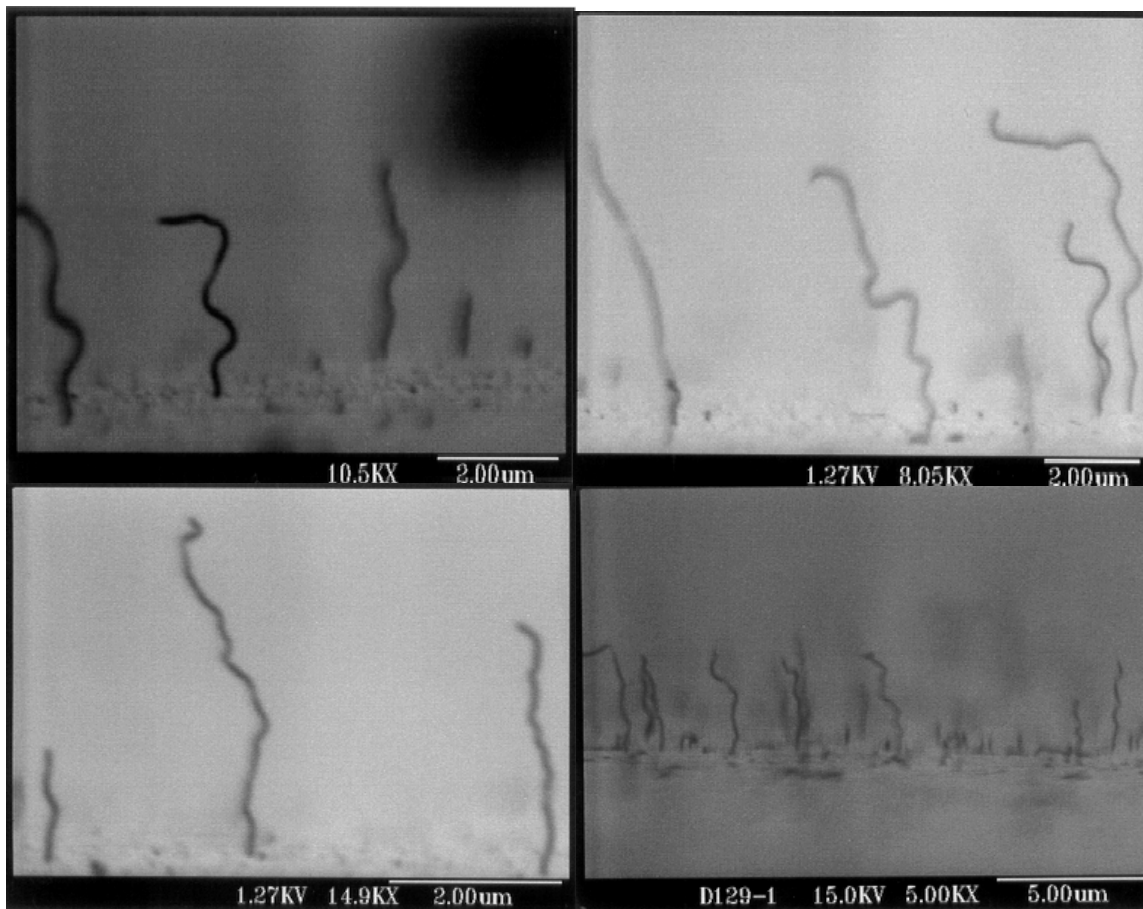


**Figure 5** MWNT grown in flat silica surface at 800 °C employing benzene as the carbon source. The MWNT are seen growing in single strand and are about 70 – 100 nm in diameter

## 4.2 Reduction at 400 °C and reaction at 900 °C

The reduction was carried at the same conditions as given in section 4.1. At the reaction temperature, an extra amount of helium was also introduced since large amount of carbon was observed to form (given in results). The reaction temperature of 900 °C has given consistent and good reproducibility for carbon nanotubes formation and hence in depth study was performed. The following sections would delineate the procedure followed. The samples were spin coated with 2 mmol/L FeCl<sub>2</sub> at 4000 rpm for all cases given below.

**Table 1** Results for reaction at 900 °C and no removal of sample between the reduction and reaction conditions.

Sample no.	Temp. °C	Reaction time (min)	Helium flow (ml/min)	Benzene flow (ml/min)	Extra He flow (ml/min)	Results
1	700	5	180	19.71 (8.97%)	0	No MWNT
2	800	5	180	19.71 (8.97%)	0	Abundant single MWNT
3	900	5	180	19.71 (7.31%)	50	Bundles of MWNT
4	900	5	180	19.71 (6.16%)	100	Less MWNT

#### 4.2.1 Sample was kept inside the reactor from reduction to reaction temperature

The sample was reduced at 400 °C and then kept in the furnace until reaction temperature of 900 °C was reached (at a ramp of 70 °C/min). The sample in this case was not removed out of the furnace in between reduction and reaction time. The results are given in Table 1. The results here show that the nanotubes are produced at a temperature of 800 °C and above. The growth of carbon nanotubes in a straight well aligned manner did not occur again at 800 °C after repeating the experiment several times. At 900 °C, the sample showed growth of long tubes of MWNT which were not straight and aligned because of the usually larger length of tubes formed (about few 10s of microns). The results for sample no. 3 (Table 1) are given in Figure 6. The diameters of the nanotubes formed are in the range of 100 to 130 nm.

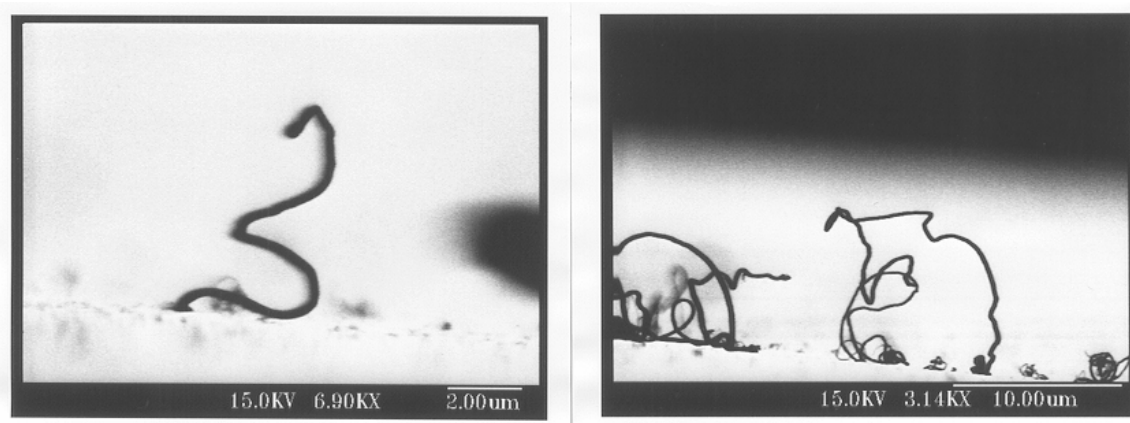


**Figure 6** Growth of carbon nanotubes at 900 °C and 180 ml/min flow rate of helium that leads to higher benzene to hydrogen flow rate

#### **4.2.2 Sample was removed after reduction and again introduced in to the furnace chamber at reaction conditions**

The sample was first reduced at 400 °C as described in section 4.1. If the sample is kept with in the furnace until the reaction temperature is reached, it might allow for large agglomeration of catalyst clusters. In order to prevent this, sample was removed from the furnace after reduction (no part of the sample containing tube was opened; only the sample was removed out of the furnace using a sliding mechanism). When the furnace reached the reaction temperature, the tube was inserted again. The hydrogen was started about 50 °C before the furnace reached the reaction temperature (before the sliding of the sample in to the furnace). Once the sample is inside the reactor, benzene flow was started. The experiments conducted and the results are given in Table 2.

The experiments showed that no carbon nanotubes are produced at 800 °C. The growth of carbon nanotubes were observed only at 900 °C. At reduced flow rates of helium through saturator whereby we reduce the ratio of flow rate of benzene to hydrogen, the production of carbon nanotubes is more refined in the sense we observe more carbon nanotubes with respect to the carbon formed on the surface. Results are shown in Figure 7. At reduced ratio of benzene to hydrogen, the size of carbon nanotubes is between 70 – 100 nm.



**Figure 7** SEM scan of sample reacted at 900 °C at reduced benzene to hydrogen ratio shows ample amount of carbon nanotubes formed. Helium flow rate through saturator was 87.3 ml/min

### **4.2.3 Sample was spin coated with higher concentration of salt to have higher loading of catalyst**

The effect of high catalyst loading will of course be higher number of CNT per unit area. We spin coated the silica flat support with 40 mmol/L salt solution at 5000 rpm. Under AFM, we observe almost a continuous film on the surface. The sample was reduced at 400 °C under pure hydrogen for one hour and then reacted at both 800 °C and 900 °C. The following were the details of the reactions:

#### **Reaction conditions**

Temperature: 800 °C and 900 °C

H<sub>2</sub> flow rate: 20 ml/min

He flow rate (through saturator): 87.3 ml/min

Corresponding Benzene flow rate: 9.56 ml/min (5.73%)

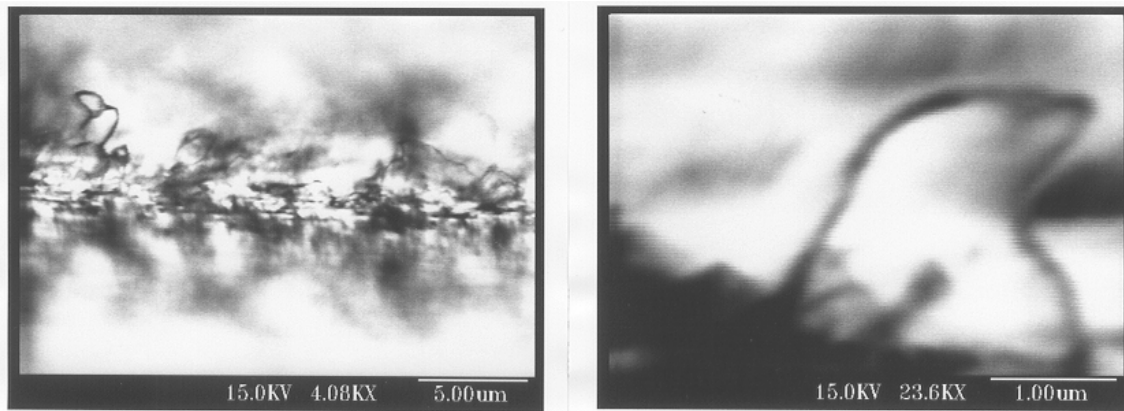
Extra He flow rate: 50 ml/min

#### **Results**

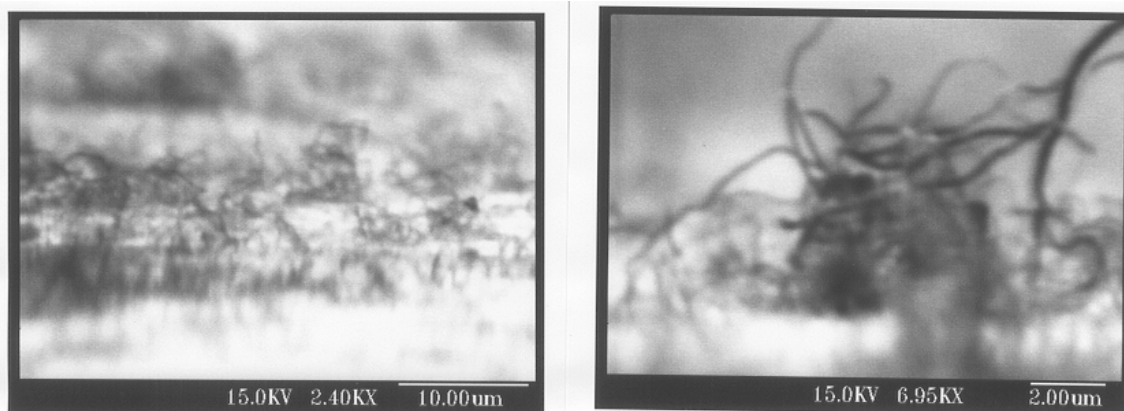
The SEM results show formation of dense layer of MWNT on the surface at 900 °C. At 800 °C, the formation of CNT is limited and most of the surface is covered with carbon. The results are given in Figure 8. It goes to prove that under sufficient number of trial and conditions of reaction, 900 °C is the suitable temperature for growth of MWNT.

**Table 2** Experimental conditions and results for samples kept out of the furnace between the reduction and reaction period.

Sample no.	Temp. °C	Reaction time (min)	Helium flow (ml/min)	Benzene flow (ml/min)	Extra He flow (ml/min)	Results
1	800	5	180	19.71 (7.31%)	50	No MWNT
2	900	5	180	19.71 (7.31%)	50	MWNT, C deposit
3	900	5	87.3	9.56 (5.73%)	50	MWNT
4	800	5	87.3	9.56 (5.73%)	50	No MWNT, C Deposit
5	900	5	180	19.71 (7.31%)	50	No MWNT



**SEM picture of sample treated at 800 °C**



**SEM picture of sample treated at 900 °C**

**Figure 8** Growth of carbon nanotubes occurs both at 800 and 900 °C from iron catalyst deposited from 40 mmol/L salt solutions. A dense growth of carbon nanotubes is observed throughout especially so for reaction at 900 °C

## **5 Reaction of FeCl<sub>2</sub> on SiO<sub>2</sub>/Si with Propylene as carbon source**

The reaction of benzene was successful with iron chloride as carbon source in growing multi walled carbon nanotubes. Sacco et al. [1, 2] has shown that growth of CNT takes place only on Fe<sub>3</sub>C (cementite) formed by saturation of iron with carbon under reaction conditions. The formation of cementite usually occurs at around 500 – 600 °C [3]. Benzene produced carbon nanotubes in the temperature range of 800 – 900 °C. Propylene is more reactive compared to benzene and its behavior of propylene as carbon source would be interesting study to compare the influence of different carbon source on growth of multi and single walled carbon nanotubes. The carbon source should vary the environment of production of carbon nanotubes and should give hint in to the growth of carbon nanotubes. The conditions employed were similar to the previous case of benzene. The catalyst was first reduced at 400 °C for 30 minutes in 4% H<sub>2</sub> flow, rest being helium. The second step was increasing the temperature of the system to 800 – 900 °C with a gradient of 70 °C/min while the catalyst is kept out of the furnace. As the temperature reaches the set reaction temperature, the reactor is pushed in again with the catalyst with helium flowing and a switch of the valve starts propylene and hydrogen flow rate maintained at respective concentration. This ensures that there is no lag in starting the flow rate of reactants as the temperature is reached. Propylene concentration and temperature were varied for growth of carbon nanotubes. Analysis and characterization were performed by Raman, AFM and TEM techniques. Following are the conditions and the results:

## 5.1 Reaction with 1.5% Propylene concentration at 900 °C

The following conditions were employed for the reduction and reaction of iron clusters for formation of carbon nanotubes.

### Reduction:

Temperature  $T_1 = 400\text{ °C}$       Time  $t_1 = 30\text{ minutes}$       Ramp  $R_1 = 4\text{ °C/min}$

Hydrogen flow rate = 9.3 ml/min (4.4 %)

Helium flow rate = 200 ml/min

### Reaction:

Temperature  $T_2 = 900\text{ °C}$       Time  $t_2 = 10\text{ minutes}$       Ramp  $R_2 = 70\text{ °C/min}$

Hydrogen flow rate = 9.3 ml/min (4.4 %)

Helium flow rate = 200 ml/min

Propylene flow rate = 3.1 ml/min (1.5%)

The AFM shows large agglomerated clusters with carbon deposit. The reaction treatment provides instability to the clusters present on the surface. Raman shows a faint indication of D or G band characteristic of structured carbon molecules indicating that few carbon nanotubes or similar structures were formed. Raman and AFM results are given in Figure 9.

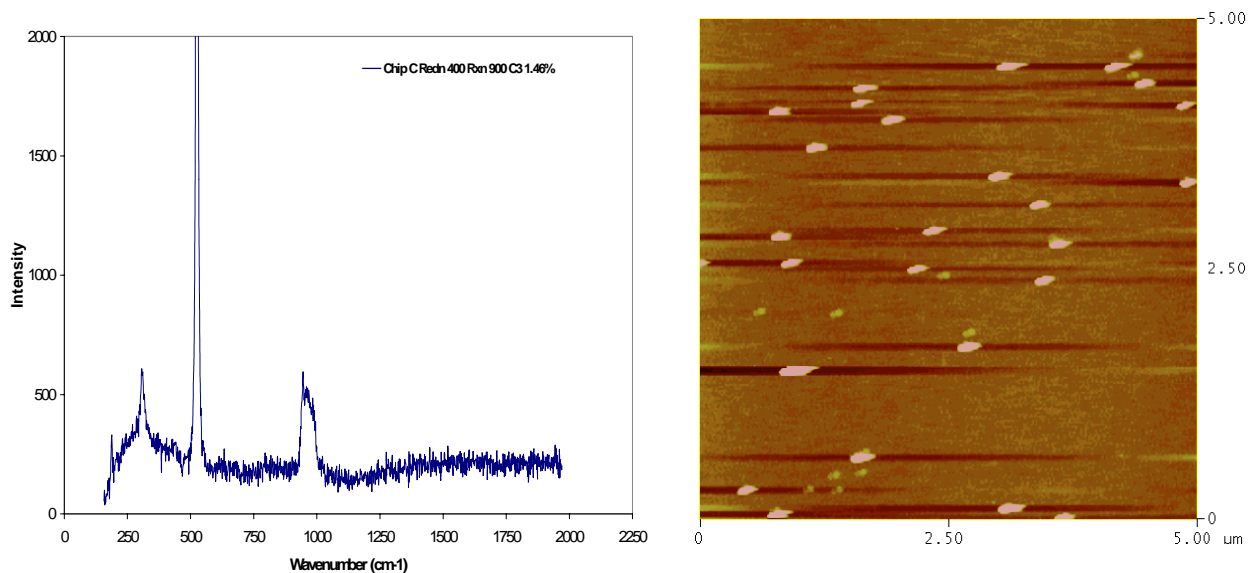


**Figure 9** The reaction of iron clusters at 900 °C after being reduced at 400 °C from iron chloride shows a large agglomeration of clusters. The average diameter is about 30 - 70 nm.

## 5.2 Reaction with 3% Propylene concentration at 900 °C

The reaction conditions were kept same except that the concentration of propylene was increased from 1.5 to 3%. The AFM measurement shows a large deposition of carbon present as huge semi-spheres. It is clear that cracking of excess of propylene takes place at 900 °C and deposits on the surface. Raman shows a weak signal for D and G band indicating presence of carbon but does not indicate anything definite (Figure 10).

The reaction conditions are as follows:

Temperature  $T_2 = 900\text{ °C}$       Time  $t_2 = 10\text{ minutes}$       Ramp  $R_2 = 70\text{ °C/min}$

Hydrogen flow rate = 9.3 ml/min (4.3 %)

Helium flow rate = 200 ml/min

Propylene flow rate = 6.5 ml/min (3.0 %)

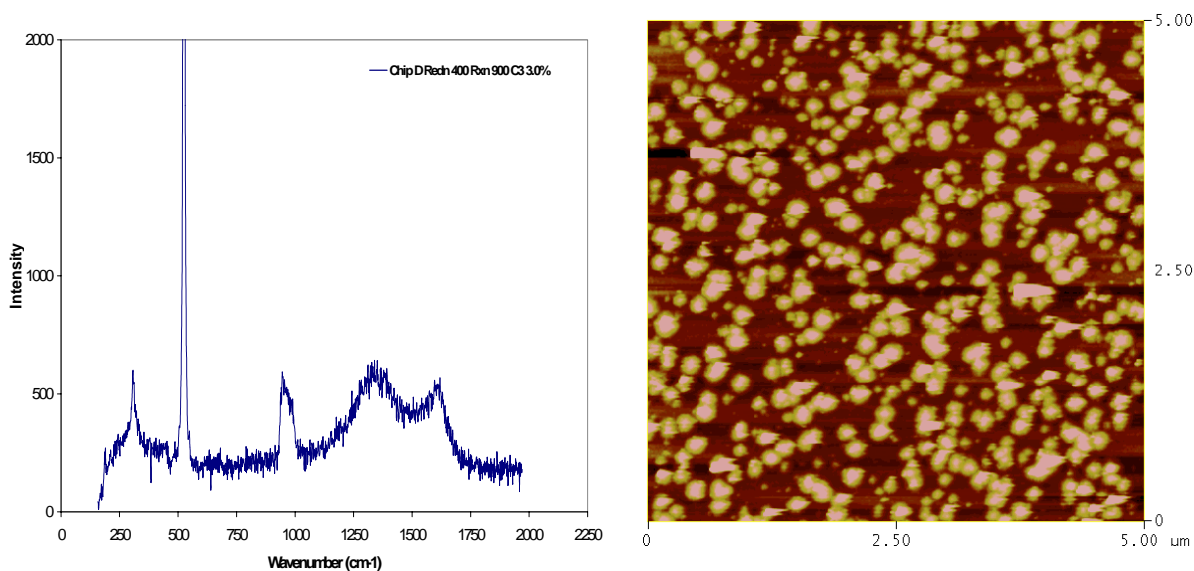


**Figure 10** High concentration of propylene leads to its homogenous pyrolysis resulting in deposition of high amount of carbon as observed by AFM. The Raman indicates the presence of carbon deposition.

### 5.3 Reaction with 3% Propylene concentration at 850 °C

To prevent homogenous pyrolysis of propylene, the temperature of reaction was reduced to 850 °C maintaining the concentration same as in chip d. The results are similar with large deposition of carbon on the surface though the sizes of deposited carbon hemispheres are small compared to previous of chip d. The lower temperature results in low deposition of carbon but does not yield any carbon nanotubes. Raman shows a very faint peak for carbon but does not indicate any growth of single walled carbon nanotubes. AFM also does not yield any information about it. The results are given in Figure 11 and the conditions are given below:

Temperature  $T_2 = 850\text{ °C}$       Time  $t_2 = 10\text{ minutes}$       Ramp  $R_2 = 70\text{ °C/min}$

Hydrogen flow rate = 9.3 ml/min (4.3 %)

Helium flow rate = 200 ml/min

Propylene flow rate = 6.5 ml/min (3.0 %)

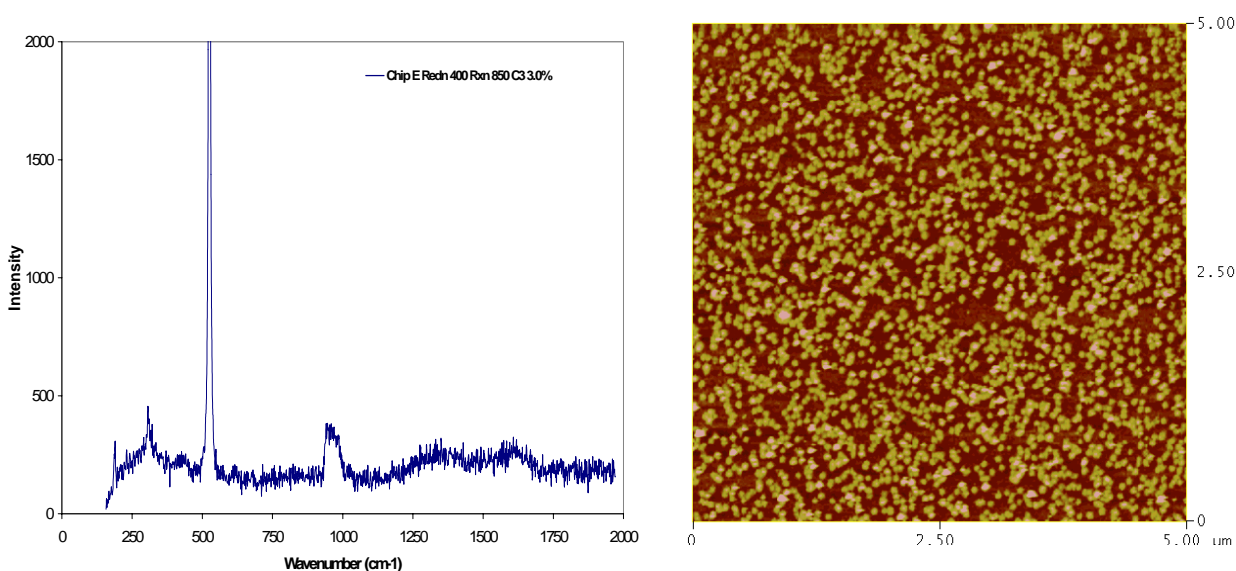


**Figure 11** Drop in reaction temperature does reduce the size of carbon deposited but also indicates that the pyrolysis of propylene does take place. The analysis does not conclusively prove about the nature of clusters after reaction conditions.

## 5.4 Reaction with 3% Propylene concentration at 800 °C

The temperature was even further reduced to 800 °C to obtain the pyrolysis temperature of propylene. At 800 °C of reaction temperature, almost no carbon is observed by Raman, which is characterized by presence of D and G band. AFM shows very diffuse picture of clusters. Results are given in Figure 12 and the conditions of reactions are given below:

Temperature  $T_2 = 800$  °C      Time  $t_2 = 10$  minutes      Ramp  $R_2 = 70$  °C/min

Hydrogen flow rate = 9.3 ml/min (4.3 %)

Helium flow rate = 200 ml/min

Propylene flow rate = 6.5 ml/min (3.0 %)

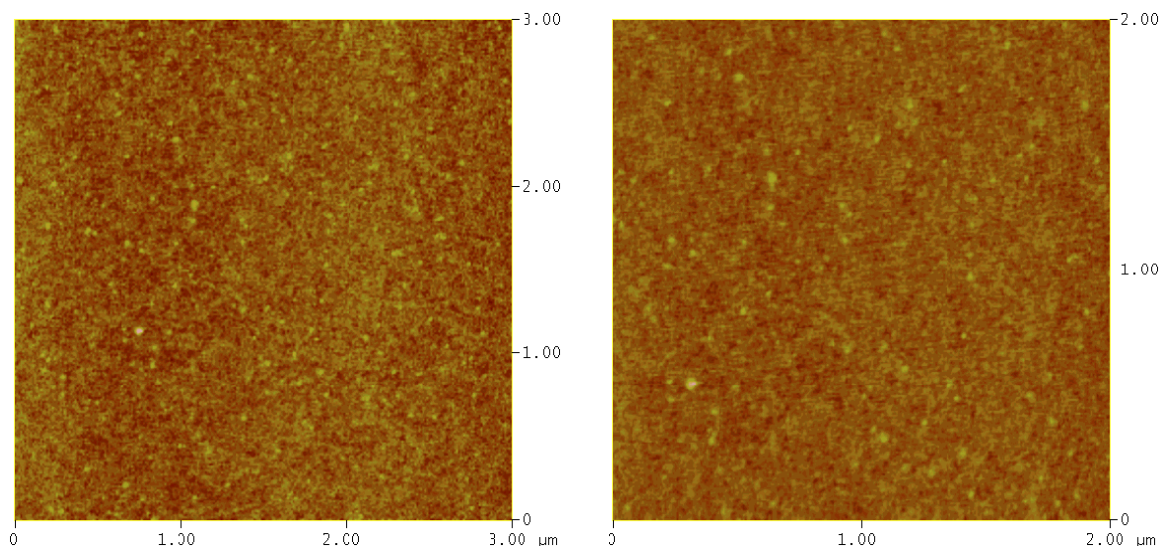


**Figure 12** The reaction at reduced temperature of 800 °C at 3% propylene concentration does not lead to formation of carbon nanotubes as observed by AFM. Very few clusters are seen in this case with heights considerably reduced (1 – 3 nm) compared to the ones spin coated with (4 – 7 nm).

## **5.5 TEM analysis of reaction performed at 900 °C with 3% Propylene concentration**

AFM though an effective technique in determining the status of the clusters after spin coating and reduction/reaction conditions is not useful for determining the yield of carbon nanotubes since most of the clusters do not seem to produce carbon nanotubes. They are either rendered inactive during reaction conditions or covered with carbon due to homogenous pyrolysis of carbon source. SEM shows the carbon nanotubes limited to the external surface only. It is not applicable for discerning the internal structure of carbon nanotubes. Bulk technique such as TEM was employed to ascertain the formation of carbon nanotubes and determine the internal and external structure properties. The sample selected was the one reacted with 3% propylene concentration at 900 °C. TEM images show a low amount of carbon nanotube production (Figure 13). The multi-wall of the structure is clearly visible. The structure also shows defects in form of twists in the wall and the incomplete formation of inner walls. Iron clusters are seen trapped within the carbon nanotubes and some are adhered to the base or tip of the nanotubes. The diameter of carbon nanotubes formed varies between 30 – 60 nm, a number that agrees with the agglomerated clusters on silica after reaction conditions. A lot of soot is also visible along with the nanotubes. In summary, formation of carbon nanotubes is not free of defects and is of large diameters as grown on silica/Si surface, the starting diameter being small.

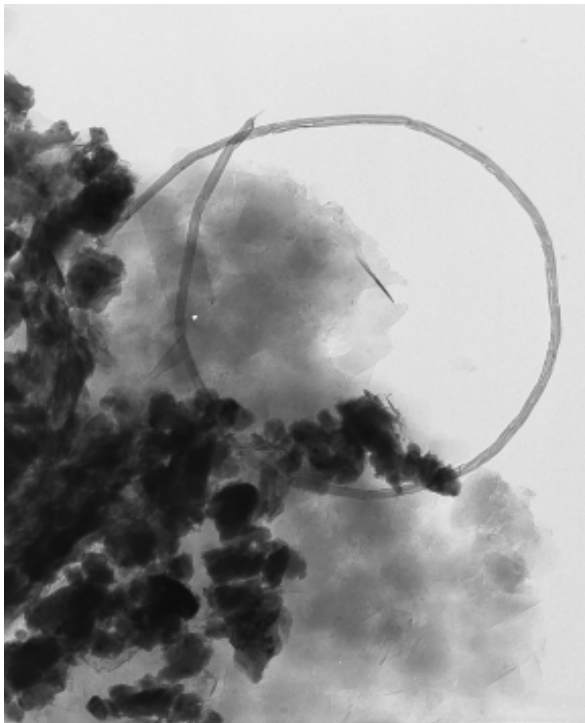
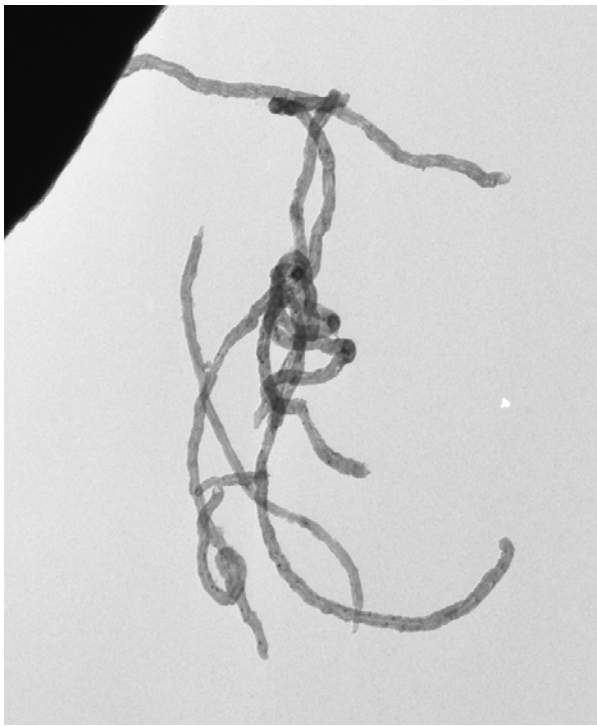


**Figure 13** TEM images of multi-walled carbon nanotubes grown on iron deposited on silica/Si wafer with propylene as carbon source. The diameter varied between 30 – 60 nm. Walls of the nanotubes do not show uniformity of structure showing many defects.

## 6 Discussion and Conclusion

- 1) MWNT are observed to grow at 900 °C with benzene and propylene as carbon source. The reaction temperature of 800 °C does not seem to reproduce the results for benzene while propylene cracks at this temperature.
- 2) The effect of keeping the sample within the reactor during the time between reduction and reaction and keeping it out of the reactor affects the size of the carbon nanotubes formed. The former results in larger tube size ranges.
- 3) Carbon nanotubes are produced in the size ranges of 100 - 130 nm for higher benzene to hydrogen ratio and reduces to 70 to 100 nm for reduced ratio. Below a particular flow rate of benzene (40 ml/min) with respect to hydrogen flow rate (20 ml/min) no carbon nanotubes were observed to form by SEM.
- 4) In all cases, carbon nanotubes growth was accompanied with formation of carbon.
- 5) A higher catalyst loading produces greater number of MWNT per unit area throughout the surface at 900 °C. A higher catalyst loading also produces MWNT at 800 °C but it is almost all covered with carbon.
- 6) It is thought necessary that as the catalyst clusters agglomerate, the temperature of formation of MWNT (900 °C with benzene) should be reduced. This is possible with using compounds that can crack at lower temperatures. The low temperature was employed with the case of propylene as the carbon source but resulted in the larger defects in the structure.

## 7 Reference

1. Sacco, A., Jr., Thacker, P., Chang, T. N. and Chiang, A. T. S., *Journal of Catalysis*, 85, (1984), p. 224.
2. Thacker, P. and Sacco, A., Jr., *Int. Congr. Catal., [Proc.]*, 8th, 2, (1985), p. II647.
3. Arabczyk, W., Konicki, W., Narkiewicz, U., Jasinska, I. and Kalucki, K., *Applied Catalysis A: General*, 266, (2004), p. 135.

# **Chapter 4**

## **Growth of Carbon Nanotubes on Ni catalyst on Silica/Si model catalyst**

## Table of Contents

<b>1</b>	<b>EXPERIMENTAL PROCEDURE TO PRODUCE CARBON NANOTUBES</b>	<b>126</b>
<b>2</b>	<b>SPIN COATING OF NiCl<sub>2</sub> ON SiO<sub>2</sub>/Si (100) SUPPORT AND BLANK REACTION</b>	<b>128</b>
2.1	AFM STUDIES ON SAMPLE SPIN COATED WITH NiCl <sub>2</sub>	128
2.2	REDUCTION AND REACTION OF NiCl <sub>2</sub> IN ABSENCE OF HYDROGEN AND BENZENE	129
2.3	REDUCTION AND REACTION OF NiCl <sub>2</sub> IN ABSENCE OF BENZENE	131
<b>3</b>	<b>PRODUCTION OF CARBON NANOTUBES ON NiCl<sub>2</sub></b>	<b>133</b>
3.1	1% BENZENE CONCENTRATION AT 900 °C	133
3.2	0.5% BENZENE CONCENTRATION AT 1000 °C	138
3.3	0.15% BENZENE CONCENTRATION AT 1000 °C	140
3.4	0.5% BENZENE AT 600 °C, 700 °C, 800 °C AND 1% BENZENE AT 800 °C	142
<b>4</b>	<b>CONCLUSION</b>	<b>144</b>

## List of Figures

- Figure 1 The reactor design for growth of carbon nanotubes. The design consists of flow tube reactor with reactants fed through manifold. .... 127
- Figure 2 AFM picture of NiCl<sub>2</sub> clusters formed by spin coating on silica/Si (100) surface shows well distributed clusters in good density. The diameter of the clusters is large (~40 – 60 nm)..... 128
- Figure 3 Ni salt after reduction at 300 °C and blank reaction at 900 °C in absence of hydrogen and benzene..... 130
- Figure 4 Reaction in presence of hydrogen reduces the density of cluster though it increases the height and diameter of clusters formed. The agglomeration under reaction conditions is clearly visible..... 132
- Figure 5 AFM image of Ni metal on silica/Si surface shows growth of structures after reaction at 900 °C. The structures are not easily resolved by AFM and needs SEM. .... 134
- Figure 6 SEM analysis shows a very good growth of carbon nanotubes on nickel catalyst. The reaction temperature employed were 900 °C with 1% benzene concentration..... 135
- Figure 7 Raman spectra of the sample reacted at 900 °C shows the presence of D and G band characteristic of the structured carbon and defects in the structured carbon respectively. Peak at 521 cm<sup>-1</sup> indicates the silicon from the substrate..... 136
- Figure 8 Raman spectra of sample obtained from reaction at 900 °C. No Si peak is observed in this case as the Raman is concentrated in the area of dense carbon nanotube growth..... 136

Figure 9 SEM pictures of CNT grown on Ni catalyst at 1000 °C for 20 minutes and 0.5% benzene concentration. The growth of carbon nanotubes is accompanied with deposition of carbonaceous materials seen at the base of the nanotubes growth. .... 139

Figure 10 SEM pictures of CNT grown on Ni catalyst at 1000 °C for 5 minutes and 0.15% benzene concentration. For such a low concentration of benzene, there was still homogenous decomposition of benzene leading to vapor deposition of carbon..... 141

## List of Tables

Table 1 Summary of growth of carbon nanotubes on nickel catalyst at different temperatures and benzene concentration. .... 143

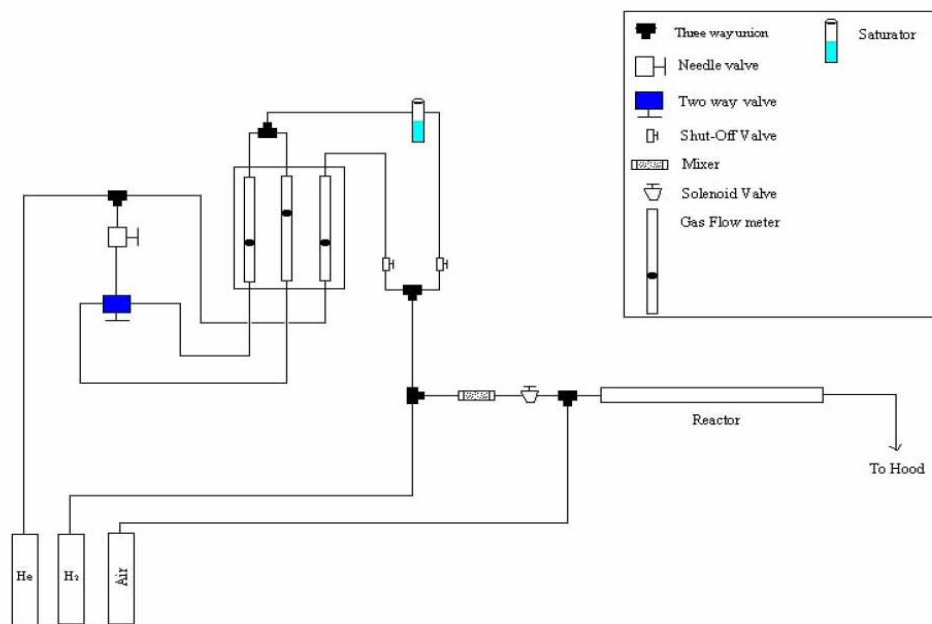
## 1 Experimental Procedure to produce carbon nanotubes

The procedure involves reduction of the  $\text{NiCl}_2$  catalyst with hydrogen at 300 °C and reaction of benzene over the metallic catalyst at elevated temperatures to produce carbon nanotubes. The experimental setup for the reaction is given in Figure 1.

The Silicon wafer spin coated with the catalyst salt is cut into small pieces. They are then placed on small quartz crucible. They are then inserted into the reaction tube made up of quartz placed in a furnace. The inlet to the reactor tube includes the connection of benzene, hydrogen and helium, which can be controlled individually with flow meters. This helps regulate the concentration of benzene and hydrogen in helium and the residence time in the reactor.

The wafer chip is inserted into the reactor tube placed inside the furnace. Flow of hydrogen diluted with Helium flow, is started. The temperature is ramped at a rate of 50 °C/min until it reaches 300 °C. The temperature is maintained at 300 °C for a period varying from 25 to 60 minutes. The temperature is increased to the required reaction temperature at a ramp of 50°C/min. The tube containing the wafer chip loaded with catalyst (sample) is removed out from the furnace by a sliding mechanical motion until the reaction temperature is reached to prevent sintering of the catalyst particles at high temperature. At reaction temperature, the sample is reinserted into the furnace. The sample is kept sealed inside the quartz tube during its sliding in and out of the furnace. The sample is maintained at the reaction temperature from 5 to 40 minutes. After this, the

tube containing the sample is withdrawn immediately and allowed to cool to room temperature. Once the tube cools down to room temperature, it is opened and the sample is removed out for study on AFM and SEM.



Reactor design for Carbon Nanotube production

**Figure 1** The reactor design for growth of carbon nanotubes. The design consists of flow tube reactor with reactants fed through manifold.

## 2 Spin coating of NiCl<sub>2</sub> on SiO<sub>2</sub>/Si (100) support and blank reaction

### 2.1 AFM studies on sample spin coated with NiCl<sub>2</sub>

In order to observe the effect of high temperatures on the catalyst particles deposited on the surface, we first conducted temperature increase study without carrying out reaction (not introducing benzene in the reaction chamber) but following the reaction procedure exactly as given in experimental section. The effect of hydrogen was studied by completely shutting off the hydrogen or allowing it to flow during reaction conditions. Concentration of NiCl<sub>2</sub> solutions was 4 mmol/L and was deposited on SiO<sub>2</sub>/Si flat surface at 6000 rpm using spin coating. The AFM pictures of salt clusters deposited after spin coating is shown in Fig. 2. The clusters of NiCl<sub>2</sub> are densely deposited with relative roughness of 1.515 nm. The size range of clusters varies from 5 – 10 nm in height and 40 – 60 nm in diameter.

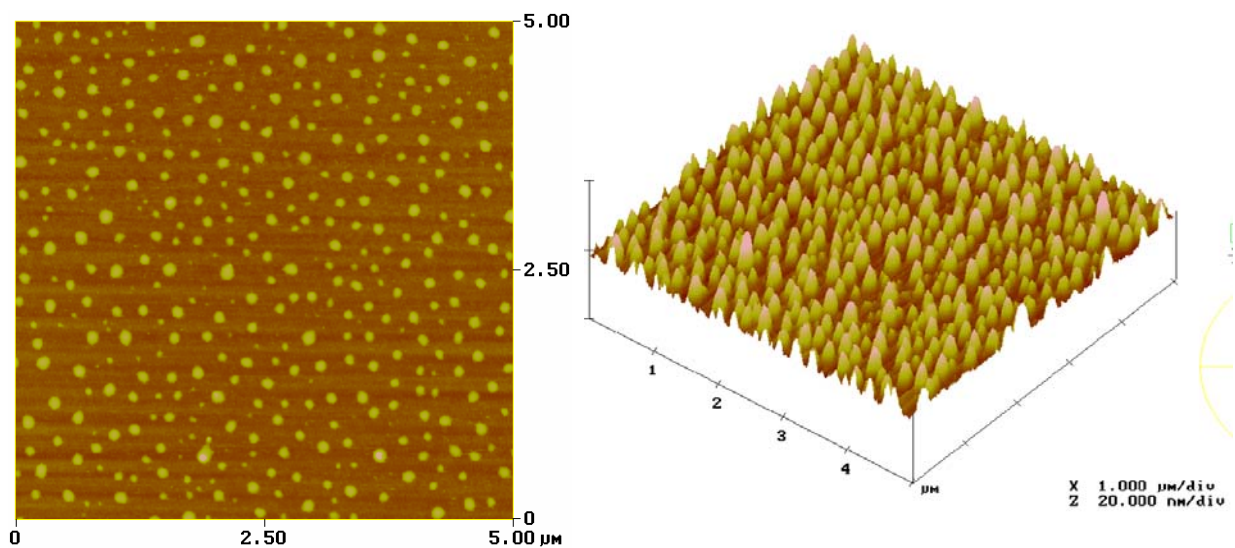


**Figure 2** AFM picture of NiCl<sub>2</sub> clusters formed by spin coating on silica/Si (100) surface shows well distributed clusters in good density. The diameter of the clusters is large (~40 – 60 nm).

## **2.2 Reduction and reaction of NiCl<sub>2</sub> in absence of hydrogen and benzene**

The reduction was carried at 300 °C in 1.6% H<sub>2</sub> concentration followed by blank reaction at 900 °C. By blank reaction, we imply no hydrogen or benzene was introduced in to the reaction chamber. The clusters were only heated in inert atmosphere to observe the agglomeration of clusters. The reduction and reaction conditions are given below:

### **Reduction Conditions:**

Temperature	: 300 °C
Time	: 25 minutes
Hydrogen flow rate	: 3.97 ml/min
Helium flow rate	: 250 ml/min

### **Reaction Conditions (without hydrogen):**

Temperature	: 900 °C
Time	: 40 minutes
Helium flow rate	: 475 ml/min
Hydrogen flow rate	: 0 ml/min
Benzene flow rate	: 0 ml/min

The flow of hydrogen was stopped as soon as temperature begins to rise above 300 °C. We observe by AFM (Figure 3) that the cluster of NiCl<sub>2</sub> reduces in size. The relative roughness of NiCl<sub>2</sub> is 0.863 nm. The relative roughness indicates that the number of particles of NiCl<sub>2</sub> is greatly reduced in size on the support surface. The AFM scan size is 5 μm x 5 μm.

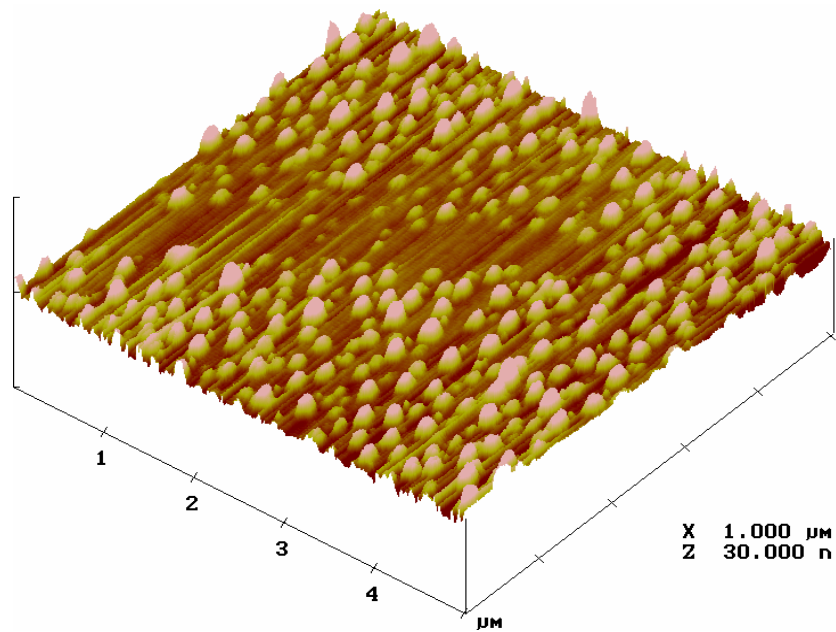


**Figure 3** Ni salt after reduction at 300 °C and blank reaction at 900 °C in absence of hydrogen and benzene

### 2.3 Reduction and Reaction of NiCl<sub>2</sub> in absence of benzene

Reaction carried in absence of hydrogen indicated that clusters though reduced in size were still present on the surface. To observe the effect of hydrogen, the model catalyst was reduced in hydrogen at conditions as mentioned before in section 2.2. Reaction was carried at 900 °C with hydrogen flow on while benzene flow was not started. This would help us to understand the role played by each reactant on the size of clusters and their stability under reaction conditions. The reaction conditions are given below:

#### Reaction Conditions (With hydrogen)

Temperature	: 900 °C
Time	: 40 minutes
Helium flowrate	: 475 ml/min
Hydrogen flowrate	: 3.97 ml/min
Benzene flowrate	: 0 ml/min

Hydrogen was allowed to flow after 300 °C until the reaction at 900 °C was over. The AFM picture of the samples is given in Figure 4. The relative roughness of NiCl<sub>2</sub> is 1.070 nm. The cluster density and size is maintained on the surface when compared with the reaction performed in the absence of hydrogen. The overall density is reduced compared to spin coating. The height of clusters increases to 10 – 15 nm and the diameter increases to 60 – 100 nm, indicating agglomeration under reaction conditions.

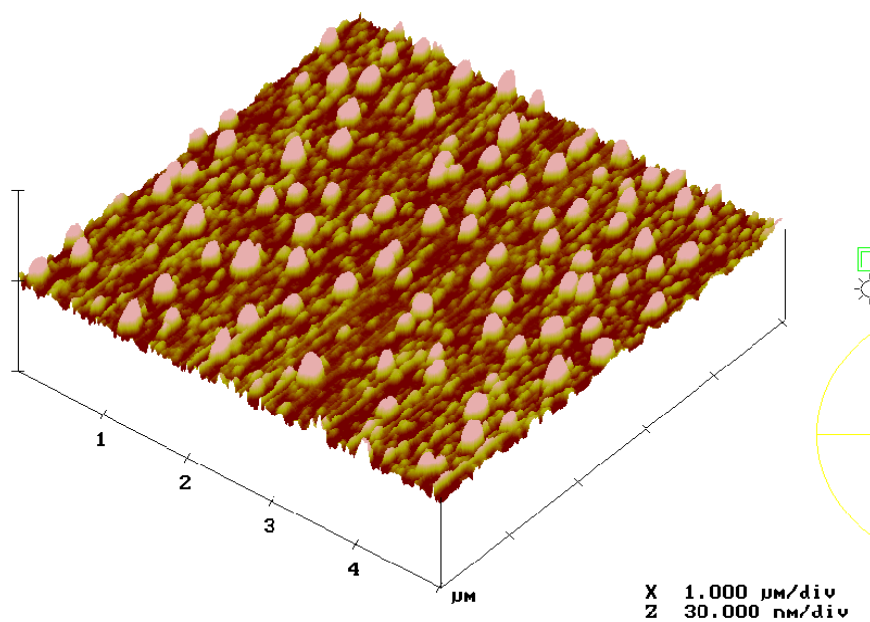


**Figure 4** Reaction in presence of hydrogen reduces the density of cluster though it increases the height and diameter of clusters formed. The agglomeration under reaction conditions is clearly visible.

### 3 Production of Carbon Nanotubes on NiCl<sub>2</sub>

The procedure for reaction is given above. The reaction was carried in the presence of hydrogen and low benzene concentration. The conditions and the corresponding SEM pictures are given in this section.

#### 3.1 1% Benzene concentration at 900 °C

##### Reduction conditions:

Temperature	: 300 °C
Time	: 25 minutes
Helium flowrate	: 250 ml/min
Hydrogen flowrate	: 3.97 ml/min
Benzene flowrate	: 0 ml/min

##### Reaction Conditions:

Temperature	: 900 °C
Time	: 40 minutes
Hydrogen flowrate	: 3.97 ml/min
Helium flowrate (saturator)	: 48 ml/min
Helium flowrate (Excess)	: 472 ml/min
Benzene flowrate	: 5.26 ml/min

AFM and SEM pictures of the samples were taken. The AFM results are given in Fig. 5 for reaction on Ni clusters. The CNT being labile would be easily deformed by the AFM tip and hence exact nanotubes at this stage of experimentation cannot be observed very clearly. The picture shows elongated structures growing from the particles. The SEM pictures on Ni catalyst (Figure 6) show a good growth of Carbon nanotubes (CNT). The size of carbon nanotubes vary from 100 – 150 nm.

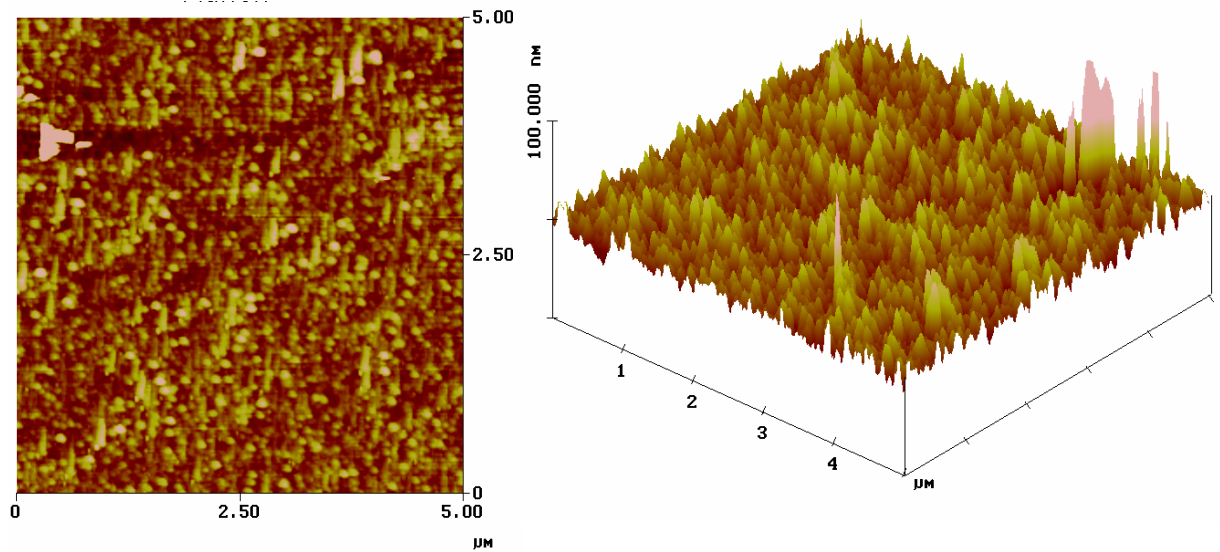


**Figure 5** AFM image of Ni metal on silica/Si surface shows growth of structures after reaction at 900 °C. The structures are not easily resolved by AFM and needs SEM.

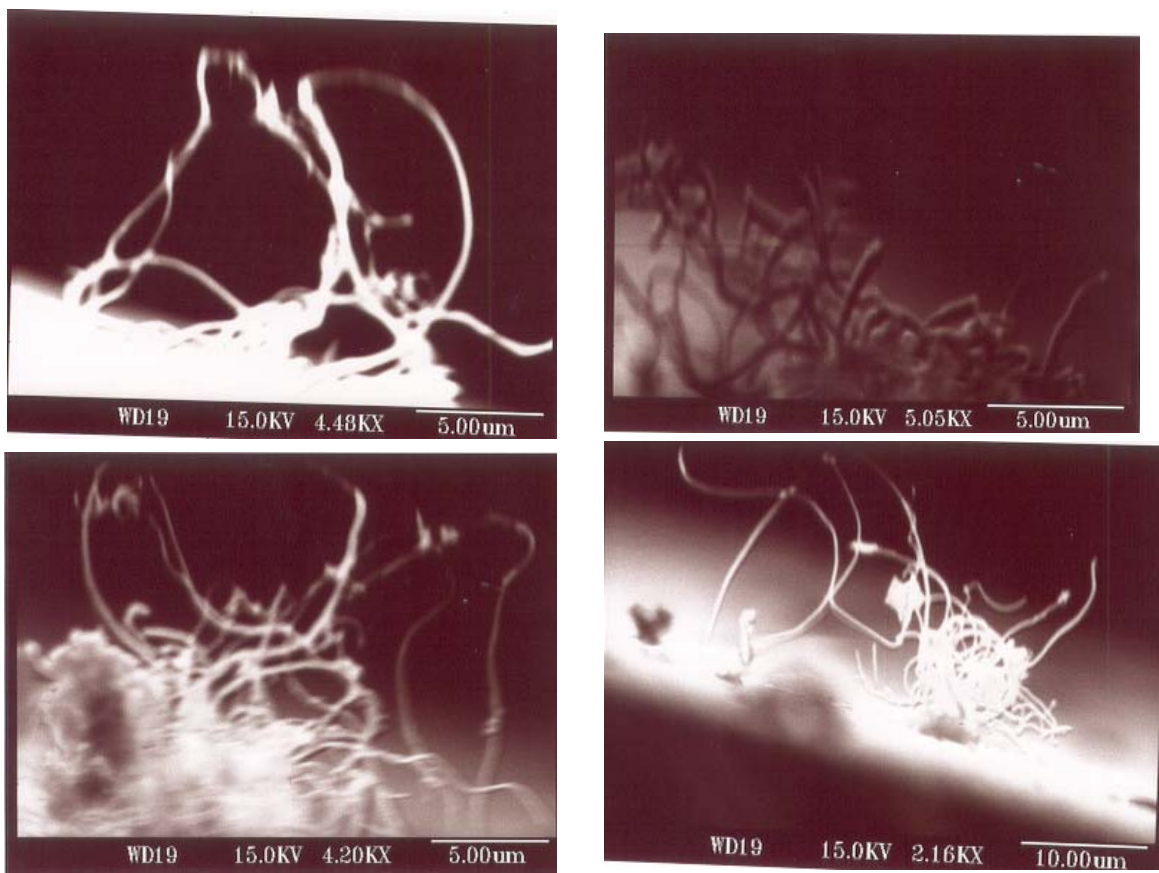


**Figure 6** SEM analysis shows a very good growth of carbon nanotubes on nickel catalyst. The reaction temperature employed were 900 °C with 1% benzene concentration

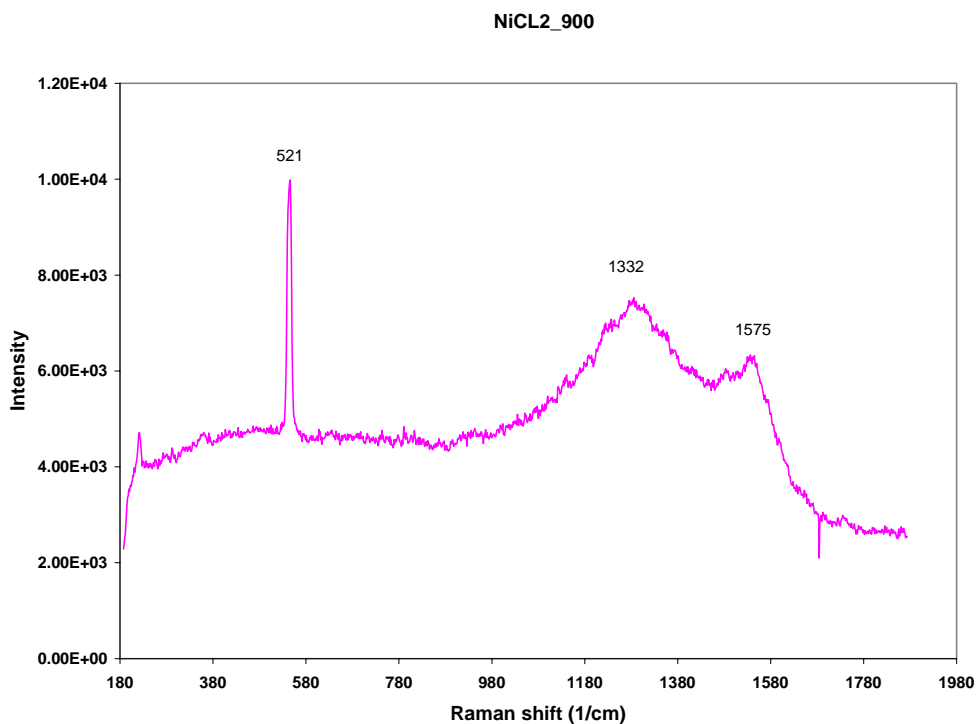


**Figure 7** Raman spectra of the sample reacted at 900 °C shows the presence of D and G band characteristic of the structured carbon and defects in the structured carbon respectively. Peak at 521  $\text{cm}^{-1}$  indicates the silicon from the substrate

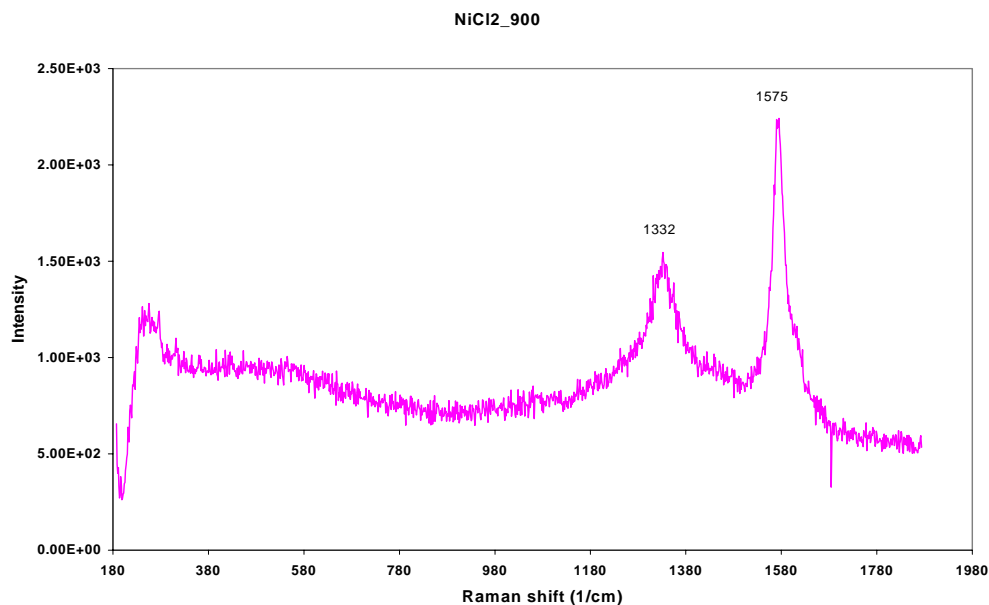


**Figure 8** Raman spectra of sample obtained from reaction at 900 °C. No Si peak is observed in this case as the Raman is concentrated in the area of dense carbon nanotube growth.

We also produce here the Raman spectra of the samples with reactions performed at above conditions. The Raman spectra show the presence of structured carbon with peaks at  $1332\text{ cm}^{-1}$  and  $1575\text{ cm}^{-1}$  (Figure 7 and 8) and that of silicon at  $521\text{ cm}^{-1}$  (Figure 7). The Raman spectra are obtained at a very fine position on the given sample. The Raman spectra of Figure 7 provide us with the information that at the position the spectra were taken, the surface was not completely covered with carbon structures and Si was exposed. The presence of G band is indicative of structured carbon such as carbon nanotubes. The presence of D band is indicative of defects in the nanotubes including the formation of multi-walled carbon nanotubes that may have their layers not aligned with each other. In Figure 8, the defects are not large in number since D band intensity is small compared to the G band.

### 3.2 0.5% benzene concentration at 1000 °C

Reaction at 900 °C did produce a high carbonaceous product as observed by SEM and also by Raman spectra. As reported in literature, the crystallinity and the defects in carbon nanotubes decrease with increase in the temperature of reaction. Most of the laser ablation and arc-discharge technique employ a large temperature (1100 – 1300 °C) for production of single walled carbon nanotubes and also defect free multi-walled carbon nanotubes. Accordingly we performed reaction at high temperature (1000 °C) and to prevent vapor deposition of carbon, we employed low concentration of benzene (0.5%).

#### **Reduction Conditions:**

Temperature	: 300 °C
Time	: 25 minutes
Helium flowrate	: 250 ml/min
Hydrogen flowrate	: 3.97 ml/min

#### **Reaction Conditions:**

Temperature	: 1000 °C
Time	: 20 minutes
Hydrogen flowrate	: 3.97 ml/min
Helium flowrate (saturator)	: 20 ml/min
Helium flowrate (Excess)	: 412 ml/min
Benzene flowrate	: 2.19 ml/min

SEM pictures (Figure 9) show carbon nanotubes produced on Ni catalyst. The average size of the CNT bundle was around 150 – 300 nm. The SEM picture shows presence of large deposition of carbon. Raman shows presence of carbonaceous material and defects in carbon nanotubes. The large diameter is most likely because of the deposition of carbon on the nanotubes themselves from homogenous decomposition of benzene.

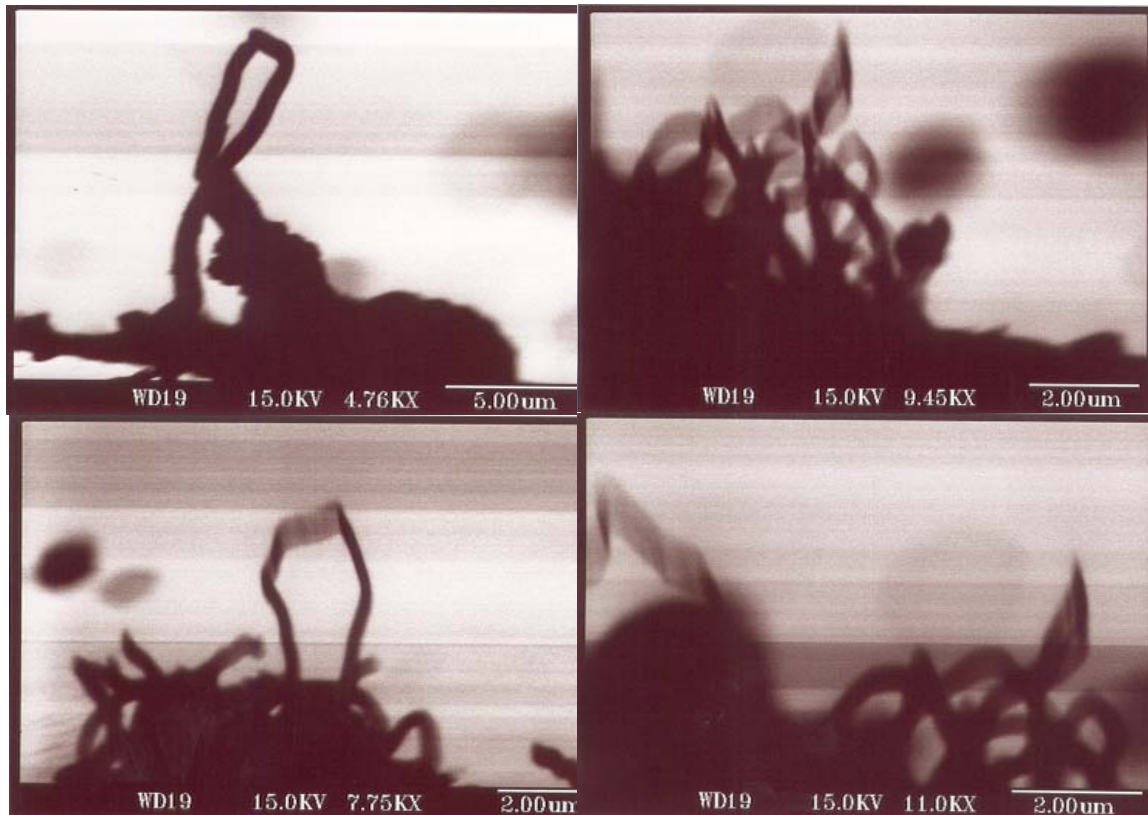


**Figure 9** SEM pictures of CNT grown on Ni catalyst at 1000 °C for 20 minutes and 0.5% benzene concentration. The growth of carbon nanotubes is accompanied with deposition of carbonaceous materials seen at the base of the nanotubes growth.

### 3.3 0.15% Benzene concentration at 1000 °C

Presence of large amount of carbon was observed along with formation of carbon nanotubes by SEM, at conditions given in section 3.2, which may be attributed to the concentration of benzene being high for temperature of reactions and also the larger time of reaction. The concentration of benzene was further reduced to 0.15% from 0.5% and the reaction time was reduced from 20 minutes to 5 minutes.

#### **Reduction Conditions:**

Temperature	: 300 °C
Time	: 25 minutes
Helium flowrate	: 250 ml/min
Hydrogen flowrate	: 3.97 ml/min

#### **Reaction Conditions:**

Temperature	: 1000 °C
Time	: 5 minutes
Hydrogen flowrate	: 3.97 ml/min
Helium flowrate (saturator)	: 15 ml/min
Helium flowrate (Excess)	: 1079 ml/min
Benzene flowrate	: 1.643 ml/min

SEM pictures show formation of carbon nanotubes on Ni catalyst (Figure 10). There is a large amount of carbon deposits observed along with the tubes and some is

seen attached to the tubes themselves. The average diameter of the bundles is about 250 – 500 nm. The carbon nanotubes were observed to grow uniformly throughout the surface. We observed that low temperature of 900 °C was necessary for formation of clean carbon nanotubes. At higher temperature, there is homogenous decomposition of benzene for concentration of benzene as low as 0.15% leading for deposition of carbon not on the surface but also on the tubes themselves. Also the size of tubes formed is large. It was not possible for us to go to a concentration lower than 0.15% given the limitation of equipment.

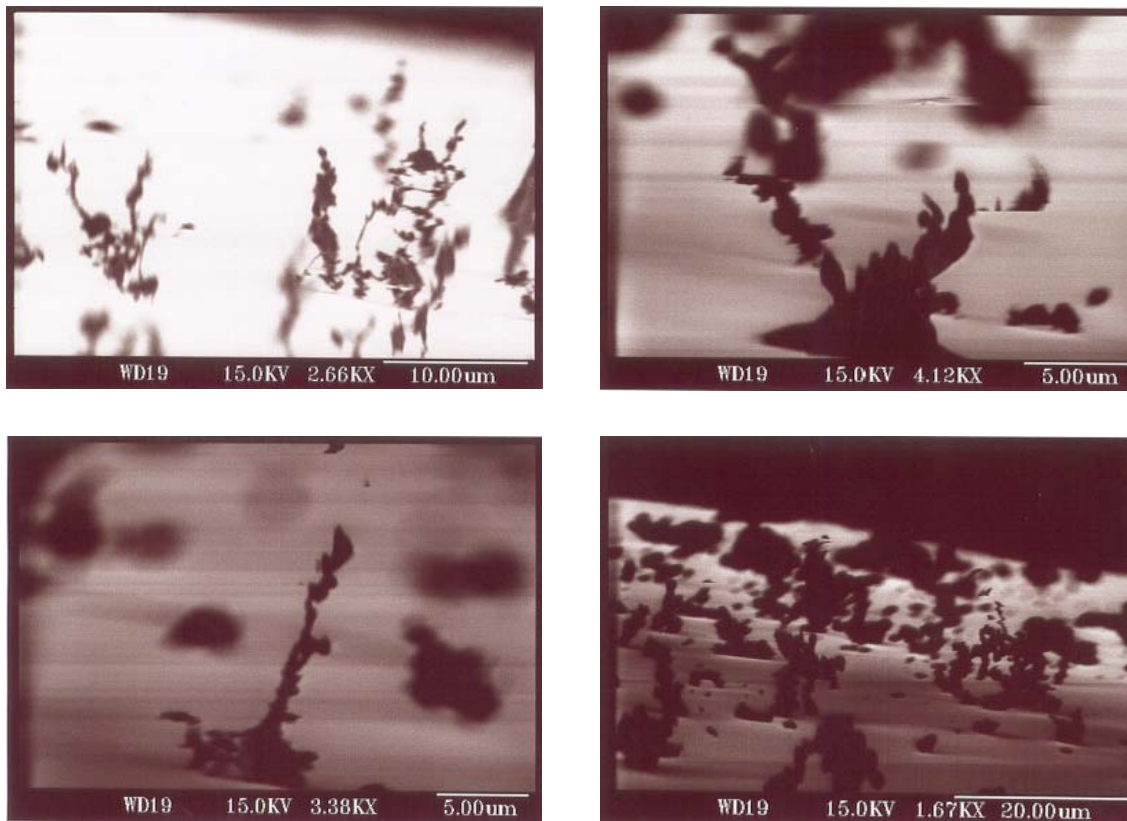


**Figure 10** SEM pictures of CNT grown on Ni catalyst at 1000 °C for 5 minutes and 0.15% benzene concentration. For such a low concentration of benzene, there was still homogenous decomposition of benzene leading to vapor deposition of carbon.

### **3.4 0.5% benzene at 600 °C, 700 °C, 800 °C and 1% benzene at 800 °C.**

It was also necessary to ascertain whether there was formation of carbon nanotubes at temperatures below 900 °C as it becomes very uneconomical of their production on industrial scale. It will also help us find the optimum conditions. We employed 0.5% - 1% concentration of benzene and temperature was varied from 600 °C – 800 °C. The conditions of reduction and reaction are given below:

#### **Reduction Conditions:**

Temperature	: 300 °C
Time	: 25 minutes
Helium flowrate	: 250 ml/min
Hydrogen flowrate	: 3.97 ml/min

#### **Reaction Conditions:**

Temperature	: 600 °C, 700 °C, and 800 °C
Time	: 40 minutes
Hydrogen flowrate	: 3.97 ml/min
Helium flowrate (saturator)	: 20 ml/min (40 ml/min for 1.0% benzene at 800 °C)
Helium flowrate (Excess)	: 412.59 ml/min (389.62 ml/min for 1.0% benzene at 800 °C)
Benzene flowrate	: 2.19 ml/min (4.38 ml/min for 1.0% benzene at 800 °C)

SEM pictures for all cases showed no presence of Carbon structures except for amorphous deposit of carbon on the surface. From the reaction conditions given in section 3.1 of this report, it becomes fairly evident that the formation of carbon nanotubes does not start at temperatures below 900 °C at the above-mentioned conditions. All of the results obtained for nickel catalyst is compiled in Table 1.

**Table 1** Summary of growth of carbon nanotubes on nickel catalyst at different temperatures and benzene concentration.

Temperature (°C)	Benzene conc. (%)	Time of reaction (min)	Total flow rate (ml/min)	Results	Remarks
600, 700, 800	0.5	40	438.16	No CNT	-
800	1.0	40	438.16	No CNT	-
900	1.0	40	529.23	CNT	-
1000	0.5	20	438.16	CNT	C deposit
1000	0.15	5	1100	CNT	C deposit

## 4 Conclusion

- 1) Carbon nanotube growth on nickel catalyst is observed at temperatures of 900 °C and above.
- 2) Benzene homogenously decomposes at concentrations as low as 0.15% at temperature of 1000 °C. Deposition of carbon takes place not only on the surface but on the nanotubes themselves and thereby may lead to apparent larger size of their diameters.
- 3) Decreasing the concentration of benzene does not prevent the thermal vapor decomposition of carbon on nanotubes. It is acknowledged that at 1000 °C, homogenous decomposition of benzene takes place along with the catalytic decomposition for formation of carbon nanotubes.
- 4) No growth of carbon nanotubes occur at temperatures below 900 °C indicating the conditions obtained in section 3.1 are the optimum ones for growing multi-walled carbon nanotubes on nickel catalyst.
- 5) The size of carbon nanotubes formed is large in general (about 100 – 150 nm) at optimum conditions of 900 °C and 1% benzene concentration. The diameter of clusters was in the range of 40 – 60 nm after spin coating indicating agglomeration of clusters under reaction conditions.
- 6) No growth of single walled carbon nanotubes is observed by Raman spectroscopy under our scope of experiments conducted.

# **Chapter 5**

## **Growth and Study of Multi-walled Carbon Nanotubes from Ferrocene**

## Table of Content

Growth and Study of Multi-walled Carbon Nanotubes from Ferrocene .....	145
1 Background.....	150
2 Experimental.....	153
3 Results and Discussion .....	155
4 TEM analysis .....	161
5 Oxidation of sample covered with carbon nanotubes grown from ferrocene.....	163
6 Discussion and Conclusion.....	166
7 Reference .....	168

## List of Figures

- Figure 1 Reactor design for the ferrocene/benzene inlet and reaction on silica surface. 153
- Figure 2 SEM image of sample obtained at conditions in experiment no. 3. We observe good amount of MWNT arising out of amorphous carbon. Reaction was carried at 700 °C for 5 minutes. .... 156
- Figure 3 Raman spectra of sample obtained with experiment no. 3. A shoulder in the peak at around 1600 indicates structured molecule of carbon such as graphite or MWNT. .... 156
- Figure 4 SEM image of the sample obtained at conditions of experiment no. 5. A single MWNT had an average diameter of about 30-50 nm. .... 157
- Figure 5 Raman spectra of sample obtained at conditions of experiment no. 5, reaction performed at 700 °C at 13.29%. .... 157
- Figure 6 SEM image of sample obtained at conditions of experiment no. 8. The reaction temperature was 900 °C and liquid benzene flow was 1.824 ml/hr. Hydrogen concentration was 10%. .... 159
- Figure 7 The D and G band are clearly seen with the ratio to be about 0.4 as compared to 1.0 seen at lower temperatures. The lower D/G intensity ratio indicates that the MWNT formed are low on defects and more crystalline. .... 160
- Figure 8 TEM images of carbon nanotubes produced at 900 °C show production of large amount of carbon nanotubes (left). The enlarged image (right) show tubular structures made of multi wall of carbon and hollow core at the center. The diameter of nanotubes varies from 10 – 30 nm. .... 162

Figure 9 AFM image of substrate surface taken after oxidation of all forms of carbon for sample obtained from conditions in experiment no. 5. We observe distinct peaks on the surface indicating agglomeration of Fe catalyst. .... 164

Figure 10 Raman spectra of sample from experiment no. 5 oxidized in air. Spectra show the presence of Iron oxide and very low peak of C, which is smaller than the silica peak..... 164

Figure 11 SEM image of sample treated with benzene after oxidation and reduction of sample containing CNT. SEM shows only amorphous carbon and few pockets of formation of carbon nanotubes indicating significance of the role played by ferrocene. .... 165

## List of Tables

Table 1 Conditions for growth of carbon nanotubes from ferrocene and benzene.....	154
---	-----

# 1 Background

The main application of carbon nanotubes envisaged for the future is in field emission transistor (FET) which imposes that the nanotubes should be freely standing on the surface of the substrate [1, 2]. The nanotubes should be present in large amount with tightly packed density. The second advantage of well packed and aligned carbon nanotubes is in the storage of hydrogen that may help in the development of alternative fuel sources. The popular technique to grow well-aligned multi-walled carbon nanotubes is from organometallic precursor such as ferrocene, nickelocene, or cobaltocene (metallocene). Single walled carbon nanotubes have been synthesized from organometallic precursor at relatively high temperature and dilute concentration of carbon source. It is also easier to separate the nanotubes from the substrate by just scraping the nanotubes off without any of the expensive separation procedures. For the growth of carbon nanotubes, both the carbon source and the metallic nano-particle are required in a catalytic growth mode. Metallocene provides the dual requirement of catalyst and carbon source in a single molecule for CNT growth since it contains both the metal particle sandwiched between two organic ring molecules. The first carbon nanotubes synthesized by this route was by C. N. R. Rao's group [3, 4]. This work was followed with excellent work in this area [5, 6, 7, 8]. The other advantage of this method is that the growth of carbon nanotubes takes place on selected sites only. It is shown to grow only on silica support (model) but will not grow on silicon surface [8, 9]. It is easy to pattern a silica/Si wafer such that silica surface in desired pattern are created on top of silicon wafer by plasma etching, lithography or any other suitable technique. Carbon nanotubes grown from ferrocene will selectively grow on the silica surface and not on the

silicon surface resulting in the patterned nanotubes, which has potential application in nanofabrication of components involving carbon nanotubes. The reason for growth of carbon nanotubes on silica as compared to silicon is the reaction of silicon with iron to form corresponding iron silicide while the iron clusters are stable on silica under the short reaction time [10].

The experimental set up employs a two stage furnace reactor where the first furnace is maintained at  $\sim 180$  °C to evaporate the metallocene molecule in to the second furnace maintained at 900 °C. Pyrolysis of the metallocene occurs in the second furnace producing multi-walled carbon nanotubes. The system is kept under reducing atmosphere with presence of hydrogen and diluted with argon or helium. To increase the yield of carbon nanotubes, another additional carbon source could also be employed along with the metallocene. The concentration of carbon source and the metallocene would in this case help to decide the diameter and properties of carbon nanotubes formed.

In our case, study of growth of carbon nanotubes through ferrocene provided a unique opportunity to investigate their production conditions and their growth mechanism. The growth of carbon nanotubes easily occurs on silica or quartz material and especially so on model silica/Si support. The growth of multi-walled carbon nanotubes on model silica support will hopefully provide us with insights in to some of the questions regarding the model catalyst produced by spin coating. Ferrocene was chosen as the metallocene precursor and benzene was employed as the carbon source. The reaction temperature was varied between 600 – 900 °C in presence of hydrogen and

helium as inert diluent. Ferrocene is dissolved in to benzene and introduced in to the reactor where it decomposes to form iron clusters surrounded by carbon atmosphere resulting in the formation of carbon nanotubes. Ferrocene cracks at temperatures above 550 °C. The catalyst in this form of reaction is produced in-situ and hence more effective in production of carbon nanotubes and hence the large yield as compared to the model catalyst. The following objectives were maintained in current study:

- a) Produce well-aligned Carbon nanotubes.
- b) Remove CNT's from the surface by oxidation and study the nature of catalyst deposited on the surface.
- c) Reproduce conditions that lead to the production of CNT using conventional spin-coating experiment, which give better control over regulating catalyst size and structure.

## 2 Experimental

The ferrocene was dissolved in benzene to form 5% solution by weight. Ferrocene in benzene was injected in to the system using syringe pump that could be adjusted to give variable flow rate. The system was optimized for various flow rates of benzene. The hydrogen concentration was kept constant at 10% of the total flow of helium. The experimental setup is given in Figure 1. The reactor consists of a quartz tube kept in a furnace maintained at the reaction temperature. The sample consists of silicon wafer calcined at 750 °C for 24 hours to form about 80 nm of silica. It is placed inside the furnace inside the quartz tube and maintained at the temperature of reaction. The tube of quartz preceding the sample and kept outside the furnace is heated with a heating tape to 175 °C. A small stainless steel tube of 1/16<sup>th</sup> of an inch is inserted in to the main reactor quartz tube (diameter of tube is 0.5”) to introduce the ferrocene/benzene mixture.

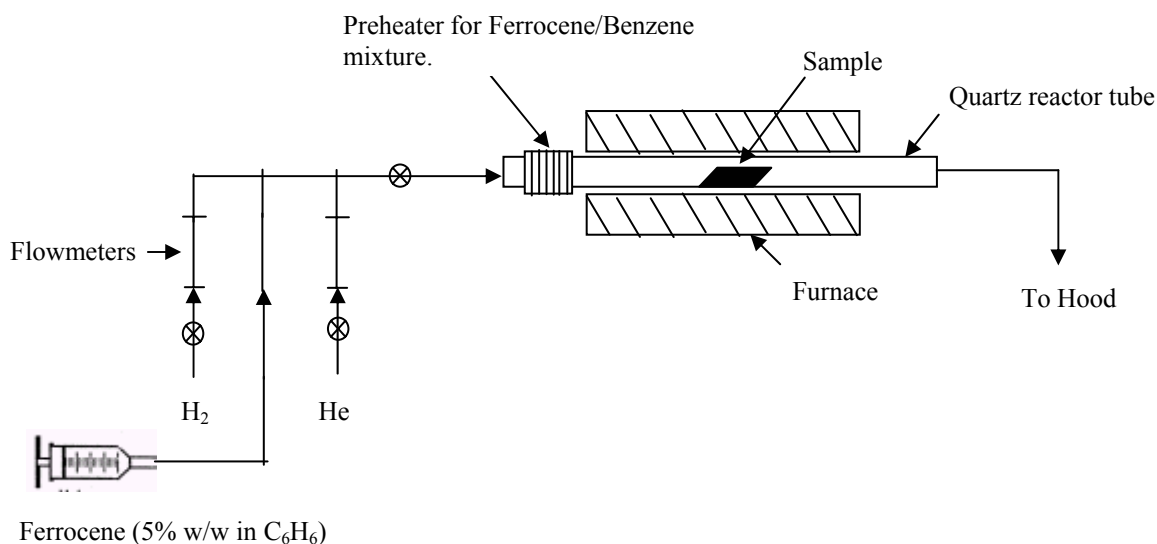


**Figure 1** Reactor design for the ferrocene/benzene inlet and reaction on silica surface

Several coils are made of this tube that is actually heated by the external heating coil to 175 °C. The reaction conditions employed for the study are summarized in Table 1. The ferrocene evaporates at 160 °C while benzene evaporates at 80 °C. Both the vapor mixtures are mixed intimately with hydrogen and helium and carried to the furnace where it undergoes decomposition and catalytic reaction to form carbon nanotubes.

**Table 1** Conditions for growth of carbon nanotubes from ferrocene and benzene.

Expt.	Temp (°C)	Time (min)	C <sub>6</sub> H <sub>6</sub> Flow (ml/hr)	Helium flow	H <sub>2</sub> flow	C <sub>6</sub> H <sub>6</sub> conc. (%)	Results
1	700	15	4.44	650	20 (3%)	4.38	Huge C deposit
2	700	5	1.33	180	20 (10%)	4.39	No C deposit
3	700	5	1.824	180	20 (10%)	6.46	Some C deposit. A peak in the Raman
4	700	5	2.987	180	20 (10%)	9.35	C deposit. Peak in the Raman
5	700	5	4.44	180	20 (10%)	13.29	- do -
6	600	5	1.824	180	20 (10%)	6.46	No C observed. No C peak in Raman.
7	800	5	1.824	180	20 (10%)	6.46	C deposit. Peak in the Raman
8	900	5	1.824	180	20 (10%)	6.46	- do -
9	1000	5	1.824	180	20 (10%)	6.46	- do -

### 3 Results and Discussion

The optimum flow rate of ferrocene/benzene mixture to be used for CNT growth was obtained to be 1.824 ml/hr of liquid flow from various reactions carried at 700 °C. At this flow rate of benzene, the temperature was varied to observe for results in terms of well-aligned CNT. We observe that 900 °C produces well-aligned CNT.

Carbon formation occurs at a temperature of 700 °C and above. A Raman peaks at 1325  $\text{cm}^{-1}$  (D band) and 1600  $\text{cm}^{-1}$  (G band) approximately indicates the presence of some form of carbon. In certain Raman spectra (Experiment # 3, 4, 5, less distinct in 7 and 8, Table 1) show a shoulder on the peak at 1600  $\text{cm}^{-1}$  indicating presence of structured material such as graphite. The samples were also analyzed using SEM.

Experiment 1 was only a trial setup that indicated the growth of huge carbon at 4.4% benzene concentration and 3% hydrogen concentration. SEM showed presence of MWNT growing all over the surface and also a huge deposit of amorphous carbon. Experiment 2 shows the same conditions but a higher percentage of hydrogen concentration. No MWNT or carbon deposits were observed by SEM and Raman spectroscopy. Experiment 3 had increased concentration of benzene and showed substantial growth of MWNT and some amorphous carbon. A representative SEM image is given in Figure 2. A zoom in on a single MWNT shows a diameter of about 30 – 50 nm. Figure 3 shows corresponding Raman spectra. Both D and G band are clearly visible in this case. The ratio of intensity of both the peaks is approximately 1.0.

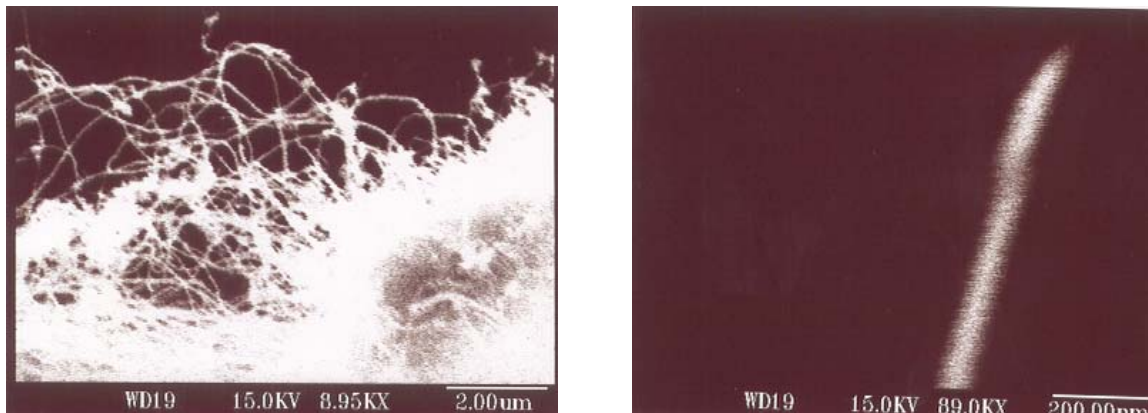


**Figure 2** SEM image of sample obtained at conditions in experiment no. 3. We observe good amount of MWNT arising out of amorphous carbon. Reaction was carried at 700 °C for 5 minutes.

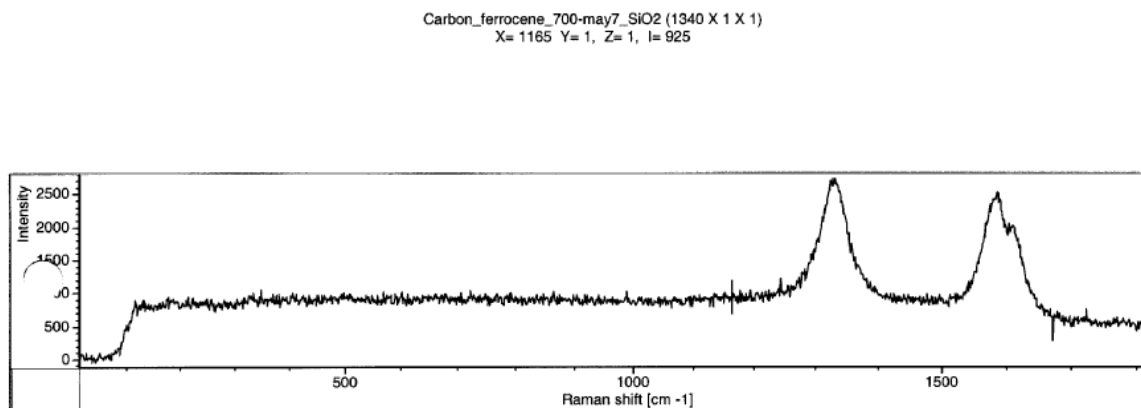


**Figure 3** Raman spectra of sample obtained with experiment no. 3. A shoulder in the peak at around 1600 indicates structured molecule of carbon such as graphite or MWNT.

Experiment no. 4 and 5 produced more amount of amorphous carbon with few Multi walled carbon nanotubes (MWNT) which were in increasing order of benzene concentration. A representative SEM image of MWNT is given in Figure 4, which clearly

shows large amount of amorphous carbon. Corresponding Raman spectra is given in Figure 5. The higher amount of amorphous carbon is in lieu with the increase in the concentration of benzene.

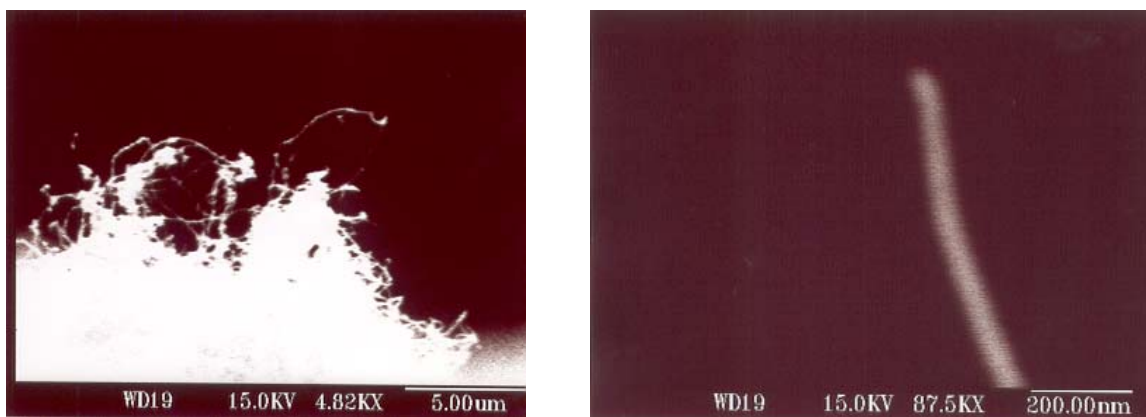


**Figure 4** SEM image of the sample obtained at conditions of experiment no. 5. A single MWNT had an average diameter of about 30-50 nm.

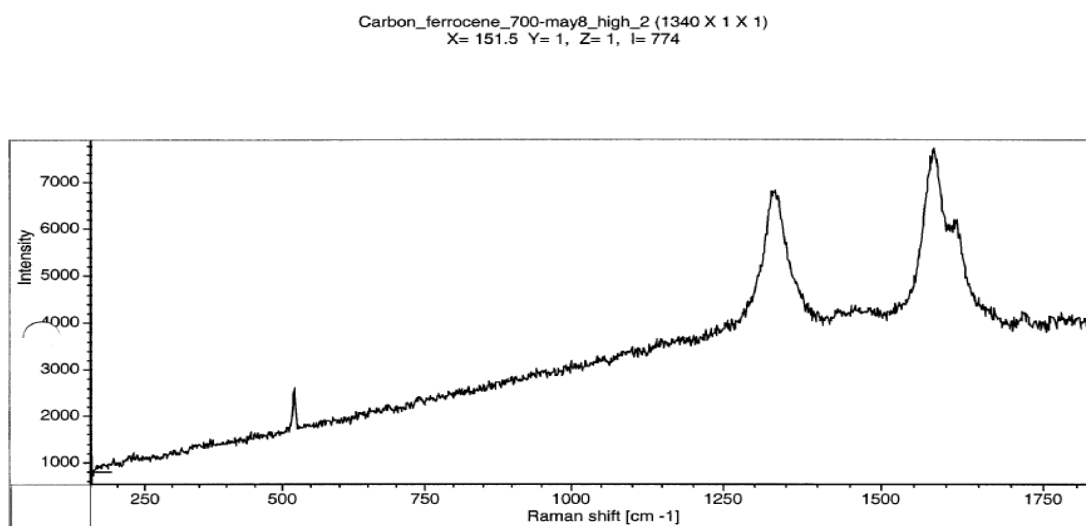
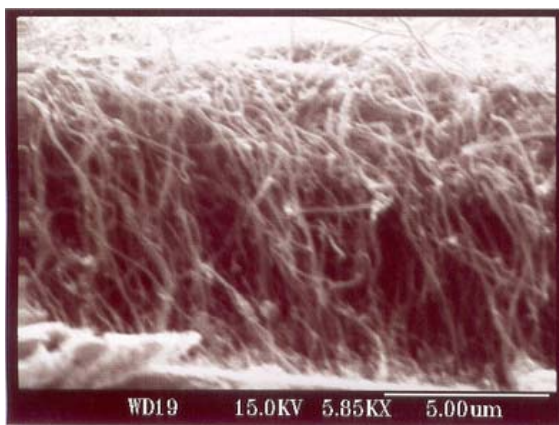
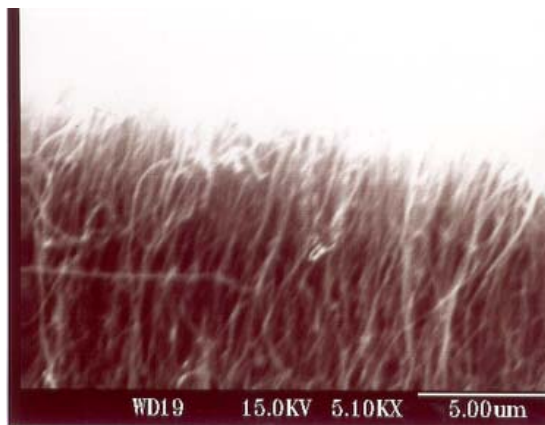


**Figure 5** Raman spectra of sample obtained at conditions of experiment no. 5, reaction performed at 700 ° C at 13.29%.

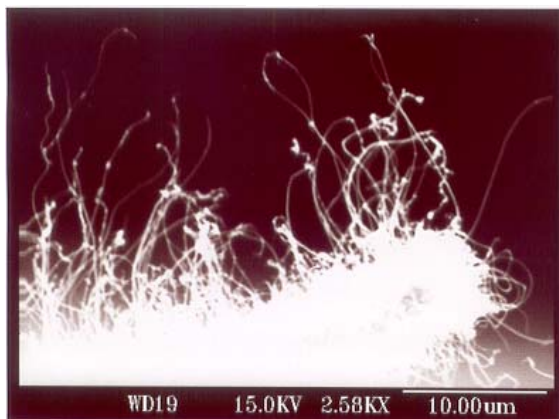
Ample MWNT were produced at liquid benzene flow rate of 1.824 ml/hr and 10% hydrogen flow. As the flow rate of benzene increased more amorphous carbon was produced and hence 1.824 ml/hr of benzene flow was selected as the optimum value at 10% hydrogen concentration. The next set of experiments involved varying the temperature to ascertain the temperature where we could obtain aligned MWNT. At 600 °C (experiment no. 6) we did not observe any CNT or amorphous carbon. At 800 °C (experiment no. 7) we did observe both MWNT and amorphous carbon but it was at 900 °C (experiment no. 8) that we first observed aligned MWNT. The SEM result given in Figure 6 show copious amount of CNT with formation of small quantity of amorphous carbon. Figure 6a and 6b shows aligned MWNT that are seen in a good number of areas of the silica sample. Figure 6c, 6d, and 6e show bundles of MWNT that form the largest portion of CNT observed. Figure 6f shows amorphous carbon deposited in some pockets of sample. This is to be observed since the sample size is of the order of mm and we are observing objects at nanometer scale. A variation in conditions and deposition of catalyst will give rise to variable production of aligned, bundles of CNT and amorphous carbon. Corresponding Raman spectra is given in Figure 7. The D/G intensity ratio is about 0.4. The G band is indicative of crystallinity of the carbon nanotubes and D band indicates the number of defects and other carbonaceous material. The low ratio compared to carbon nanotubes grown at lower temperatures clearly proves that besides good alignment, the system is low in defects and impurities.



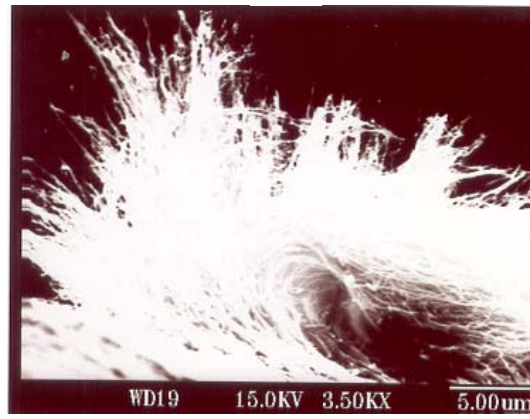
6a



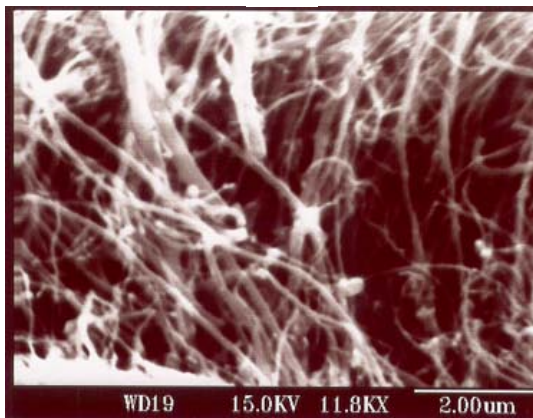
6b



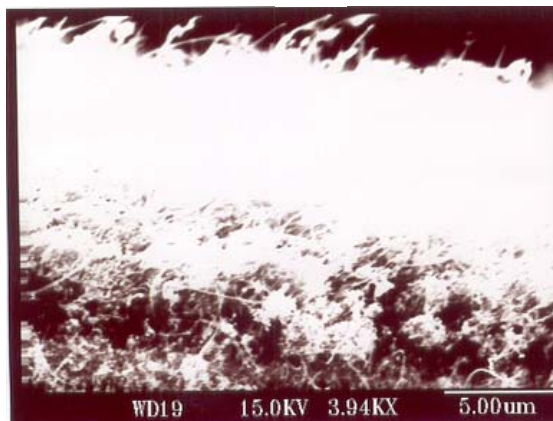
6c



6d



6e



6f

**Figure 6** SEM image of sample obtained at conditions of experiment no. 8. The reaction temperature was 900 °C and liquid benzene flow was 1.824 ml/hr. Hydrogen concentration was 10%.

Experiment no. 9 conducted at 1000 °C did not produce any aligned CNT and gave rise to more amorphous carbon. Hence the optimum conditions to be further investigated are 2 ml/hr of liquid benzene flow, 10% hydrogen concentration and temperature of 900 °C.

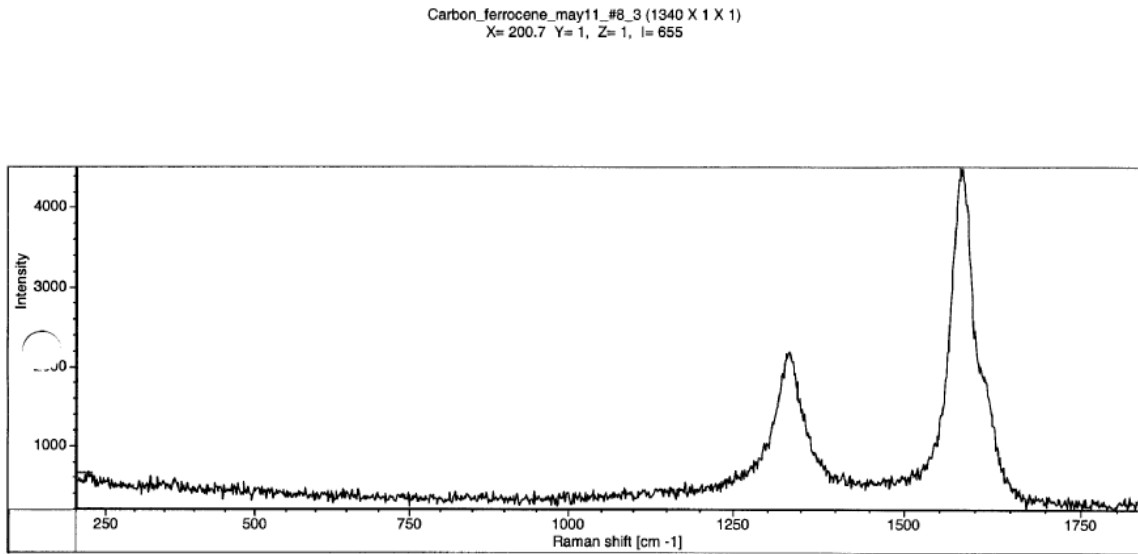


**Figure 7** The D and G band are clearly seen with the ratio to be about 0.4 as compared to 1.0 seen at lower temperatures. The lower D/G intensity ratio indicates that the MWNT formed are low on defects and more crystalline.

## 4 TEM analysis

The sample reacted at 900 °C was analyzed using Transmission electron microscopy (TEM). TEM will be able to provide the structures of nanotubes and the defect and growth mechanism if possible. The results are shown in Figure 8. The production of carbon nanotubes occur in large number with tubes closely packed. The tubes show a hollow core with multi-walls of carbon. The iron particles are trapped inside tubes both at the base and inside the tubes. Some of the walls while growing split to form a cap inside the tube. The rest of the tube continues further to form longer tube. There are defect visible along the tube in the form of kinks. The imperfection of the tubes is also visible through the presence of D band in Raman spectroscopy which is less than half the height as the G band. In absence of any carbonaceous material and defects, the D/G will be less than 0.1. The iron particles are seen sometimes throughout the tube indicating that the deposition of ferrocene takes place over another nanotubes leading to formation of all types of structures. With further tuning the conditions of growth of carbon nanotubes can be made to be cleaner.

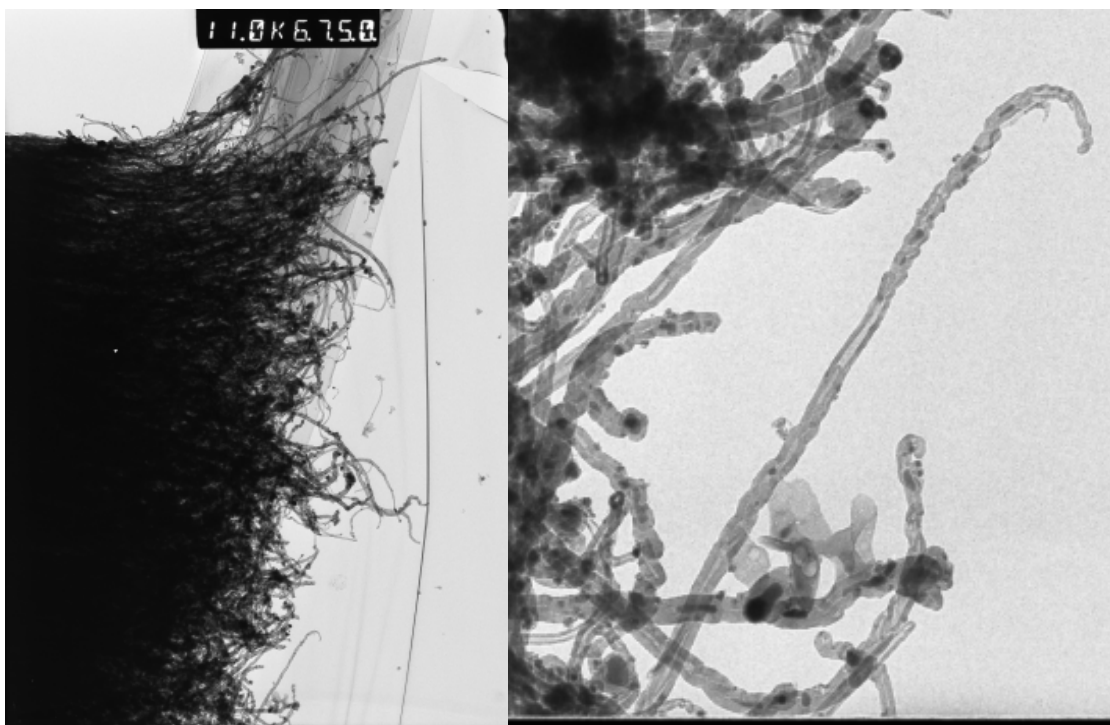


**Figure 8** TEM images of carbon nanotubes produced at 900 °C show production of large amount of carbon nanotubes (left). The enlarged image (right) show tubular structures made of multi wall of carbon and hollow core at the center. The diameter of nanotubes varies from 10 – 30 nm.

## **5 Oxidation of sample covered with carbon nanotubes grown from ferrocene**

In order to study the catalyst deposition on the flat silica surface from ferrocene that result in the formation of CNT, sample from experiment # 5 was oxidized in atmosphere at 800 °C for 3 hours. AFM pictures were taken and are given in Figure 9. We observe a layer of iron oxide that shows agglomeration of clusters leading to the formation of “hills” on the surface. The complete oxidation of sample was ascertained by Raman spectra that showed very low peak of carbon in 1325  $\text{cm}^{-1}$  and no peak at 1600  $\text{cm}^{-1}$  region (Figure 10). The sample was reduced and the topography observed did not seem to change much with reduction. Reduction was carried at 300 °C for 30 minutes followed by reduction at 400 °C for 120 minutes in pure hydrogen.

The sample was then treated with benzene at 700 °C for 5 minutes. The benzene concentration was 9.87%, concentration chosen close to the one in experiment no. 4 hoping to reproduce the results obtained with ferrocene. SEM pictures shows presence of essentially amorphous carbon and very few pockets of carbon nanotubes (Figure 11) indicating that the ferrocene provides the necessary molecule to initiate the formation of CNT as it provides the catalyst in the right size and activity surrounded by carbon atmosphere.

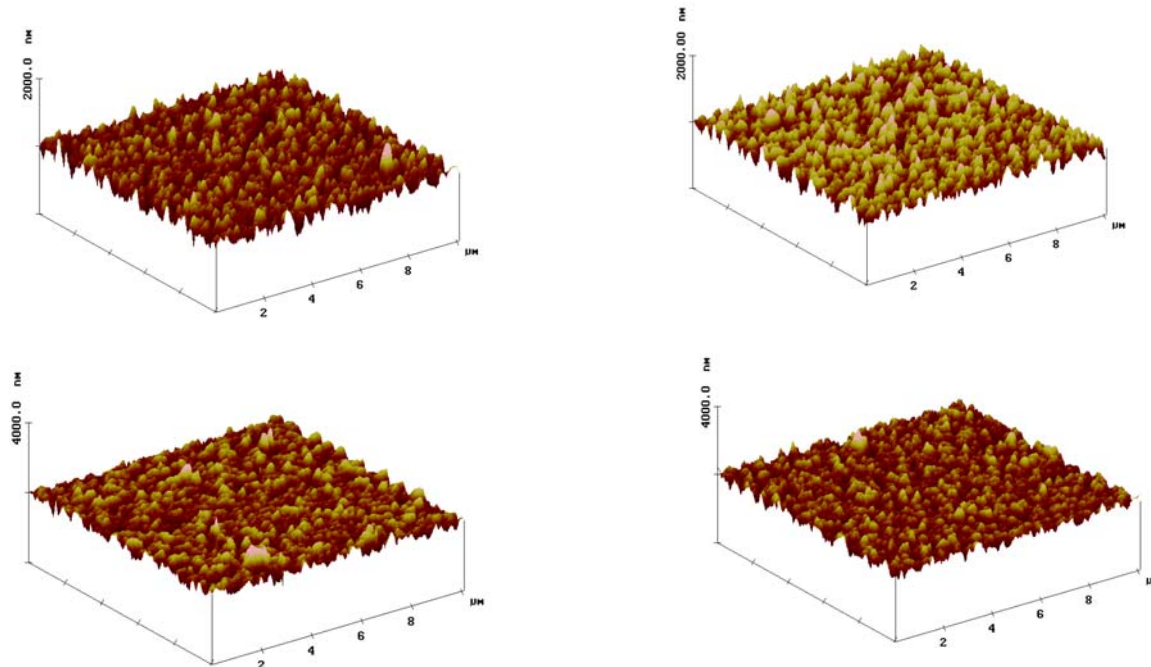


**Figure 9** AFM image of substrate surface taken after oxidation of all forms of carbon for sample obtained from conditions in experiment no. 5. We observe distinct peaks on the surface indicating agglomeration of Fe catalyst.

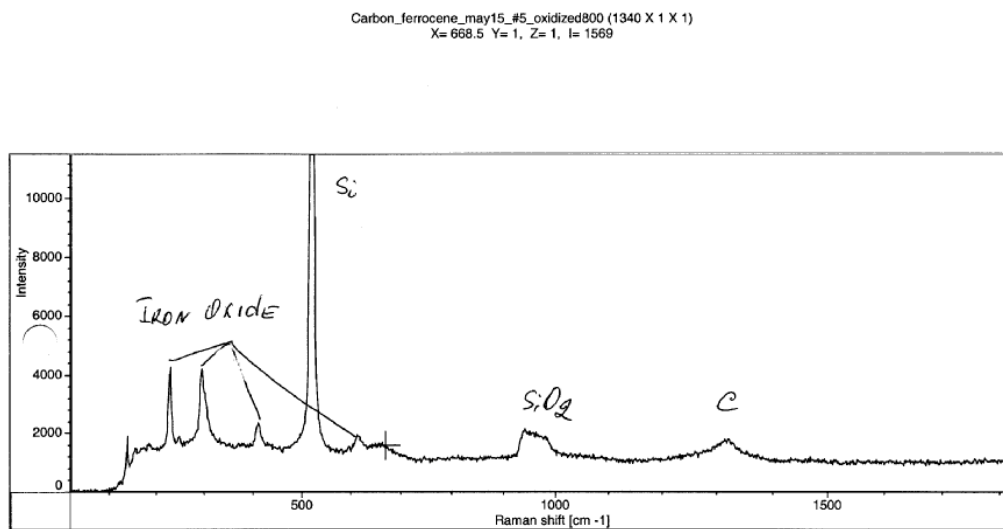


**Figure 10** Raman spectra of sample from experiment no. 5 oxidized in air. Spectra show the presence of Iron oxide and very low peak of C, which is smaller than the silica peak.

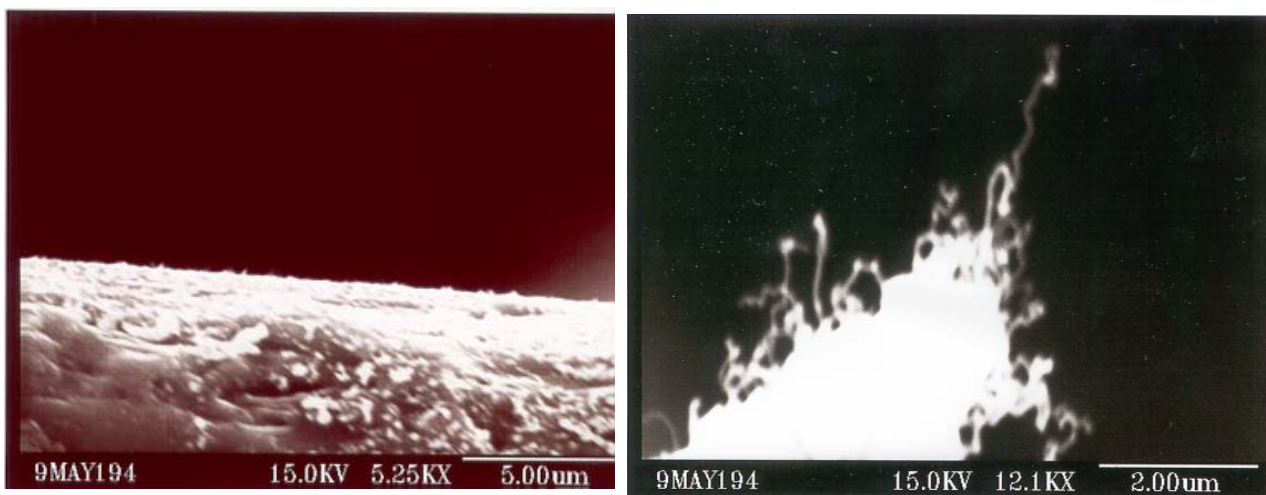


**Figure 11** SEM image of sample treated with benzene after oxidation and reduction of sample containing CNT. SEM shows only amorphous carbon and few pockets of formation of carbon nanotubes indicating significance of the role played by ferrocene.

## 6 Discussion and Conclusion

Ferrocene has shown to be one of the best catalysts for production of carbon nanotubes because of the high yield and density of carbon nanotubes. In our system of ferrocene and benzene, no growth of carbon nanotubes takes place up to 600 °C. Carbon nanotubes growth occurs from 700 °C along with formation of carbon as determined by Raman and SEM. The carbon nanotubes do show defects in their structures as determined by the high D/G intensity of about 1.0. The defects are not greatly improved with reaction temperature though the alignment improves. At 900 °C of reaction temperature with the concentration of ferrocene determined for 700 °C to produce carbon nanotubes, we get well aligned carbon nanotubes. Further the carbon nanotubes formed are of greater crystallinity and contain less impurities. The results are confirmed by Raman and SEM. At lower temperatures a mangled mass of carbon nanotubes is formed though the yield is high.

The interaction of the support with the metallocene needs to be investigated at different temperatures but is beyond the scope of current work. The defect in the carbon nanotubes and the carbon formation can be reduced to certain extent if the introduction rate in to the furnace is reduced though we were limited by the speed of the syringe pump. Removal of carbon nanotubes from the silica surface by calcination at 800 °C in air exposes the iron oxide surface as indicated by the Raman and AFM. The growth of carbon nanotubes was attempted on this surface by first reducing it and then reacting with benzene but did not produce carbon nanotubes equivalent to the original density observed. A large deposit of amorphous carbon was observed. It is therefore necessary

that for high density growth of carbon nanotubes, production of catalyst is to be done in-situ.

The TEM analysis shows carbon nanotubes and their interior structures. Carbon nanotubes formed show a hollow core enveloped with walls of carbon. Defects are clearly visible in the forms of kinks and loops. The size of carbon nanotubes is 10 – 50 nm depending on the temperature of reaction. The iron particles are seen on the carbon nanotubes and on the surface indicating that the decomposition of ferrocene takes in the atmosphere along with that on the surface.

## 7 Reference

1. Rao, A. M., Jacques, D., Haddon, R. C., Zhu, W., Bower, C. and Jin, S., *Applied Physics Letters*, 76, (2000), p. 3813.
2. Cao, A., Ci, L., Li, D., Wei, B., Xu, C., Liang, J. and Wu, D., *Chemical Physics Letters*, 335, (2001), p. 150.
3. Sen, R., Govindaraj, A. and Rao, C. N. R., *Chemistry of Materials*, 9, (1997), p. 2078.
4. Sen, R., Govindaraj, A. and Rao, C. N. R., *Chemical Physics Letters*, 267, (1997), p. 276.
5. Andrews, R., Jacques, D., Rao, A. M., Derbyshire, F., Qian, D., Fan, X., Dickey, E. C. and Chen, J., *Chemical Physics Letters*, 303, (1999), p. 467.
6. Singh, C., Shaffer, M. S. P. and Windle, A. H., *Carbon*, 41, (2003), p. 359.
7. Eres, G., Puzos, A. A., Geohegan, D. B. and Cui, H., *Applied Physics Letters*, 84, (2004), p. 1759.
8. Zhang, Z. J., Wei, B. Q., Ramanath, G. and Ajayan, P. M., *Applied Physics Letters*, 77, (2000), p. 3764.
9. Wei, B. Q., Vajtai, R., Jung, Y., Ward, J., Zhang, R., Ramanath, G. and Ajayan, P. M., *Nature (London, United Kingdom)*, 416, (2002), p. 495.
10. Jung, Y. J., Wei, B., Vajtai, R., Ajayan, P. M., Homma, Y., Prabhakaran, K. and Ogino, T., *Nano Letters*, 3, (2003), p. 561.

# **Chapter 6**

## **Growth of Single Walled Carbon Nanotubes on Supported Iron Catalyst**

## Table of Contents

Growth of Single Walled Carbon Nanotubes on Supported Iron Catalyst .....	169
1 Introduction.....	175
2 Experimental.....	176
3 Results and Discussion .....	178
3.1 Reaction Conditions.....	178
3.2 TEM Analysis.....	185
3.3 Reaction with iron oxide.....	187
3.4 Reaction with methane.....	188
4 Discussion.....	191
5 Conclusion .....	193
6 Reference .....	194

## List of Figures

- Figure 1 Raman spectra for reaction 1 to 3 (Table 1) carried respectively at 700 °C, 750 °C, and 800 °C. Peaks for MWNT are observed but no SWNT RBM peaks are observed. .... 181
- Figure 2 Raman spectra for reaction no. 4 and 5 conducted at 850 °C and 900 °C respectively. Formation of SWNT above is evident by RBM peak at around  $\sim 190 \text{ cm}^{-1}$  for both cases. .... 181
- Figure 3 The Raman spectra obtained for reaction carried at 950 °C shows intense peak in the RBM region. There is a split in the G band indicative of presence of metallic SWNT along with Semi-conducting SWNT. .... 182
- Figure 4 Raman spectra for single wall carbon nanotubes for reaction 6 (950 °C – 1.66% benzene concentration) and reaction 10 (950 °C – 0.91% benzene concentration) indicates difference in SWNT of different dimensions being formed. .... 182
- Figure 5 Apparent activation energy of carbon formation is 170.1 kJ/mol. The temperature variation is between 750 °C to 900 °C. .... 183
- Figure 6 The rate of carbon formation decreases with time while the yield of carbon levels off after 30 minutes. .... 184
- Figure 7 TEM images of carbon nanotubes growth on iron on alumina support at 950 °C and 0.91% benzene concentration. The size of SWNT is about 1.2 nm, a size in close agreement with the one calculated from Raman. Carbon nanotubes with 2-3 carbon layers are also observed. .... 186

Figure 8 Raman spectra for carbon nanotubes formed on iron oxide as catalyst without reduction .....	187
Figure 9 Raman spectra for reaction of iron oxide with methane shows presence of only MWNT.....	190
Figure 10 Raman spectra for reaction of iron with methane shows presence of MWNT. .....	190

## List of Tables

Table 1 Conditions for growth of CNT and yield of carbon formation show temperatures at which single walled carbon nanotubes grow. ....	178
Table 2 The diameters for carbon nanotubes vary between 1.1 to 1.4 depending on the temperature and the carbon source concentration.....	179
Table 3 Reaction conditions for formation of carbon nanotubes with iron oxide as catalyst. ....	188
Table 4 Reaction conditions for methane with iron oxide and iron catalyst clusters yielded only multi-walled carbon nanotubes .....	189

## **ABSTRACT**

Single wall carbon nanotubes (SWNT) have been synthesized on 5% wt iron-alumina supported catalyst using catalytic decomposition of benzene. SWNT were characterized employing Raman spectra and TEM. The results indicate the production of carbon nanotubes consisting of mainly single and double walled carbon nanotubes of uniform diameter. Along with the production of SWNT, MWNT and carbon have also been observed in certain regions of supported catalyst. The diameter of SWNT produced varies from 1.0 to 1.5 nm as calculated from the Raman data. The activation energy for production of carbon on iron catalyst has been determined to be 170.1 kJ/mol. Usually, SWNT of single diameter are observed but at higher temperatures and lower benzene concentration, diameter of varying sizes are formed.

# 1 Introduction

Single wall carbon nanotube has been found to have a variety of applications because of their unique mechanical [1, 2, 3] and electronic properties [4, 5, 6, 7]. SWNT can be either metallic or non-metallic depending on diameter and chirality [8, 9, 10, 11]. The ability to form both metallic and semi-conductors without any external doping is unique among the solid state materials and places SWNT as key material for nano-electronics [6]. SWNT is chiefly grown by arc-discharge method [12, 13] or by laser ablation method [14, 15, 16]. These techniques produce almost pure SWNT, but they are highly energy intensive with low yield. Catalytic decomposition of carbon source is more promising way for production of SWNT [17, 18, 19]. In addition to the prospect of continuous production of SWNT, the method involves great progress in producing SWNT with diameters varying within a narrow range [20] and up to 90% selectively semi-conducting [21]. In this study we describe catalytic decomposition of benzene on Fe catalyst supported on alumina. Raman and TEM are employed for characterization of SWNT [22, 23]. The effect of temperature and concentration of carbon source on the quality and yield of carbon is determined.

## 2 Experimental

Iron nitrate (99%, Aldrich) was impregnated in alumina (obtained from Hyperion Inc.) employing wet impregnation method that gave a loading of 5 wt% of iron. The catalyst was dried at 110 °C for 3 hours, reached at a ramp of 1 °C/min in flowing air. Temperature was further raised to 300 °C at 1 °C/min and calcined for 3 hours in flowing air to form iron oxide. The catalyst so produced was stored and a sample of it was used for each reaction.

A small sample of the catalyst was collected in a boat and placed in a flow reactor. Temperature was ramped at 2 °C/min up to 300 °C and reduced in pure hydrogen for one hour. The temperature was then ramped at 5 °C/min to 400 °C and reduced at this temperature for one hour. The catalyst was then pulled out of the furnace while the temperature of the system increased from 400 °C to the reaction temperature. This was carried out to prevent excessive agglomeration of clusters during increase in temperature. The catalyst during the temperature ramp from reduction to reaction temperature was kept under helium atmosphere. Reaction was carried out at varying temperature and benzene concentration. When the temperature was about 20 °C short of the reaction temperature, the tube was inserted in to the reactor slowly and the whole system was allowed to come to the reaction temperature. Benzene, hydrogen and helium as diluent were started immediately. Reaction was carried for 30 minutes. After reaction, the flow of the reactants was shut off; catalyst was pulled out of the furnace immediately and was kept under helium atmosphere. The furnace was cooled down to room temperature, and

the product was removed and weighed. The difference in the weight provided the yield and rate of reaction. Raman analysis and TEM was carried out to assess the results.

### 3 Results and Discussion

#### 3.1 Reaction Conditions

A series of experiments was performed with temperature varying between 700 °C to 950 °C and benzene concentration varying between 1 to 3%. The various parameters and reaction conditions are given in Table 1 and 2. Table 1 shows the temperature of reactions employed and results obtained thereof. Table 2 shows the yield of product and diameter of single walled carbon nanotubes formed at those conditions. Diameter of SWNT were evaluated using equations given by Rao et al. from radial breathing mode (RBM) peaks in Raman data [24].

**Table 1** Conditions for growth of CNT and yield of carbon formation show temperatures at which single walled carbon nanotubes grow.

Reaction no.	Temperature	Total flow rate (ml/min)	Concentration of benzene	Carbon Yield (wt/wt)	Results
1	700 °C	308.77	2.84 %	1.099	MWNT
2	750 °C	308.77	2.84 %	1.022	MWNT
3	800 °C	308.77	2.84 %	1.045	MWNT
4	850 °C	308.77	2.84 %	1.103	MWNT and SWNT
5	900 °C	308.77	2.84 %	1.289	MWNT and SWNT
6	950 °C	264.39	1.66 %	1.500	SWNT
7	900 °C	264.39	1.66 %	-	MWNT and strong peak for SWNT
8	950 °C	264.39	1.66 %	-	SWNT
9	950 °C	242.19	0.91 %	1.130	SWNT/C
10	950 °C	242.19	0.91 %	1.146	SWNT

**Table 2** The diameters for carbon nanotubes vary between 1.1 to 1.4 depending on the temperature and the carbon source concentration.

Reaction no.	Temperature	Concentration of benzene	Carbon Yield (wt/wt)	Results	Rate ( $10^{-3}$ mol mol <sup>-1</sup> s <sup>-1</sup> )	Wave Number	Dia (nm)
1	700 °C	2.84 %	1.099	MWNT	5.11		-
2	750 °C	2.84 %	1.022	MWNT	1.14		-
3	800 °C	2.84 %	1.045	MWNT	2.31		-
4	850 °C	2.84 %	1.103	MWNT and SWNT	5.35	195	1.1
5	900 °C	2.84 %	1.289	MWNT and SWNT	14.96	187	1.2
6	950 °C	1.66 %	1.500	SWNT	25.86	207, 192	1.1, 1.2
7	900 °C	1.66 %	-	MWNT and SWNT	-	191	1.2
8	950 °C	1.66 %	-	SWNT	-	214, 192	1.1, 1.2
9	950 °C	0.91 %	1.130	SWNT	6.72	192	1.2
10	950 °C	0.91 %	1.146	SWNT	7.57	215, 193, 172, 158	1.0, 1.2, 1.3, 1.4

As observed in Raman spectra in Figure 1 for reactions 1 – 3, peaks for only multi-walled carbon nanotubes (MWNT) located at  $\sim 1325$  cm<sup>-1</sup> and  $\sim 1595$  cm<sup>-1</sup> are observed, known respectively as D and G band for graphite. G band is characteristic of graphitic structure and D band is characteristic of defects in the graphitic structures and carbon structures [25]. Presence of single walled carbon nanotubes are characterized by presence of peaks in the region of  $150$  cm<sup>-1</sup> to  $250$  cm<sup>-1</sup>, called breathing mode region, produced due to the vibration of the SWNT molecule in the radial direction. Single wall carbon nanotubes are not formed in appreciable amount to be detected by Raman below 800 °C

with benzene. Presence of D and G band indicates presence of multi-walled carbon nanotubes (MWNT) that is well graphitized though not free from defects. Raman for experiments conducted at 850 °C and above (Figure 2 and 3, reaction 4, 5, 6) shows the presence of peaks for SWNT in breathing mode region along with the D and G band. Corresponding location of peaks for SWNT are given in Table 2. Reaction 7 and 8 gives results similar to their predecessors in reaction 5 and 6 respectively proving the reproducibility of results. Reaction 9 and 10, carried at similar condition as those of reaction 6 and 8 but at lower benzene concentration, provide up to four peaks in the breathing mode region. A comparison between Raman spectra of reaction 6 and that of reaction 10 (different benzene concentration) is given in Figure 4. One more observation to be made here is the loss of the D band intensity compared to G band indicating the formation of nearly defect free SWNT. In reaction 6, the G band is split to the left indicating that along with the semi-conducting SWNT, there are metallic SWNT present too [25, 26]. The relative ratio of these two peaks will roughly estimate the relative amount of these two kinds, which in our case is  $\frac{3}{4}$ . TEM results indicate this along with the presence of Multi walled carbon nanotubes that are formed in 2-3 layers that contribute little to the D band. Finally increasing concentration of benzene at a given temperature and time of reaction increases the rate of reaction and correspondingly the yield of carbon formation.

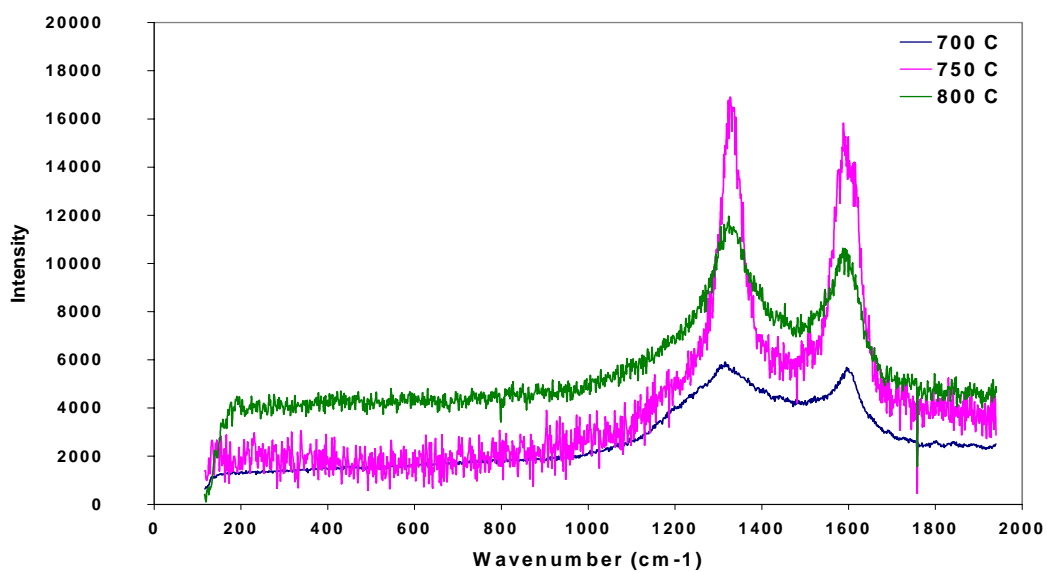


**Figure 1** Raman spectra for reaction 1 to 3 (Table 1) carried respectively at 700 °C, 750 °C, and 800 °C. Peaks for MWNT are observed but no SWNT RBM peaks are observed.

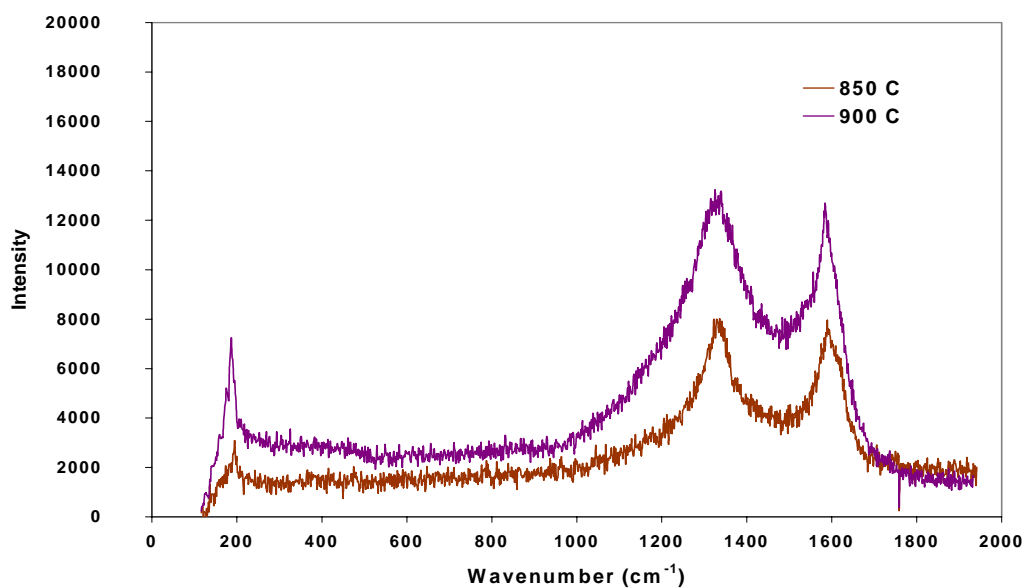


**Figure 2** Raman spectra for reaction no. 4 and 5 conducted at 850 °C and 900 °C respectively. Formation of SWNT above is evident by RBM peak at around  $\sim 190$   $\text{cm}^{-1}$  for both cases.

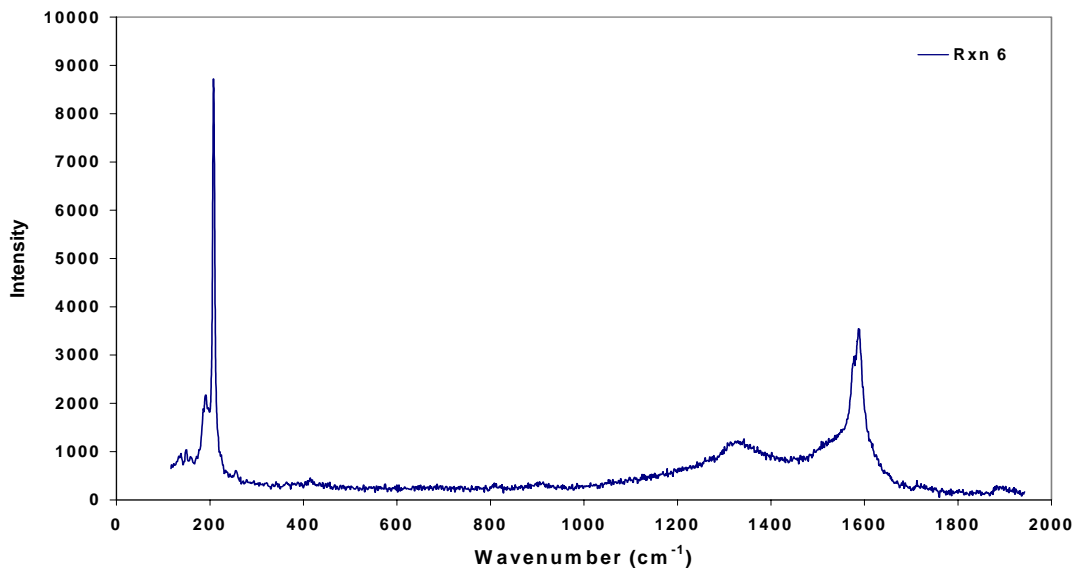


**Figure 3** The Raman spectra obtained for reaction carried at 950 °C shows intense peak in the RBM region. There is a split in the G band indicative of presence of metallic SWNT along with Semi-conducting SWNT.

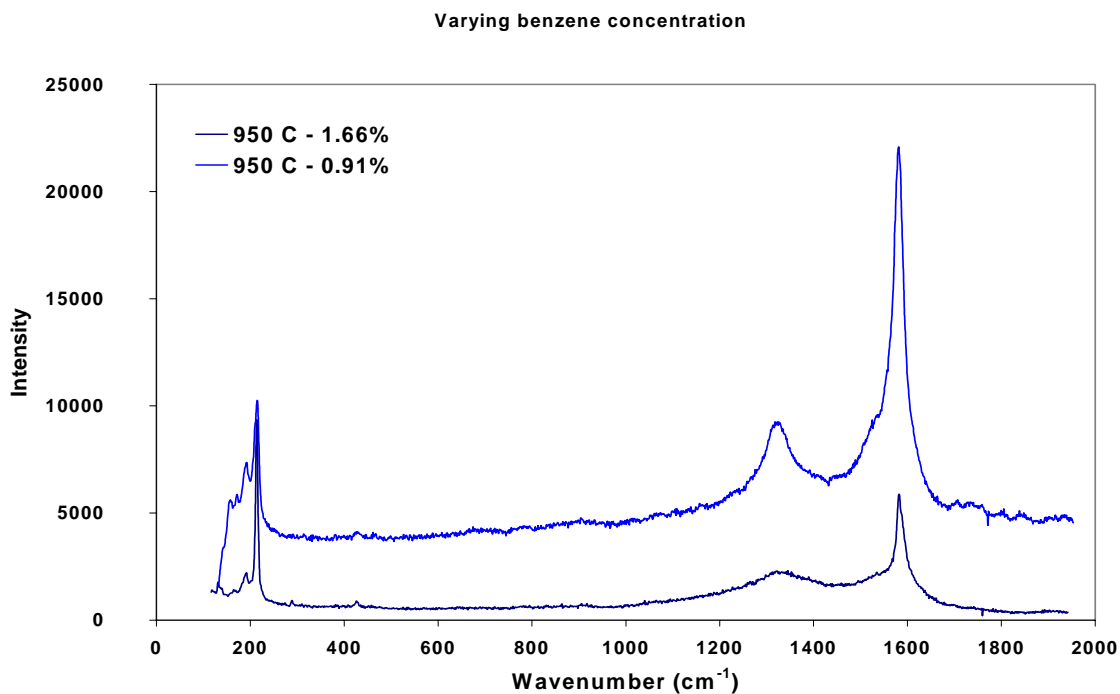


**Figure 4** Raman spectra for single wall carbon nanotubes for reaction 6 (950 °C – 1.66% benzene concentration) and reaction 10 (950 °C – 0.91% benzene concentration) indicates difference in SWNT of different dimensions being formed.

Calculations were carried for determining apparent activation energy of carbon product formation. Figure 5 shows Arrhenius plot of natural log of rate of reaction v/s inverse temperature. The plot is for data from reaction 2 to 5, temperature varying from 750 °C to 900 °C. The calculated apparent activation energy of carbon formation is 170 kJ/mol of Fe, which is close to formation of carbon on iron reported in literature [27].

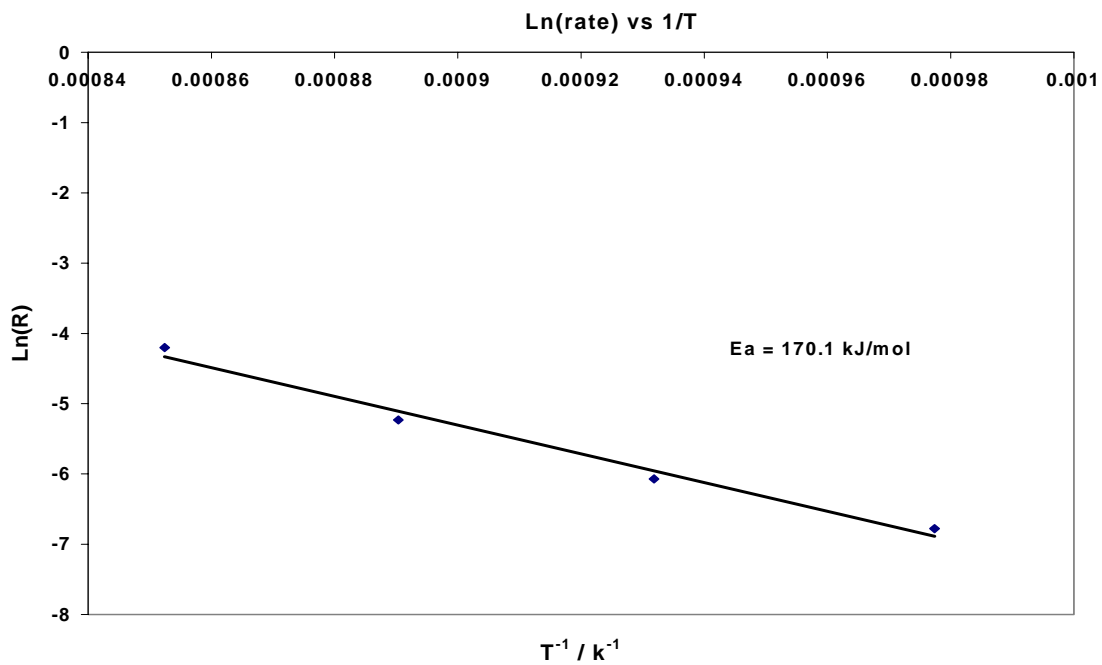


**Figure 5** Apparent activation energy of carbon formation is 170.1 kJ/mol. The temperature variation is between 750 °C to 900 °C.

The rate of carbon formation was observed to decrease as the reaction time progresses (Figure 6). The yield of carbon is high initially but reaches a saturation limit. This can be explained with the low yield of carbon nanotubes observed with Transmission Electron Microscopy (TEM), the results discussed below. Majority of Fe clusters were covered with graphitic material rendering them inactive. The amount of carbon nanotube formed does not contribute much to the total mass of the product. The initial large formation of carbonaceous material and carbon nanotubes lead to the higher rate of carbon formation. As the carbonaceous material cover most of the iron on the supported catalyst, further decomposition of benzene and formation of more carbon is prevented. Some Fe clusters that remain active for carbon nanotubes formation will lead to their growth but not significantly contribute to the total mass of the product. The yield study was done at 950 °C with 0.91% benzene concentration.

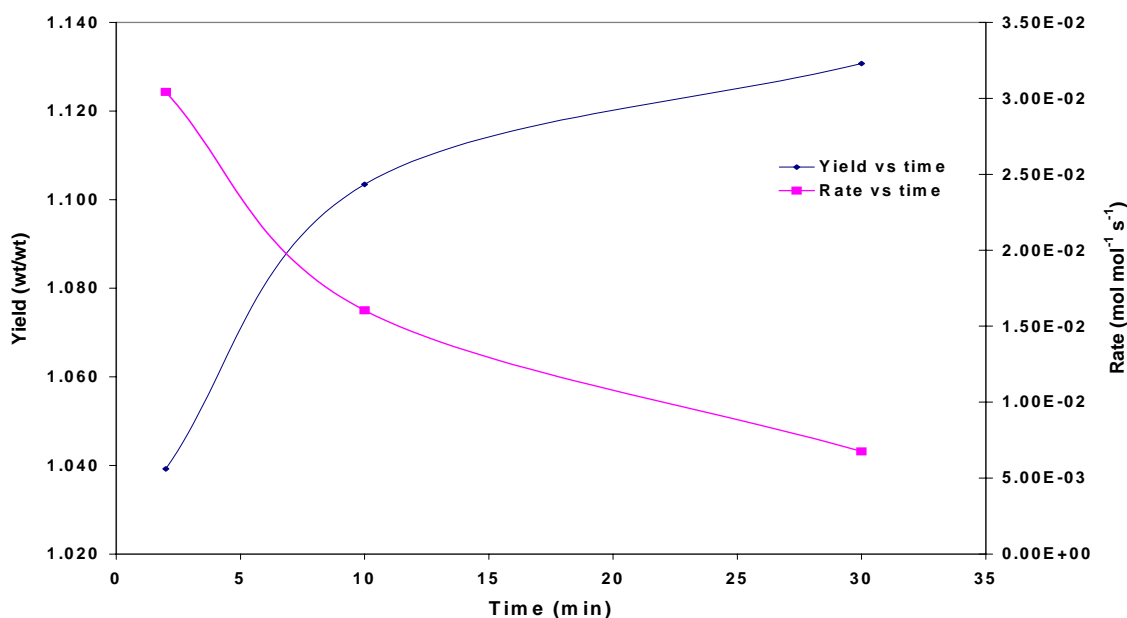


**Figure 6** The rate of carbon formation decreases with time while the yield of carbon levels off after 30 minutes.

### 3.2 TEM Analysis

TEM provides proof of the presence of single wall carbon nanotubes and their dimensions. It also provides information on the size of catalyst clusters and other byproducts. From Figure 7a, we observe the iron catalyst supported on alumina with bundles of single walled carbon nanotubes (SWNT) growing from them. The size of nanotubes observed is  $\sim 1.2$  nm, well in accordance with size provided by Raman analysis. Figure 7b shows presence of multi-walled carbon nanotubes that have 2 – 3 layers of graphite. The single and multi walled carbon nanotubes do form bundles. Figure 7c and 7d show that the yield of carbon nanotubes is low though the selectivity to form single wall carbon nanotubes or multi walled carbon nanotubes that are 2 to 3 graphitic layers. Most of the catalyst clusters seems to have been covered with graphite. Figure 7e shows presence of tubular nanostructures along with single wall carbon nanotubes. The catalyst cluster size observed was between 3 to 20 nm.

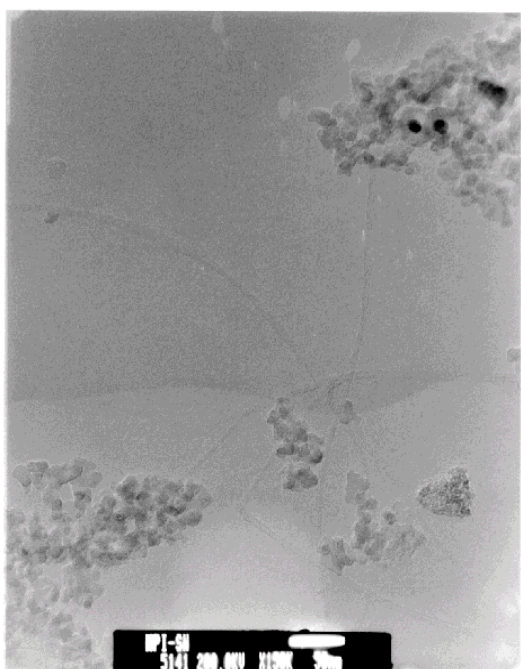


**Figure 7a** Single wall carbon nanotubes with diameter  $\sim 1.2$  nm

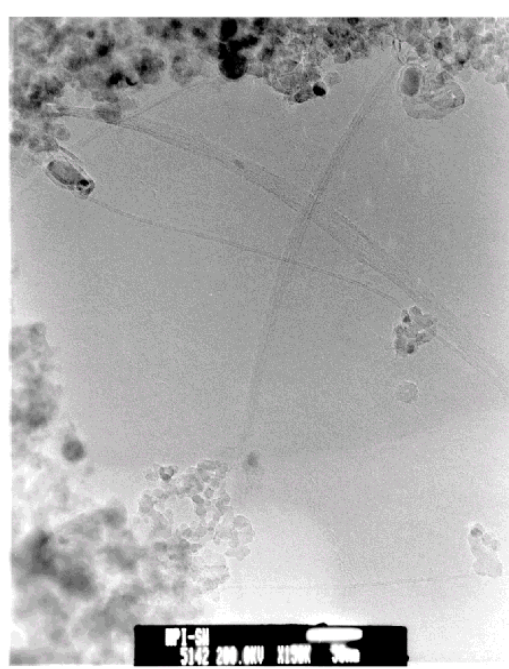


**Figure 7b** Bundles of single and multi walled carbon nanotubes with 2 to 3 graphitic layers.

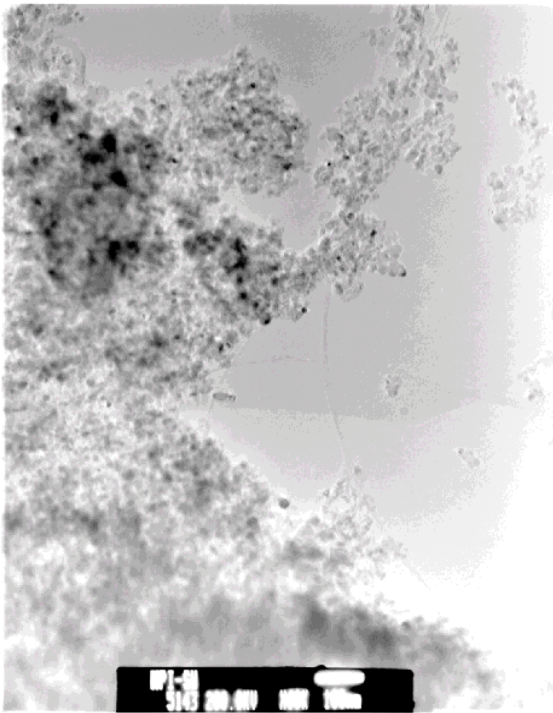


**Figure 7c** TEM shows the large bulk of support with dark spots of catalyst clusters. SWNT are seen interspersed with support. Scale 100 nm

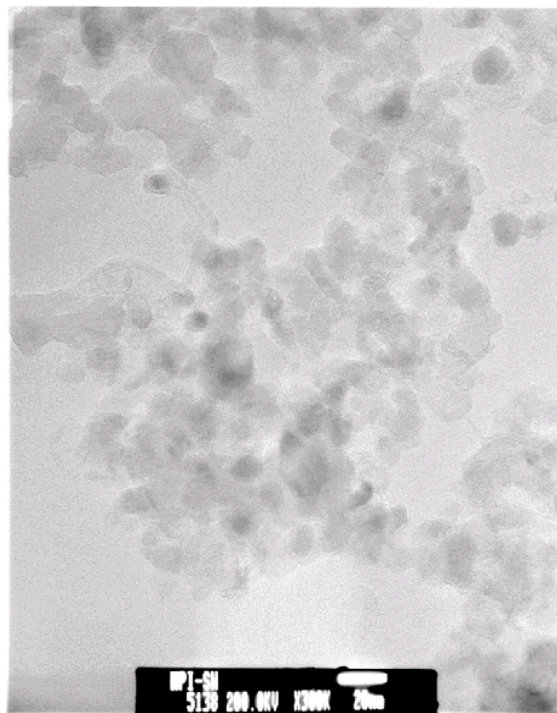


**Figure 7d** Catalyst clusters on support. Catalyst cluster size varies from 5 to 20 nm. Some clusters were covered with graphitic carbon.



**Figure 7e** Presence of nanostructures along with single wall carbon nanotubes.

**Figure 7** TEM images of carbon nanotubes growth on iron on alumina support at 950 °C and 0.91% benzene concentration. The size of SWNT is about 1.2 nm, a size in close agreement with the one calculated from Raman. Carbon nanotubes with 2-3 carbon layers are also observed.

### 3.3 Reaction with iron oxide

In all above reactions, Fe was the active catalyst for growth of carbon nanotubes. To ascertain whether  $\text{Fe}_2\text{O}_3$  can be active for production of SWNT, the catalyst ( $\text{Fe}_2\text{O}_3$ ) was not reduced but reacted directly with benzene at reaction temperature of 900 °C. Raman analysis showed both MWNT and SWNT. Presence of large D band indicates the presence of defects in their structure. The results indicate reduced iron is better catalyst to form defect free SWNT. Iron oxide will be reduced in the carbon and hydrogen atmosphere under reaction conditions and this delay in reduction is probably responsible for deposition of large carbonaceous material. The conditions are given in Table 3. The corresponding Raman spectrum is given in Figure 8.

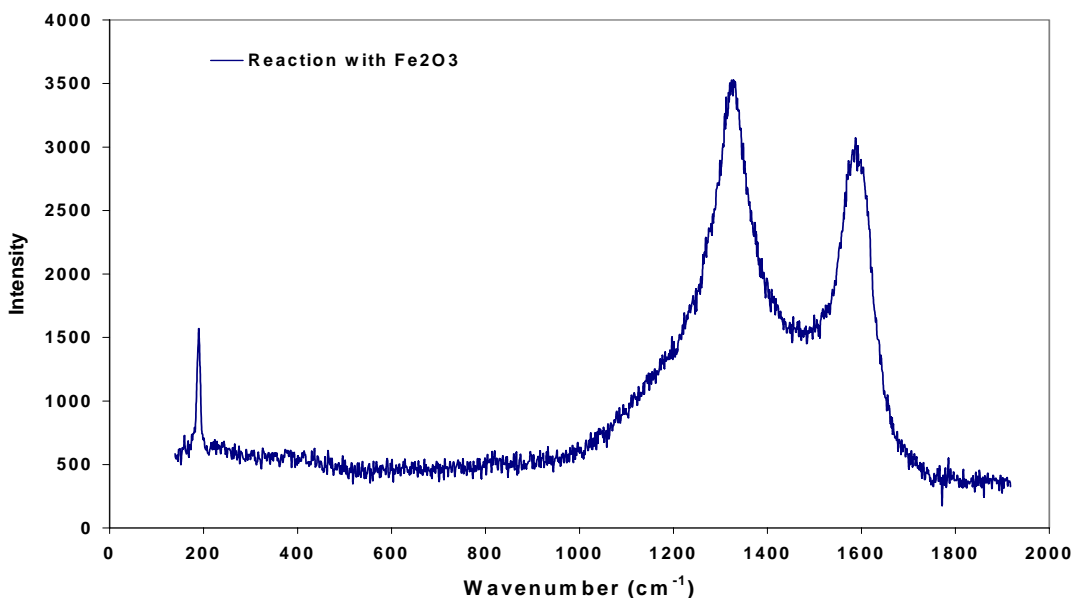


**Figure 8** Raman spectra for carbon nanotubes formed on iron oxide as catalyst without reduction

**Table 3** Reaction conditions for formation of carbon nanotubes with iron oxide as catalyst.

Rxn no.	Temp	Conc. of benzene	Carbon Yield (wt/wt)	Rate / $10^{-3}$ mol mol <sup>-1</sup> s <sup>-1</sup>	Wave number	Diameter (nm)	Results
1	900 °C	1.66 %	1.287	14.8	190	1.2	SWNT/ MWNT

### 3.4 Reaction with methane

To observe the effect of carbon source on growth of single wall carbon nanotubes, the carbon source was changed to methane. Methane is more stable compared to benzene and should exhibit different reactivity. We carried reaction both with iron and iron oxide as the catalyst. In all cases, we observed only multi walled carbon nanotubes by Raman. Reaction conditions are given in Table 4. Methane concentration was 2.0 %. No excess helium was flown since the diluent gas for methane was helium that was about 98% of the total flow. The reduction conditions and temperature ramp used were similar to the ones used in reaction with benzene. The rate of reaction in case of both iron oxide and iron from reaction 1 to 3 is almost of equal order of magnitude. In reaction 4, hydrogen was also used in the reaction mixture introduced at the flow rate of 20 ml/min. The rate of reaction is higher in presence of hydrogen. Hydrogen plays a role in removal of carbon by methane formation and this in turn acts to remove excessive carbon from the surface

of catalyst keeping it active for formation of carbon nanotube formation. Representative Raman spectra are given in Figure 9 and 10.

**Table 4** Reaction conditions for methane with iron oxide and iron catalyst clusters yielded only multi-walled carbon nanotubes

Reaction no.	Temp	Time (min)	Conc. Of methane	Carbon Yield (wt/wt)	Rate / $10^{-3}$ mol mol <sup>-1</sup> s <sup>-1</sup>	Results
Rxn 1 (Fe <sub>2</sub> O <sub>3</sub> )	950 °C	10	2.08%	1.079	12.25	MWNT
Rxn 2 (Fe)	950 °C	10	2.08 %	1.108	16.72	MWNT
Rxn 3 (Fe <sub>2</sub> O <sub>3</sub> )	950 °C	10	2.08 %	1.125	19.39	MWNT
Rxn 4* (Fe)	950 °C	10	2.04 %	1.25	38.78	MWNT

\* Use of hydrogen in reaction shows increase in rate of formation of carbon products.

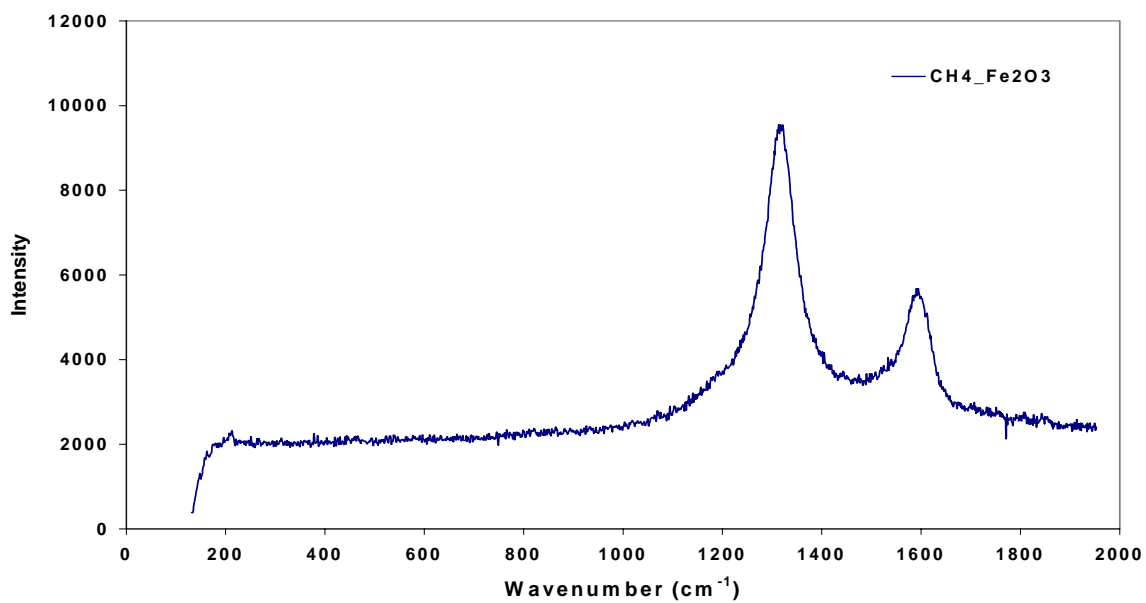


**Figure 9** Raman spectra for reaction of iron oxide with methane shows presence of only MWNT.

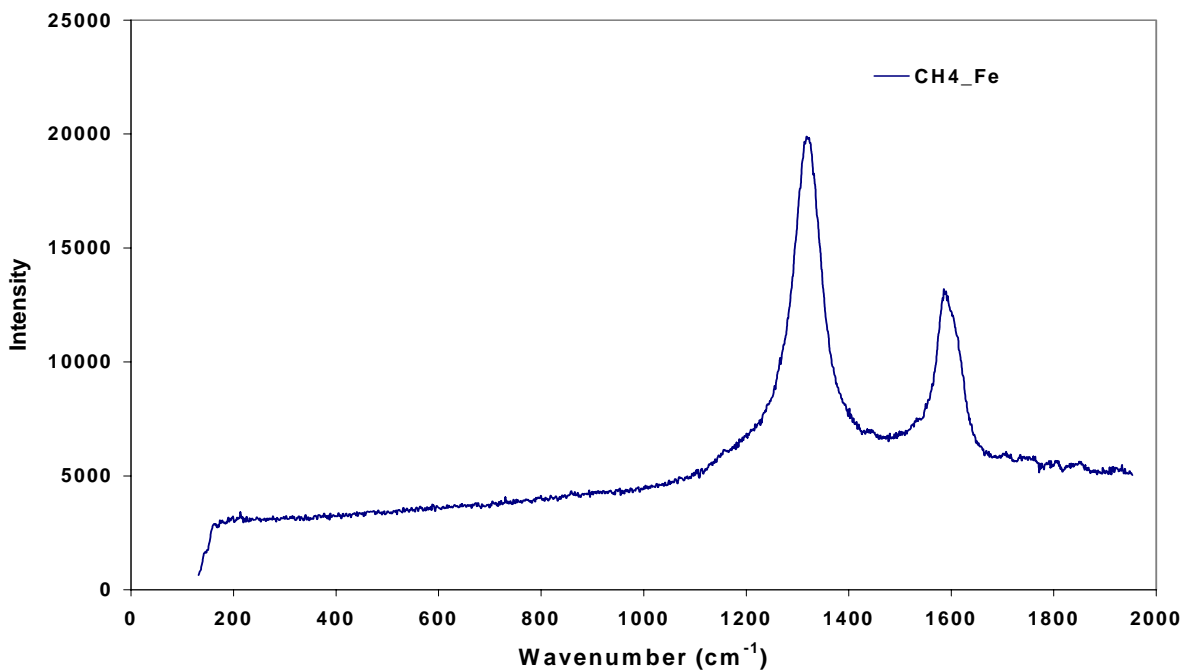


**Figure 10** Raman spectra for reaction of iron with methane shows presence of MWNT.

## 4 Discussion

Formation of single wall carbon nanotubes from benzene requires temperature to be sufficiently high. Single walled carbon nanotubes are readily formed above 850 °C with good reproducibility but are not formed below 800 °C. Multi walled carbon nanotubes are observed to form from 700 °C and up. The yield and rate of carbon formation also goes up with temperature (Table 1) as observed for reaction 2 to 6 (reaction 1 is an exception which may be an error point). At 950 °C, when we decrease the concentration of benzene (reaction 6 and 9), we simultaneously observe decrease in yield and rate of carbon formation. The results are similar in both cases. This follows what we expect intuitively.

From the Raman data, we can evaluate the size of single wall carbon nanotubes formed using Rao et al. equation [24]. According to their equation, diameter of SWNT (D) is given by

$$D \text{ (nm)} = 223.75 \text{ (cm}^{-1}\text{)}/\lambda \text{ (cm}^{-1}\text{)}$$

where  $\lambda$  = Wave number of Raman spectra observed. The diameter of SWNT formed varies from 1.0 to 1.4 nm, the dominant size being 1.2 nm. This is confirmed by the results from TEM. TEM also indicate that the selectivity of SWNT is high with minimum formation of MWNT, which are usually 2 to 3 graphitic layers, and other nanostructures. The yield of SWNT is however low. Usually they occur in bundles. A good number of clusters are covered with carbon or carbonaceous material. This answers the decrease in the rate of carbon formation with time and leveling of yield of carbon. The active clusters

that form SWNT do not contribute to the total yield to a large extent and clusters that only form carbon are covered with it and inactive for any more carbon formation. The large number of clusters being rendered ineffective has to do with the type of interaction the metal catalyst has with the support material. The topic needs to be investigated in more depth.

Size of catalyst clusters that participate in the formation of carbon nanotubes is between 3 – 20 nm. Iron and iron oxide both result in the formation of SWNT at suitable temperatures. This may indicate that iron oxide gets reduced under reaction conditions with benzene and hydrogen present in the reaction stream to form metallic iron though it results in larger deposition of carbonaceous material. The type of carbon source greatly affects the formation of SWNT. No SWNT were observed to grow in presence of methane up to a concentration of 2%. MWNT and C were the dominant products as observed with Raman. The rate of carbon formation is slightly higher in magnitude compared to reaction with benzene of comparable concentration.

## 5 Conclusion

The growth of SWNT was successfully attempted on iron supported on alumina. The SWNT is preferentially formed above 850 °C and shows good selectivity at temperatures of 900 – 950 °C. Iron oxide as well as iron is effective for growth of SWNT at suitable temperatures suggesting that iron oxide is reduced under reaction conditions to form metallic iron. Methane with a maximum concentration of 2% produced only MWNT up to a temperature of 950 °C. Size of carbon nanotubes formed varied from 1.0 to 1.4 nm with dominant size being 1.2 nm. This result was independently confirmed with TEM.

### **Acknowledgement:**

We would like to acknowledge the help of Dr. Jun Ma, Hyperion Inc., for the alumina support and TEM analysis of our samples.

## 6 Reference

1. Saito, R., *Physical Properties of Carbon Nanotubes*, p. 259 pp (1998).
2. Yakobson, B. I., Brabec, C. J. and Bernholc, J., *Physical Review Letters*, 76, (1996), p. 2511.
3. Yu, M.-F., *Journal of Engineering Materials and Technology*, 126, (2004), p. 271.
4. Dekker, C., Tans, S. J., Devoret, M. H., Geerligs, L. J., Groeneveld, R. J. A., Venema, L. C., Wildoer, J. W. G., Verschueren, A. R. M. and Bezryadin, A., *Molecular Nanostructures, Proceedings of the International Winterschool on Electronic Properties of Novel Materials, 11th, Kirchberg, Austria, Mar. 1-8, 1997*, (1998), p. 467.
5. Gonzalez, J., *Encyclopedia of Nanoscience and Nanotechnology*, 3, (2004), p. 163.
6. McEuen, P. L., *Nature (London)*, 393, (1998), p. 15.
7. Odom, T. W., Huang, J.-L., Kim, P. and Lieber, C. M., *Journal of Physical Chemistry B*, 104, (2000), p. 2794.
8. Mintmire, J. W., Dunlap, B. I. and White, C. T., *Physical Review Letters*, 68, (1992), p. 631.
9. Wildoer, J. W. G., Venema, L. C., Rinzler, A. G., Smalley, R. E. and Dekker, C., *Nature (London)*, 391, (1998), p. 59.
10. Kim, P., Odom, T. W., Huang, J. and Lieber, C. M., *Carbon*, 38, (2000), p. 1741.
11. Odom, T. W., Huang, J.-L., Kim, P. and Lieber, C. M., *Nature (London)*, 391, (1998), p. 62.
12. Ebbesen, T. W. and Ajayan, P. M., *Nature (London, United Kingdom)*, 358, (1992), p. 220.

13. Journet, C., Maser, W. K., Bernier, P., Loiseau, A., Lamy de la Chapells, M., Lefrant, S., Deniard, P., Lee, R. and Fischer, J. E., *Nature (London)*, 388, (1997), p. 756.
14. Zhang, Y., Gu, H. and Iijima, S., *Applied Physics Letters*, 73, (1998), p. 3827.
15. Yudasaka, M., Ichihashi, T. and Iijima, S., *Journal of Physical Chemistry B*, 102, (1998), p. 10201.
16. Nishide, D., Kataura, H., Suzuki, S., Okubo, S. and Achiba, Y., *Chemical Physics Letters*, 392, (2004), p. 309.
17. Resasco, D. E., Alvarez, W. E., Pompeo, F., Balzano, L., Herrera, J. E., Kitiyanan, B. and Borgna, A., *Journal of Nanoparticle Research*, 4, (2002), p. 131.
18. Hongo, H., Yudasaka, M., Ichihashi, T., Nihey, F. and Iijima, S., *Chemical Physics Letters*, 361, (2002), p. 349.
19. Murakami, Y., Chiashi, S., Miyauchi, Y., Hu, M., Ogura, M., Okubo, T. and Maruyama, S., *Chemical Physics Letters*, 385, (2004), p. 298.
20. Bachilo, S. M., Balzano, L., Herrera, J. E., Pompeo, F., Resasco, D. E. and Weisman, R. B., *Journal of the American Chemical Society*, 125, (2003), p. 11186.
21. Li, Y., Mann, D., Rolandi, M., Kim, W., Ural, A., Hung, S., Javey, A., Cao, J., Wang, D., Yenilmez, E., Wang, Q., Gibbons, J. F., Nishi, Y. and Dai, H., *Nano Letters*, 4, (2004), p. 317.
22. Dresselhaus, M. S., Dresselhaus, G., Jorio, A., Souza Filho, A. G. and Saito, R., *Carbon*, 40, (2002), p. 2043.
23. Souza, M., Jorio, A., Fantini, C., Neves, B. R. A., Pimenta, M. A., Saito, R., Ismach, A., Joselevich, E., Brar, V. W., Samsonidze, G. G., Dresselhaus, G. and Dresselhaus,

- M. S., *Physical Review B: Condensed Matter and Materials Physics*, 69, (2004), p. 241403/1.
24. Rao, A. M., Bandow, S., Richter, E. and Eklund, P. C., *Thin Solid Films*, 331, (1998), p. 141.
25. Jorio, A., Pimenta, M. A., Souza Filho, A. G., Saito, R., Dresselhaus, G. and Dresselhaus, M. S., *New Journal of Physics*, 5, (2003), p. 1.
26. Jorio, A., Souza Filho, A. G., Dresselhaus, G., Dresselhaus, M. S., Righi, A., Matinaga, F. M., Dantas, M. S. S., Pimenta, M. A., Mendes Filho, J., Li, Z. M., Tang, Z. K. and Saito, R., *Chemical Physics Letters*, 351, (2002), p. 27.
27. Arabczyk, W., Konicki, W., Narkiewicz, U., Jasinska, I. and Kalucki, K., *Applied Catalysis A: General*, 266, (2004), p. 135.

# **Chapter 7**

**Atomic Layer Deposition of alumina on  
Silica/Si (100) substrate and their Thermal  
Properties**

## Table of Content

<b>CHAPTER 7</b> .....	<b>197</b>
<b>ATOMIC LAYER DEPOSITION OF ALUMINA ON SILICA/SI (100)</b>	
<b>SUBSTRATE AND THEIR THERMAL PROPERTIES</b> .....	<b>197</b>
<b>1 INTRODUCTION</b> .....	<b>205</b>
<b>2 BACKGROUND OF ATOMIC LAYER DEPOSITION</b> .....	<b>206</b>
<b>3 CHARACTERIZATION OF THIN FILMS USING ELLIPSOMETRY</b> .....	<b>208</b>
<b>4 EFFECT OF SUPPORT ON PRODUCTION AND GROWTH OF CARBON NANOTUBES</b> .....	<b>210</b>
<b>5 ATOMIC LAYER DEPOSITION EQUIPMENT DESIGN</b> .....	<b>212</b>
5.1 DESIGN OF ALD EQUIPMENT: .....	212
5.2 REACTOR DESCRIPTION .....	212
5.3 INLET SYSTEM FOR REACTANTS .....	213
<b>6 ATOMIC LAYER DEPOSITION OF ALUMINA ON SILICA/SI MODEL SUPPORT</b> .....	<b>215</b>
6.1 ALUMINA COATING ON HF TREATED SI (100) SURFACE .....	216
6.2 ALUMINA COATING ON THERMALLY GROWN SILICON OXIDE ON Si (100): THICKNESS VARIATION WITH NUMBER OF ALUMINA COATINGS .....	218
6.2.1 Alumina deposition by ALD at 177 °C.....	219
6.2.2 Alumina deposition by ALD at 300 °C.....	221
6.2.3 AXPS Analysis of alumina films deposited at 177 °C and 300 °C.....	223

6.2.4	<i>Thickness measurement of alumina film deposited at 177 °C and 300 °C by Ellipsometry</i> .....	225
6.3	DEPOSITION OF ALUMINA ON NATIVE SILICA ON Si (100).....	228
<b>7</b>	<b>THERMAL STABILITY OF ALUMINA FILM</b> .....	<b>230</b>
7.1	CALCINATION OF ALUMINA FILM DEPOSITED AT 177 °C .....	231
7.1.1	<i>Calcination at 500 °C</i> .....	231
7.1.2	<i>Calcination at 600 °C</i> .....	232
7.1.3	<i>Calcination at 800 °C</i> .....	233
7.1.4	<i>Blank reaction on the alumina film calcined at 600 °C</i> .....	234
7.2	CALCINATION OF ALUMINA FILM DEPOSITED AT 300 °C .....	235
7.2.1	<i>Calcination of film at 600 °C</i> .....	236
7.2.2	<i>Blank reaction on alumina film calcined at 600 °C</i> .....	237
<b>8</b>	<b>DEPOSITION OF CATALYST CLUSTERS ON ALUMINA COATED SILICA/SI WAFER</b> .....	<b>239</b>
8.1	SPIN COATING ON CALCINED ALUMINA SURFACE .....	240
8.2	TREATMENT OF ALUMINA SURFACE FOR PRODUCTION OF HYDROXYL GROUPS FOR DEPOSITION OF CLUSTERS .....	242
8.2.1	<i>Treatment with 0.5 Torr of water for 30 minutes</i> .....	242
8.2.2	<i>Treatment with basic Piranha solution (high concentration)</i> .....	243
8.3	DEPOSITION OF CLUSTERS ON UNCALCINED ALUMINA ON SILICA/SI SURFACE .	244
8.3.1	<i>Treatment of alumina surface with 1 - 10% RCA-1 solution to produce –OH groups</i> 245	

8.3.2 *Spin coating of alumina surface treated with 10% RCA-1 solution with Iron Nitrate 246*

<b>9</b>	<b>REACTION ON IRON SALT DEPOSITED ON ALUMINA COATED SILICA/SI WAFER.....</b>	<b>248</b>
9.1	IRON SALT ON UNCALCINED ALUMINA SURFACE .....	248
9.2	IRON SALT ON CALCINED ALUMINA SURFACE.....	250
<b>10</b>	<b>DISCUSSION .....</b>	<b>252</b>
<b>11</b>	<b>CONCLUSION .....</b>	<b>255</b>
<b>12</b>	<b>REFERENCES.....</b>	<b>256</b>

## List of Figures

- Figure 1 The AFM scan shows surface to be rough compared with deposition on the native silicon oxide. The relative roughness of the surface is about 0.2 nm. .. 216
- Figure 2 The AFM figures from left to right show alumina coating of 50, 100, 150 and 200 cycles. The surface is very flat and the roughness does not change much from the silica surface or the number of alumina coatings..... 220
- Figure 3 AFM analyses performed on alumina coatings carried at 300 °C shows smooth topography. The relative roughness of the surface measured as the rms value is about 0.2 nm in average..... 222
- Figure 4 AXPS result for 50 and 100 layers deposited at 177 °C show presence of alumina. Al signal increases with number of coatings as is obvious. The Si signal correspondingly decreases..... 224
- Figure 5 AXPS result for 20 and 100 layers for alumina deposited at 300 °C. The Al intensity increases with number of coatings as expected. The Si signal decreases though does not disappear..... 225
- Figure 6 The thickness of alumina deposited at 177 °C varies linearly with the number of cycles of coating. .... 226
- Figure 7 Growth of film thickness is linear with the number of cycles of alumina deposition at 300 °C. The growth rate is approximately 1 Å/cycle, a value that matches closely with the literature..... 227

Figure 8 The thickness vs. No. of cycles plot shows almost no variation in the error bar for the thickness of alumina deposited on native silicon oxide. The growth rate is also constant at  $\sim 1.2 \text{ \AA}/\text{cycle}$  for both the cases. .... 229

Figure 9 Alumina coated  $\text{SiO}_2/\text{Si}$  wafer shows almost no change after calcination at  $500 \text{ }^\circ\text{C}$ . The relative roughness is about  $0.24 \text{ nm}$ . .... 231

Figure 10 Wafer calcined at  $600 \text{ }^\circ\text{C}$  for one hour at a low temperature ramp of  $0.5 \text{ }^\circ\text{C}/\text{min}$  does not change the surface to a great extent. Relative roughness is about  $0.24 \text{ nm}$ . .... 232

Figure 11 Calcination of 200 layers of alumina coated surface when calcined at  $800 \text{ }^\circ\text{C}$  shows pits that indicate that the layers are not stable to temperatures of  $800 \text{ }^\circ\text{C}$ . .... 233

Figure 12 Treatment of pre-calcined wafer sample ( $600 \text{ }^\circ\text{C}$ ) develops pinhole structure on the alumina-coated surface when treated at  $900 \text{ }^\circ\text{C}$  for 5 minutes. This indicates that the surface is not stable at  $900 \text{ }^\circ\text{C}$ . .... 234

Figure 13 Alumina coated samples on Silicon wafer coated at  $300 \text{ }^\circ\text{C}$  shows a smooth surface. Average roughness was about  $0.17 \text{ nm}$ . .... 235

Figure 14 Alumina film deposited at  $300 \text{ }^\circ\text{C}$  after calcination at  $600 \text{ }^\circ\text{C}$  shows formation of clusters that are distinctly distributed in two sizes. The cluster formation may be because of crystallization of film. .... 236

Figure 15 Carrying a blank reaction (only in He) produces a discontinuous film about  $1 - 2 \text{ nm}$  thick. The film is not uniformly spread across the surface, at places covering only a small area. .... 237

Figure 16 The cluster deposition on alumina coated silica/Si wafer shows almost no deposition for low concentration of iron nitrate solution (top left and right) while for a high concentration of salt (2 mmol/L, bottom) a very large salt deposition more likely because of precipitation occurs..... 241

Figure 17 Treatment with water vapors at 0.3 Torr for 30 minutes at 120 °C did not lead to any deposition of clusters after spin coating..... 242

Figure 18 The treatment of the calcined alumina surface with RCA-1 solution leads to its roughening (left). Spin coating of 0.1 mmol/L iron nitrate solution deposits good density of clusters on the surface but are somewhat difficult to discern from the AFM images..... 243

Figure 19 No clusters of appreciable density are deposited on as produced alumina coating. The few clusters seen deposited are separated very far away and the large particles are probably from the dust contamination..... 245

Figure 20 Alumina surface when treated with 1% RCA-1 (left) shows almost no deposition of clusters on the surface. Treatment of the surface with 10% RCA-1 solution (right) does lead to good number of clusters though the density is still not so high as the one obtained on silica surface..... 246

Figure 21 Alumina coated SiO<sub>2</sub>/Si wafer was treated with 10% RCA-1 solution and then spin coated with 0.2 mmol/L iron nitrate solution at 4000 rpm. The distribution of clusters seems uneven on the surface. .... 247

Figure 22 AFM shows the clusters before reaction (left) and after reaction (right). The clusters are seen on the surface after reaction conditions but no carbon nanotubes could be easily discerned..... 249

Figure 23 The spin coated alumina surface is shown by the AFM image to the left. The surface after the reaction is shown to the right. The AFM shows presence of structures on the catalyst but is not clearly discernible..... 251

# 1 Introduction

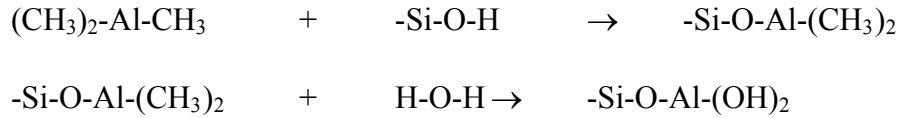
Atomic layer deposition (ALD) was first reported by Aleskovskii [1] for atomic layer growth of titania and germania on top of silica. Suntola [2] first invented the technique of atomic layer epitaxy in 1974 for forming thin amorphous films of semiconductor material. Current potential application for ALD is in the development of high dielectric gate applications. The reduction in size of metal oxide on silicon for advanced gate dielectrics has made atomic layer deposition a very attractive technique. The traditional gate oxide employed was silica on top of Si thermally grown under controlled environment. The current requirement of Ultra large-scale Integration units is pushing the thickness of silica layer to as low as 30 Å and needs to go further down. Around ~20 Å of gate oxide thickness, various problems creep in such as high leakage current and the stability of oxide. To overcome this fundamental limitation, materials other than silica with higher dielectric constant need to be incorporated as gate oxides, which will also be compatible with the silicon. To reduce the leakage current, the small thickness of the new material should provide a high capacitance. This is accomplished by employing dielectric material with high permittivity (K). Typical materials employed are ZrO<sub>2</sub>, HfO<sub>2</sub>, TiO<sub>2</sub>, Ta<sub>2</sub>O<sub>5</sub>, Y<sub>2</sub>O<sub>5</sub>, Al<sub>2</sub>O<sub>3</sub>, Gd<sub>2</sub>O<sub>3</sub>, La<sub>2</sub>O<sub>3</sub>, Hf and Zr silicates, La silicates, and Gd silicates [3]. The dielectric constant for these materials varies from 10 – 40 range, about 3 to 10 times higher than silica ( $\epsilon = 3.8$ ).

## 2 Background of Atomic Layer Deposition

The preparation of flat model supports can be done at atomic level using atomic layer deposition on single crystal with suitable reactive surface. Atomic layer deposition involves sequential approach of saturating a surface with a reactive metallic precursor and this in turn is reacted with another species to form metal oxide [4]. The reaction is self-limiting in the sense that once the precursor reacts with the surface of the substrate, no further reaction takes place and there is no more deposition of the precursor on the surface. The excess of the first precursor is purged out and then second precursor is introduced that will regenerate the surface required for reaction with the first precursor. Alumina thin films were grown since 30 years for electroluminescent applications by atomic layer epitaxy [1] employing  $\text{AlCl}_3$  and  $\text{H}_2\text{O}$ . Presence of chlorine in the system makes it necessary to process the film at temperatures above  $500\text{ }^\circ\text{C}$  to drive away the impurities. The severe processing condition may be harmful for the integrity of the structures on which the film is deposited. Other precursors such as Al alkoxides [5], trialkyl Al and such have been used for low temperature deposition of aluminum films [6]. In case of alumina deposition, we begin with hydrogen passivated silicon or silica surface that is terminated with hydroxyl groups. A reactive organometallic compound such as trimethyl aluminum  $[(\text{CH}_3)_3\text{Al}]$  (TMA) that reacts violently with water is chosen as the metal oxide precursor. When exposed in limited amount and under dilute conditions (to prevent vapor deposition), the hydroxyl group on the surface of silica reacts with trimethyl group releasing one methane molecule and binding the alumina group to its oxygen. Exposure to water releases the excess methyl group and forms

terminal hydroxyl groups that are further available for reaction with trimethyl aluminum.

The reaction proceeds as follows:



The reaction of trimethyl group of TMA with surface hydroxyl group followed by water reaction with remaining methyl groups of TMA constitutes one cycle. The growth rate reported increases with temperature to a maximum of about 1.2 Å/cycle at ~177 °C and decreases further on [7]. Our study agrees with this observation. The biggest advantage of atomic layer deposition is the conformal deposition of one layer over another. A highly convoluted surface or surface with a very high aspect ratio can be uniformly coated without areas that typically remains shadowed during vapor deposition of metal. We also observe a constant growth rate up to 200 cycles of deposition indicating that the number of reactive sites does not increase with film growth. This indicates that the formation of film is conformal to the underlying silica surface.

### 3 Characterization of thin films using Ellipsometry

Thickness of alumina film was determined by ellipsometry. Ellipsometry studies are very sensitive to sub atomic layer coverage and hence very appropriate in the current study [8,9]. The repeatability and non-destructive nature of the technique makes it very easy to employ and compares well with some of the more sensitive techniques such as Medium Energy Ion Scattering Spectroscopy (MEIS) and High Resolution Transmission Electron Spectroscopy (HRTEM) [10].

The technique involves measuring the experimentally determined angle  $\Delta$ , which is the difference in the phase shift that occurs during reflection and  $\psi$ , the arctangent of the magnitudes of the reflection coefficients. These angles are related to the Fresnel reflection coefficients ( $R^P$  and  $R^S$ ) as follows:

$$\rho = \tan\psi e^{i\Delta} = R^P/R^S$$

The quantities  $R^P$  and  $R^S$  are functions of the incident angle, the thickness of the film present, and the refractive indices of the layers. In principle, the technique can be applied to as many layers present on the bulk substrate provided the refractive indices of the material is well known. For a superb derivation of the models and employing the equations for determining the thickness of the film on bulk substrate, we refer the reader to Tompkins' book on Ellipsometry [11]. In brief, a plot of  $\psi$  vs.  $\Delta$  is plotted for a known value of refractive index of the thin film and that of the bulk material, thickness of the

film, the angle of incidence and wavelength of light incident. The experimentally determined values of  $\psi$  and corresponding  $\Delta$  is made to lie on the plot. If the assumed values of refractive indices are accurate, the points will lie on the profile. Each point on the profile corresponds to certain thickness of the film and is thus used to determine it. In our results, we found the thickness matches very closely to the reported values in literature.

## **4 Effect of support on production and growth of carbon nanotubes**

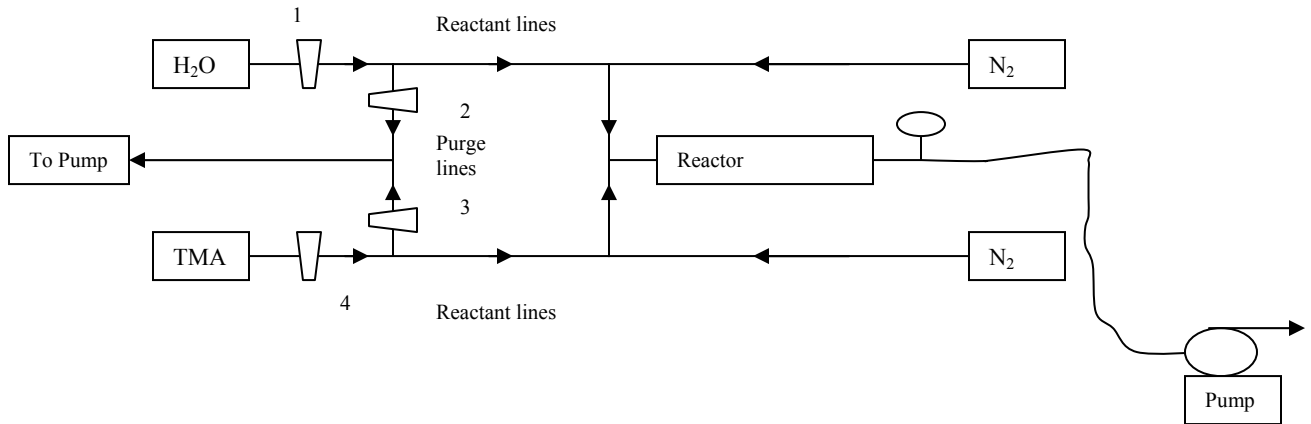
The support plays a major role in catalytic reaction. Besides providing the large exposure of catalyst material, it also leads to a specific relation with catalyst by means of charge transfer that either enhances or reduces the catalytic efficiency and selectivity of the metal towards production of desired product. One of the aims of our experiments was to observe the effect of different support material for growth of carbon nanotubes. Most of the work has been done with alumina and silica as support. Titania shows a very strong metal support interaction with metal clusters, which leads to catalyst particle's immersion in the support under strong reducing conditions at high temperature [12]. For this reason, we only carried out alumina coating deposition on silica and studied its effect. We have performed experiments with silica as model support and the growth yield has not been high. De los Arcos et al [13] have shown that alumina is indeed a better support for growth of carbon nanotubes because of its better interaction with the iron. Strong interaction between iron and silicon resulting in the formation of iron silicide phase precludes many of the iron catalyst clusters to remain active for the formation of carbon nanotubes [14]. In such case, it will be interesting to study the effect of support for the model catalyst and observe the growth of carbon nanotubes on such wide ranging support properties.

The other advantage of atomic layer deposition is formation of transition metals directly on the support surface which will be in their pure form [15, 16]. This will

necessarily give a large class of materials that can be synthesized in thin films with very interesting properties [17, 18]. We observe here that atomic layer deposition opens up a whole new area for applications in catalysis, micro and nano-electronics, and novel material synthesis. The substrate synthesis temperatures are low enough so that applications of high-quality high-k dielectrics are possible to temperature sensitive substrates, such as carbon nano-tube transistors and photo-resist patterning by liftoff.

## 5 Atomic layer deposition equipment design

### 5.1 Design of ALD equipment:



### 5.2 Reactor Description

Equipment design is based on Elam et al. work [19]. The equipment consists of a main reactor that has an internal diameter of 2.37" and can easily house a 2" wafer inside it. The wafer is mounted on a rectangular aluminum block with circumscribed recess to hold the wafer. The block also has three through holes parallel to the wafer surface with inner diameter of 0.25" to house the cartridge heaters. There is a small 0.0625" hole just below the surface to house the thermocouple. The cartridge heaters are connected to the external power supply through ultra-high vacuum seal and controlled using a temperature controller. The temperature on the silicon wafer was measured to be uniform throughout the surface. The reactors all have conflat flange connections for diameters above 0.5" and below it, VCR fittings. The pressure in the reactor was measured at the outlet of the

reactor by Baratron Capacitance Manometer (10 Torr range). Vacuum was maintained using Hitachi 160 VP mechanical pump (capacity 175 l/min) to about ~2 Torr in the reactor chamber connected via nitrogen trap. The reactor including the dosing line after the regulating needle valve (described below) is kept at ~90 °C to avoid condensation of the reactant on the chamber wall. The cartridge heater raises the temperature of the wafer surface to the desired reaction temperature. Reaction was carried at 177 °C, 250 °C and 300 °C.

### **5.3 Inlet system for reactants**

It is connected by inlet to two reactants needed for atomic layer deposition. In our case we employ trimethyl aluminum (TMA) and water in sequential order to grow alumina layers on top of silica layer. The reaction is self-limiting and needs only small exposure of reactant to the silica surface. The inlet of the reactants to the main reactor is connected via ‘reactant’ solenoid valve (1 and 4 in diagram), which controls the exposure of the reactant to the surface. The reactant stream is further connected to N<sub>2</sub> lines that help purge the reactor of the reactants preventing mixing of the reactants. A purge line for both reactants is provided that is an offshoot from the reactant line going towards another pump (Alcatel 2008A). This keeps the reactant line under N<sub>2</sub> purge when reactant solenoid valves are closed and ‘purge’ valves 2 and 3 in diagram are open.

In both reaction and purge mode, N<sub>2</sub> is continuously flown through the reactor so as to maintain the reactor pressure at about 2 Torr. TMA and water react rapidly with each

other and their mixing is to be strictly avoided to prevent any gas phase CVD deposition. We will illustrate one example of the working of the reactor. With N<sub>2</sub> continuously flowing, the solenoid valve in the purge lines is kept open. N<sub>2</sub> flows through the reactor and also through the purge lines. Keeping valve 2, 3 and 4 closed, opening solenoid valve 1 exposes TMA to the silica surface. TMA has a vapor pressure of 11 Torr and transported at supersonic speed to the reactor chamber saturating the silica surface. It takes about 0.33 seconds to saturate the surface under our reaction conditions; we provide an exposure of 1 second. To close TMA exposure, valve 1 is closed; valve 2 is opened to purge the TMA reactant line. About 25 seconds are allowed to purge the reactor and the reactant lines of the TMA vapors. Then water is exposed for 1 second in exactly the same order with valve 4 open, valve 3, 2, and 1 closed. The process continues alternatively with exposure of TMA and water constituting one cycle and 1 alumina layer. The control of the exposure of reactants with appropriate purging and the temperature of deposition are critical factors in the uniform deposition of the film. Other important aspect is the presence of hydroxyl groups on the surface of silica to make way for the formation of alumina as these provide the reactant species for the alumina deposition.

## **6 Atomic layer deposition of alumina on Silica/Si model support**

The procedure we followed for studying the growth of alumina layer was according to the experiments of Elam et al. [19, 20], determine the suitable conditions in our experimental set up and then make modifications for our requirement. This will also help us to check the working of our equipment, which had few modifications from the one in Elam's work. The experiment work carried out was in following order:

- a. Stripping the native silicon oxide from Si (100) to have H<sub>2</sub> terminated silicon surface. Perform atomic layer deposition on the surface and compare the results with Elam et al. work.
- b. Different number of alumina coating on thermally grown silicon oxide on Silicon and measuring their thickness using ellipsometer.
- c. Producing alumina coating on native silicon oxide.
- d. Effect of producing hydroxyl groups using water vapor and RCA-1 source.
- e. Thermal stability of the alumina film.
- f. AFM analysis of samples.
- g. Deposition of catalyst clusters on alumina coated wafer.
- h. Reaction with carbon source to form carbon nanotubes.

The study centers on the overall deposition and characterization of alumina film formed on silica/Si surface. Once alumina film is reproducibly deposited on the surface,

the next step is to analyze its thermal stability and then deposit the catalyst clusters on it to observe its reactivity for the formation of carbon nanotubes.

## 6.1 Alumina coating on HF treated Si (100) surface

The native silicon oxide on Si (100) was etched employing buffered HF (BHF) solution that has surface etch rate of 1000 Å/min. The wafer was cleaned with multiple rinses of toluene, propanol and ethanol and dried in nitrogen. The surface was then dipped in buffered HF for 20 seconds and then rinsed thoroughly with ultra clean DI water and dried in nitrogen. The wafer was transferred to ALD equipment and coated with 100 layers of alumina at 177 °C. The cycles were performed in 1 second of TMA and water exposure (0.1 Torr) interspersed with 25 seconds of nitrogen purge resulting in 1 – 25 – 1 – 25 seconds cycle. The preheater temperature was maintained at 90 °C. The base pressure was ~2 Torr and total flow rate of nitrogen was 200 ml/min.

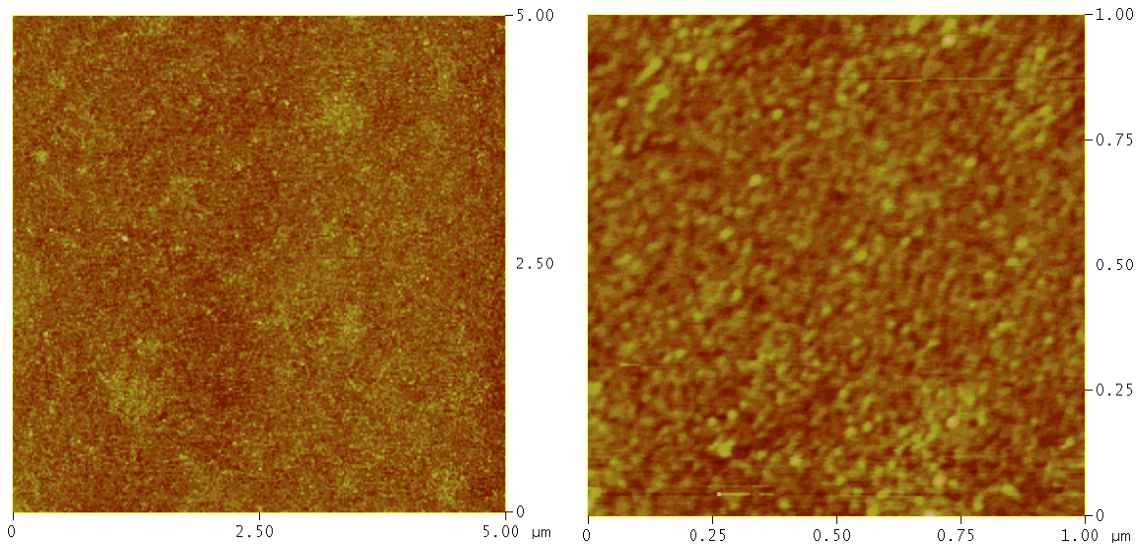


**Figure 1** The AFM scan shows surface to be rough compared with deposition on the native silicon oxide. The relative roughness of the surface is about 0.2 nm.

The AFM images (Figure 1) of the alumina coated surface on HF treated Silicon surface appears rough. The roughness is caused by etching of surface and is carried over to alumina surface. The relative roughness was still within tolerable limits (0.2 nm).

Surface coated with alumina was studied using Ellipsometer. The native silicon oxide is absent in present case so we have alumina layer on bulk silicon, whose thickness is easy to calculate. Ellipsometric readings were taken for light of wavelength 633 nm and at an angle of incidence of  $70^\circ$ . We plot  $\Delta$  vs.  $\psi$  for a given refractive index of silicon and alumina. The refractive index determined by fitting the plot with the experimental data points for bulk Silicon is  $N_1 = (3.835, -0.018)$  and for alumina is  $N_2 = (1.65, 0.0)$ , where the N's are complex numbers. The value of bulk silicon refractive index varied between  $(3.835 \pm 0.004, -0.018)$ , a small variation in the number. The fitting of the experimental readings were done by varying the refractive index of the alumina coating and intermediate silicon oxide refractive index ( $N_2$ ). The alumina refractive index varied between  $1.65 \pm 0.03$  for all calculations. The refractive index of silica in our calculations varies between  $1.46 \pm 0.02$ . These values were employed in determining the thickness of the alumina film coated on silica/Si surface.

## **6.2 Alumina coating on thermally grown silicon oxide on Si (100): Thickness variation with number of alumina coatings**

Alumina deposited on native silicon oxide tends to provide enough porosity for oxygen to diffuse and oxidize the silicon underneath [21]. Copel et al. have shown that higher the oxygen pressure, greater is the presence of Si peak at the interface. It could be attributed to the diffusion of oxygen to the interface and reacting with the silicon or silicon atoms could itself diffuse towards the interface and get oxidized. To prevent the effect of underlying silicon, it may be useful to form a large thickness of silica on top of Si (100) on which we could deposit alumina. We thermally grow silica on Si by heating the wafer at  $\sim 850$  °C for 4 – 6 hours. This produces a silica layer of about  $\sim 80$  nm as measured by ellipsometry. Following are the details of the experiment performed.

- i. Wafer samples were cleaned with DI water, dried in  $N_2$  with spinning and treated for 20 minutes with UV-Ozone to remove carbonaceous contamination from the atmosphere.
- ii. Sample after being transferred to the reaction chamber was kept in vacuum for a while and then  $N_2$  was flown to give chamber pressure of approximately 2.0 Torr. The pre-heater temperature was raised to  $\sim 90$  °C and temperature of the heater block was gradually increased to 177 °C/300 °C.
- iii. When the temperature was about 135 °C, the water valve was opened for exactly 5 minutes for the surface of Silica to be hydroxylated. The temperature at the end of 5 minutes was 160 °C.

- iv. Water and Trimethyl aluminum exposure pressure was maintained close to 0.1 Torr. Exposure for 1 second made the pressure rise above the base pressure of  $\sim 2$  Torr by  $\sim 0.1$  Torr.

### **6.2.1 Alumina deposition by ALD at 177 °C**

The reaction temperature was maintained at 177 °C during the whole process of deposition. The number of cycles coated on surface was 50, 100, 150 and 200 (Figure 2). The surface was analyzed using atomic force microscopy. The term used to characterize the smoothness of the surface is the relative roughness value. Care was taken to see that the tip was sharp to prevent unusually low relative roughness as some of the deeper surfaces do not become accessible to it. Relative roughness is the root mean square value of the difference between height of pixels and the average height of pixels. The average roughness of the silica is about 0.2 nm. Depositing the surface with alumina did not vary the roughness to a significant extent. The relative roughness of the surface after 50, 100, 150 and 200 cycles were on average 0.185, 0.248, 0.227 and 0.21. One observes that the roughness value does not have a particular trend with respect to the number of cycles of deposition indicating that the roughness is not changed much with the increase in layers up to 200 layers of coating. The AFM images also show that the surface appears smooth from a height of 10 nm. This smoothness is good enough for depositing 1 – 5 nm clusters on the surface which will be easy to discern on the surface and is of course the main concern of our experiments.

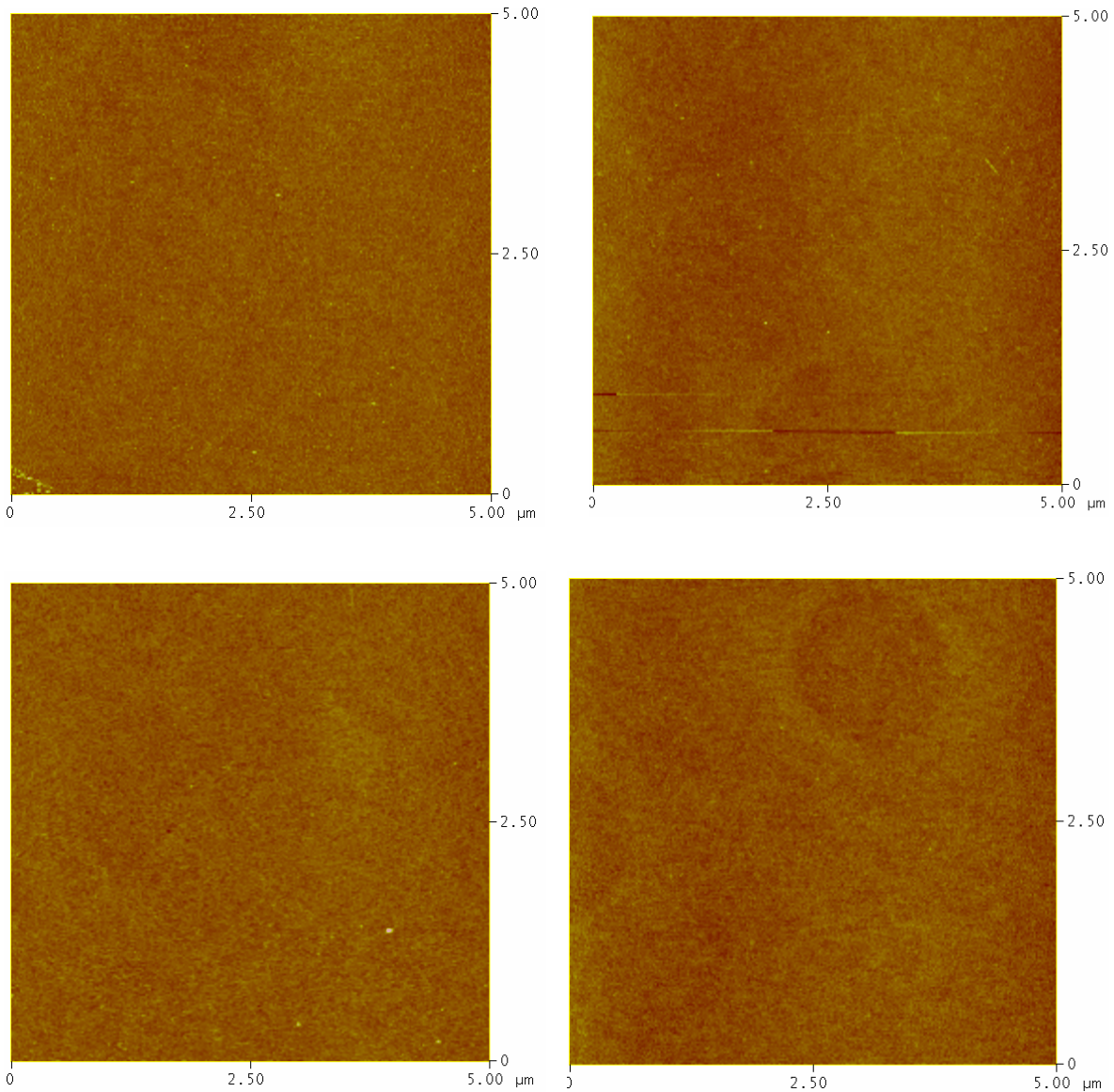


**Figure 2** The AFM figures from left to right show alumina coating of 50, 100, 150 and 200 cycles. The surface is very flat and the roughness does not change much from the silica surface or the number of alumina coatings.

## 6.2.2 Alumina deposition by ALD at 300 °C

The deposition temperature of alumina plays a part on the stability of the film under reaction conditions [21, 22]. It is generally observed that deposition of film at higher temperature results in film that can withstand high temperature processing up to 900 °C. We perform carbon nanotube growth in around these ranges of temperatures so deposition of alumina was carried at 300 °C to study the topography of the film deposited. The other objective was to see the rate of growth of film at different temperatures and compare it with the literature. This will ensure that our modified system is working properly for deposition of alumina film. The rest of the reaction conditions employed were similar to the ones conducted at 177 °C. The base pressure was ~2 Torr with reactant exposure pressure ~0.1 Torr. The number of coatings deposited was 20, 50, 100 and 150 layers. The AFM image for 50 and 100 layers of coating is shown in Figure 3. The surface appears clean and flat like the original silica surface and did not pose any problem to identify our clusters from the surface. The relative roughness is about 0.2 nm for both cases.

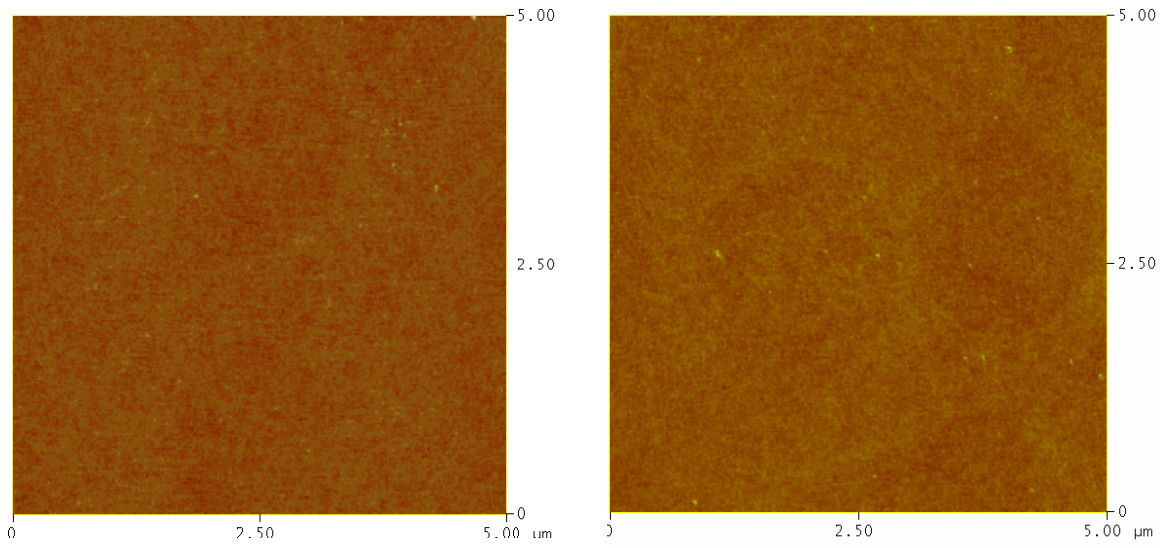


**Figure 3** AFM analyses performed on alumina coatings carried at 300 °C shows smooth topography. The relative roughness of the surface measured as the rms value is about 0.2 nm in average.

### **6.2.3 AXPS Analysis of alumina films deposited at 177 °C and 300 °C**

The surface deposited with alumina was confirmed by angle resolved X-Ray Photo electron Spectroscopy (AXPS). X-Ray Photoelectron Spectroscopy (XPS) works on the principle of emission of electron by absorption of photon of energy larger than its binding energy (BE). Besides binding energy of the electron to the nucleus of the atom, the electron has to overcome hurdles provided by atoms present in its path. Energy required for electrons to overcome its hurdles and come out of the surface is called the work – function of the system. This limits the depth under the surface of substrate from which the electrons can come to the surface, which are usually located about 5 – 10 nm. The advantage of this technique therefore lies in its ability to provide information from the surface of the material making it highly surface sensitive. Our alumina film thickness usually varies between 2 – 20 nm and so the technique is very useful in determining not only the presence of alumina but also its variation with increasing thickness. AXPS adds further to the advantage by taking XPS spectrum at different angles to the normal of the surface. For a given thin film covering a substrate surface, the total path traveled by X-ray will vary with the angle. The XPS data is reported in atomic units. The elemental ratio shows variation of one element with respect to another on the surface of the substrate.

The AXPS results are given for coatings done at 177 °C and 300 °C in Figure 4 and 5 respectively. The number of coatings performed was 50 and 100 layers at 177 °C, and 20 and 100 layers at 300 °C. If we observe coatings done at 177 °C, for 50 coatings, the intensity for Al is low as compared to silica. At 100 coatings, the intensity of Si

decreases while that of Al correspondingly increases. This is proof of alumina deposition on the surface of Si. For deposition at 300 °C, the alumina film is more crystalline in nature which shows a more prominent signal for Al compared to Si. The Al intensity with respect to Si increases with number of coatings as the number of aluminum atoms increases on the surface. We also observe presence of carbon and oxygen. Carbon comes from atmospheric contamination and also some of the methyl groups that may not be completely removed during the coating process. The oxygen arises from the alumina structure. The intensity ratios of Al with respect to Si decreases in most cases of deposition with angle of electron collection. This indicates that there is Si or Si type of structure at the surface. The Si presence on the surface may be because of its diffusion from the interface to the surface as hydroxyl groups make Si atoms very labile. The signal also has contributions from the interfacial silica [23].

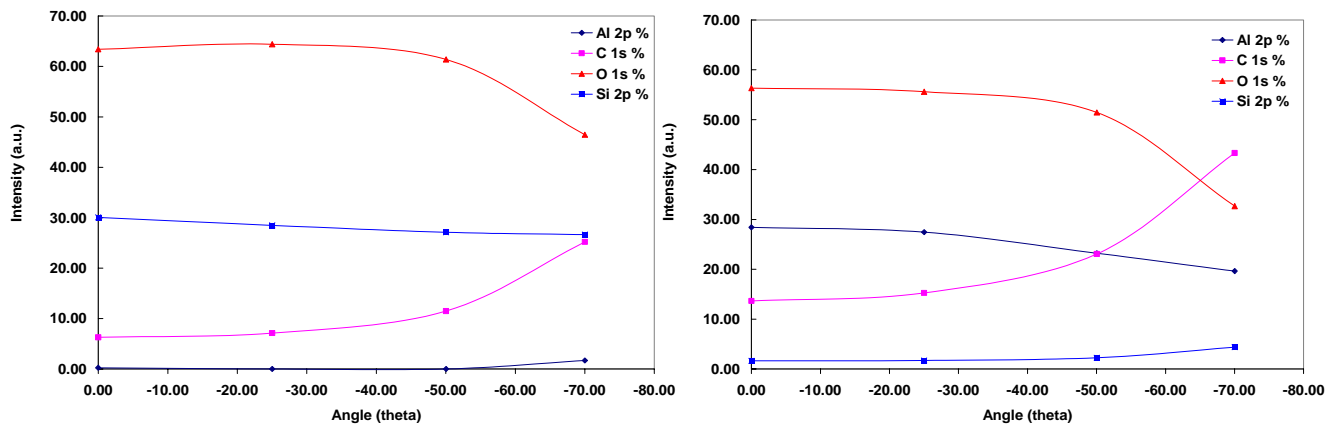


**Figure 4** AXPS result for 50 and 100 layers deposited at 177 °C show presence of alumina. Al signal increases with number of coatings as is obvious. The Si signal correspondingly decreases.

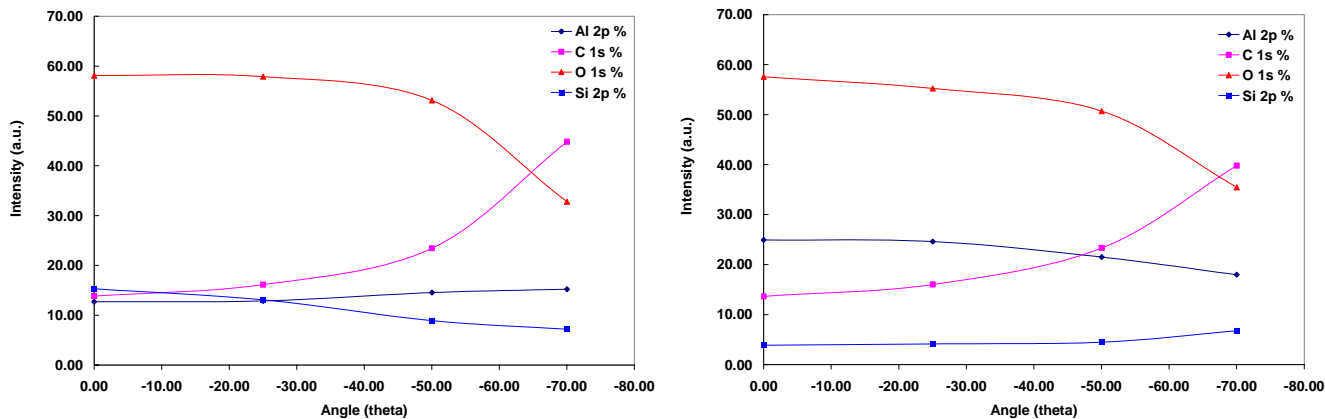


**Figure 5** AXPS result for 20 and 100 layers for alumina deposited at 300 °C. The Al intensity increases with number of coatings as expected. The Si signal decreases though does not disappear.

#### 6.2.4 Thickness measurement of alumina film deposited at 177 °C and 300 °C by Ellipsometry

Ott et al. [7] has shown that the thickness of alumina film varies with the temperature of reaction. The thickness of film deposited per cycle increases with temperature and maximum rate occurs at 177 °C and hence we chose this temperature to perform majority of our reactions. Above 177 °C, the thickness of the film deposited per cycle of alumina decreases with increasing temperature because of rising crystallinity of film that leads to more compactness of atoms. The thickness is measured, in all cases, using Ellipsometry. The refractive index of the silicon bulk sample is measured from experiments performed on HF treated sample that removes the native silicon oxide. The value of refractive index obtained was used in subsequent calculations. Wafers coated with 50, 100, 150 and 200 cycles of alumina coating were studied using ellipsometry.

The thickness of the layers determined with ellipsometry for above cases varies linearly with the number of layers. The following plot shows the results. The thicknesses for 50, 100, 150 and 200 cycles are respectively 9, 16, 24 and 31 nm.

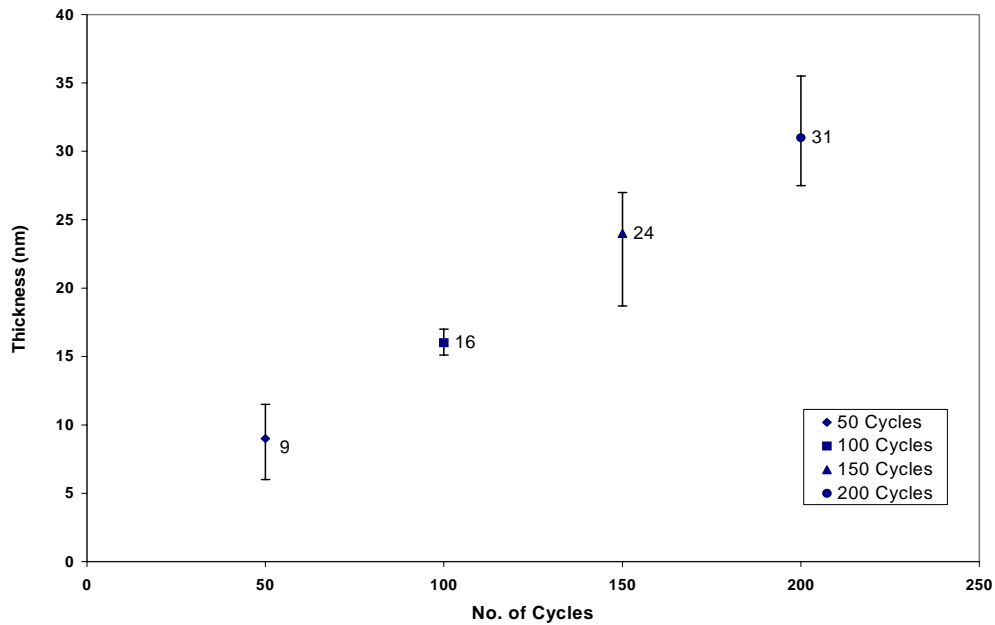


**Figure 6** The thickness of alumina deposited at 177 °C varies linearly with the number of cycles of coating.

The linear variation of film thickness is indicative of the uniformity of deposition. There is a general variation in the measurement of thickness of alumina shown by the error bar in Figure 6. The average growth rate for 50, 100, 150 and 200 cycles was respectively 1.8 Å/cycle, 1.6 Å/cycle, 1.6 Å/cycle and 1.55 Å/cycle. Experiment repeated with 200 cycles was able to give 1.2 Å/cycle as reported in literature. The variation in the thickness of the film may be because of the uneven silica thickness during calcination of the silicon wafer. In our determination of the alumina coating thickness on

silica by ellipsometry, we have assumed an average value of the silica thickness. Our ellipsometry measurements were taken ex-situ in open air and there is a possibility of contamination from air which may contribute to the error bar.

Wafers were coated with 20, 50, 100 and 150 nm of alumina layers at 300 °C. The ellipsometry study of the surface varies nearly linearly as shown in Figure 7. The growth rate for 20, 50, 100 and 150 cycles are 0.84, 1.21, 1.22 and 1.0 Å/cycle. Literature [1] shows that the growth rate is close to 0.9 Å/cycle for deposition at 300 °C, a value close to our prediction of average deposition rate of ~ 1 Å/cycle.

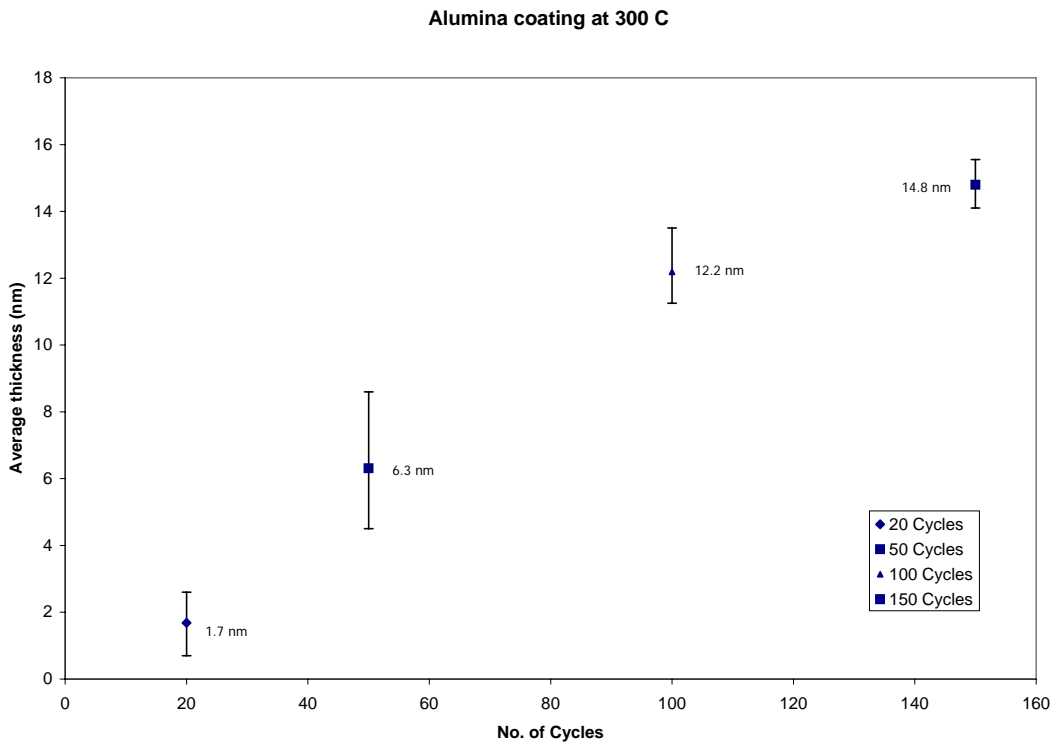


**Figure 7** Growth of film thickness is linear with the number of cycles of alumina deposition at 300 °C. The growth rate is approximately 1 Å/cycle, a value that matches closely with the literature.

### 6.3 Deposition of alumina on native silica on Si (100)

Our deposition on HF stripped native silicon oxide provides a very rough surface. HF treatment is very corrosive process and destroys the surface to a large extent and is not recommended for deposition of alumina if the flatness of the surface is a concern as in our case. On HF treated sample the calculation of refractive index is very reproducible and easy. The introduction of native silicon oxide does add to the difficulty which was circumvented to some extent using a larger thickness of silica (by thermal oxidation). This does add one difficulty though. The formation of silica on silicon by thermal oxidation leads to roughening of surface which is to be avoided as much as possible as it also adds error to the ellipsometer results. Further during the calcination of silicon wafer, the SiO<sub>2</sub>/Si interface does not move uniformly in to the depth of the bulk Silicon with time, giving a film of varying valency of silica contributing to the error in the ellipsometry results. For these reasons further deposition of alumina was carried out on native silicon oxide present on silicon at 250 °C. A higher temperature was chosen as 177 °C falls exactly in the range when silica surface starts losing water attached by hydrogen bonding and may interfere with the alumina deposition. Calculations of thickness of alumina film agreed very well with results in the literature. The average native silicon oxide thickness is 1.85 nm as calculated. For 100 layers of coating, the thickness of the film is 11.8 nm and for 200 coatings, the thickness is 25.4 nm. The growth rate is 1.18 Å/cycle and 1.27 Å/cycle, a close match to the ones reported in the literature [7]. The plot of 100 and 200 layers of alumina deposition on native silicon oxide is shown in Figure 8. The variation in thickness of the film is very low for different samples at a given number of coatings. The results could be attributed to the smoothness of the surface

independently determined by AFM as compared to calcined silicon wafer. The non-uniformity of the interface of silica/Si wafer coupled with increased roughness of the surface provides for a large variation in the thickness measurement of alumina coated on larger thickness of silica on Si against one for native silicon oxide.

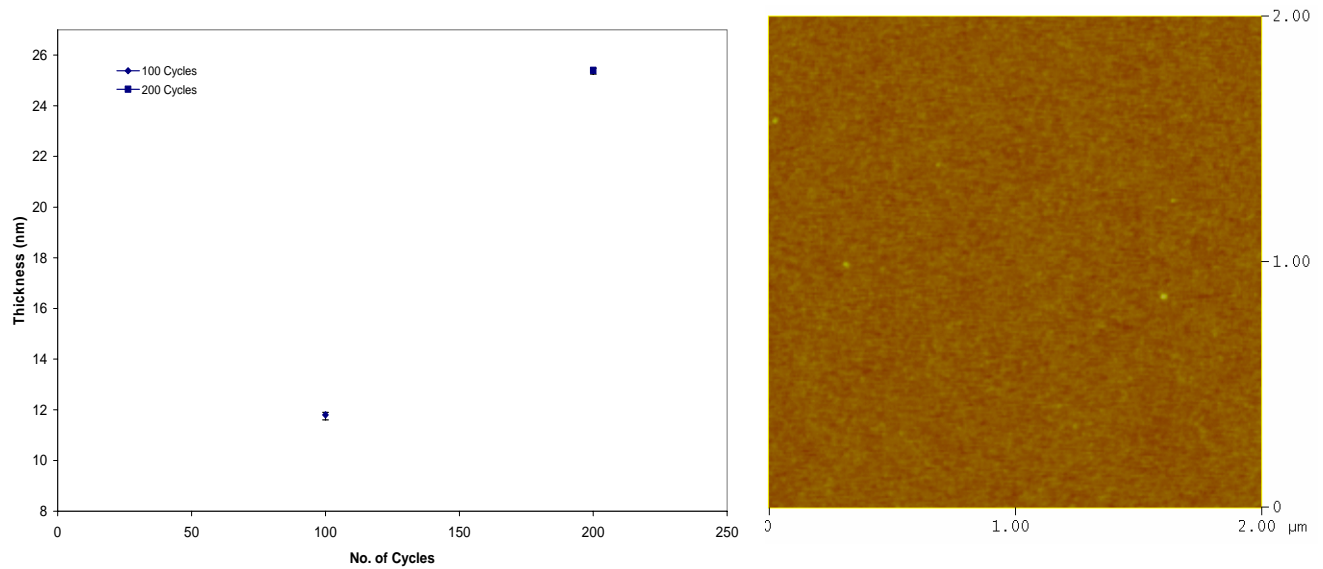


**Figure 8** The thickness vs. No. of cycles plot shows almost no variation in the error bar for the thickness of alumina deposited on native silicon oxide. The growth rate is also constant at  $\sim 1.2$  Å/cycle for both the cases.

## **7 Thermal stability of alumina film**

The performance of alumina film is crucial for both semi-conductor industry as they need processing temperatures as high as 900 °C and for our case where we perform our reactions at these extreme conditions. In literature, thermal stability analysis has been carried at relatively high temperatures from 600 °C – 900 °C but only for few seconds to couple of minutes and either under relatively inert atmosphere [21] or under vacuum [22]. Various analyses have been carried regarding the gate properties of the film after the annealing process. We decided to measure the stability of the film with respect to the processing conditions employed in growth of carbon nanotubes. We performed thermal study on the stability of alumina film deposited at 177 °C. Under the reaction condition, the film holds its structure integrity up to 900 °C. Prolonged heating at lower temperatures such as 500 °C – 600 °C and then reaction at 900 °C does destroy the structure forming pinholes in the surface. If the film is not calcined for long time, then there is no appreciable change at reaction temperature of 900 °C.

## 7.1 Calcination of alumina film deposited at 177 °C

Alumina deposition was carried at 177 °C for 200 layers. The film was analyzed using atomic force microscopy to observe changes in the surface morphology.

### 7.1.1 Calcination at 500 °C

The temperature of calcination was maintained at 500 °C for 1 hour. The calcination temperature was reached in 6 hours and after calcination the furnace was cooled in ~ 4 hours. Heating to high temperature leads to crystallization of film which in turn would align to the surface on which it is deposited. A slow heating and cooling rate is provided to prevent any misalignment in the crystal structure and resulting in cracks. Figure 9 shows the AFM image of the surface at two different scales after calcination. The surface appears flat with relative roughness of about 0.25 nm.

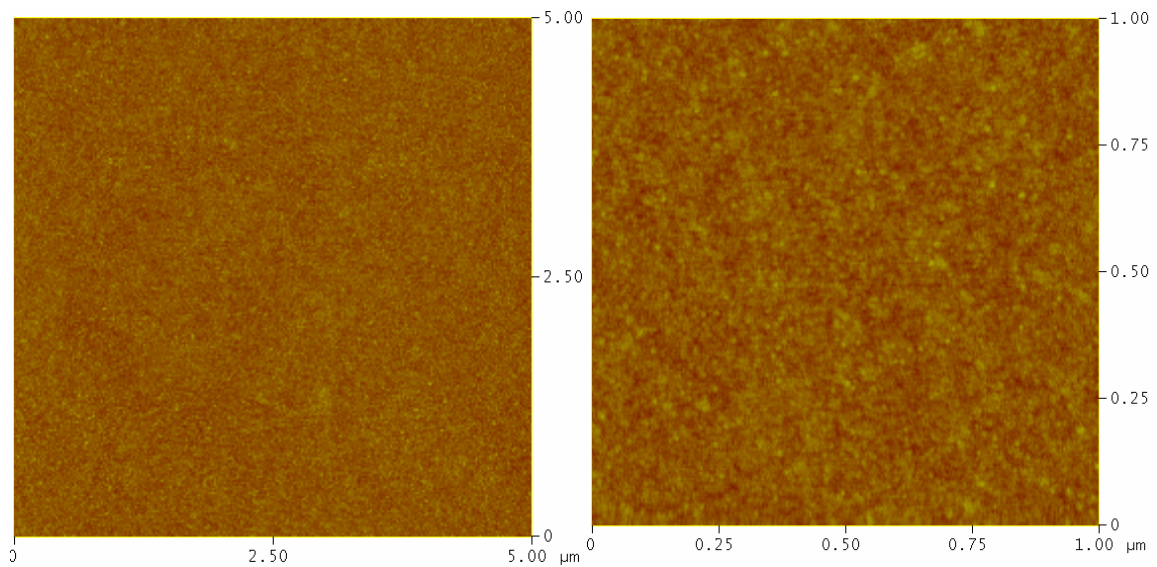


**Figure 9** Alumina coated SiO<sub>2</sub>/Si wafer shows almost no change after calcination at 500 °C. The relative roughness is about 0.24 nm.

### 7.1.2 Calcination at 600 °C

Wafer chips were calcined at 600 °C for one hour (temperature ramp about 0.5 °C/min). The cooling was carried at 1 °C/min rate to room temperature. Calcination was carried in air. There was no appreciable change in the relative roughness and structure of the surface as compared to an uncalcined alumina surface. The relative roughness is about 0.245 nm (Figure 10).

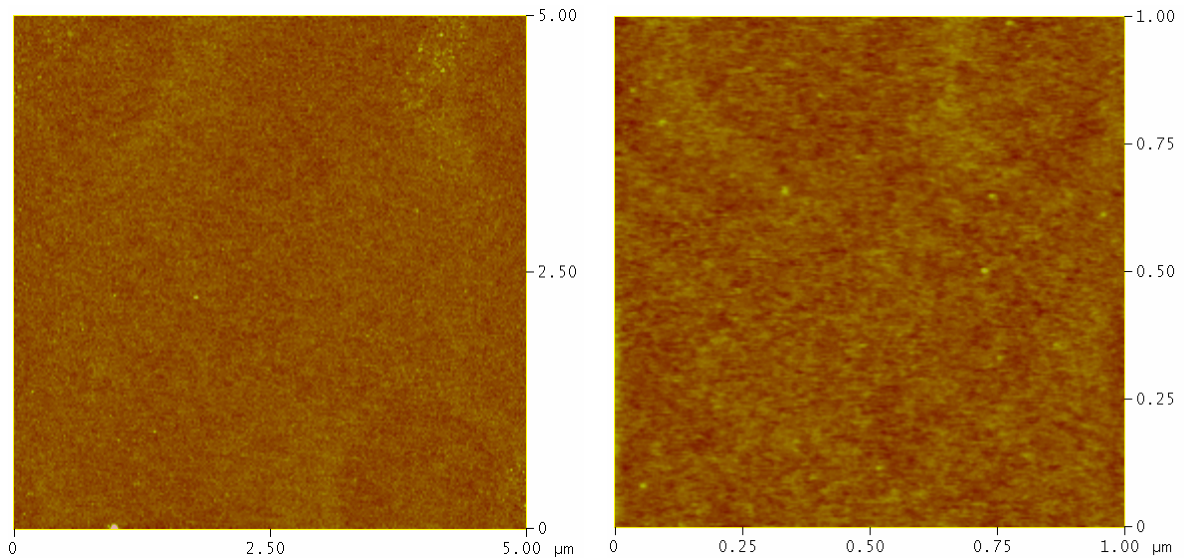


**Figure 10** Wafer calcined at 600 °C for one hour at a low temperature ramp of 0.5 °C/min does not change the surface to a great extent. Relative roughness is about 0.24 nm.

### 7.1.3 Calcination at 800 °C

Calcination was performed at 800 °C for one hour, the temperature reached at 0.5 °C/min and cooled at 1 °C/min. The surface show pits (Figure 11) whose depth varies from 2 to 5 nm. The diameter varies to a large extent from 10 to 300 nm. The thermal stability of film is not sustained at such high temperatures of 800 °C. The slow heating ramp maintains the film at high temperature for much longer time than the actual calcination period. The surface also shows large diameter particles which may be because of crystallization of alumina films. Alumina atoms lost from one part of surface during crystallization forming pits in those sections contributed to the formation of large crystallized clusters.

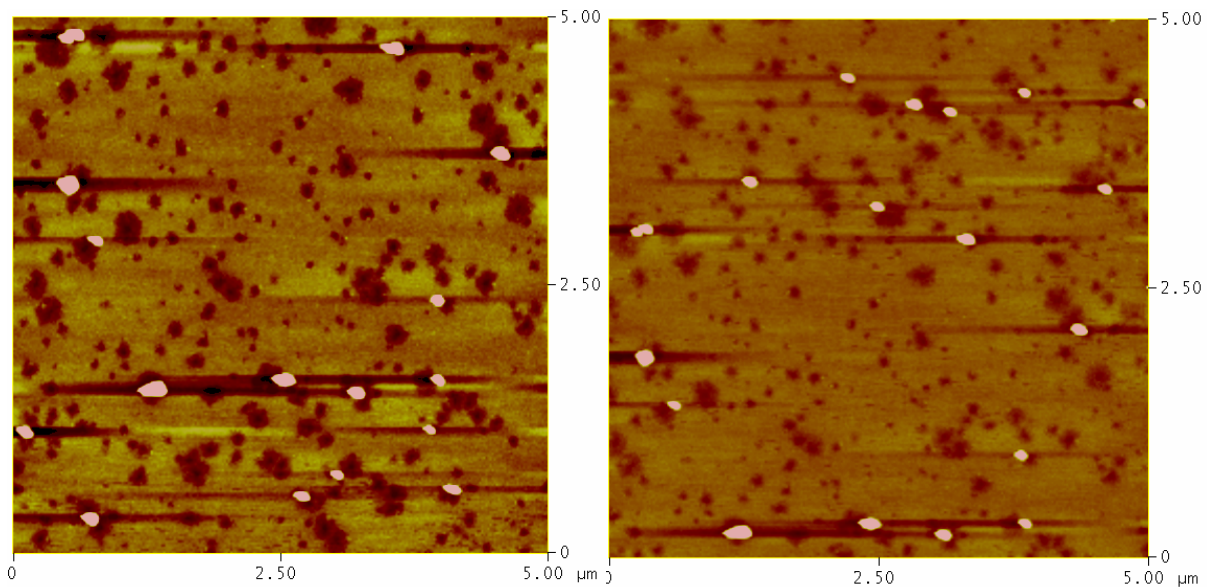


**Figure 11** Calcination of 200 layers of alumina coated surface when calcined at 800 °C shows pits that indicate that the layers are not stable to temperatures of 800 °C.

#### 7.1.4 Blank reaction on the alumina film calcined at 600 °C

Alumina film calcined at 600 °C for 1 hour was treated at 900 °C for 5 minutes (blank reaction) to observe stability of the alumina coating after calcination. The wafer was maintained under helium gas flow (300 ml/min) throughout the blank reaction treatment. After calcination was complete the wafer was pulled outside the furnace without exposing it to atmosphere and kept until the temperature reached 900 °C and then slowly inserted to equilibrate with the furnace temperature. It was kept for 5 minutes and immediately removed after the temperature started to reduce. The surface shows small pinholes being developed in the surface indicating the surface is not stable. The pinholes are about 1 nm deep. The results are given in Figure 12.

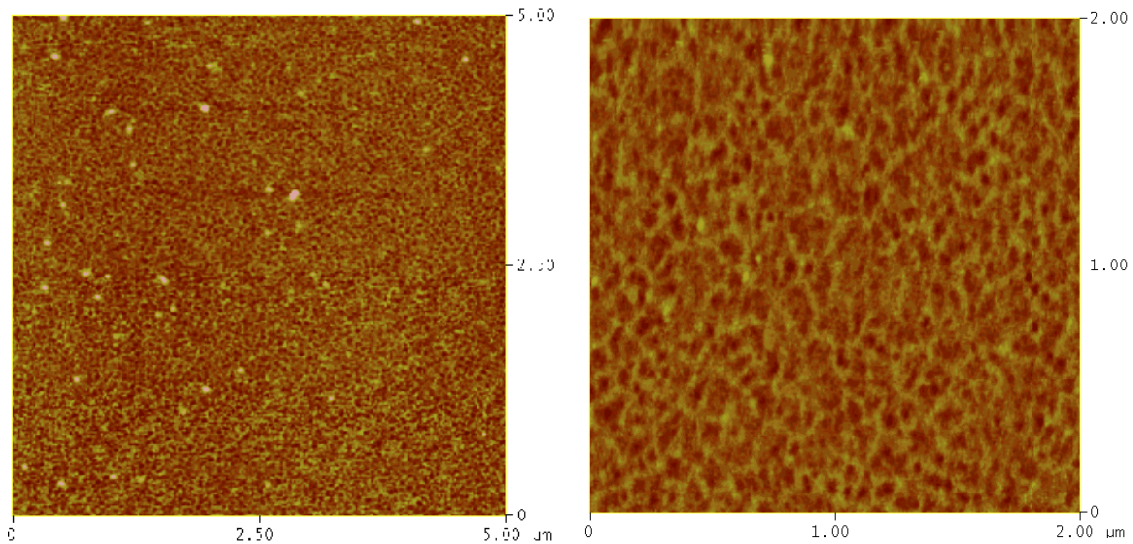


**Figure 12** Treatment of pre-calcined wafer sample (600 °C) develops pinhole structure on the alumina-coated surface when treated at 900 °C for 5 minutes. This indicates that the surface is not stable at 900 °C.

## 7.2 Calcination of alumina film deposited at 300 °C

As reported in literature [21], films deposited at 300 °C show greater stability at 900 °C. The reason for greater stability of the film is probably the semi-crystallization of the surface that will be able to withstand the rapid annealing process. We performed calcination of the film deposited at 300 °C in order to ascertain whether it will remain stable during our conditions of oxidation/reduction and reaction of catalyst. The deposited alumina layer at 300 °C on Silica/Si wafer is shown in Figure 13. Average roughness of the film was 0.17 nm.

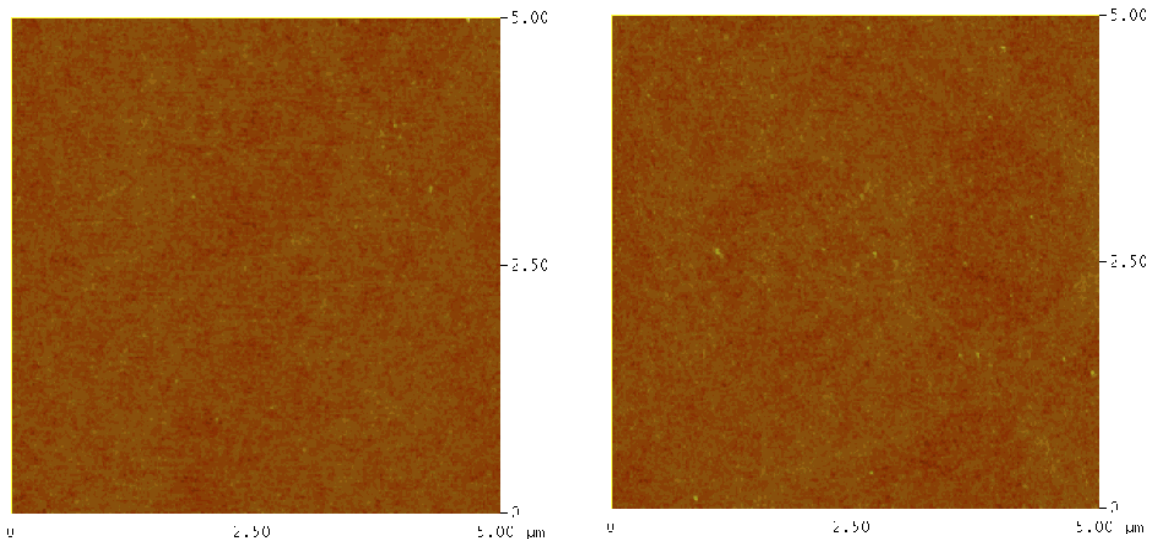


**Figure 13** Alumina coated samples on Silicon wafer coated at 300 °C shows a smooth surface. Average roughness was about 0.17 nm.

### 7.2.1 Calcination of film at 600 °C.

Calcination of the alumina coating (100 layers) show formation of clusters distributed in two size range (Figure 14). One has an average size of about 5-10 nm and other present between 40 – 60 nm. The formation of these particles may perhaps be because of agglomeration of film to form crystalline structures. The distribution of particles is probably because of Oswald ripening, where smaller clusters are consumed to contribute to the formation of larger particles. More experiments are needed to confirm this observation. The disparity in the results after being calcined at 600 °C, seen here for the film deposited at 177 °C and 300 °C may result because of the fact that deposition at 300 °C leads to partial crystallization of film which continues on at 600 °C. It may be guessed that the film deposited at 177 °C if maintained for longer time at 600 °C should show similar behavior.

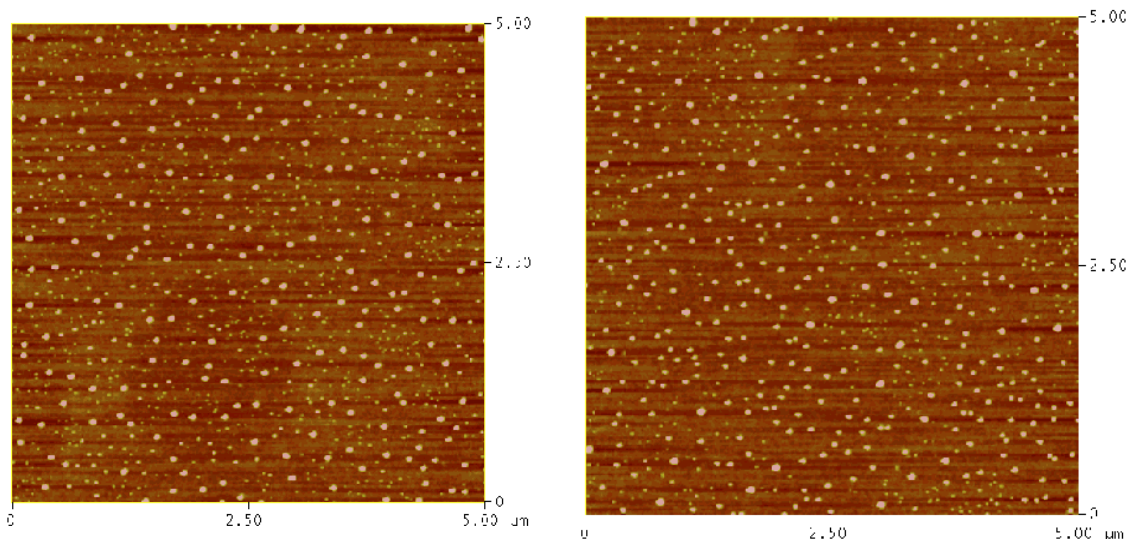


**Figure 14** Alumina film deposited at 300 °C after calcination at 600 °C shows formation of clusters that are distinctly distributed in two sizes. The cluster formation may be because of crystallization of film.

### 7.2.2 Blank reaction on alumina film calcined at 600 °C

The wafer calcined at 600 °C was subjected to treatment at 900 °C for 5 minutes. Only helium was flown (300 ml/min) to maintain inert atmosphere. The surface shows thin film separated from the background with the height of film about 1 – 2 nm in depth (Figure 15). It is interesting to observe that there is no pitting here as observed in case of film deposited at 177 °C but a discontinuous film more like an island.

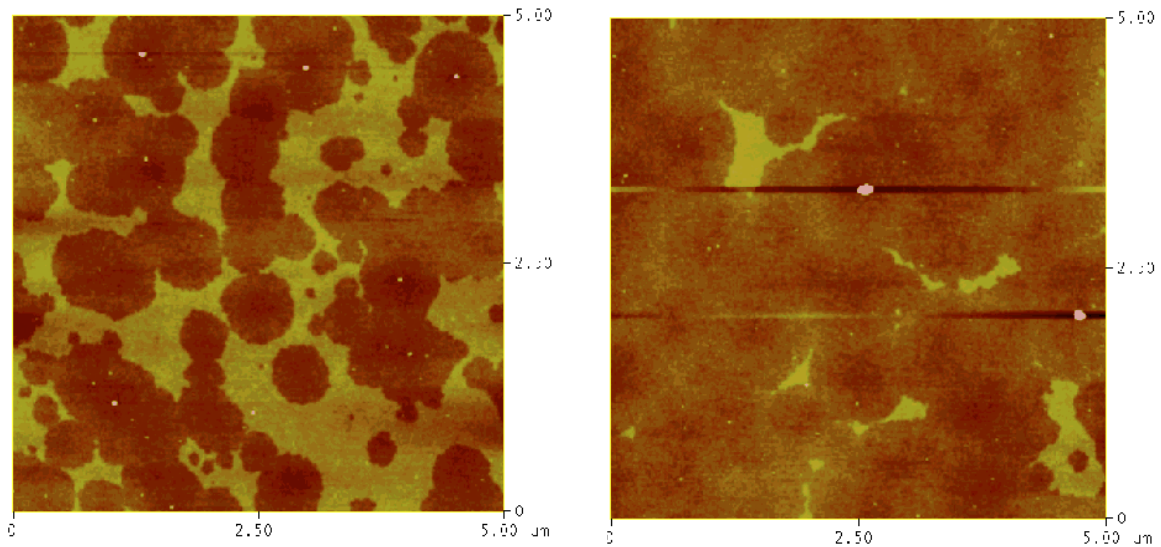


**Figure 15** Carrying a blank reaction (only in He) produces a discontinuous film about 1 – 2 nm thick. The film is not uniformly spread across the surface, at places covering only a small area.

One of the reasons for observation of the instability of film may be because of the long time of calcination that is performed on the surface. The slow ramp of heating and cooling further add time to calcination period. Further studies are needed for determining the nature of the film produced.

In our studies so far, it was concluded that calcined film though remaining flat after the calcination process does not maintain its integrity at higher temperature of reaction. Alumina film deposited at 300 °C shows more prone to crystallize and form clusters as compared to film deposited at 177 °C as it is already in semi-crystalline form at 300 °C. Comparing the calcination results at 600 °C (Figure 10 and 14) one can draw this inference.

## **8 Deposition of catalyst clusters on alumina coated Silica/Si wafer**

The deposition of clusters on alumina posed a different problem because of the surface acidity compared to the silica. It affects the type of surface charges interacting with the solute molecules being deposited from solution during spin coating. The isoelectric point of alumina surface is at pH of about 8 – 9, while that for silica is ~ pH 1 – 2. This in turn indicates that silica acts as a Brønsted acid while alumina acts as a Lewis acid under solution conditions. The proton from silica (hydroxylated silica) can easily react with the anion of the solution ( $\text{Cl}^-$ ,  $\text{NO}_3^{2-}$  etc) to form corresponding salt and help deposit the clusters. The alumina will not usually have the proton to remove the anion of the salt and help deposit the clusters. For deposition, the solution needs to be more basic compared to the surface or the surface needs to be made relatively more acidic.

Alumina surface when coated on silica surface proceeds via hydroxyl group formation on intermediate surface. At the end of the alumina deposition, the surface is terminated with hydroxyl groups. This should provide us with ample of Brønsted acid sites to help deposit the clusters on the surface. The results obtained in our case were contrary to the expected results. No clusters were deposited on calcined alumina surface and very less density on uncalcined alumina surface. We discuss the results in the following sections.

## 8.1 Spin coating on calcined alumina surface

Calcination of surface is important to remove any imperfection in the surface due to incomplete reaction. Alumina coated silicon wafer was calcined at 500 °C for one hour with 6 hours to reach the final temperature. It was set to cool within 4 hours but after a certain point it cooled naturally. Wafer was then spin coated with iron nitrate at varying concentration of salt to have different salt loading on the surface. The concentration was 0.05, 0.1 and 2 mmol/L and speed of spin coating was maintained at 4000 rpm. The results are shown in Figure 16. There was no appreciable cluster deposition on the surface for 0.05 and 0.1 mmol/L concentration of iron nitrate. Except for few clusters on the surface, most of the surface is vacant indicating there are not many sites for the clusters to nucleate and grow. To check whether the salt solution concentration falls short of deposition of enough clusters on the surface, we increased the concentration of salt solution up to 2 mmol/L and spin coating at 4500 rpm, an order of magnitude higher than the previous case. We observed very large clusters in the size range of 150 – 200 nm but they were also very largely spaced in between. The observation coupled with earlier results above indicates absence of hydroxyl groups on the surface that provides the anchoring sites for deposition of clusters. Higher concentration of salt results in precipitation of salt rather than nucleation and growth. The loss of hydroxyl groups occurs primarily because of the calcination treatment.

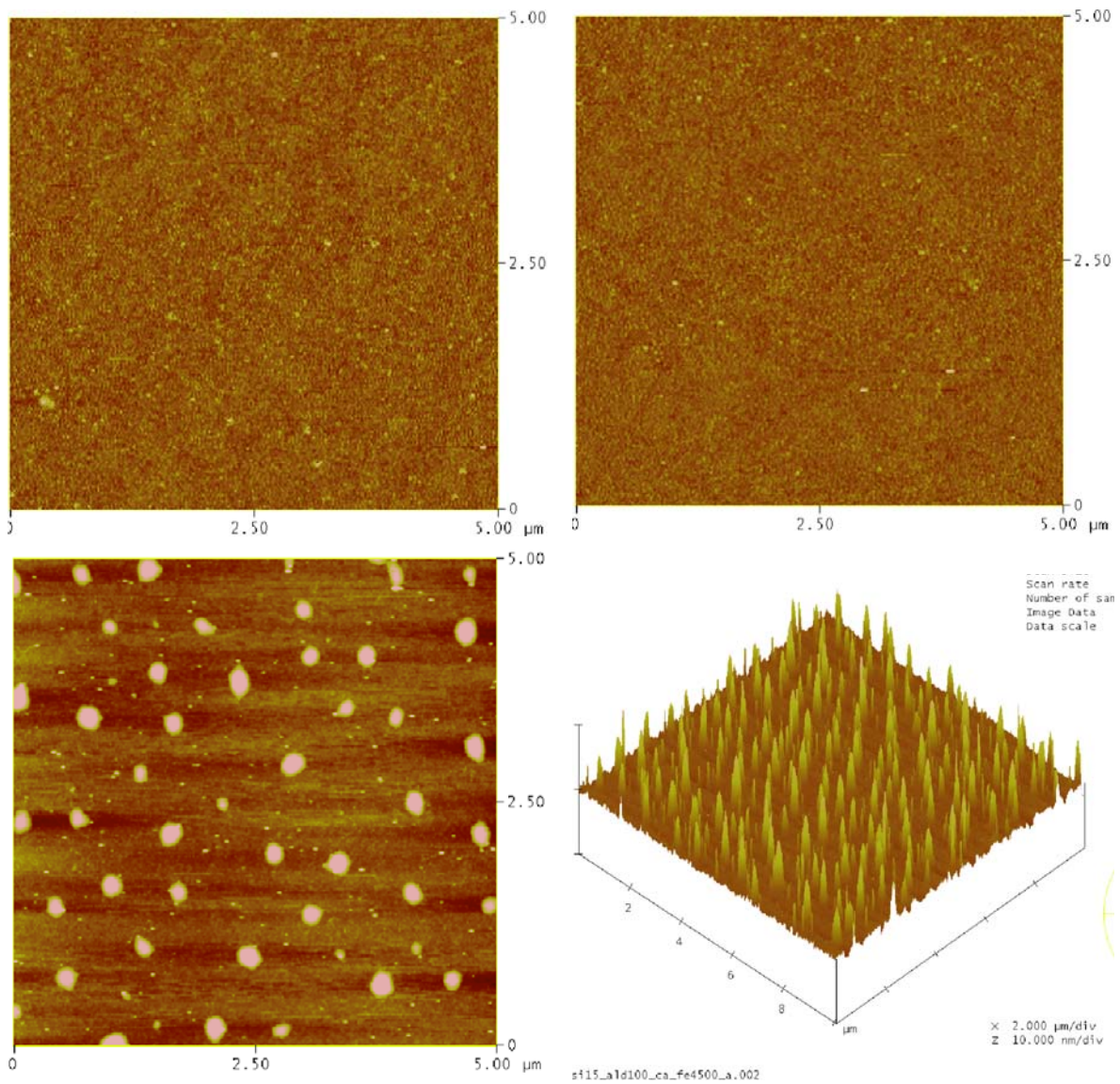


**Figure 16** The cluster deposition on alumina coated silica/Si wafer shows almost no deposition for low concentration of iron nitrate solution (top left and right) while for a high concentration of salt (2 mmol/L, bottom) a very large salt deposition more likely because of precipitation occurs.

## 8.2 Treatment of alumina surface for production of hydroxyl groups for deposition of clusters

The presence of hydroxyl groups for Brønsted acid sites are necessary for the formation of clusters and are essentially completely lost during the calcination process. Our efforts were motivated to that end. The literature [24, 25] shows that exposing the surface to water vapor at around 0.3 Torr produces the necessary hydroxyl groups. More hydroxyl groups can be effectively produced using water plasma which was independently determined in other experiments. Attempts were made to hydroxylate the surface by various techniques and spin coating with 0.1 mmol/L of iron nitrate or iron chloride solution to observe any deposition possible. The results are given below:

### 8.2.1 Treatment with 0.5 Torr of water for 30 minutes

The surface was treated with 0.5 Torr water vapor at 120 °C for 30 minutes expecting this treatment will produce surface -OH group. The surface was then spin coated with 0.1 mmol/L solution of iron nitrate at 3500 rpm. We observed no significant deposition of iron nitrate clusters (Figure 17) indicating no significant change in the surface hydroxyl groups.

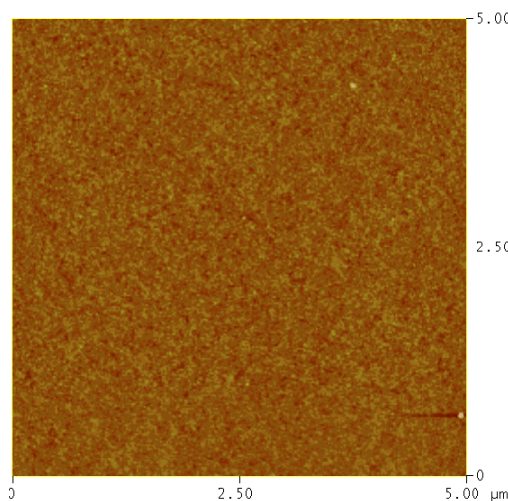


**Figure 17** Treatment with water vapors at 0.3 Torr for 30 minutes at 120 °C did not lead to any deposition of clusters after spin coating.

## 8.2.2 Treatment with basic Piranha solution (high concentration)

The wafer was treated with Piranha solution or RCA-1 solution (70:30 v/v  $\text{NH}_4\text{OH}$ :  $\text{H}_2\text{O}_2$ ) for 10 minutes at room temperature. It was then cleaned and thoroughly washed with deionized water. The surface was then spin coated with 0.1 mmol/L iron nitrate solution at 3500 rpm. AFM images show surface after RCA-1 cleaning of the alumina surface and after spin coating this cleaned surface with iron nitrate (Figure 18). The surface becomes quite rough (relative roughness 0.67 nm) when treated with basic piranha. The cluster size varies between 5 – 10 nm.

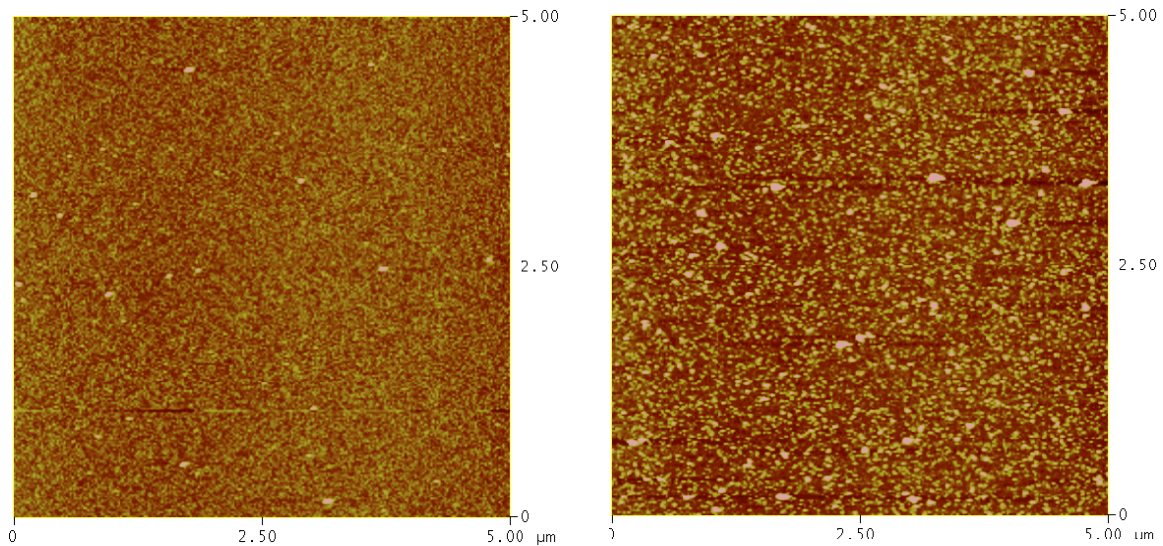


**Figure 18** The treatment of the calcined alumina surface with RCA-1 solution leads to its roughening (left). Spin coating of 0.1 mmol/L iron nitrate solution deposits good density of clusters on the surface but are somewhat difficult to discern from the AFM images.

### **8.3 Deposition of clusters on uncalcined alumina on Silica/Si surface**

The Silica/Si wafers were coated with 100 layers of alumina at 177 °C. The alumina should be terminated with hydroxyl groups but since they are lost during the calcination process, attempt was made to spin coat on the alumina surface as it is prepared. The only drawback of this process will be that any defects during deposition will remain with the alumina film. When we spin coated the alumina coated silica/Si surface with 0.2 mmol/L iron chloride solution at 4000 rpm, almost negligible amount of clusters were deposited (Figure 19). Some of the larger clusters were probably dust contamination from the atmosphere. The reason for such observation could be because of the high basicity of the surface that prevents any cluster deposition. Another reason may be because of the high temperature of deposition (250 °C) which may lead to condensing of the hydroxyl groups to form water. We need more investigation into this case. In any case we could not deposit the clusters on as produced alumina surface or calcined surface.

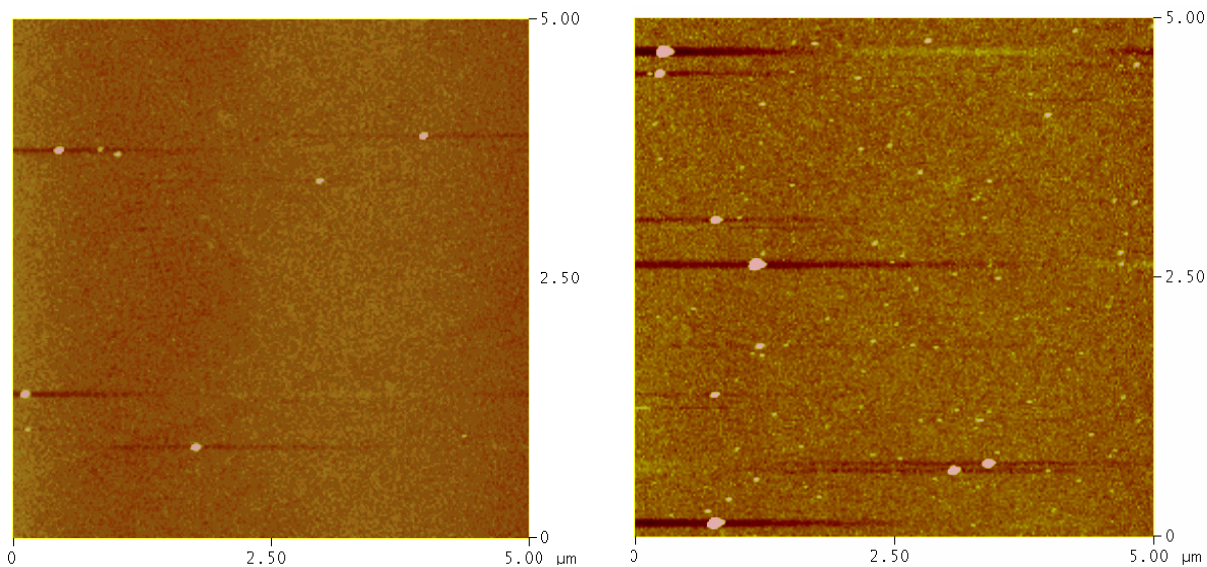


**Figure 19** No clusters of appreciable density are deposited on as produced alumina coating. The few clusters seen deposited are separated very far away and the large particles are probably from the dust contamination.

### 8.3.1 Treatment of alumina surface with 1 - 10% RCA-1 solution to produce –OH groups

To prevent extensive roughening of surface because of strong interaction with the RCA-1 solution, a 1% RCA solution in DI water was produced. The alumina coated Si surface was soaked in the 1% RCA-1 solution for 10 minutes and then cleaned thoroughly with DI water. The water was dried under N<sub>2</sub> in spin coater with spinning. The surface was then spin coated with 0.2 mmol/L of FeCl<sub>2</sub> solution at 4000 rpm. The surface still do not show the good density of salt clusters. When the concentration of RCA-1 solution is increased to 10%, we observe good deposition of clusters without much roughening of the surface. The comparative results are given in Figure 20.

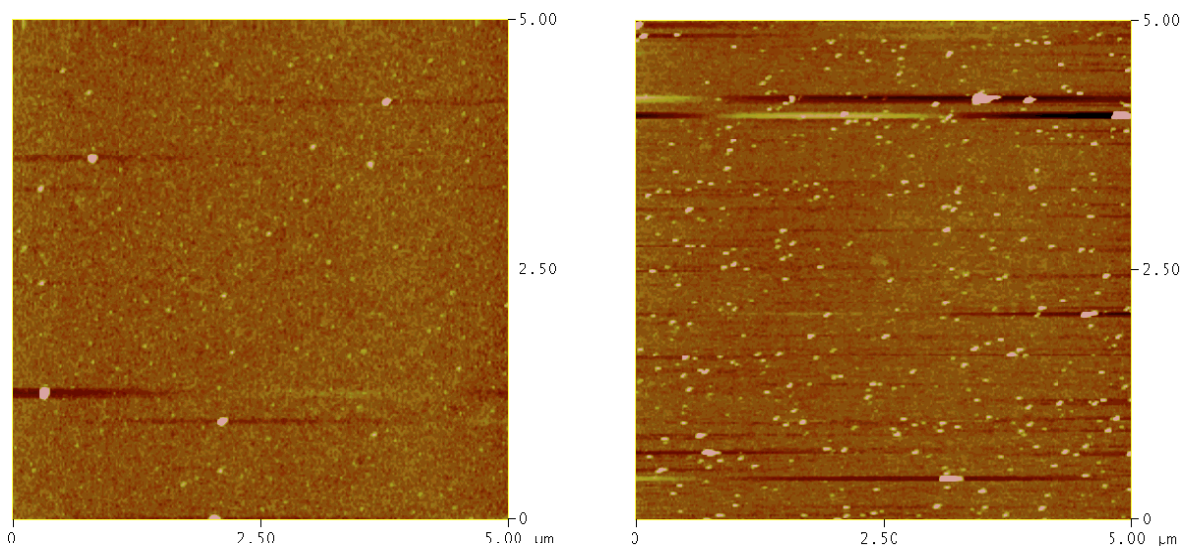


**Figure 20** Alumina surface when treated with 1% RCA-1 (left) shows almost no deposition of clusters on the surface. Treatment of the surface with 10% RCA-1 solution (right) does lead to good number of clusters though the density is still not so high as the one obtained on silica surface.

### **8.3.2 Spin coating of alumina surface treated with 10% RCA-1 solution with Iron Nitrate**

The study of supported catalyst was performed with iron nitrate and it is our aim to also deposit the iron nitrate salt on alumina coated silica surface to study growth of carbon nanotubes on it. We deposited with 100 layers of alumina on native silica on Si at 250 °C and then treated the surface of alumina with 10 % RCA-1 solution at room temperature for 10 minutes. The surface was then spin coated with 0.2 mmol/L of solution of iron nitrate in water at 4000 rpm. The distribution and density of clusters as

observed by AFM was uneven. The results are shown in Figure 21. It may be deduced that from Figure 20 and 21, the type of salt also makes a difference.

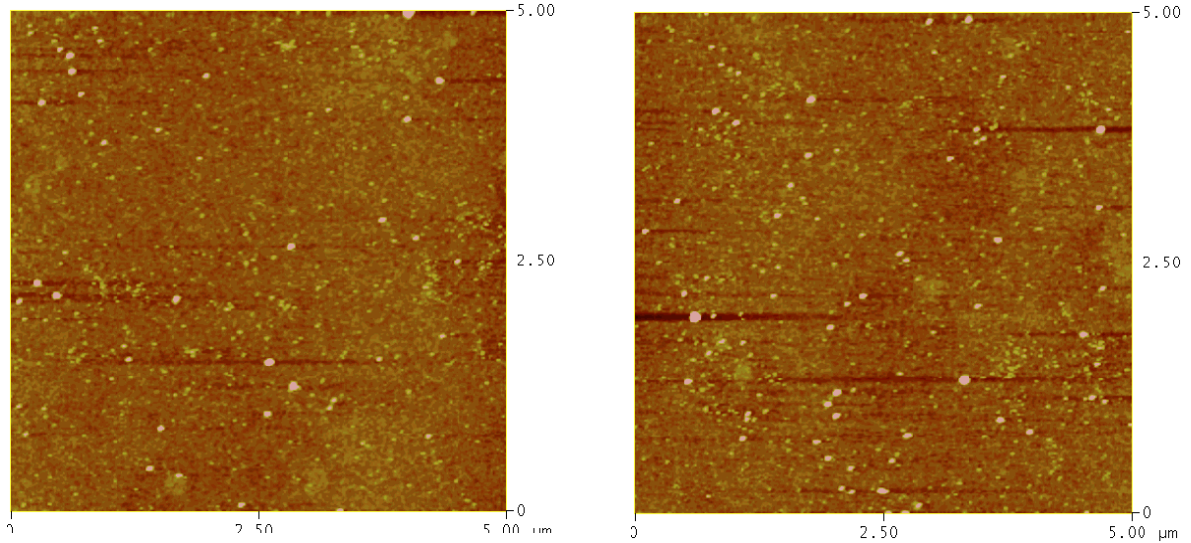


**Figure 21** Alumina coated  $\text{SiO}_2/\text{Si}$  wafer was treated with 10% RCA-1 solution and then spin coated with 0.2 mmol/L iron nitrate solution at 4000 rpm. The distribution of clusters seems uneven on the surface.

## 9 Reaction on iron salt deposited on alumina coated silica/Si wafer

The final aim of all the alumina coating was to perform experiments on growing carbon nanotubes on alumina and compare it to the growth on silica model catalyst. Two samples of different loading of catalyst on alumina surface were chosen for the growth of carbon nanotubes, one on calcined and one on uncalcined surface. AFM done on both the surfaces were not very conclusive on the growth of carbon nanotubes. The results in general indicated that no large growth of carbon nanotubes was observed. They are discussed in following sections.

### 9.1 Iron salt on uncalcined alumina surface

The clusters deposited were first calcined at 300 °C in air for 1 hour gradually ramped. It was then allowed to cool down and then reduced in hydrogen at 300 °C for one hour. It was then reacted at 900 °C for 5 minutes with benzene. The complete conditions of treatment are given below:

#### Calcination:

Temperature<sub>1</sub> = 120 °C                      time<sub>1</sub> = 20 minutes                      Ramp<sub>1</sub> = 0.5 °C/min

Temperature<sub>2</sub> = 300 °C                      time<sub>2</sub> = 60 minutes                      Ramp<sub>2</sub> = 1 °C/min

#### Reduction:

Temperature<sub>3</sub> = 300 °C                      time<sub>3</sub> = 60 minutes                      Ramp<sub>3</sub> = 10 °C/min

H<sub>2</sub> flow rate = 20 ml/min

**Reaction:**

Temperature<sub>4</sub> = 900 °C

time<sub>4</sub> = 5 minutes

Ramp<sub>4</sub> = 70 °C/min

H<sub>2</sub> flow rate = 20 ml/min

He flow rate (saturator) = 20 ml/min

He flow rate (excess) = 200 ml/min

Benzene flow rate = 2.19 ml/min

AFM shows no growth of any nanotubes (Figure 22). The clusters are observed clearly on the surface after the reaction period.

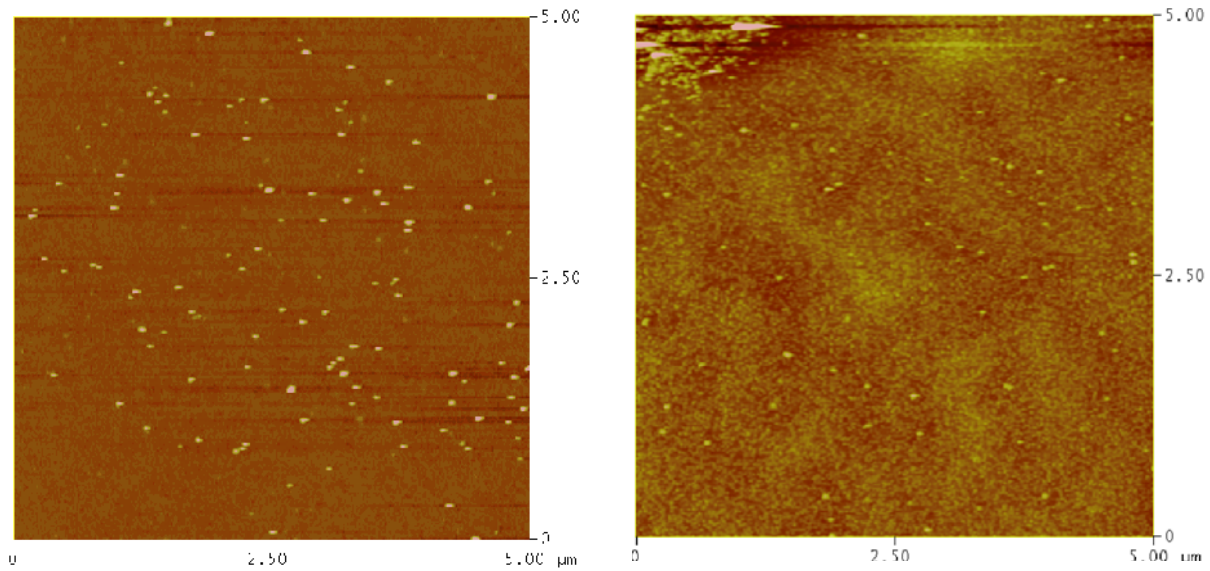


**Figure 22** AFM shows the clusters before reaction (left) and after reaction (right). The clusters are seen on the surface after reaction conditions but no carbon nanotubes could be easily discerned.

## 9.2 Iron salt on calcined alumina surface

The calcined alumina coated with iron nitrate salt at very high concentration was employed to see the effect of reaction conditions. The alumina surface was deposited with 2 mmol/L solution of iron nitrate at 4000 rpm leading to a larger loading of catalyst. The higher loading was chosen because it was not possible to get good deposition of catalyst from a low concentration of solution on calcined surface. The carbon source in this case employed was propylene instead of benzene. A lower temperature of reaction (800 °C) was chosen for propylene as it is more reactive. Following conditions were employed for reaction.

### Calcination:

$T_1 = 120\text{ °C}$                        $t_1 = 20\text{ minutes}$                        $R_1 = 1\text{ °C/min}$

$T_2 = 400\text{ °C}$                        $t_2 = 5\text{ minutes}$                        $R_2 = 5\text{ °C/min}$

### Reduction:

$T_3 = 300\text{ °C}$                        $t_3 = 20\text{ minutes}$                        $R_3 = 10\text{ °C/min}$

$H_2$  flow rate = 9.3 ml/min

### Reaction:

$T_4 = 800\text{ °C}$                        $t_4 = 10\text{ minutes}$                        $R_4 = 25\text{ °C/min (tube inside furnace)}$

$H_2$  flow rate = 9.3 ml/min

He flow rate = 300 ml/min

Propylene flow rate = 3.1 ml/min (1.0 %)

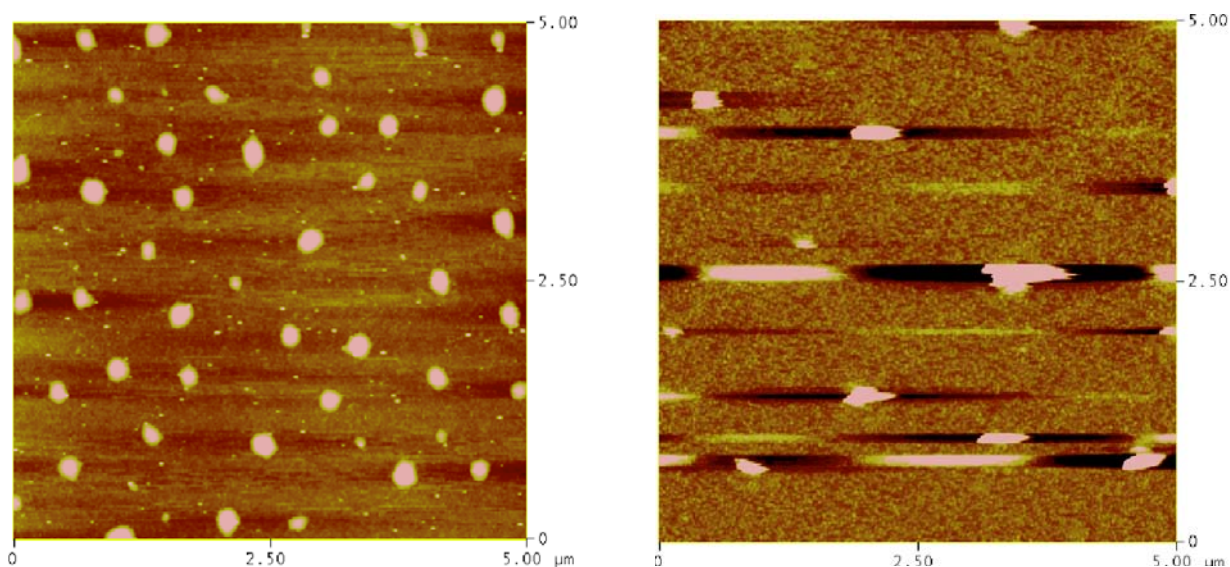


**Figure 23** The spin coated alumina surface is shown by the AFM image to the left. The surface after the reaction is shown to the right. The AFM shows presence of structures on the catalyst but is not clearly discernible.

Reaction on high loading of catalyst does produce structures on the catalyst particles but the results are not clearly discernible from the AFM images (Figure 23). The height of the cluster after calcination is about 40 nm while after reaction is about 150 nm. Further analysis is needed to ascertain the results with other techniques. At this stage of experimentation, it is not possible to comment on the suitability of one support material over the other. There are factors concerning the growth of alumina on silica surface which are complex in themselves such as retaining the Brønsted acidity of the surface to have a uniform and high density of clusters. In all above cases of reaction conditions, the pretreatment of the surface such as calcination and reduction of catalyst are not severe so it maintains its integrity during the reaction process as we do not observe pin holes or any such breakdown of alumina layer.

## 10 Discussion

In this study, attempt was made to form conformal films of alumina on silica or Si bulk surface using atomic layer deposition. The deposition was carried using alternate cycles of exposures of trimethyl aluminum and water on the surface. The reaction between trimethyl aluminum and water proceeded strictly on the surface and was self-limiting. Bulk reaction and chemical vapor deposition of alumina was prevented by purging each exposure of reactant with nitrogen. The films were deposited on bulk silicon (100) by stripping out the native silicon oxide, on native silica and on thick silica on Si (100) produced by calcination above 750 °C for few hours. The stripping of native silicon oxide leaves a rough surface and consequently the alumina deposited on the bulk Si (100) is rough. The roughness is not acceptable for our case of model catalyst support so deposition was carried out on native and bulk silica on Si (100). The bulk silica on Si (100) was employed for preventing the silica and Si interface playing any role in the growth of alumina surface. The ellipsometric results show more unreliability for alumina coating thickness on bulk silica compared to thickness of alumina on native oxide. The bulk silica has an uneven interface between silica and bulk Si (100) which will give an error in the measured thickness for silica. Further the roughness of the film adds its own error to the thickness of the film. Alumina film deposited on the native silicon oxide at 250 °C shows a growth rate of  $\sim 1.2 \text{ \AA}/\text{cycle}$ , a value that matches very closely to the literature. The certain advantage in growing films on native silicon oxide is obviously a more smooth surface compared to the one deposited on the bulk silica surface.

Alumina films were deposited at 177 °C, 250 °C and 300 °C. The maximum growth rate is observed for temperatures of 177 °C and the temperature increase leads to the decrease in the growth rate of alumina film on the surface. The reason for this may be because of the crystallinity changes at increasing temperature. The crystallinity of the film increases with temperature leading to compactness of molecules.

The film of alumina deposited at 177 °C is stable up to a temperature of 600 °C calcined at slow rate of 1 – 3 °C/min for one hour. The film deposited at 300 °C does show formation of clusters after calcination at 600 °C, a phenomenon that occurs from the crystallization of the film. The deposition of film at 177 °C is amorphous as compared to the one at 300 °C and may lead to formation of clusters at higher temperature of calcination. Calcination at 800 °C for film deposited at 177 °C shows development of pin holes which are 2 – 5 nm indicating the instability of the surface. Same is the case for film deposited at 300 °C only that the film shrinks forming large voids which are about 2 nm deep and forms disconnected island type structure. The difference in behavior in both cases is definitely because of different deposition temperature and the crystallinity of the film deposited. Film is not stable under reaction conditions (temperature of 900 °C) for film calcined at 600 °C but remains stable for film calcined at 500 °C under reaction conditions.

Deposition of iron clusters on the surface of alumina films provides a great challenge. The film if calcined to remove any defect present does not easily lead to any deposition on its surface. The number of clusters is almost non-existent. This is

contradictory to the deposition of clusters observed on silica surface. The reason lies in the fact that the surface after calcination may lose some of the hydroxyl groups present after deposition. Treatment of the alumina surface with RCA-1 solution leads to the formation of hydroxyl groups necessary for the deposition of clusters. The only drawback of the process is the roughening of the surface.

Deposition on uncalcined surface also does not deposit a high density of clusters. The reason probably lies in the acidity of the silica surface compared to the alumina surface. Silica with its low isoelectric point of pH 1.5 – 2 easily provides the Brønsted acid sites for cation exchange. The case is not true for the alumina case which shows a very high basicity at pH of 8 – 9. There are almost no Brønsted acid sites to exchange for the  $H^+$  ion to remove the anion of iron salt. The treatment of the surface with RCA-1 solution does help deposit the iron clusters.

Reaction of the clusters with benzene did not yield any carbon nanotubes as observed or discernible by AFM. The clusters were observed to be present after the reaction conditions. The limited reactions done on the catalyst clusters on alumina are not sufficient for the determining the effect of the support on the growth of carbon nanotubes.

## 11 Conclusion

Conformal alumina coating was successfully done on the silica/Si surface at temperatures of 177 °C, 250 °C and 300 °C. The growth rate of alumina film is comparable to the ones reported in the literature. The AFM indicates a smooth topography surface at all temperatures of deposition and is sufficient for model catalyst support study for various reactions. The film is usually stable up to 500 °C for calcination in air. Above 500 °C, the film properties start degrading depending on the time and temperature of treatment. Pin holes develop at temperature of 800 °C and above. If the calcination is done at 500 °C and reaction is carried at temperatures of up to 900 °C, the film maintains its integrity during the period of reaction. Reaction on clusters on alumina film did not yield any carbon nanotubes as observed by AFM. At this stage it is difficult to compare the effect of support on the growth of carbon nanotubes because of limited number of experiments performed in this area.

## 12 References

1. Shevyakov, A. M., Kuznetsova, G. N. and Aleskovskii, V. B., *Khim. Vysokotemp. Mater., Tr. Vses. Soveshch., 2nd*, 149-55, (1965), p. 149.
2. Suntola, T. and Antson, J., Apparatus and method for growing thin compound films, in *Ger. Offen.*, (Instrumentarium Oy, Finland). De, p. 30 pp. (1976).
3. Gusev, E. P., Cartier, E., Buchanan, D. A., Gribelyuk, M., Copel, M., Okorn-Schmidt, H. and D'Emic, C., *Microelectronic Engineering*, 59, (2001), p. 341.
4. Leskela, M. and Ritala, M., *Thin Solid Films*, 409, (2002), p. 138.
5. Hiltunen, L., Kattelus, H., Leskela, M., Makela, M., Niinisto, L., Nykanen, E., Soininen, P. and Tiitta, M., *Materials Chemistry and Physics*, 28, (1991), p. 379.
6. Suntola, T., *Handb. Cryst. Growth*, 3, (1994), p. 601.
7. Ott, A. W., Klaus, J. W., Johnson, J. M. and George, S. M., *Thin Solid Films*, 292, (1997), p. 135.
8. Ho, J. H., Lee, C. L., Jen, C. W. and Lei, T. F., *Solid-State Electronics*, 30, (1987), p. 973.
9. Tompkins, H. G., *Thin Solid Films*, 181, (1989), p. 285.

10. Cho, H. M., Lee, Y. W., Lee, I. W., Moon, D. W., Lee, H. J., Kim, B. Y., Kim, H. J., Kim, S. Y. and Cho, Y. J., *Journal of Vacuum Science & Technology, B: Microelectronics and Nanometer Structures*, 19, (2001), p. 1144.
11. Tompkins, H. G., *User's Guide to Ellipsometry*, Academic Press, Boston (1993).
12. Bond, G. C., Modification of catalytic properties by metal-support interaction., in *Studies in Surface Science*, Vol. 11.
13. de los Arcos, T., Vonau, F., Garnier, M. G., Thommen, V., Boyen, H. G., Oelhafen, P., Duggelin, M., Mathis, D. and Guggenheim, R., *Applied Physics Letters*, 80, (2002), p. 2383.
14. Jung, Y. J., Wei, B., Vajtai, R., Ajayan, P. M., Homma, Y., Prabhakaran, K. and Ogino, T., *Nano Letters*, 3, (2003), p. 561.
15. Lim, B. S., Rahtu, A. and Gordon, R. G., *Nature Materials*, 2, (2003), p. 749.
16. Keranen, J., Carniti, P., Gervasini, A., Iiskola, E., Auroux, A. and Niinisto, L., *Catalysis Today*, 91-92, (2004), p. 67.
17. Gordon, R. G., *Polymeric Materials Science and Engineering*, 90, (2004), p. 726.
18. Goswami, I. and Laxman, R., *Semiconductor International*, 27, (2004), p. 49.
19. Elam, J. W., Groner, M. D. and George, S. M., *Review of Scientific Instruments*, 73, (2002), p. 2981.

20. Ott, A. W., McCarley, K. C., Klaus, J. W., Way, J. D. and George, S. M., *Applied Surface Science*, 107, (1996), p. 128.
21. Copel, M., Cartier, E., Gusev, E. P., Guha, S., Bojarczuk, N. and Poppeller, M., *Applied Physics Letters*, 78, (2001), p. 2670.
22. Afanas'ev, V. V., Stesmans, A., Mrstik, B. J. and Zhao, C., *Applied Physics Letters*, 81, (2002), p. 1678.
23. Renault, O., Gosset, L. G., Rouchon, D. and Ermolieff, A., *Journal of Vacuum Science & Technology, A: Vacuum, Surfaces, and Films*, 20, (2002), p. 1867.
24. Eng, P. J., Trainor, T. P., Brown, G. E., Jr., Waychunas, G. A., Newville, M., Sutton, S. R. and Rivers, M. L., *Science (Washington, D. C.)*, 288, (2000), p. 1029.
25. Elam, J. W., Nelson, C. E., Cameron, M. A., Tolbert, M. A. and George, S. M., *Journal of Physical Chemistry B*, 102, (1998), p. 7008.

# **Chapter 8**

## **Discussion and Conclusions**

The aim of the experiments was to deposit well controlled sizes of clusters on model silica or silicon surface and attempt to grow carbon nanotubes from them. The study of growth of carbon nanotubes on this system will be facilitated by the easy access to the catalyst on the model support (in our case silica on top of Si (100)). Model support provides the ideal condition for study of growth of carbon nanotubes. They are easily accessible by surface sensitive technique such as AFM, STM, XPS, LEED and others, thereby making it easy to study the behavior of catalyst on the surface very accurately. The deposition of clusters is easily manageable on them.

Spin coating gives a good control on the size, density and distribution of clusters deposited from salt solution of a given concentration at a given speed with nitrogen as evaporation gas. The parameters used to control the clusters sizes are the speed of spin coating, type of salt, concentration of salt and the type of solvent used for evaporation. Atomic force microscopy was employed for studying the salt distribution on the model support. Some of the observations were that the density of clusters decreases from the center of the wafer to its edge because of the effect of centrifugal force. Among the type of salt clusters deposited, iron citrate showed the smallest cluster size because of its large ligand molecule which prevents it from excessive agglomeration. Solvent that evaporates rapidly forms a thinner film on the silica surface as compared to more viscous liquid resulting in smaller cluster size. In general, higher the speed of spin coating, smaller is the film formed by its adhesion to the silica surface because of larger centrifugal force, smaller is the size of clusters formed. With drop in concentration, the total amount of salt

present to be deposited decreases and thereby reduces the cluster size. One of the side effects is that the density of salt also decreases with above parameters.

The salts studied were iron chloride, iron acetate, iron citrate, iron nitrate and nickel nitrate. All salts except iron nitrate showed stability under reduction/oxidation conditions and further treatment under reaction conditions. Reaction with dicyclopentadiene produced carbon nanotubes with clusters obtained from iron chloride only. Nickel chloride produced them with benzene as the carbon source. Iron nitrate did not produce carbon nanotubes to the extent as the other two salts. Iron chloride was selected to be best among the lot followed by iron nitrate to study on model catalyst. Nickel chloride was used to study the effect of other salts.

Iron nitrate showed peculiar results with respect to its treatment under reaction conditions. When rest of the salts were observed under blank reaction conditions (in absence of hydrogen or benzene or both), iron nitrate clusters seem to be “lost” from the surface except trace of one or two large ones in  $25 \mu\text{m}^2$  area. The other salt clusters were observed under reaction conditions though agglomerated to some extent (about 3 times) but not absent from the surface. All these clusters were deposited on silica formed from Si (100) by calcination for 24 hours at  $750 \text{ }^\circ\text{C}$ . When iron nitrate is deposited on silica surface on Si (100) obtained by calcination at  $350 \text{ }^\circ\text{C}$  for 24 hours, the surface show clusters about 5 – 10 times larger than the original. It is not clear as to what gives rise to such an observation at this stage of research, the factors that varied in two cases was the

thickness of silica film. One lesson to take from this observation is that the type of ligand (nitrate vs. chloride) decides the chemistry of clusters in growth of carbon nanotubes along with the support chemistry.

Iron chloride being the most suitable catalyst on silica/Si surface, we pursued further studies on growth of carbon nanotubes with it as the iron catalyst precursor. On model catalyst, based on Raman and SEM, only MWNT were observed to grow at temperatures of 900 °C. No SWNT were ever observed on the surface. The reason for this is agglomeration of clusters on the surface during reaction conditions. It was beyond our limits to prevent the agglomeration of clusters. The MWNT produced on the surface were in very good density and some grew vertical to the surface. MWNT were observed to grow with both benzene and propylene as the carbon source. TEM indicates the presence of graphitized wall with defects in form of kinks.

Nickel chloride was employed to observe the effect of different metal catalyst known for growth of carbon nanotubes. The growth of MWNT is observed at temperatures of 900 °C and above. The size of carbon nanotubes obtained in general are larger (100 – 150 nm) compared to the ones obtained from iron salt (60 – 100 nm). No growth of single walled carbon nanotubes is observed by Raman Spectroscopy.

One of the well developed techniques of growing multi-walled carbon nanotubes is from Ferrocene and other metallocene molecules. The research was pursued to

understand the nature of catalyst surface conducive for effective growth of carbon nanotubes. Growth of carbon nanotubes occurred at 650 °C and above. At low temperatures of up to 800 °C, growth of MWNT is accompanied with deposition of carbonaceous material. At 900 °C, the alignment of the carbon nanotubes becomes vertical to the surface. The impurity of the MWNT formed at 900 °C decreases and crystallinity increases as seen with the relative intensity of D/G bands in Raman spectra. One of the samples was heated in air at 800 °C to remove all the MWNT and C deposits and expose the surface. The oxidized iron surface was visible by naked eye and confirmed by Raman. The surface was reduced in hydrogen and reacted with benzene (without ferrocene) at 800 °C. Very few number of MWNT grew on the surface with majority of the surface covered only with carbon. It is clear from these experiments that production of iron clusters in-situ is very important for effective growth of carbon nanotubes. The diameter of the nanotubes varied from 10 – 50 nm.

In order to produce single walled carbon nanotubes, we chose supported catalyst. One advantage of supported catalyst is that in the pores of their bulk, there is little movement possible for solid iron clusters to move around and agglomerate. The advantage is that once a small size is achieved, a certain possibility exists for their stability under reaction conditions. We employed 5% by weight of iron (from iron nitrate) on alumina with benzene as the carbon source. At 800 °C and below, only MWNT were formed on the supported catalyst. The first SWNT were observed at 850 °C along with MWNT. Almost pure SWNT were observed at 900 °C and above by Raman. This was

confirmed by Raman and TEM independently. The size of single walled carbon nanotubes is approximately  $1.2\pm 0.2$  nm. The active clusters for growth of SWNT are low compared to overall loading and the rest of them are covered by carbon. The percentage being low is not deterrent to the formation of carbonaceous material. The cluster size varies between 3 – 20 nm. Methane as a carbon source was not able to produce any carbon nanotubes up to a 2% by volume in gas phase.

Atomic layer deposition of alumina on silica or Si (100) surfaces was pursued at 177 °C, 250 °C and 300 °C. The study was undertaken to produce different support layer to observe its effect on growth of carbon nanotubes. Conformal flat alumina deposition was carried out on HF stripped Si (100), on native silicon oxide and on silicon oxide deliberately grown on top of Si (100) by calcining it. HF stripping of native silicon oxide makes the surface rough and inappropriate for our purpose in employing AFM to observe nano-clusters. The thickness was measured by ellipsometer. The best coating occurred on top of native silicon oxide because of its natural smooth surface. Film deposited at 177 °C is stable up to 600 °C of calcining temperature in air for 1 hour. Calcining alumina film deposited at 300 °C for one hour did produce large clusters produced because of crystallization of the film itself. Calcination at higher temperatures produces pin-hole defects in the surface. Alumina films are not stable under reaction conditions (temperature of 900 °C) for cases prior calcined at 600 °C in air. Amorphous films showed stability under reaction conditions. The interaction of alumina with inorganic salt is not favorable from the point of view of depositing the salt on its surface. The

deposition takes place when the alumina surface is treated with RCA-1 solution though roughening occurs to a large extent because of the corrosive nature of the solution. Reaction of the clusters with benzene did not yield any carbon nanotubes as observed by AFM and TEM. The number of reaction carried were very few and not enough to determine the effect of support on growth of carbon nanotubes.

# **Chapter 9**

## **Future Work**

Our aim of experiments was to grow single walled carbon nanotubes on catalyst deposited on model support and with the help of surface sensitive techniques and study their growth mechanism. Deposition of clusters on silica model support grew only multi-walled carbon nanotubes. The main reason for this observation was that the clusters were not stable under reaction conditions which entailed temperatures as high as 950 °C. Model catalyst have the clusters open to the reaction environment which in certain cases provides an advantage (negligible heat and mass transfer) but in our case proved to be a disadvantage since there was practically nothing to stop their agglomeration. Metal or metal oxides at 950 °C are usually above their melting point when they are present in nanometer sized clusters. Unless there is a very strong interaction between clusters and surface, the clusters will become mobile at temperatures usually half that of its melting point at atmospheric pressure. In case of supported catalysts we were very successful in growth of single walled carbon nanotubes. In supported catalyst, the mobility of clusters is restricted to a large extent because of the pore sizes of the support material being distributed in 1 – 10 nm. The tortuosity of the pores further prevents the movements of catalyst. The case is indeed suitable for production of single walled carbon nanotubes if the catalysts remain active under the reaction conditions and is accessible to the reactants.

An attempt was made based on the strong interaction between alumina and iron to deposit iron clusters on alumina model support. Alumina model support was produced on top of silicon model catalyst and its behavior is studied under different calcination conditions, reaction conditions and thickness of silica on top of Si (100). We were able to deposit clusters on top of the surface only with great difficulty and not without making

the surface rough. This was accomplished by treating alumina surface with RCA-1 solution. It is not a recommended technique of depositing the clusters and other methods exists. One way is to make the salt solution more basic so that its overall pH value becomes higher than the isoelectric pH value of alumina surface. Deposition of clusters occurs on a surface that has a Brønsted acid site to exchange its hydrogen with the anion of the salt and deposit the cluster on the surface. In case of silica the isoelectric pH value is about 1.5 which is usually below the pH value of most of salt solutions. The one for alumina is about 9.0 and special treatment of the surface such as increasing the basicity of the salt solution may be needed for depositing the clusters. After successful deposition of clusters, one needs to control the size and density of clusters on the surface by studying the effect of spin coating parameters on salt deposition. The salt solution being basic would add its own complexity to the system.

Reaction on clusters on alumina surface with benzene did not yield any carbon nanotubes at conditions of reactions employed with silica as the support. We did not perform many reactions to study this case in its depth. This case provides the biggest challenge and also prospect of doing better than silica since we did not observe much agglomeration of clusters under reaction conditions. The reason of no production of carbon nanotubes is probably that the chemistry of reaction on alumina surface provides a different route and needs independent optimization for growth of carbon nanotubes. More reactions at different conditions of calcination, reduction, reaction temperature, concentration of carbon source and other parameters need to be investigated in greater details. The type of carbon source will also be very important in this case since the

adsorption of one particular carbon source on a given support material will be different in case of silica and alumina because of their very different acidity. An in depth study will greatly advance our understanding of the mechanism of growth of carbon nanotubes based on the properties of different support and relating the results to these properties.

Atomic layer deposition provides a unique opportunity to study different support materials for growth of carbon nanotubes. Besides alumina, the other support materials that can be employed are Zirconia, and Titania. They can both be deposited by the same principles as alumina. In fact the ALD process in their case will only need to have the precursor changed and the temperature of reaction. The two supports are well characterized in literature and easy to adopt for our system. The system will provide valuable insight in to the process of metal support interaction. Most of the catalytic studies have been carried over the high surface area porous supports. Very few reactions have been carried on model support with Zirconia or Titania as support either because they are difficult to prepare from wet chemistry or in case of single crystals being very expensive. Atomic layer deposition provides a relatively inexpensive technique to produce model catalyst support. The availability of ALD will make it easy to study different reaction systems besides the growth of carbon nanotubes. Further ALD gives conformal coatings which may be useful in special reaction design.

We have studied a great variation in the responses of the catalyst clusters produced from different precursors. It is possible by atomic layer deposition to deposit transition metals using appropriate metal precursor and hydrogen or water. The area is

not yet developed and it has its competing techniques for depositing thin films. The advantage of this technique is the conformal coating and extremely thin film (of the order of 0.5 – 2 nm) not easily achievable by other techniques. The deposition of film instead of clusters is that the surface is readily available with metal catalyst and reaction on it can be performed right away. The surface need not be exposed to external atmosphere at all. One may argue that we are out of model catalyst regime which is not necessarily true. Conformal coating will still ensure that we have a flat surface for characterizing with surface sensitive technique and treatment of metal surface at high temperature will lead to sintering of film forming small clusters, the size of which will depend on the thickness of the film. With this route, we eliminate the entire process of treatment of catalyst precursor for producing metal catalysts and thereby rendering it inactive in majority of cases. Many successful experiments in growth of carbon nanotubes on thin film of catalyst have been reported in literature.

We did not perform reactions on bimetallic catalyst clusters with promoter effect that has been reported to produce single walled carbon nanotubes on model catalyst albeit the catalyst was deposited by different techniques. It will be useful to try different transition metals with promoters to grow carbon nanotubes. The properties of the carbon nanotubes produced could be associated with the metal and promoter properties. It will also be useful to tune the reaction system to produce carbon nanotubes of particular orientation and chirality once the system starts producing good yield of carbon nanotubes. The scientific community working in carbon nanotubes want to produce carbon nanotubes with definite diameter and chirality (and in turn metallic or semi

conductors) to make them useful. Studying the interaction between support and catalyst will help to modify the system producing carbon nanotubes to meet these requirements. The knowledge will also be able to make contribution to other areas such as catalysis, thin film properties, nanomaterials and composites.

# Acknowledgement

At the juncture of completing my dissertation, it is a great pleasure to have the opportunity to thank those who contributed in completing my research and adding to my education. My association with colleagues and Professors both at WPI and Purdue University during pursuit of M.S. and Ph.D. degree has been fun and highly educational.

I would like to begin first by thanking my advisor Prof. Fabio Ribeiro. In three years of association with him, I have come to realize Fabio to be a highly enthusiastic researcher who settles for nothing less than the very best. His sincerity, diligence, hard work and integral approach to research has left an indelible impression on me. I am grateful to him in more than one way for his teaching me the path of incessant toil for achievement of goal, and providing me with the opportunity to work on this project. My education would have been incomplete without his guidance and help throughout. I thank my co-advisor Prof. Robert Thompson for his guidance and help with my dissertation, without which it would not have been complete in its present form. My special thanks to Prof. Venkat Thalladi for being on my advisory committee and for the helpful hints and ideas. During the course of my research, help was extended by various faculty members, here at WPI and my one year of research at Purdue University. Special thanks to Prof. Terri Comesano at WPI for allowing us use of her Atomic Force Microscopy, which forms the major part of our experimental data. Thanks to Prof. Elias Franses for allowing us use of their Ellipsometer for determining thickness of alumina film deposited.

For successful completion of research, help from colleagues is indispensable. I am grateful to Dr. Yury Zvinevich for his help with Raman spectroscopy and help in general. My thanks are due to Dr. Dmitri Zemlianov for his help with XPS. I would also like to thank specially to Dr. David Taylor at Purdue University for helping me setup the controls for valves in atomic layer deposition equipment. I am also grateful to Mr. Richard Lowe for his invaluable help in constructing the electrical cabinet for the equipment. The TEM analysis was done by Dr. Jun Ma at Hyperion Inc, Cambridge, Boston, to whom I am very grateful. My special thanks to Vikrant Urade at Purdue University for performing TEM analysis on model catalyst samples. I would like to thank Mr. Jack Ferraro and Mr. Douglas White for their invaluable help in building equipment at the start of my research.

I would like to extend my sincere thanks to the Faculty at WPI and Purdue University for their guidance and help throughout my pursuit of M.S. and Ph.D. degree. My acknowledgements are due for the staff members at both these Universities for handling all the paper work and allowing me to concentrate on finishing my thesis. A special thanks to Tom Thomsen, Director of International Student Council at WPI, for his help in student activities I participated in.

I would like to thank my friends both at WPI and Purdue University who made my stay a wonderful experience. My special thanks to Nikhil Jalani, Ritesh Shukla, Dharmesh Thakkar, Aditya Nadkarni, Vishal Phirke, Abhijit Phatak, Dr. Guanghui Zhu, Dr. Nan Chen, Dr. Jinyi Han, Dr. Tony Thampan, and all the friends at WPI. I sincerely

appreciate my association with Shadab Mulla, Ajay Joshi, Rahul Sharma, Yogesh Joshi, Aditya Bhan, Rahul Kasat, Patrick Figaro, Joshua Ratts, Scott McClellan, and all my friends at Purdue University. It has been my privilege.

Finally I would like to thank my family for their unrelenting support, care and love without which I would never have been able to achieve my career goals.